UNIVERSITY OF CALIFORNIA SAN DIEGO

Neural progenitor cell/neural stem cell graft functional integration and maturation in spinal cord injury

A dissertation in partial satisfaction of the requirements for the degree
Doctor of Philosophy

in

Biomedical Sciences

by

Steven Lee Ceto

Committee in charge:

Professor Mark Tuszynski, Chair
Professor Martin Marsala, Co-Chair
Professor Bruce Hamilton
Professor David Kleinfeld
Professor Axel Nimmerjahn
Professor Binhai Zheng

2019

The Dissertation of Steven Lee Ceto is approved, and it is acceptable in quality and form for publication on microfilm and electronically:

_____

_____

_____

_____

_____
Co-Chair

_____
Chair

University of California San Diego

2019

DEDICATION

This doctoral dissertation is dedicated to all the friends and family that have supported me from the time I was a naive young lad who changed his career goals every month until now, the culmination of my formal education. Here's to the next adventure.

EPIGRAPH

Although the neuron doctrine and single neuronal techniques have focused on the exhaustive analysis of the individual 'pixels' of the brain, it is possible that the function of neural circuits may not be apparent unless one can visualize many, or most, 'pixels' in the screen.

Rafael Yuste

TABLE OF CONTENTS

LIST OF FIGURES AND TABLES

ACKNOWLEDGEMENTS

I would like to acknowledge Professor Mark H. Tuszynski for his support as the chair of my committee. His vision inspired me to take on an ambitious project, and in the end I came out a neuroscientist.

I would also like to thank the members of the Tuszynski Lab, past and present, for all their support and guidance throughout my journey.

Chapter 2, in full, is currently being prepared for submission for publication of the material. Ceto, Steven; Sekiguchi, Kohei J.; Takashima, Yoshio T.; Nimmerjahn, Axel; Tuszynski, Mark H. The dissertation author was the primary investigator and author of this material. He designed and performed the experiments, processed and analyzed the data, and wrote the manuscript.

Chapter 3, in full, is a reprint of the material as it appears in The Journal of Clinical Investigation. Lu, P; Ceto, Steven; Wang, Yaouzhi; Graham, Lori; Wu Di; Kumamaru, H; Staufenberg, E; Tuszynski, Mark H., American Society for Clinical Investigation, 2017. The dissertation author was the second author of this material. He captured images, designed analysis methods, processed and analyzed data, wrote a portion of the manuscript, and edited the manuscript.

VITA

2011	Bachelor of Science, University of Washington
2011-2013	Research Technician II, Fred Hutchinson Cancer Research Center
2019	Doctor of Philosophy, University of California San Diego

PUBLICATIONS

London N, Ceto S, Ranish JA, Biggins S. “Phosphoregulation of Spc105 by Mps1 and PP1 regulates Bub1 localization to kinetochores” Current Biology, 22;22(10):900-6, April 2012.

Akiyoshi B, Nelson CR, Duggan N, Ceto S, Ranish JA, Biggins S. “The Mub1/Ubr2 ubiquitin ligase complex regulates the conserved Dsn1 kinetochore protein” PLoS Genetics, 9(2):e1003216, February 2013.

Ng TM, Lenstra TL, Duggan N, Jiang S, Ceto S, Holstege FC, Dai J, Boeke JD, Biggins S. “Kinetochore function and chromosome segregation rely on critical residues in histones H3 and H4 in budding yeast” Genetics, 195(3):795-807, September 2013.

Sarangapani KK, Duro E, Deng Y, Alves Fde L, Ye Q, Opoku KN, Ceto S, Rappsilber J, Corbett KD, Biggins S, Marston AL, Asbury CL. “Sister kinetochores are mechanically fused during meiosis I in yeast” Science, 346(6206):248-51, September 2014.

Lu P, Ceto S, Wang Y, Graham L, Wu D, Kumamaru H, Staufenberg E, Tuszynski MH. “Prolonged human neural stem cell maturation supports recovery in injured rodent CNS” Journal of Clinical Investigation, 127(9):3287:3299, August 2017.

Ceto S, Sekiguchi KJ, Takashima Y, Nimmerjahn A, Tuszynski MH. “Graft-Host Synaptic Connectivity in Spinal Cord Injury Revealed by Calcium Imaging” In Preparation.

FIELDS OF STUDY

Major Field: Biochemistry

Studies in DNA quaternary structure and kinetochore assembly
Professors Nancy Maizels and Sue Biggins

Major Field: Muscle Physiology

Studies in muscle satellite cell populations in patients with cerebral palsy
Professor Richard Lieber

Major Field: Neuroscience

Studies in axon regeneration and neural stem cell treatments for spinal cord injury
Professors Yishi Jin, Binhai Zheng, Axel Nimmerjahn, and Mark H. Tuszynski

ABSTRACT OF THE DISSERTATION

Neural progenitor cell/neural stem cell graft functional integration and maturation in spinal cord injury

by

Steven Lee Ceto

Doctor of Philosophy in Biomedical Sciences

University of California San Diego, 2019

Professor Mark H. Tuszynski, Chair
Professor Martin Marsala, Co-Chair

Neural progenitor cell/neural stem cell (NPC/NSC) grafts integrate into sites of spinal cord injury (SCI) and show anatomical and electrophysiological evidence of forming neuronal relays across lesions. To determine how signals may be propagated through grafts, we performed ex vivo and in vivo calcium imaging of NPC grafts and

host spinal cord neurons in mice. Following optogenetic stimulation of corticospinal tract axon terminals ex vivo, we detected consistent calcium responses throughout grafts. Grafts exhibited spontaneous activity in both independently-firing neurons and emergent neuronal networks, which were also activated by corticospinal stimulation. These patterns of activation resembled those present in intact spinal cord. In turn, optogenetic stimulation of graft axons extending out of lesion sites triggered excitatory post-synaptic responses in caudal host spinal cord neurons. Finally, distinct sensory stimuli elicited responses in the dorsal aspect of grafts in vivo. Thus, NPC/NSC grafts form local networks that are activated by host inputs and can activate host neurons on the distal side of spinal cord lesions.

In order to properly assess the potential benefit of neural stem cell grafts in humans, we sought to understand the rate at which human grafts mature in the injury site. We grafted human NSCs into sites of SCI in immunodeficient rats and assessed anatomical and functional outcomes over a 1.5-year period. Although mature neuron markers appeared 3 months after grafting; neurogenesis, neuronal pruning, and neuronal soma enlargement progressed over the next year. Graft size remained stable as axons emerged in large numbers early on, with half of these projections persisting after 1.5 years. Astrocytes expressed mature markers after 6 months, while oligodendrocytes did not display mature markers until 1 year after grafting. A slow migration of astrocytes from graft sites into host tissue was observed. Importantly, functional improvement did not occur until over 1 year after grafting. Thus, human NSCs mature at their intrinsic rate even when grafted into a rodent environment, and they

support functional recovery only at this delayed timepoint, a key finding in human clinical trial planning.

CHAPTER 1

Introduction

Spinal Cord Injury

Spinal cord injury (SCI) encompasses both traumatic and non-traumatic damage to the spinal cord that results in changes to its function. These changes arise from both primary injuries that occur with the initial insult and secondary damage from the injury response. The clinical manifestations of these changes may be temporary or permanent and include partial or complete loss of sensorimotor and sympathetic nervous system function below the level of injury, with many resulting complications (Ahuja et al., 2017). In the United States, which has the highest incidence of SCI, approximately 291,000 people are currently living with the condition (NSCISC, 2019), while a similar number of new injuries occur worldwide every year (WHO, 2013). In addition to placing an incredible emotional toll on patients and their friends and families, SCI represents a significant economic burden that can result in over $5 million of lifetime expenses (NSCISC, 2019). Currently, there is no cure for SCI, but recent studies have shown promise for several new therapeutic approaches.

The spinal cord extends from the brainstem at the base of the brain to the lumbar region of the vertebral column (**Principles of Neural Science**). It is made up of gray matter that contains neuronal cell bodies and surrounding white matter containing myelinated axons. When viewed in transverse section, the gray matter appears as a pair of butterfly wings on an oval of white matter. This organization stands in contrast to

the brain, in which cortical gray matter envelops underlying white matter. A central canal runs through the middle of the cord and provides circulation of supportive cerebrospinal fluid (CSF) to the tissue. Sensory nerves enter the spinal cord bilaterally at the dorso-lateral aspect (dorsal roots), while motor nerves exit the spinal cord at the ventro-lateral aspect (ventral roots). This follows the organization of the gray matter neurons, which generally encode sensory information in the dorsal gray and motor information in the ventral gray. Neurons of the central and ventral gray matter are involved in integrating sensory and motor information and forming the central pattern generators (CPGs) and reflex circuits intrinsic to the spinal cord. The white matter is organized into many ascending and descending tracts, with sensory axons slightly more concentrated dorsally and motor axons more ventrally. While many of these axons connect with cells in the brain and periphery, some are propriospinal axons that serve to relay information between neuron populations within the cord (Watson and Kayalioglu, 2009). Motor signals are sent from the spinal cord to muscles by motor neurons that project axons out of the cord through the ventral roots. In contrast, sensory neuron cell bodies are located in the dorsal root ganglia (DRG) that lie along each of the dorsal roots. The axons of DRG neurons bifurcate, sending one branch to the periphery and one to the spinal cord, where it may terminate or project to the brainstem (Gardner and Johnson, 2013)

Protecting the spinal cord with encircling bone and ligament, the vertebral column is organized into 7 cervical, 12 thoracic, 5 lumbar, and 5 sacral vertebrae. Intervertebral discs allow neighboring vertebrae to move smoothly with respect to one another, giving the spine flexibility. Compared to the cranium, much more space exists between the

bone of the vertebrae and the meninges surrounding the spinal cord. This space is comprised of connective and lymphatic tissue, fat, spinal nerve roots, and a concentration of veins termed the internal venous plexus. Meningovertebral ligaments attach the outer meninges of the spinal cord, the dura mater, to the vertebral column. This allows a limited range of movement of the cord within the column. The dura is a stiff membrane composed of longitudinally oriented collagen fibers and fibroblasts. Closely attached to the dura is the arachnoid mater, a thinner and more pliable membrane of collagen and elastic fibers with several cell layers. A loose layer of leptomeningeal cells is attached to the inner surface of the arachnoid and forms trabeculae that bridge the subarachnoid space to connect to the pia mater. About one third of the vertebral canal is occupied by the subarachnoid space, which is filled with CSF and provides hydromechanical protection of the spinal cord from the vertebral walls. The pia mater is the final meninge separating the spinal cord from the CSF and is made up primarily of collagen and elastic fibers, fibroblasts, and small vessels. It connects to a layer of foot processes formed by spinal cord astrocytes, known as the glia limitans. Together, these layers form a redundant system of protection of the spinal cord, but they also play important roles in the occurrence and ongoing pathophysiology of SCI (Sakka et al., 2016; Watson and Kayalioglu, 2009).

In cases of traumatic SCI, the injury-causing event produces forces strong enough to disrupt and dislocate the vertebral column, causing compression or transection of the spinal cord. The outcomes of these insults can be grouped into four categories: solid cord injury, contusion/cavity, laceration, and massive compression (Bunge et al., 1993). Solid cord injury (10% of cases) refers to a site in the spinal cord

that appears normal by gross morphology but shows signs of damage when examined by histology. The most common classification at 49%, contusion/cavity shows intact surface anatomy and no adhesion of the spinal cord to the dura. However, the cord parenchyma displays regions of hemorrhage and necrosis that eventually progress into cystic cavities referred to as syringomelia, and the damage is often spread in a tapering manner rostrally and caudally from the core injury site. Twenty-one percent of injures are lacerations, usually caused by sharp bone fragments or penetrating missiles. Clear disruption of the cord surface is observed, but damage is generally restricted to the immediate vicinity of the penetration site. Complete transections of the spinal cord are rare. The collagenous connective tissue that invades the lesion is often connected to the overlying meninges. Maceration or pulpification of the cord is termed massive compression (20% of cases). These injuries are typically seen with major vertebral body fractures and display similar pathology to laceration, with invading fibrous tissue and in some cases nerve root fragments present in the lesion site. The extent of all four types of injury can vary dramatically, and in some cases injuries at multiple spinal levels are present. Depending on the location, even a relatively small injury can have severe clinical outcomes (Norenberg et al., 2004).

Though the leading cause of traumatic SCI in the United States has long been automobile accidents, this figure has dropped from 47.0% in the 1970s to 38.1% between 2010 and 2014. Other major causes include falls (31.0%, increasing with the aging population), violence (13.5%), sports (8.9%), and medical/surgical (4.7%) (Chen et al., 2016). Non-traumatic SCI results from disease processes that affect the environment in or around the spinal cord, such as infection, tumor growth, or spine

malformations (New and Marshall, 2014). Perhaps because non-traumatic SCI is seen as a side effect other disease conditions, far less data is available for its overall prevalence than for traumatic SCI, and the two have not been compared within a single demographical study. However, studies from Canada and Australia indicate that non-traumatic SCI is far more common. In Canada, 1,227 cases per million people were reported for non-traumatic SCI, whereas 39 cases of traumatic SCI were reported per million North Americans. Australia had lower numbers for both classes, but the same trend appeared in the ratio between them, with 364 non-traumatic vs 16 traumatic cases per million (New et al., 2013; Noonan et al., 2012). While these statistics indicate the importance of non-traumatic cases within the field of SCI, this dissertation focuses on traumatic SCI.

The majority of traumatic SCI cases occur in males (79.8%), but the difference in incidence between males and females is more marked among young adults than old. Although the highest incidence of new cases is in young adults (34.4% ages 16-30), this figure has nearly halved since the 1970s, whereas the incidence in adults aged 46-60 increased from 9.0% to 25.2% in the same time period. This increased incidence among older Americans was seen across all injury etiologies except for violence, with the largest increases occurring in falls and vehicle accidents. Incidence among different ethnic backgrounds in the United States reflects the proportions of the general population, though blacks have a higher overall incidence rate than whites, and, together with Hispanics, were affected by a spike in violence-related SCI in the 1990s (Chen et al., 2016). A decline in the marriage rate in the overall population is

compounded by a lower rate specifically among SCI patients, who benefit psychosocially from the support of a marriage partner (Cao et al., 2015).

Diagnoses of SCI are initially made by first responders, who attempt to stabilize the patient with standard life support measures and immobilization of the spinal column with a cervical collar and backboard. Once at the hospital, patients typically undergo a voluntary neurological examination, and X-ray or computed tomography (CT) scans are performed to evaluate damage to the spinal column (Acheson et al., 1987). Magnetic resonance imaging (MRI) is used to assess the soft tissue of the spinal cord, nerve roots, intervertebral discs, and ligaments (Lammertse et al., 2007). Determining the extent and location of edema or laceration of these tissues is an important step in surgical planning and developing a prognosis. Electrophysiological measurements are often taken and appear to be promising tools to understand the function of the spinal cord in different states of injury, providing direct information about spared connectivity, but they have not been shown to consistently improve the accuracy of outcome predictions in awake and alert patients (Curt et al., 2008). Once sufficient information about the state of the spinal column and soft tissue integrity has been gathered, surgeons perform spinal decompression, removing any bone or foreign objects that may be impinging on the spinal cord or nerve roots. Early decompression has been shown to improve impairment scores in prospective studies. Hardware may be installed to realign and stabilize the spinal column thereafter (Ahuja et al., 2017). Even after stabilization, SCI patients may persist in a state of spinal shock for weeks to months after the injury event. Spinal shock begins as a depression of spinal reflexes below the injury in the immediate aftermath of the traumatic event. Reflexes begin to return 1-3 days later but

then progress to spasticity and hyper-reflexia over the following days to months, which may persist up to a year. These symptoms can prevent an accurate assessment of the true extent of the injury (Ditunno et al., 2004).

The clinical outcomes of SCI depend on the level and severity of injury. Although vertebral fractures are defined by the vertebral level, the neurological injury to the spinal cord is defined by the level at which the nerve roots emerge from the spinal column. The discrepancy between levels becomes more pronounced at the lower thoracic vertebrae; a fracture of the thoracic level 12 (T12) vertebra could results in damage to the sacral level 1 (S1) spinal cord. In terms of sensorimotor function, the cervical level 5 (C5) through T1 spinal cord segments communicate with the arms and hands, thoracic segments innervate the trunk, and the lumbar level 1 (L1) through L5 segments connect with the legs and feet (Watson and Kayalioglu, 2009). Bowel, bladder, and sexual function may all be affected by injuries even as low as the sacral segments, though most dysfunction is seen with injuries at or above L1-L2 (Benevento and Sipski, 2002; Hess and Hough, 2012). More immediately critical to patient survival, innervation to the diaphragm may be disrupted by injuries above C5, and injuries between C5 and T12 can affect chest and abdominal muscle innervation, all potentially leading to respiratory problems (Tator, 1972). The distribution of injury levels of new cases is roughly even for C1-4, C5-8, and T1-12 (each about 30%), whereas L1-S3 injuries are more rare at 9.1% (Chen et al., 2016). In addition to sensorimotor systems, the autonomic nervous system, with preganglionic neurons throughout the spinal cord, is susceptible to SCI. Disruptions to sympathetic outflow to the heart cause decreased heartrate (bradycardia) and cardiac output. The imbalance between sympathetic and parasympathetic output can

result in acute episodes of both hypotension and hypertension under different circumstances. Furthermore, disrupted connectivity to the lymphatic organs can result in secondary immunodeficiency (immune paralysis), increasing susceptibility to infections (hwab et al., 2014). Otherwise treatable conditions such as urinary tract infections or pneumonia are often fatal in SCI patients (Ahuja et al., 2017).

SCIs are graded on three scales developed by the American Spinal Injury Association (ASIA) and adopted by the international SCI communities in the form of the International Standards for Neurological Classification of Spinal Cord Injury (ISNCSCI). The motor and sensory scores evaluate muscle power and light touch and pinprick sensation, respectively, at each nerve root level. The impairment scale (AIS) is a more direct evaluation of injury severity, relying on the presence or absence of spared functions to assess the completeness of the lesion. Grade A injuries are the most severe, with complete loss of sensorimotor function, while Grade E indicates normal function at all levels in patients with previous deficits (Kirshblum et al., 2011). Though AIS A injuries are most common in the total SCI population (45.6%), only 33.7% of cases from 2010-2014 were of the highest severity. This change was accounted for by rises in the incidence of all grades B through D. Improvements in the medical and surgical management (van Middendorp et al., 2013), as well as changing epidemiology may account for this trend.

Across injury levels and severities, several common comorbidities affect SCI patients. Spasticity, a state of increased muscle tone due to exaggeration of the stretch reflex that contracts muscles in response to their stretching, occurs in 65-78% of chronic SCI cases. This condition arises from hyperexcitability of spinal reflex circuits following

the loss of inhibition from supraspinal inputs (Adams and Hicks, 2005). Three types of spasticity may occur: intrinsic tonic (increased muscle tone in response to passive stretch), intrinsic phasic (exaggerated reflex to tendon tap, known as hyper-reflexia; or clonus, an involuntary rhythmic contraction) and extrinsic spasticity (exaggerated flexion or extension reflexes to perceived noxious stimuli outside the muscle) (Decq, 2003). These symptoms can be detrimental to mobility, performance of daily living activities and sleep. Neuropathic arthropathy, the destruction of a joint over time due to microtraumas not felt after loss of sensory innervation, can cause deformity as well as ulcerations of the skin overlying the joint (Alpert et al., 1996). Similarly, pressure ulcers may result from prolonged sitting or lying with no sensation of discomfort to induce patients to reposition themselves. Resulting infections can be fatal. Heterotopic ossification, the buildup of ectopic bone in the connective tissue around joints, affects 10-53% of patients and begins within months of SCI. This may contribute to spasticity as well as cause localized pain, redness, and low-grade fever (van Kuijk et al., 2002). Finally, neuropathic pain is present in 40% of SCI patients, significantly affecting their mental health and quality of life. This inappropriately triggered and sometimes chronic pain can be present at the level of injury, due to sprouting sensory fibers around damaged nerve roots, or below the injury, hypothetically from the loss of spinal and supraspinal inhibition and simultaneous hyperexcitability of pain responsive areas in the brain (Cardenas and Felix, 2009).

To prioritize treatment goals, a number of studies have been performed surveying SCI patients regarding the functions they most desired to regain. Across these studies, patients with tetraplegia placed highest priority on arm and hand function,

while improved mobility was more important to patients with paraplegia. In one study of 681 patients, sexual function ranked as the highest priority for paraplegic patients. Restoring bladder and bowel function was important to both injury groups (Anderson, 2004). As the most researched functions have historically been motor and bladder function, a clear need is present for more research on bowel and sexual function (Simpson et al., 2012).

Rehabilitation is a critical component in the ongoing management of SCI complications and restoration of function that can improve quality of life and independence. Exercise focused on cardiovascular and respiratory conditioning are important for patients that may be immobilized for much of the day, and transfer and mobility training are key to allowing the patient move between their bed and a wheelchair or walker to go about their daily activities. Strength training and stretching support spared function and prevent muscle shortening as well as maintain the potential use of limbs that have lost functional input (Ahuja et al., 2017). Although it has been observed that changes in cell signaling and expression of growth factors that result from early mobilization after injury can increase axon regeneration in animal models (Hwang et al., 2014), ventilator dependence, acute SCI comorbidities, and resource limitations limit the amount of early rehabilitation that can logistically occur in the clinical setting (Ahuja et al., 2017). Once patients' conditions have stabilized after initial injury, more specialized rehabilitation programs may be employed that target their particular deficits and daily living tasks. Many exercises can be performed at home, but rehabilitation in walking requires weight support from physical therapists and/or assistive devices. Such weight-supported locomotor training (WSLT) devices include Hocoma's Lokomat and

HealthSouth's AutoAumbulator, which provide adjustable levels of weight support during walking on a treadmill or over open ground. Though no difference in functional improvement between WSLT and similar-intensity traditional physical therapy was seen in a study of patients with incomplete SCI, both groups improved significantly with training (Dobkin et al., 2006). These results highlight the importance of rehabilitation in enhancing the strength of spared connectivity between above-lesion inputs and CPGs below the injury that retain the capacity to generate locomotor patterns.

Cellular Events in Spinal Cord Injury

Mechanical trauma to the spinal cord causes transection of axons and direct strain at the tissue and cellular level. The limited capacity for regeneration of the central nervous system was has been noted since the early days of neuroscience (Cajal, 1928). Once cut, both the proximal and distal ends of axons die back hundreds of microns from the lesion site, as seen in in vivo imaging experiments of sensory axons (Kerschensteiner et al., 2005). The proximal axon segment may then undergo further retraction, but this often stabilizes over time. The distal segment invariably is destroyed through an active process known as Wallerian degeneration (Rotshenker, 2011; Waller, 1851). Strain at the cell soma may take the form of extensional strain (compression or stretch) or shear strain, in which the force is tangential to the surface upon which it is applied. While both types of strain are capable of disrupting the plasma membrane of a cell, shear strain has been shown to cause more damage at a given strain, and it is thought to be the primary mode of CNS tissue failure (LaPlaca et al., 2007; Sahay et al., 1992). Once the integrity of the plasma membrane of a cell has been compromised,

uncontrolled ion flux across the membrane leads to cell death or dysfunction (such as excitotoxicity in neurons) and pro-apoptotic signaling. Local ischemia due to disrupted microvascular supply can further exacerbate these effects. Additionally, breakdown of the blood-spinal cord barrier (BSCB) leads to destructive inflammatory responses. The BSCB, the spinal cord ortholog of the blood-brain barrier, is made up of nonfenestrated endothelial cells, pericytes, basal lamina, and astrocyte foot processes. Together, these structures prevent blood-borne molecules and cells from entering the CNS, protecting it from pathogens and cytotoxins while allowing the passage of O_2, CO_2, and other small molecules. Many of the ongoing forms of secondary damage in SCI result from BSCB disruption (Bartanusz et al., 2011).

Hemorrhage in the spinal cord permits the invasion of inflammatory cells and an influx of proinflammatory cytokines, such as tumor necrosis factor (TNF) and IL-1β (Pineau and Lacroix, 2007). Combined with the activity of inflammatory cells such as macrophages, neutrophils, and lymphocytes; these factors cause an overwhelming inflammatory response that can persist past the acute injury phase (<48 hours) and into the subacute phase (48 hours to 14 days). The resulting swelling within the cord can cause further compression and mechanical damage that in turn leads to additional secondary damage; ultimately, significant rostro-caudal expansion of the lesion can occur (Ahuja et al., 2017). Neurons and glia that do not die during the acute injury phase may still suffer the effects of excitoxicity and ischemia, which disrupt ion homeostasis both intracellularly and extracellularly. Elevated intracellular calcium levels activate calpains, which can trigger mitochondrial dysfunction and eventual cell death (Kwon et al., 2004; Schanne et al., 1979). As cells die, they release ATP, DNA, and

potassium; potent activators of microglia. Activated microglia and other inflammatory immune cells exacerbate the immune response and contribute to further apoptosis of neurons and oligodendrocytes. In the process of clearing cellular debris, phagocytes release cytotoxic by-products such as free radicals, which cause oxidative damage to DNA, proteins, and lipids (Dizdaroglu et al., 2002). The numerous feedforward mechanisms of secondary insults can lead to greater secondary damage to the spinal cord than the original mechanical injury. However, this damage is not evenly spread throughout the spinal cord tissue. For example, studies in humans have shown that ischemia has a greater effect on gray matter than white matter, partially accounting for the sparing of below injury level functions (Benton and Hagg, 2011; Ng et al., 2011).

As the subacute phase shifts into the intermediate phase (14 days to 6 months post-injury), further damage as well as attempts at self-repair begin to take place. In the wake of massive cell death, cystic cavitations of extracellular fluid, macrophages, and thin bands of connective tissue form (Norenberg et al., 2004). These spaces do not support the regrowth of axons and prevent cell migration that could otherwise create a more hospitable environment (Tator, 1995). The solid tissue of the lesion core develops as cellular debris is cleared and an influx of fibroblasts, pericytes, and other stromal or mesenchymal cells arrives. Ultimately, the mature lesion core consists of non-neural stromal cells and extracellular matrix molecules, such as proteoglycans, collagens, laminins, and fibronectins (Burda and Sofroniew, 2014; O'Shea et al., 2017). This non-neural lesion core has also been termed the fibrotic scar, stromal scar, and mesenchymal scar.

Separating these regions from viable neural tissue, an astrocycte scar forms from elongated astrocytes derived from local astroglial progenitor cells. The borders of the astrocyte scar are similar in structure and function to the glia limitans that border the meninges and blood vessel surfaces. The term ‘glial scar’ has been a point of controversy in its meaning within the SCI field, often being used in a general sense that encompasses non-neural cells and may generate confusion as to its pathological role. Thus, ‘astrocyte scar’ presents a clearer, cell type-based terminology (Sofroniew, 2018). Only several cells thick, the astrocyte scar typically surrounds the lesion core by 2-3 weeks post-injury, and disruptions to it can lead to prolonged secondary damage (Wanner et al., 2013). While during the acute stage the signaling of reactive astrocytes, microglia, and macrophages causes secretion of extracellular matrix (ECM) proteins that inhibit axonal growth, astrocytes also express molecules known to enhance axon growth. In one RNA sequencing study of astrocytes and non-astrocytes harvested from SCI lesions, both groups downregulated more axon growth inhibitors than they upregulated and upregulated more axon-permissive molecules than they downregulated (Anderson et al., 2016). Dissecting the dual role of the astrocyte scar is an ongoing endeavor.

Outside the lesion, the proximal ends of injured axons swell into spherical retraction bulbs within 1 day after injury and may persist several months. In a study in mice, the majority of corticospinal axons stopped dieback after 4 weeks at a distance of approximately 2.5 mm from the lesion, though some retraction bulbs were seen as far as 19 mm after 16 weeks (Seif et al., 2007). In vivo imaging of sensory axons showed that one mechanism that can stabilize damaged axons is the presence of an intact

branch proximal to the lesion. As previously discussed, neurons of the dorsal root ganglia project an axon that bifurcates, with one branch innervating the peripheral target organ and the other innervating the spinal cord. Once in the spinal cord, the CNS portion of the axon bifurcates again, with a descending branch targeting spinal cord neurons and an ascending branch targeting the brain. Dieback of both ascending and descending branches in the spinal cord usually halted at this second bifurcation point. Interestingly, axotomy of the main branch (proximal to the spinal cord bifurcation), resulted in more frequent regeneration than axotomy of either the ascending or descending branches alone. Combined, these results suggest that a surviving branch may act as a stabilizer, suppressing both degeneration and regeneration (Lorenzana et al., 2015). In addition to dieback, axons around the injury site can also undergo demyelination, slowing conductance of action potentials and exposing them to further injury (Fehlings and Tator, 1995). Although local oligodendrocyte precursors can differentiate into mature oligodendrocytes and remyelinate these axons, this process is inefficient due to inhibition by molecules of the injury milieu, including the debris of the very myelin in need of replacement (Kotter et al., 2006; Syed et al., 2016).

Despite historical pessimism regarding the ability of the central nervous system to regenerate, partial regeneration can occur to a limited extent through endogenous mechanisms. Patients with incomplete SCI can show substantial spontaneous improvements in function, which are maximized with rehabilitation (Ahuja et al., 2017; Curt et al., 2008; Dietz et al., 1998). This is in large part a result of the preservation of CPGs below the lesion that contain much of the circuitry encoding movement paradigms. Experiments in spinalized cats (with complete spinal cord transection above

the hindlimb motor neuron pools) have shown that, once activated, CPGs are capable of generating coordinated stepping on a treadmill even in the complete absence of supraspinal input, although the same capacity has not been observed in humans without additional stimulus (Barbeau and Rossignol, 1987; Hodgson et al., 1994; de Leon et al., 1998). Plasticity of spinal cord circuits allows detour connections to be made around partial injuries, restoring some behavioral function. For instance, following a mid-thoracic hemisection (transection of one half of the spinal cord), injured corticospinal axons sprout laterally across the midline of the spinal cord and form new synapses onto long descending propriospinal neurons (PSNs). These long PSNs in turn make connections onto lumbar motor neurons, effectively restoring corticospinal connectivity to the original target neuron population via a PSN relay. Electrophysiological and behavioral testing confirm the function of these relays (Bareyre et al., 2004). Such detour circuits are well documented, and they can also include descending supraspinal projections from the brainstem (Ballermann and Fouad, 2006; Courtine et al., 2008; Rosenzweig et al., 2010; Ruder et al.; Takeoka and Arber, 2019; Takeoka et al., 2014; Zörner et al., 2014).

In addition to new circuitry, new neural tissue can form from the ependymal layer lining the central canal. Neural progenitor cells (NPCs) contained within are capable of generating neurons, oligodendrocytes, and astrocytes *in vitro*. It is populations of these cells that allow primitive vertebrates such as zebrafish and lizards to regenerate spinal tissue, including motor neurons, that supports remarkable functional recovery after severe spinal cord injury (Becker et al., 2004; Fisher et al., 2012; Reimer et al., 2008, 2013). However, mammalian NPCs only generate glial subtypes after SCI *in vivo*, which

contribute mostly to the inflammatory response and astrocyte scar formation (Barnabé-Heider et al., 2010; Mao et al., 2016; Meletis et al., 2008). Thus, endogenous spinal cord regeneration is limited to stabilization of the injury site and the rewiring of existing neurons to compensate for lost connectivity.

Barriers to Regeneration

As previously stated, the CNS is far more refractory to regeneration than the peripheral nervous system (PNS), and it is this contrast that has been the basis of many discoveries in the mechanisms that prevent CNS axon regeneration. These include extrinsic factors in the CNS environment as well as intrinsic deficiencies in the regenerative potential of CNS axons. Extrinsically, lack of proper growth substrate, the presence of inhibitory factors in the environment, and loss of neurotrophic support combine to impede growth. Within CNS neurons, genetic programs for regeneration fail to sufficiently activate following injury. Understanding these barriers to regeneration is key to developing new therapeutics for SCI.

Axon regeneration vs axon sprouting

Before discussing in detail the regulation of axon regeneration, it is important to define precisely what is meant by this term, as not all new axon growth is considered regeneration. Under normal conditions of neural plasticity such as motor learning, axon branches may sprout to form new connections with post-synaptic targets. Sprouting also occurs after injury as part of the previously discussed endogenous repair that allows compensatory connections with spared circuitry to mediate functional recovery.

Tuszynski and Steward differentiate sprouting from regeneration with the requirement that regeneration must occur as new growth from a cut axon into or beyond a lesion (Tuszynski and Steward, 2012). Sprouting, on the other hand, is defined as new growth from uninjured axons. Regeneration can be further divided into subtypes that distinguish the fundamentally different processes that may occur. Canonical regeneration is new growth from the transected axon tip that leads to reinnervation of its normal target neuron population. New growth from an injured axon near the injury or remote from it has been labeled “regenerative sprouting,” but both cases may be considered subtypes of regeneration because they initiate from damaged axons. Ultimately, both sprouting and regeneration can support functional improvement following injury, so each merits examination in assessing outcomes. However, clear descriptions of observed phenomena (indicating the exact origin, path, and termination of axons whenever possible) are more useful than general terminology and can help to avoid confusion and misleading claims that may set back progress in the field.

Physical barriers

Perhaps the most obvious obstacles facing successful regeneration following spinal cord injury are the physical barriers created by the disruption of intact tissue. As described earlier, the cystic cavities formed within many injuries are not permissive to axon growth. Dense collagenous scar tissue made by invading fibroblasts at the lesion core also exclude axon penetration in a simple mechanical fashion (Berry et al., 1983; Norenberg et al., 2004). While many small animal models of spinal cord injury are able

to reproduce these lesion structures, the size of human injuries is much greater, making the anatomy of the injury a formidable barrier in its own right (Zhang et al., 2014).

CNS vs PNS injury environment

Even in the presence of a physical substrate upon which to grow, however, a permissive molecular environment is also required for axon regeneration. Aguayo and colleagues showed in the 1980s that while peripheral nerve axons regenerate poorly into the glial milieu of the optic nerve (part of the CNS), CNS axons can regenerate robustly into a transplanted peripheral environment (Aguayo et al., 1978; David and Aguayo, 1981; Richardson et al., 1980). In one experiment, sciatic nerve “bridges” were grafted between the medulla oblongata and the lower cervical or upper thoracic spinal cord of rats. Prior to sacrificing the animals, the graft was transected at the rostral or caudal end and horseradish peroxidase (HRP) was applied to the exposed ends of the grafts. Twenty-four to 48 hours later, animals were killed, and the number of labeled neurons in the brainstem or spinal cord distal from the graft transection site was assessed. In each animal, tens to hundreds of cells were seen in both regions, indicating that ascending and descending CNS axons grew over 30 mm through peripheral nerve grafts, far further than any regeneration seen within a CNS environment. Light and electron microscopy showed that these axons were often ensheathed by peripheral Schwann cells (David and Aguayo, 1981). These results provided striking evidence of the limiting effect of the CNS environment on the regenerative potential of CNS axons.

Scar-associated molecules

In the years following, several groups sought to uncover the molecular mechanisms by which the CNS environment impedes axon regeneration. Early on, the astrocyte scar and CNS myelin were both found to contain axon growth inhibitors (Davies et al., 1999; McKeon et al., 1991; Rudge and Silver, 1990; Schwab and Caroni, 1988). In vitro experiments of axon outgrowth from retinal ganglion neurons demonstrated that, while nonreactive astrocytes supported axon outgrowth, reactive astrocytes explanted from lesions in adult animals did not. Previously known inhibitors of axon growth, cytotactin/tenascin (CT) and chondroitin-6-sulfate proteoglycan were found to be present around the lesion and associated with reactive astrocytes (McKeon et al., 1991). Subsequently, other chondroitin sulfate proteoglycans (CSPGs) were found to be secreted by reactive astrocytes after injury (Jones et al., 2003; McKeon et al., 1999; Tang et al., 2003) and to contribute to the inhibition of axon growth (Dou and Levine, 1994; Mckeon et al., 1995; McKeon et al., 1999). In mature synaptic circuits, CSPGs from neurons and astrocytes contribute to the formation of perineuronal nets that regulate synaptic plasticity (Wang and Fawcett, 2012). During development, CSPGs provide guidance cues for the initial extension of axons, directing them away from inappropriate targets (Cole and McCabe, 1991; Katoh-Semba et al., 1995; Pindzola et al., 1993; Snow et al., 1990). Reflecting developmental axon guidance, growth inhibition by CSPGs is dependent on their concentration relative to growth promoters; they are not absolute inhibitors (Tom et al., 2004). It should also be noted that the astrocyte scar is not the only source of CSPGs after SCI. Prevention of astrocyte scar formation in one set of studies in transgenic mice did not significantly

change total CSPG levels or CSPG immunolabeling density in or around spinal cord lesions, nor did it increase axon growth into lesions (Anderson et al., 2016). Indeed, astrocyte bridges are the only viable endogenous substrate for axon growth into the lesion core (Sun et al., 2011; Zukor et al., 2013). The inhibitory role of CSPGs is highly dependent on the specific subtype and relative concentration and varies in different lesion compartments. It may be that CSPGs don't directly inhibit axon growth; rather, they may interfere with action of growth enhancers such as laminin (Silver and Miller, 2004).

Although CSPGs are the most widely researched, other scar-associated inhibitors of axon growth are produced in spinal cord lesions. The ligand-receptor pair Ephrin-B2 and EPHB2 are important for cell migration, axon guidance, and tissue patterning during development. Expression of ephrin-B2 increases in astrocytes following injury, and its binding to EPHB2 on fibroblasts facilitates the formation of the glial/mesenchymal scar (Bundesen et al., 2003). Another group of cell migration and axon guidance regulators, the slit proteins, are upregulated along with their glycipan 1 receptors, in reactive astrocytes (Hagino et al., 2003). To date, though, neither ephrin nor slit proteins have been directly implicated as inhibitors of axon regeneration after SCI. In contrast, repulsive guidance molecule (RMG) binding to neogenin has been reported to inhibit axon sprouting and/or regeneration through the RhoA-Rho kinase signaling pathway (Hata et al., 2006). It is expressed by oligodendrocytes and neurons, and it appears at elevated levels around spinal cord injury sites. Finally, the chemorepellent semaphorin 3, which acts through its receptor neuropilin 1, is present in the CNS injury environment and has demonstrated potent axon growth inhibiting

properties in several studies (Mecollari et al., 2014). SEMA3A has also demonstrated its role as an inhibitor of axon growth after SCI (Kaneko et al., 2006).

Myelin-associated molecules

Myelin-associated proteins are the final major class of known axon regrowth inhibitors, and, like CSPGs, are the center of much controversy in the field. Over thirty years ago, isolated myelin from adult rat spinal cord was observed to inhibit axon outgrowth, whereas myelin from sciatic nerve promoted growth, narrowing down an important factor in the differing CNS and PNS environments (Schwab and Caroni, 1988). Interestingly, Davies and colleagues later showed that transplanted DRG neurons can extend into both intact and degenerating adult myelinated white matter tracts if astrocyte scarring is minimized, emphasizing the growth-limiting effects of reactive astrocytes and calling into question the inhibitory properties of CNS myelin (Davies et al., 1997, 1999). Despite ongoing debate over the overall role of myelin in axon regeneration, several myelin-associated inhibitors (MAIs) have been identified, including myelin-associated glycoprotein (MAG), oligodendrocyte myelin glycoprotein (OMgp), and neurite outgrowth inhibitor (Nogo), all of which bind to the Nogo Receptor (NgR) (Geoffroy and Zheng, 2014; Sofroniew, 2018). MAG, a myelin maintenance protein produced by both Schwann cells and oligodendrocytes, was the first MAI characterized, with the dual effect of promoting axon growth in newborn DRG neurons while inhibiting growth in older neurons, in a neuron type-dependent manner (Mukhopadhyay et al., 1994). A glycosylphosphatidylinositol (GPI)-linked protein, OMgp is expressed by both oligodendrocytes and adult CNS neurons. It has roles in

developmental axon sprouting as well as the regulation of synaptic strength and plasticity (Chang et al., 2010; Raiker et al., 2010), and it has a specific inhibitory effect on axon sprouting (Ji et al., 2008). Nogo and NgR are the most widely studied MAIs. Three subtypes of Nogo are expressed through alternative splicing: Nogo-A, Nogo-B, and Nogo-C; though Nogo-A has been most thoroughly researched. Through activation of the signal transducer RhoA and ROCK, Nogo-A binding to NgR1 induces axonal growth cone collapse and arrest of neurite outgrowth (Chivatakarn et al., 2007). Other Nogo-A signaling pathways through multiple domains of the protein have been proposed but are less well characterized (Schwab and Strittmatter, 2014). In a comprehensive study of MAG, OMgp, and Nogo deletion in mice, single mutants showed enhanced sprouting of corticospinal and raphespinal serotonergic fibers after injury, but no synergistic effect on sprouting or improvement in axon regeneration was observed with any mutant combination, indicative of their redundant actions in binding to NgR (Lee et al., 2010). Several studies have confirmed that MAIs have an important role in limiting axon sprouting and experience-dependent plasticity, but they do not seem to be a primary cause of axon regeneration failure (Geoffroy and Zheng, 2014; Schwab and Strittmatter, 2014).

Lack of neurotrophic support

Neurotrophic factors are secreted proteins critical not only for axon regeneration, but for the very survival of neurons. In the 1970s, Campenot found that distal neurites of sympathetic neurons in culture required nerve growth factor (NGF) for their growth and survival, but NGF was not required around the neuron soma or proximal portions of

neurites (Campenot, 1977). A decade later, a well-established theory of the dependence of neurites on neurotrophic factors produced by their target cells was in place, with NGF remaining the prime example of such a factor (Purves, 1986). This doctrine had mainly been developed with assays of the PNS, but it soon became clear that CNS axons also required trophic support in much the same way. Following up on the studies of Aguayo, experiments manipulating peripheral nerve grafts in the CNS found that viable Schwann cells were an essential component of grafts for CNS axon regeneration unless substituted with NGF (Hagg et al., 1991; Smith and Stevenson, 1988). In another study, corticospinal neuron survival was completely restored by brain-derived neurotrophic factor (BDNF) and partially enhanced by neurotrophin-3 (NT-3) following axotomy at the level of the internal capsule, which killed 46% of neurons within one week without intervention (Giehl and Tetzlaff, 1996). As axons transected by SCI retract, they become separated from their target cells and thus lose neurotrophic support. While collaterals of these axons may be able to maintain the surviving structures by finding trophic support from other targets, the lesion site lacks neurotrophic factors. Induction of regeneration into SCI lesions through delivery of these factors by gene therapy or cell transplantation has demonstrated their necessity (Alto et al., 2009; Blesch et al., 2002; Kadoya et al., 2009).

Insufficient activation of intrinsic growth programs

One factor contributing to the inconsistent results seen between studies manipulating the environment of CNS axon regeneration is the varying age and subtype of the neurons examined. A growth permissive extracellular milieu for one set of

neurons may not prove as permissive for another set due to the intrinsic growth potential of each. Separating the cellular changes after injury that are due to intrinsic properties vs extrinsic influences is difficult, as they are often interdependent. Nevertheless, clever approaches have provided some insights into the innate growth capacity of CNS neurons. Evidence that dormant regenerative programs could be reactivated to induce CNS axon regeneration came from studies in DRGs showing that a conditioning lesion of the peripheral branch could prime the neuron for regeneration following a subsequent lesion of the central branch (Kadoya et al., 2009; McQuarrie and Grafstein, 1973; Richardson and Verge, 1986). Laser axotomies that sever axons while causing little damage to the surrounding tissues allow researchers to observe the intrinsic ability of different neuron types to regenerate their axons with minimal injury response in the environment (Canty et al., 2013; Lorenzana et al., 2015). While most CNS axons do not regenerate, 55% of layer 6 cortical neurons initiated regeneration from the axon stump, whereas only 20% of axons from other cortical layers and thalamus showed such regrowth (Canty et al., 2013). Comparing different neuron populations that undergo axotomy from the same lesion allows direct assessment of the relative regenerative capacity of injured axons in same environment. Optic nerve crush experiments, which disrupt the axons of retinal ganglion cells (RGCs) revealed that, although alpha-RGCs and M1 RGCs preferentially survive following lesion compared to other RGC subtypes, only alpha-RGC axons regenerate following inhibition of phosphatase and tensin homolog (PTEN). Among supraspinal projection neurons that send axons to the spinal cord, serotonergic axons from the brainstem have shown remarkable resistance to astrocyte scar-associated inhibitors and response to pro-

regenerative interventions compared to glutamatergic corticospinal axons (Hawthorne et al., 2011; Hellal et al., 2011; Lang et al., 2014; Ruschel et al., 2015). In addition to differing neuron subtypes, the age of injured neurons plays a large role in injury response across all neurons (He and Jin, 2016). Despite a life-cycle of only 3 days, the microscopic nematode *C. elegans* shows age-dependent axon regeneration, which can be reversed by manipulation of insulin signaling (Byrne et al., 2014). Similarly, age-dependent effects of PTEN deletion on corticospinal and reticulospinal axon regeneration after SCI has also been shown (Geoffroy et al., 2016).

Several mechanisms have been proposed to explain varying intrinsic regeneration potential. When an axon is cut, it must first seal the ruptured membrane and form a growth cone. Whereas developing neurons form growth cones near the soma or a branch point, transected axons must form growth cones from the freshly sealed stump, often in the middle of a degenerating white matter tract. One of the primary injury signals that induces changes within the damaged cell is a flux of calcium into the injured axon tip, which triggers several signaling cascades. In *C. elegans*, elevated calcium levels can increase the activity of dual leucine zipper kinase-1 (DLK-1), which in turn activates the mitogen-activated protein kinase (MAPK) cascade that mediates neuronal survival as well as axonal transport and growth (Holland et al., 2016; Huntwork-Rodriguez et al., 2013; Watkins et al., 2013; Yan and Jin, 2012). Leucine zipper-bearing kinase (LZK), which shares much sequence similarity with DLK, has similar activations patterns and downstream effects, suggesting they act through a common pathway (Chen et al., 2016b). Another important pathway implicated in neuronal survival and axon growth is JAK/STAT signaling, which is activated by

cytokines produced by glia in the injury site such as ciliary neurotrophic factor (CNTF) and is inhibited by suppressor of cytokine signaling 3 (SOCS3) (Bareyre et al., 2011; Jin et al., 2015; Müller et al., 2007; Smith et al., 2009). Finally, the mammalian target of rapamycin (mTOR) pathway, a central regulator of cell metabolism that is notably inhibited by PTEN, has been shown to influence the growth-competency of neurons, with marked effects on axon regeneration in spinal cord injury (Belin et al., 2015; Liu et al., 2010; Park et al., 2008). Even if primed for axon growth, mature neurons face major hurdles when attempting to achieve long-distance axon regeneration. Much of the length of adult axons is derived from “tethered growth,” in which the axon lengthens with the increasing size of the organism while already synapsed onto its target(s). In contrast, injured axons must grow much further from their distal ends than occurs during development. This places a large metabolic requirement at a location far from the cell soma (He and Jin, 2016). Thus, axonal transport of the building blocks of new growth; such as neurofilaments, tubulin, membranous organelles, and actin; may be a rate-limiting process in axon regeneration that differs in the PNS and CNS (Wujek and Lasek, 1983). Many other neuron-intrinsic pathways are involved in injury response signaling and subsequent axon regeneration, and understanding the complex interactions of all these processes is the subject of numerous ongoing proteomics, transcriptomics, and epigenomics studies (He and Jin, 2016).

Therapeutic approaches

Due to the multifaceted nature of SCI, from the molecular to the gross morphological and systems level changes that occur, it is now the general consensus

that an accordingly comprehensive approach to treatment will likely yield the best functional outcome. Although standard practice SCI treatment is currently limited to the stabilizing measures previously described in addition to rehabilitation, many therapeutic avenues have shown promise in preclinical studies and are now in various stages of clinical testing. These include interventions aimed at neuroprotection, neuroregeneration, augmenting plasticity of spared circuitry, and tissue replacement. Translation from preclinical results to clinical efficacy has proven difficult due to interspecies differences in lesion size and pathology as well as the heterogeneity of injuries among human patients. Each SCI is unique and occurs in a unique individual; thus, each SCI patient has a different potential to respond to treatment. This leads to high variability in the observed efficacy in clinical trials, and subgroup analyses that attempt to account for some variables may draw scrutiny (Bracken, 1997). Therefore, the best approach may be to only move forward with treatments that have shown efficacy in multiple animal models while narrowing recruitment requirements to patients most likely to respond to treatment, based on clinical factors and biomarker assessment (Ahuja et al., 2017; Kwon et al., 2010).

Neuroprotection

The first step in any comprehensive treatment approach to SCI is avoiding as much secondary damage to perilesional tissue as possible. Perhaps the most controversial neuroprotective intervention in the field of SCI to date is the acute intravenous administration of methylprednisolone sodium succinate (MPSS). A steroid of the glucocorticoid class, MPSS is thought to attenuate lipid peroxidation and

subsequent tissue destruction that results from ischemia and hemorrhage immediately following SCI (Braughler and Hall, 1984; Hall and Braughler, 1982a, 1982b). Despite association with substantial recovery and structural preservation in animal models of SCI (Braughler and Hall, 1984; Green et al., 1980; Hall and Braughler, 1982a), human clinical trials showed marginal efficacy of 24-hour acute MPSS administration, while increased incidences of gastrointestinal hemorrhage, wound infection, and other serious side effects were observed alongside higher mortality rates in MPSS-treated groups (Ahuja and Fehlings, 2016; Bracken, 1997; Bracken et al., 1990; Fehlings et al., 2014; Hurlbert, 2000, 2014). In light of the limited benefit and risk of morbidity, MPSS has fallen out of favor with many physicians, and its administration is now only recommended as a treatment option with 8-hours of acute SCI at the discretion of the physician (Ahuja et al., 2017; Hurlbert, 2014).

Several new pharmaceuticals with neuroprotective effects in preclinical studies are currently in the clinical trial phase. Minocycline, a synthetic derivative of the antibiotic tetracycline, is proposed to reduce oligodendrocyte apoptosis, local inflammation, and neuronal excitotoxicity (Lee et al., 2003; Wells et al., 2003). Seven-day delivery of minocycline resulted in a 6-point improvement in ASIA motor score over one year in a phase II placebo-controlled, randomized clinical trial, with minimal side-effects observed (Casha et al., 2012). A phase III multi-center trial is currently underway (NCT01828203). The sodium channel blocker riluzole may attenuate neuronal swelling, excitotoxicity, and death by preventing continuous activation of voltage-gated sodium channels (Wilson and Fehlings, 2014). In a Phase I trial comparing riluzole treatment to matched patient records, motor and impairment scores improved more in riluzole-

treated patients with cervical injuries, while no serious adverse events or deaths were reported (Grossman et al., 2014). A phase II/III multi-center, randomized trial of 14-day riluzole treatment in acute SCI patients is ongoing (NCT01597518). Other small molecules undergoing clinal trials for neuroprotection include glyburide (NCT02524379), which blocks cation influx after CNS injury (Jeffery et al., 2018), and imatinib (NCT02363361), a tyrosine kinase inhibitor that modulates the inflammatory response after SCI (Abrams et al., 2012). Finally, two growth factors with neuroprotective properties are currently being evaluated in clinical trials: granulocyte-colony stimulating factor (G-CSF, IRCT201108297441N1) and basic fibroblast growth factor (bFGF, delivered as the structural analogue SUN13837, NCT01502631).

Systemic hypothermia has also shown neuroprotective potential through an anti-inflammatory effect (Batchelor et al., 2010). While decompression of the spinal cord is critical to preventing further damage after the initial injury, many hours may elapse before surgery can be performed. Hypothermia slows the basal metabolic rate of the CNS and thereby delays contusive damage caused by compression until decompression can be performed. A small phase I study of intravascular hypothermia in 14 patients with complete cervical SCI (AIS A) demonstrated safety and increased conversion to lower impairment scores compared to age- and injury-matched historical controls (Levi et al., 2010). Currently, a multi-center study is in the recruitment phase (NCT0299169).

Neuroregeneration

As discussed previously, the adult spinal cord does not produce new neurons following injury. Thus, most neuroregeneration research has focused on axon regeneration or sprouting in existing neurons. However, neurogenesis is observed in the spinal cord regeneration of adult zebrafish and other lower vertebrates, and post-mortem studies have suggested that neurogenesis may occur in the hippocampus of adult humans (Eriksson et al., 1998; Moreno-Jiménez et al., 2019; Spalding et al., 2013). While the existence of meaningful adult human neurogenesis has been challenged (Cipriani et al., 2018; Sorrells et al., 2018), these findings have inspired research aimed at inducing neurogenesis from endogenous neural progenitor cells to regenerate spinal cord tissue after SCI. A few groups have reported *in vivo* induction of neurogenesis from adult spinal cord ependymal cells using various interventions, but these studies relied on expression of immature neuronal markers alone to substantiate their findings, failing to perform rigorous cell fate tracking techniques to show newly-born, mature neurons (Carelli et al., 2019; Guo et al., 2014; Zhang et al., 2018). Following a similar trend of insufficient evidence, an actively recruiting clinical trial for the endothelin B receptor agonist sovateltide claims that the drug aids in damage repair through the formation of new neurons (NCT04054414). Published animal studies report increases in vascular endothelial growth factor (VEGF), neuroprotective effects, and increased in angiogenesis with sovateltide delivery in stroke models; however, no evidence of neurogenesis associated with the drug is presented (Gulati, 2015; Leonard et al., 2015). As research progresses in the molecular mechanisms of primitive spinal cord regeneration and human cell reprogramming, new approaches to endogenous tissue regeneration may emerge. Even if this can be achieved at some level, though,

the large volume of human SCIs may prove difficult to replace with endogenously derived tissue alone.

Remarkable progress has been made in recent years in overcoming extrinsic and intrinsic barriers to induce axon regeneration across lesion sites and into intact tissue on the distal side (termed “bridging”). To combat the axon-repellant properties of CSPGs, a CSPG-degrading bacterial enzyme called chondroitinase ABC has been administered in sites of SCI in animal models (Bartus et al., 2014; Bradbury et al., 2002; Cafferty et al., 2007; Kanno et al., 2014; Muir et al., 2019; Nori et al., 2018; Wu et al., 2017). Because CSPGs are only one form of axon growth inhibitor, chondroitinase is often used as a component in combinatorial treatment strategies. When growth-promoting interventions are employed, chondroitinase can aid in maximizing the growth potential while opening perineuronal nets to new synaptic connections that mediate functional recovery (Muir et al., 2019; Soleman et al., 2012; Wang and Fawcett, 2012; Wu et al., 2017). This mechanism can likewise benefit rehabilitation programs (García-Alías and Fawcett, 2012). Chondroitinase also aids in survival and integration of cell transplants to sites of SCI, and it may enhance remyelination of spared axons (Kanno et al., 2014; Nori et al., 2018; Suzuki et al., 2017). The optimal delivery method and timing for chondroitinase is still unclear, and it will likely depend on the nature of the other treatments with which it is combined. Intrathecal infusion (Bradbury et al., 2002), intraspinal injection (Zhao et al., 2013), and lentiviral gene therapy (Bartus et al., 2014) have all shown positive outcomes in SCI. In a recent clinical trial in naturally occurring canine SCI, lipid microtube-embedded chondroitinase showed safety as well as mild improvements in forelimb-hindlimb coordination (Hu et al., 2018). Besides directly degrading CSPGs, one

may simply disrupt their binding to axonal membranes. For instance, a peptide that blocks CSPG binding to protein tyrosine phosphatase σ (PTPσ) has been shown to restore serotonergic axon innervation below spinal cord lesions, resulting in improvements to locomotor and urinary function (Lang et al., 2014).

As one of the classic sets of environmental inhibitors of axon regeneration, Nogo and other MAIs have been the target of many preclinical therapeutic approaches in SCI (Freund et al., 2006, 2009; Geoffroy et al., 2015; Merkler et al., 2001; Zhao et al., 2013; Zörner and Schwab, 2010). When combined with chondroitinase treatment, anti-Nogo-A antibodies resulted in more sprouting and greater improvements in forelimb function after cervical SCI than either of the two treatments alone (Zhao et al., 2013). Two strategies for disrupting NgR activation have moved to clinical trials. A recombinant human antibody against Nogo-A, ATI355 is thought to sterically hinder the inhibitory domain of Nogo-A as well as downregulate its protein levels (Weinmann et al., 2006). In animal studies anti-Nogo-A antibodies enhanced sprouting of CST axons and contributed to locomotor recovery (Brösamle et al., 2000; Freund et al., 2006, 2009; Merkler et al., 2001). A first-in-human trial of intrathecal administration of ATI355 demonstrated safety (Kucher et al., 2018), and a phase II trial of repeat bolus injections is currently recruiting (NCT03935321). Another approach, termed “Nogo Trap” by makers ReNetX uses a decoy Nogo receptor to capture MAIs and prevent them from binding to NgR (Wang et al., 2014). A phase I clinical trial is recruiting patients to undergo repeat dosage of lumbar puncture and slow bolus infusion of the Nogo Trap molecule (NCT03989440). Potentially concerning for the promise of Nogo-based therapies is the recent failure of a phase II/III clinical trial of VX-210, also known as Cethrin. This Rho GTPase antagonist

disrupts RhoA-mediated inhibition of axon growth, which is initiated by NgR signaling (Fehlings et al., 2011). Despite demonstrating significant motor improvement in the absence of safety issues in Phase I/IIa trial (NCT0050081), the follow-up trial of a single dose in 71 patients was terminated early (NCT02669849).

A more mechanical approach, microtubule stabilization provides the dual benefit of reducing fibroblast scarring and directly promoting axon growth (Ertürk et al., 2007; Hellal et al., 2011; Witte et al., 2008). By stabilizing microtubule networks, taxol administration can interfere with transforming growth factor–β (TGF-β) signaling, an important fibrosis pathway that is increased after SCI (Hellal et al., 2011). Microtubule stabilization within damaged axons prevents retraction bulb formation and decreases axonal degeneration in vivo, and it increases axon growth through myelin in cultured neurons (Ertürk et al., 2007). Because taxol does not cross the blood-brain barrier, it lacks clinical potential for use in SCI. Therefore, a recent study aimed to determine whether the blood-brain barrier-permeable drug epothilone B delivered intraperitoneally (I.P.) could recapitulate the effects of taxol. Indeed, epothilone B reduced fibrotic scarring and promoted both sensory and serotonergic axon growth in rats after dorsal hemisection (Ruschel et al., 2015). These anatomical improvements were associated with increased accuracy in horizontal ladder stepping that was abrogated when serotonergic innervation was pharmacologically ablated, emphasizing the functional benefit of serotonergic axon regeneration.

One of the most consistently effective manipulations of intrinsic growth capacity is activation of the mTOR pathway, which is negatively regulated by PTEN (Bei et al., 2016; Du et al., 2015; Geoffroy et al., 2016; Jin et al., 2015; Liu et al., 2010; Sun et al., 2011; Zukor et al., 2013). However, the role of PTEN as a tumor suppressor does not

make it an ideal candidate for clinical application. The mediation of the activity of growth factors by the mTOR pathway led the He group to seek growth factors that could similarly enhance axon regeneration. Upregulation of receptors for insulin-like growth factor 1 (IGF-1) and the mTOR-activating secreted protein osteopontin (OPN) in regeneration-competent α-RGCs made these proteins attractive targets (Ahmed and Kundu, 2010; Duan et al., 2015). Although delivery of either IGF-1 or OPN with adeno-associated viruses (AAVs) had little effect, combinatorial delivery of both resulted in extensive axon regeneration and sprouting as well as improved functional recovery in both SCI and cortical stroke models (Liu et al., 2017). The behavioral improvement was significantly enhanced by administration of 4-amino-pyridine-3-methanol (4-AP-3-MeOH), which enhances conduction in unmyelinated axons such as those that underwent regeneration (Bei et al., 2016).

Electrical stimulation

While restoring neuronal connectivity within the spinal cord is the obvious means for a true cure for SCI, several electrical stimulation approaches directly address functional deficits with quick and sometimes lasting results. Devices for functional electrical stimulation (FES) of peripheral nerves or muscles below the level of SCI are already on the market, while stimulation of the brain and spinal cord transcutaneously or with epidural or penetrating electrodes is showing promise in the preclinical and clinical stages. Implementation of closed-loop feedback is being actively researched and has the potential to dramatically increase the functionality and efficiency of all these methods (Ahuja et al., 2017).

FES has enjoyed clinical success in augmenting several functions. Patients with cervical injuries often have difficulty grasping objects, which makes even the most basic activities challenging. Skin surface electrodes on the forearm can produce muscle contractions that aid in grasping and releasing. One such device utilizes a splint-like design, is completely wireless while in use, and is currently on the market (Bioness H200). Another device that used electrodes implanted in the muscles of the forearm and hand, the Freehand (Cleveland Functional Electrical Stimulation Center/NeuroControl Corp.), allowed users to modulate grasp opening and closing by changing the elevation of their contralateral shoulder. This device went to market, but production was discontinued despite clinical success (Ho et al., 2014). A clinical trial with an updated version named IST-12 that uses myoelectric signals to control grasp is currently underway (NCT00583804). The Parastep I from Sigmedics, Inc. facilitates ambulation with a walker in SCI patients through sequential, user-controlled stimulation of the quadriceps muscles and reflex-generating sensory nerves. Although not intended as a replacement for a wheelchair, the Parastep I allows walking for short distances and standing in some patients, which can aid in rehabilitation and daily living tasks. Similar devices have been created for rehabilitation with stationary bicycles, such as ERGYS 3 by Therapeutic Alliances, Inc. and RT300 by Restorative Therapies. Surgical implantation of electrodes on the anterior sacral nerve roots allows modulation of bowel and bladder function. For example, Finetech Medical's Bladder Control System (branded as VOCARE in the US) gives users remote control over muscle contractions that primarily aid in emptying the bladder, but some control over bowel evacuation and penile erection is also possible. Proper device function has typically required surgical

lesioning of dorsal sensory roots to eliminate interfering sensory feedback-induced reflexes of the bladder and urethra (Ho et al., 2014), but a clinical trial is currently underway to circumvent this procedure (NCT02978638).

A major disadvantage of FES is that it requires a large amount of current to activate muscles and can quickly lead to muscle fatigue. A few different approaches to stimulation of the spinal cord itself have been taken address these issues. Transcutaneous stimulation using cathodes and anodes placed on the skin has been demonstrated to facilitate locomotor-like movements in paraplegic patients with incomplete injuries but no voluntary control of rhythmic stepping movements (Gerasimenko et al., 2015). Stepping-like movements could be generated with stimulation alone during the first session, and after 18 weeks of weekly training, patients could perform such movements voluntarily with or without stimulation, suggesting that transcutaneous stimulation can augment spared brain-spine connectivity. Functional improvements after transcutaneous stimulation were also seen in chronic cervical SCI patients (Gad et al., 2018). This clinical trial (NCT01906424) emphasized the use of stimulation levels that did not evoke movements directly, but rather modulated the supraspinal-spinal networks to improve voluntary task performance with a protocol termed transcutaneous enabling motor control (tEmc). In addition to increased amplitude of electromyography (EMG) responses in proximal and distal arm muscles and improved grip strength, some patients also experienced improvements in autonomic function including recovery of the ability to perspire, bowel function, bladder fullness sensation, and penile erection duration. Patients additionally reported a variety of quality of life improvements resulting from improved strength and sensation at and

even below the level of stimulation. These improvements outside the clinic demonstrate the lasting benefit of tEmc in promoting functional plasticity in spared spinal cord circuitry.

Epidural electrical stimulation (EES) is a more invasive method of spinal cord stimulation that in turn allows more precise functional control. First used in a human patient in 1971 (Shimoji et al., 1971), this technology has since seen widespread use for pain management (Kumar et al., 1998). In more recent years, its application in restoring motor function has been explored extensively in animal and human trials and demonstrated remarkable efficacy (Alam et al., 2017; Angeli et al., 2018; Capogrosso et al., 2016; Courtine et al., 2009; Gill et al., 2018; Mishra et al., 2017; Moxon and Knudsen, 2017; Wagner et al., 2018). Theoretical modeling and experimental studies suggest that EES activates motor neurons of the spinal cord trans-synaptically through proprioceptive afferent fibers in the dorsal roots and dorsal columns (Capogrosso et al., 2013; Gerasimenko et al., 2006; Sayenko et al., 2014). Through precise placement on the dural surface, an array of electrodes can engage distinct muscle groups in a temporally-controlled fashion to elicit rhythmic locomotion patterns that, combined with intensive weight-support training, enable over-ground walking and provide stability during standing (Wagner et al., 2018; Wenger et al., 2016). Despite additional technical challenges due to increased movement of the spinal cord at the neck level, cervical EES has shown promise in improving arm and hand function (Alam et al., 2017; Lu et al., 2016; Mishra et al., 2017). However, the complex and diverse movements of the upper motor systems, especially single digit manipulation, will require more advanced

stimulation protocols and more electrode contacts, possibly supplemented with peripheral FES.

A more invasive but potentially more beneficial stimulation method is intraspinal microstimulation (ISMS), which uses fine microwires inserted into the anterior horn of the spinal cord (Holinski et al., 2016; Sunshine et al., 2018). Although ISMS electrodes are placed in lamina IX of the spinal cord, in the vicinity of lower motor neurons, the mechanism of action of ISMS is thought to be mostly trans-synaptic, through activation of pre-synaptic axons with lower activation thresholds than motor neurons (Holinski et al., 2016; Roberts and Smith, 1973). In addition to enabling even greater precision stimulation than EES, ISMS can produce comparable muscle forces to FES and EES with 1/100th the stimulus amplitude while inducing far less muscle fatigue (Ho et al., 2014; Holinski et al., 2016; Lemay and Grill, 2004). In an anesthetized cat, ICSMS in the hindlimb motor pools produced over 1 kilometer of walking without appreciably fatiguing muscles (Ho et al., 2014). Beneficial effects of ICMS have also been observed in forelimb and respiratory function (Kasten et al., 2013; Sunshine et al., 2018). ICMS is a relatively new therapeutic approach to SCI, and its particularly invasive nature presents unique challenges to its clinical implementation. Work is underway in optimizing surgical techniques and fabrication of mechanically stable electrode arrays for use in humans (Toossi et al., 2017). Meanwhile, significant financial backing is accelerating development of more flexible and electrode-dense “threads” and robotic devices to implant them (Musk and Neuralink, 2019). Mimicking the pliant nature of the nervous tissue will likely prove critical to the long-term functionality of implants in the brain and spinal cord, as encapsulation and ultimate failure of electrodes is partially mediated by

the inflammatory response to objects of foreign mechanical properties (Adewole et al., 2016).

All of these electrical stimulation methods can enhance activity-dependent plasticity, and they may also enhance neuronal survival and new axon growth (Al-Majed et al., 2000; Mondello et al., 2018; Yang et al., 2014). Maximizing the benefits of stimulation will require thoughtful design of each component to generate a durable, user-friendly device that keeps patients engaged with assisted rehabilitation. While current devices and those close to market allow users and their physical therapists to program tailored stimulation protocols, it is likely that brain-spine interfaces that allow users to naturally control neuroprosthetic stimulation could further improve functional outcomes (Bonizzato et al., 2018; Capogrosso et al., 2016). Tightly synchronized stimulation of motor areas in the brain and spinal cord could have a similar benefit (Mishra et al., 2017). Clinical application of these technologies will depend their proven safety and success rates, as patients with varying levels and severity of SCI must decide if the risk of such an intervention is worth the potential functional gains.

Non-neuronal tissue replacement

Regardless of interventions to promote axon regeneration or plasticity of spared circuitry, replacement of fibrotic, necrotic, and/or cystic volumes of spinal cord tissue with a growth permissive substrate is necessary to restore connectivity across complete lesions and may provide additional benefit even to patients with partial lesions. Such a substrate may be prefabricated or injected as a liquid suspension before forming a more stable structure once in the lesion site. The amount and type (healthy or necrotic/scar)

of tissue that should be removed from the injured area to facilitate substrate integration varies among injuries and is still a matter of debate. Additionally, substrates may simply act as a bridge for axon regeneration, or they may contain cells that form neurons capable of relaying signals from regenerated axons which synapse onto them (Ahuja and Fehlings, 2016). Non-neuronal substrates will be discussed first.

Biomimetic scaffolds can be custom-made to conform to unique lesion morphologies (as determined by MRI or lesion model parameters) and may contain linear channels or mesh-like structures (Koffler et al., 2019; Pawar et al., 2015; Stokols and Tuszynski, 2006; Stokols et al., 2006; Theodore et al., 2016; Wen et al., 2015; Xiao et al., 2016). Hydrogels and other polymers such as fibrin can also be injected to perfectly fill a lesion cavity before gelling into a stable structure (Anderson et al., 2018; Lu et al., 2012; Nowak et al., 2002). While scaffolds alone may have scar-attenuating and tissue-sparing properties (Koffler et al., 2019; Teng et al., 2002), they are often seeded with growth factors, cells, or other therapeutics aimed at enhancing axon regeneration and neuroprotection. For example, hydrogels containing fibroblast growth factor 2 (FGF2) and epidermal growth factor (EGF) injected into the center of severe crush SCIs increased levels of axon growth-supportive laminin in the lesion core. When combined with additional interventions to increase intrinsic growth capacity of propriospinal neurons and hydrogel deposits containing chemoattractants on the distal side of lesions, this substrate allowed robust descending propriospinal axon regeneration across a complete lesion, a remarkable result for a noncellular substrate (Anderson et al., 2018).

Non-neuronal cell grafts are a widely-used substrate to support regeneration. These can include bone marrow stromal cells (BMSCs), Schwann cells, olfactory ensheathing cells (OECs), oligodendrocyte precursor cells (OPCs), and neural progenitor cells/neural stem cells (NPC/NSCs) (Assinck et al., 2017). BMSCs have been a popular cell type for transplants due to their ease of access for autologous transplantation and ability to support certain types of axon regeneration and enhance neuroprotection (Assinck et al., 2017; Parr et al., 2007). Early reports concluded that BMSCs, which include mesenchymal stem cells, could differentiate into neurons *in vitro* and could potentially replace damaged spinal cord tissue (Black and Woodbury, 2001; Woodbury et al., 2000), but the bulk of in vivo studies have shown that BMSCs do not form substantial numbers of neurons when grafted into sites of spinal cord injury or delivered intravenously or intrathecally (Parr et al., 2007; Tetzlaff et al., 2011). Some studies have suggested that BMSCs enhance endogenous neural progenitor cell proliferation and neurogenesis, but not to the point of contributing to functional improvement by cell replacement (Hofstetter et al., 2002; Mahmood et al., 2004; Wu et al., 2003). The beneficial effects of BMSCs seem to most likely stem from formation of cellular bridges to support axon growth, the scar-modifying properties of the proteins they secrete (such as fibronectin), upregulation of astrocytic expression of growth factors (such as BNDF, VEGF, and FGF2), and through remyelination of injured axons (Gao et al., 2005; King et al., 2006; Parr et al., 2007; Sasaki et al., 2001; Zurita and Vaquero, 2004). BMSCs can also be combined with additional therapeutics and grafted in scaffolds for structural stability and mitigation of potentially tumorigenic ectopic cell growth. For example, Koda and colleagues grafted BMSCs infected with a BDNF

expression adenovirus and embedded in Matrigel into a complete removal of the T8 spinal segment (Koda et al., 2007). This intervention resulted in increased motor and sensory axon growth into the lesion/graft site and small improvements in hindlimb function. In another study, delivery of the chemoattractant growth factor neurotrophin 3 (NT-3), combined with a conditioning peripheral nerve lesion, elicited sensory axon regeneration across a marrow stromal cell graft placed in a C1 dorsal column lesion (Alto et al., 2009). Remarkably, these axons formed synapses onto their appropriate brainstem targets on the distal side of the lesion, although they did not enhance post-synaptic potentials in the brainstem after sciatic nerve stimulation in lesioned animals. Several clinical trials involving BMSCs for SCI have been conducted, but none resulted in approved therapies despite demonstrating safety and modest benefit (Parr et al., 2007). A trial of autologous BMSCs delivered to the injury site concluded this year and showed improvements in sensation and somatosensory stimulation-evoked potentials (NCT01909154).

One potential fate of BMSCs is Schwann cell differentiation. Inspired by the success of peripheral nerve grafts in supporting CNS axon regeneration, the Bunge laboratory began to implant cultured Schwann cells into SCI in the 1990s (Xu et al., 1995, 1997). Although these grafts supported modest levels of axon regeneration on their own, combinatorial strategies with growth factors and scar-modifying agents such as chondroitinase yielded the most axon regeneration, Schwann cell survival, and remyelination of regenerated axons (Enomoto et al., 2013; Golden et al., 2007; Kanno et al., 2014; Xu et al., 1995). Many studies did not show functional improvement, possibly due to the failure of regenerating axons to exit the caudal end of the graft

(Bunge, 2016). Locomotor gains and reduction of allodynia (pain responses to normally non-noxious stimuli) were seen with induced expression of a modified neurotrophin that mitigated an apoptosis-triggering side effect as well as chondroitinase to allow better integration of the graft in the lesion site (Kanno et al., 2014). Two safety studies of autologous Schwann cell grafts derived from patients' peripheral nerve tissue have recently completed and are pending results (NCT02354625 and NCT01739023).

Olfactory ensheathing cells are specialized glia that form fascicles around the unmyelinated axons of olfactory neurons (Yao et al., 2018). While the cell bodies of olfactory neurons lie in the periphery, the axons terminate in the CNS. These neurons are unique in that they undergo continuous, lifelong neurogenesis. It was therefore proposed that OECs aid in axon guidance and extension into the adult CNS environment, which made them an intriguing potential therapy for SCI. OECs have, however, had a controversial history. Several studies that made claims of robust regeneration of several axon types were not replicated by other groups, and the anatomical outcomes have been similarly variable (Tetzlaff et al., 2011; Yao et al., 2018). For instance, olfactory nasal mucosa transplant into a T10 complete transection model was reported to support regeneration of serotonergic raphespinal axons across the transplant site and substantial open field locomotion recovery (Lu et al., 2002), but these results were not reproduced by a formal replication study (Steward et al., 2006). Human trials have also been plagued by high outcome variability, perhaps due to the fact that most trials have reported little to no purification of OECs prior to grafting, leading to inconsistent graft cell composition (Yao et al., 2018). A follow-up clinical trial to a study that made international headlines with claims of marked improvement in

motor and sensory function (Tabakow et al., 2014) is currently recruiting to test autologous olfactory bulb-derived OECs in complete lesions (NCT03933072).

Finally, oligodendrocyte precursor cells, which proliferate endogenously after SCI, may also be grafted to sites of SCI to further support remyelination (Parr et al., 2007; Tetzlaff et al., 2011a). Several studies have shown that both rodent- and human-derived OPCs are capable of remyelinating axons after SCI with correlated functional improvements (Cao et al., 2013; Kawabata et al., 2016; Keirstead et al., 2005; Nori et al., 2015). Interestingly, a study of moderate thoracic contusion SCI in which endogenous oligodendrocyte differentiation was genetically ablated just prior to injury concluded that spontaneous recovery of hindlimb stepping occurs before remyelination normally takes place and is not affected when remyelination is prevented (Duncan et al., 2018). These results suggest that it may be the neuroprotective properties of OPCs rather than remyelination by differentiated oligodendrocytes that provide therapeutic benefit (Filous et al., 2014; Kang et al., 2013). Indeed, demyelinated axons remain capable of conduction over at least 2.5 mm (Felts et al., 1997), and regions of demyelination are generally focalized around the lesion site (Powers et al., 2012). Notwithstanding this controversy, a Phase I/IIa clinical trial of OPCs grafted in subacute cervical SCI has recently been completed, with results pending (NCT02302157).

Neurogenic grafts

Reports of successful transplantation of developing neural tissue into the injured CNS were made throughout the first half the 20th century, but extensive and reproducible integration of fetal spinal cord tissue into the injured adult spinal cord was

not achieved until the studies of Reier and colleagues in the 1980s (Reier, 1985). Anatomical tracing techniques revealed bidirectional axon projections between host spinal cord and transplant tissue, providing the first evidence that graft neurons could potentially relay signals across lesions rather than the graft merely acting as a tissue bridge for host axons across the injury site (Jakeman and Reier, 1991). However, it may be said that the modern era of grafts aimed at neuronal replacement began with the implantation of dissociated cells from embryonic substantia nigra into the adult rat neostriatum (Björklund et al., 1980). The use of dissociated cells rather than pieces of tissue allowed superior graft integration and opened the door to grafts of more clinically relevant cultured cells, which could be expanded, genetically manipulated, and purified prior to grafting (Bjorklund and Stenevi, 1984). This early study also showed a marked reduction in amphetamine-induced turning (a behavior characteristic of unilateral lesions of the nigro-striatal dopamine system) in mice with grafts that was dependent on survival of graft neurons in the target area. Later, using human telencephalic neuroblasts that allowed species-specific antibody labeling of grafts in rats, the Björklund group showed that grafts extended axons up to 20 mm from a lesion site in the striatium (Wictorin et al., 1990). Furthermore, these axons innervated their normal target regions in the brain and spinal cord. These results showed that, not only do developing neurons have the ability to extend axons long distances in the injured adult CNS, but at least some of the guidance cues that facilitate their proper pathfinding remain present long after development. Similar results were seen with GFP-expressing mouse embryonic cortical neurons grafted into the damaged motor cortex, including

confirmation of host-to-graft and graft-to-host synapses by electron microscopy (Gaillard et al., 2007).

Despite success in grafting developing neural cells in the brain, sites of spinal cord injury proved to be a difficult location in which to achieve high cell survival and extensive axon outgrowth of grafts. Human neural stem cell grafts derived from fetal brain showed only modest survival in a mild spinal cord contusion site and supported very small improvements in hindlimb locomotor function (Cummings et al., 2005). Human induced pluripotent stem cells (iPSCs) differentiated toward a neuroepithelial fate also failed to completely fill a spinal cord contusion site (Fujimoto et al., 2012). In another mild injury model of the lateral spinal cord white matter (lateral funiculus), dissociated rodent NPCs from embryonic day 14 (E14) rat spinal cords filled lesion cavities well but only extended axons a few millimeters from the lesion site (Lepore and Fischer, 2005). Targeting restoration of sensory function, the same group performed a unilateral lesion of the dorsal columns at C1 and acutely grafted E14 NPCs into the lesion site (Bonner et al., 2011). In addition, they delivered a chemoattractant gradient of BDNF expression via lentivirus to the dorsal column nuclei (DCN) of the brainstem, the normal target of many ascending sensory axons of the spinal cord dorsal columns. Graft axons innervated and made synaptic contacts in the (DCN), and host afferents regenerated into grafts and made synaptic contacts onto graft neurons. Electrical stimulation of the sciatic nerve resulted in responses in the (DCN) with a delayed latency, suggesting the presence of a polysynaptic relay through the graft. Additionally, electrical responses to pinching/stroking of the forelimb ipsilateral to the injury were

observed in the dorsal column nuclei of grafted animals, indicating functional sensory restoration. Again, however, axon extension from grafts was limited to a few millimeters.

In 2012, Lu and colleagues demonstrated that both rat E14 spinal cord NPCs and human fetal spinal cord-derived neural stem cells could fill a T3 complete transection site when grafted with a cocktail of growth factors in a fibrin matrix (Lu et al., 2012). These grafts supported regeneration of host reticulospinal and serotonergic (raphespinal) axons and extended axons long-distances both rostrally and caudally from the lesion site. Graft axons grew 1-2 mm/day and ultimately reached distances of over 25 mm from the upper thoracic lesion site, innervating both cervical and lumbar spinal cord gray and white matter. The number of axons emerging caudally from the graft was counted stereologically at a site 0.5 mm below the graft. Though many axons overlapped and could not be individually counted, a conservative approach resulted in an estimate of 29,000 graft axons extending caudally, an extraordinarily high number. Host-to-graft and graft-to-host synapse formation was confirmed by immunohistochemistry and electron microscopy, including graft axon synapses on host motor neurons below the injury. Reminiscent of the sensory relay grafts described previously (Bonner et al., 2011), the response latency caudal to the lesion to electrical stimulation of the dorsal spinal cord rostral to the injury was increased, indicative of a neuronal relay through the graft. Significant improvement was observed in hindlimb locomotor function, a rare finding in complete transection models, which leave no fibers intact through which spontaneous recovery may be mediated. Similar anatomical results were observed with induced pluripotent stem cells (iPSCs) generated from fibroblasts of an 87-year-old man and differentiated to NSCs (Lu et al., 2014). However, this study

and a formal replication of the previous study did not show functional improvement, likely due to the presence of collagenous rifts in the center of most grafts, which could interrupt relays through grafts (Lu et al., 2014; Sharp et al., 2014). While these results highlight the importance of continuity of neural tissue through entire grafts, they may have been largely an artifact of the complete transection model. Though useful as an unambiguous model for assessing anatomical and functional gains, complete transections are rare in human patients (Norenberg et al., 2004), and the extensive disruption of the meninges around the spinal cord allows excessive infiltration of fibroblasts that can generate rifts. In line with this hypothesis, behavioral improvement with NSC/NPC grafts has since been more consistent in more clinically relevant injury models that do not completely disrupt the meninges (Brock et al., 2017; Kadoya et al., 2016; Kumamaru et al., 2018; Lu et al., 2017) or with scaffolds that physically prevent fibroblast invasion (Koffler et al., 2014).

The exciting promise of stem cells throughout the field of regenerative medicine has provided momentum to push neural stem cell preparations from two U.S. companies; Stem Cells, Inc. and Neuralstem; into clinical trials (NCT01772810, NCT02163876, NCT01321333, NCT01725880). These trials have employed perilesional cell injections (as opposed to intraslesional injections) while providing little justification for this approach (Cummings et al., 2005, 2013; Curtis et al., 2018; Levi et al., 2018). Additionally, relatively low-density cell suspensions were used (~71,400 cells/μl in Stem Cells, Inc. trials and 20,000 cells/μl in the Neuralstem trial vs 200,000 cells/μl in rodent studies that demonstrate superior lesion site filling in several injury models (Brock et al., 2017; Kadoya et al., 2016; Kumamaru et al., 2018; Lu et al., 2012).

It is important to perform dose escalation studies in human trials from a safety perspective, but meaningful spinal cord repair may be precluded with insufficient graft cell numbers. In the case of Stem Cells, Inc.'s human neural stem cell (HuCNS-SC) line, rodent studies of the clinical cell line to be grafted into humans showed no neuronal differentiation and reduced oligodendroglial differentiation in sites of SCI compared to research cell lines (Anderson et al., 2017). Additionally, the previously observed functional benefit of research cell lines was not observed in the clinical cell line. Despite this lack of efficacy, Stem Cells, Inc. initiated a clinical trial of these cells in cervical SCI. Ultimately, the trial was terminated after less than two years due to lack of efficacy, though no safety concerns were reported (Anderson et al., 2017). Stem Cells, Inc. defended their decision to move forward with a clinical trial despite concerns about the clinical cell line by stating that the fate of the cells in a human injury environment might not necessarily be the same as in the rodent. As the Neuralstem clinical trial continues, having reported safety in four subjects (Curtis et al., 2018), an ambitious clinical trial of allogenic iPSC clones differentiated to NPC/NSCs is in preparation in Japan (Tsuji et al., 2018).

Toward a Neuronal Relay Mechanism

Many ascending and descending axons regenerate into NPC/NSC grafts; thus many pathways may form neuronal relays through grafts. This dissertation focuses on the corticospinal tract (CST) of axons that descends from the cerebral cortex to the spinal cord. It is the most important pathway for fine, dexterous movements in humans, and it is also one of the most refractory to regeneration (Liu et al., 2011; Tuszynski and

Steward, 2012). Boosting the intrinsic growth capacity of CST neurons with genetic manipulations such as PTEN deletion has induced growth of modest numbers of CST axons across partial lesion sites, but this growth only occurred in very narrow lesions with intact tissue bridges (Liu et al., 2011). In contrast, CST axons regenerate robustly into rodent spinal cord NPC or human fetal spinal cord-derived NSC grafts, even in complete transections (Dulin et al., 2018; Kadoya et al., 2016; Kumamaru et al., 2019). Importantly, it was determined that grafts must be of caudal spinal cord identity to elicit such regeneration; E14 NPC grafts from hindbrain or telencephalon did not support substantial regeneration (Kadoya et al., 2016). Significant evidence of functional synapse formation by CST axons onto graft neurons now exists. Immunofluorescence, electron microscopy, and retrograde transsynaptic tracing have shown such synapses anatomically (Adler et al., 2017; Kadoya et al., 2016; Kumamaru et al., 2018), and optogenetic stimulation of CST axons and single unit records from graft cells has shown functional connectivity both in vivo (Jayaprakash et al., 2019) and ex vivo (Kadoya et al., 2016). As previously discussed, field recordings from below grafts detected responses to stimulation above with an increased latency compared to intact animals, likely due to the signal being relayed through one or more synapses with graft cells (Lu et al., 2012). Behaviorally, spinal cord NPC grafts support significant improvements in skilled forelimb function, as measured by a pellet retrieval task, indicating partially restored CST function (Brock et al., 2017; Kadoya et al., 2016). These experiments do not, however, address the nature of the neuronal networks that form within grafts and the activity patterns they generate. Understanding the mechanism by which activity

propagates across grafts requires techniques for specific stimulation of defined host inputs and recording of a large population of graft neurons simultaneously.

Techniques for Interrogation of Host-Graft Connectivity

In classical electrophysiological connectivity experiments, populations of neurons in gray matter or axon tracts are stimulated with electrodes, and responses are recorded with electrodes in the cells of interest. Although these techniques have been used to build much of our understanding of nervous system function, their accuracy relies heavily on measurements of well-characterized anatomical structures. Even in rodent models, spinal cord lesions are variable in both size and structure, and grafts into them are correspondingly unique, with the added inconsistencies of cell survival and integration with host tissue. Furthermore, scar tissue formation over the injury site can often make it difficult to determine the precise boundaries of a lesion/graft. Therefore, electrical recording from grafts, particularly in vivo, is a matter of guesswork and post-hoc tissue analysis to determine electrode location (Jayaprakash et al., 2019). Additionally, the number of single units (neurons) from which recordings can be made depends on the number of electrodes that can fit in the tissue without causing excessive damage.

Over the past few decades, calcium imaging has emerged as a powerful tool to optically record from defined populations of up to thousands of neurons simultaneously (Grienberger and Konnerth, 2012; Prevedel et al., 2016; Tian et al., 2012). Purified from the hydromedusan, *Aequorea*, aequorin was the first molecule identified to change its light-emitting properties when bound to Ca^{2+} ions (Shimomura et al., 1962). It was used

shortly after to monitor calcium flux during muscle contraction (Ashley and Ridgway, 1968), but Tsien and colleagues brought calcium imaging to the wider biological field with the introduction of highly sensitive synthetic calcium indicators that could be readily loaded into cells (Grynkiewicz et al., 1985; Tsien, 1980). One of these dyes, fura-2, was used to demonstrate that neuronal activity could be optically traced by calcium imaging (Yuste and Katz, 1991). During electrical activity, intracellular calcium concentrations transiently increase 10- to 100-fold from baseline, which dramatically increases the proportion of calcium indicator molecules bound to calcium and in turn the overall brightness of cell fluorescence (Grienberger and Konnerth, 2012). The advent of genetically encoded calcium indicators (GECIs) allowed imaging of neural activity in genetically defined populations of neurons, a major breakthrough in dissecting neural circuitry (Miyawaki et al., 1997; Tian et al., 2012). Single-fluorophore GECIs, such as the GCaMP family, combine an enhanced green fluorescent protein (EGFP) domain with a calmodulin and a M13 domain that change conformation upon calcium binding, increasing EGFP fluorescence (Grienberger and Konnerth, 2012). Recently, highly sensitive GCaMPs that rival the fast kinetics and bright fluorescence of synthetic dyes were developed (Chen et al., 2013). The fastest of this generation, GCaMP6f, can resolve individual action potentials separated by 50-75 ms in vivo.

Stimulation of neurons can also be performed in an optical, genetically restricted manner with channelrhodopsins (Fenno et al., 2011; Yamawaki et al., 2016). First described in 2003, Channelrhodopsin-2 is a light-gated ion channel produced in the unicellular green alga *Chlamydomonas reinhardtii* (Nagel et al., 2003). Boyden and colleagues quickly adapted this protein for use in the mammalian nervous system by

incorporating its gene into a lentivirus and infecting cultured cells (Boyden et al., 2005). Stimulation with 10 ms pulses of blue light could drive spiking in high expression neurons with 1:1 spike-to-pulse ratio at 5 Hz, an unprecedented level of optical control. These results set off an explosion in the field of optogenetics, leading to the development of many opsin variants and stimulation methods in vivo. In addition to depolarizing (neuron-exciting) channelrhodopsins, hyperpolarizing (neuron-silencing) halorhodopsins and G-protein coupled receptor rhodopsins (OptoXRs) allowed bidirectional control of excitability on short and long timescales (Fenno et al., 2011). Red-shifted channelrhodopsins; such as C1V1 (Yizhar et al., 2011), ReaChR (Lin et al., 2013), and Chrimson (Klapoetke et al., 2014); enabled robust stimulation with longer wavelengths of light that penetrate tissue more efficiently due to decreased light scattering. Importantly, channelrhodopsin-expressing axons can be efficiently stimulated at the location of their post-synaptic targets, far from their parent cell bodies. In fact, axons can be stimulated even after being severed from the soma, as often occurs in acute slice preparations (Petreanu et al., 2007). Fusion of fluorophores such as tdTomato to membrane-bound channelrhodopsins provides excellent visualization of axonal processes by native fluorescence.

Optogenetic methods for both recording and stimulation may be combined to perform all-optical circuit mapping (Emiliani et al., 2015; Packer et al., 2014). Several important considerations exist when designing such an approach. First, the wavelength of light used for stimulation must not significantly overlap with either the excitation or emission spectrum of the calcium indicator; otherwise, a stimulation artifact could mask potential responses, and light used for excitation of the calcium indicator or the light

emitted by the indicator itself could potentially stimulate the opsin-expressing axons. This naturally leads to two options: stimulate with short-wavelength light and record at longer wavelengths, or vice versa. Although several red-shifted GECIs have been developed, those with the best sensitivity and kinetics display photoconversion to a bright state following exposure to blue light, complicating their combination with optogenetic stimulation (Emiliani et al., 2015). The blue excitation and green emission of GCaMPs can be combined with orange to far-red light stimulation of red-shifted channelrhodopsins, but the blue light must be held at low intensity due to the long tails of the action spectrums of these opsins in the blue-to-green range. For example, although subthreshold currents can be induced in Chrimson-expressing neurons at low blue light intensities, in acute slices spiking is not induced until the intensity reaches 0.5 mW/mm^2, considerably higher than that needed for calcium imaging of modern GCaMPs (Chen et al., 2013; Klapoetke et al., 2014).

Light-scattering white matter overlying much of the spinal cord as well as significant respiratory motion artifacts has made it a particularly challenging a structure in which to perform calcium imaging. Recently, spinal stabilization hardware has been developed that allows chronic in vivo imaging of superficial spinal cord structures through a glass coverslip window in adult mice (Farrar et al., 2012). These techniques have been used to perform 2-photon calcium imaging in restrained mice and widefield calcium imaging with miniaturized microscopes in freely-behaving animals (Sekiguchi et al., 2016). Two-photon imaging provides superior resolution in a thin focal plane, but wide-field imaging results in a larger depth of field, allowing imaging of neurons in multiple z-planes simultaneously, albeit with more background fluorescence. Sensory

stimuli as well as grooming and locomotion induced reproducible calcium transients in ensembles of dorsal horn neurons and astrocytes. Some neurons responded to only a single stimulus, whereas others responded to multiple stimuli, with varying stimulus strength thresholds, providing unique insight to the complex patterns of sensory encoding in the adult mammalian spinal cord.

The limited depth at which in vivo imaging may currently be performed prevents access to much of the spinal cord and likewise to grafts placed therein. In contrast, acute slice preparations provide unobstructed access to any region of the spinal cord under highly controlled extracellular conditions (Husch et al., 2011; Mitra and Brownstone, 2012). A block of the spinal column containing the site of interest and several spinal cord segments rostral and caudal is removed from a deeply anesthetized animal, and the spinal cord is quickly dissected from the column while submerged in a slurry of superoxygenated artificial cerebrospinal fluid (aCSF). Slices of a few hundred micron thickness are then cut with a vibrating microtome and allowed to recover before being placed into a recording chamber perfused with continuously oxygenated aCSF. Stable recordings of neuronal activity can then be performed for many hours, during which time optogenetic stimulation and bath application of drugs can be used to dissect the properties of synaptic connections within the slice. While the dense network of myelinated axons in the spinal cord can make whole-cell patch recordings difficult, calcium imaging provides immediate access to neurons deeper in the slice, which tend to be healthier and with better-preserved axonal and dendritic processes (Flynn et al., 2011). In this dissertation, acute slice and in vivo calcium imaging are combined with optogenetic and physiological sensory stimulation to uncover the mechanism(s) of graft

activation and signal propagation. Additionally, the maturation of human NSC grafts is assessed over 18-months, providing important information concerning the expectations for the timeline of graft functional development in human translation.

Rationale and Hypotheses

Host axons, including those of the CST, regenerate into NPC/NSC grafts in sites of SCI and make functional synaptic contacts onto graft neurons. Graft neurons in turn extend axons long distances rostral and caudal to lesion sites and make synaptic connections with host neurons. Gross electrophysiological recordings suggest the presence of neuronal relays within grafts that can partially restore connectivity across lesion sites. However, the mechanism of graft activation and signal propagation remains unknown. Host inputs may affect graft activity through three possible mechanisms. First, single regenerating host axons may contact single graft neurons and form circumscribed connections that function independently of the graft as a whole. Second, regenerating host axons may activate assemblies of multiple or dozens of graft cells that act as units of a larger graft network. Third, areas of dense axon regeneration may act as initiation points of high frequency spiking activity that then activates neighboring populations of neurons. This would result in a slow spread of excitation across the graft, reminiscent of the slow waves of activation or depression that occurs in epilepsy and other neural disorders (Bikson et al., 2003; Pinto et al., 2005; Wenzel et al., 2017). Elucidating which of these mechanisms may contribute to propagation of activity across grafts is critical for optimizing both graft content and rehabilitation programs that seek to maximize the functional benefit of NPC/NSC grafts.

In this dissertation, spontaneous activity patterns and the effects of corticospinal input on E12 mouse spinal cord NPC graft activity were assessed through optogenetic stimulation of CST axons expressing the red-shifted channelrhodopsin ChrimsonR and simultaneous calcium imaging of graft neurons expressing GCaMP6f. Next, the influence of axons extending from grafts on host spinal cord neuron activity below the lesion was assessed by expressing Chrimson in graft neurons and GCaMP6f in host neurons. An acute slice preparation in the sagittal plane was used to access the entire dorso-ventral and rostro-caudal extent of the graft. Additionally, in vivo calcium imaging was performed to assess graft activity in response to sensory stimulation. A dorsal column lesion model of SCI was used because it causes disruption of both descending CST and ascending sensory axons (Weidner et al., 2001) and NPC grafts consistently survive and fill these lesion sites with minimal disruption of graft continuity by collagenous rifts (Adler et al., 2017; Kadoya et al., 2016). Furthermore, neither growth factors nor fibrin matrices are required for cell filling of these lesions, allowing direct assessment of graft cell function alone.

To assess human stem cell maturation in rodent SCI, we grafted the widely available H9 human NSCs (Gibco) into a C5 lateral hemisection 2 weeks after injury. These cells are derived from embryonic stem cells and differentiate into neurons, oligodendrocytes, and astrocytes (Chang et al., 2013). Cells were embedded in a fibrin matrix containing a growth factor cocktail to promote retention in the lesion site and cell survival. Animals were sacrificed at intervals of 1 month, 3 months, 6 months, 12 months, and 18 months for histological analysis. Function of the affected forelimb was

tested monthly in grafted animals that survived 12 or 18 months and control animals that received only fibrin and growth factors and survived 12 months.

In **Chapter 2**, we test the hypothesis that regenerating host neurons directly activate both single neurons and established clusters of neurons in grafts through synaptic connections, and that outgrowing graft axons directly activate populations of host neurons through synaptic connections.

In **Chapter 3,** we test the hypothesis that human neural stem cell grafts follow an intrinsic human timeline of maturation when grafted into an injured rodent environment.

References

Adams, M., and Hicks, A. (2005). Spasticity after spinal cord injury. Spinal Cord *43*, 577.

Adewole, D.O., Serruya, M.D., Harris, J.P., Burrell, J.C., Petrov, D., Chen, I.H., Wolf, J.A., and Cullen, K.D. (2016). The Evolution of Neuroprosthetic Interfaces. Crit Rev Biomed Eng *44*, 123–152.

Adler, A.F., Lee-Kubli, C., Kumamaru, H., Kadoya, K., and Tuszynski, M.H. (2017). Comprehensive Monosynaptic Rabies Virus Mapping of Host Connectivity with Neural Progenitor Grafts after Spinal Cord Injury. Stem Cell Reports *8*, 1525–1533.

Aguayo, A.J., Dickson, R., Trecarten, J., Attiwell, M., Bray, G.M., and Richardson, P. (1978). Ensheathment and myelination of regenerating PNS fibres by transplanted optic nerve glia. Neurosci Lett *9*, 97–104.

Ahuja, C.S., and Fehlings, M. (2016). Concise Review: Bridging the Gap: Novel Neuroregenerative and Neuroprotective Strategies in Spinal Cord Injury. Stem Cell Transl Med *5*, 914–924.

Ahuja, C.S., Wilson, J.R., Nori, S., Kotter, M., Druschel, C., Curt, A., and Fehlings, M.G. (2017). Traumatic spinal cord injury. Nature Reviews Disease Primers *3*.

Alam, M., Garcia-Alias, G., Jin, B., Keyes, J., Zhong, H., Roy, R.R., Gerasimenko, Y., Lu, D.C., and Edgerton, V. (2017). Electrical neuromodulation of the cervical spinal cord

facilitates forelimb skilled function recovery in spinal cord injured rats. Experimental Neurology *291*, 141–150.

Al-Majed, A., Brushart, T., and Gordon, T. (2000). Electrical stimulation accelerates and increases expression of BDNF and trkB mRNA in regenerating rat femoral motoneurons. European J Neurosci *12*, 4381–4390.

Alpert, S.W., Koval, K.J., and Zuckerman, J.D. (1996). Neuropathic Arthropathy: Review of Current Knowledge. J Am Acad Orthop Sur *4*, 100–108.

Alto, L., Havton, L.A., Conner, J.M., Edmund, H.R., Blesch, A., and Tuszynski, M.H. (2009). Chemotropic guidance facilitates axonal regeneration and synapse formation after spinal cord injury. Nat Neurosci *12*, 1106–1113.

Anderson, K.D. (2004). Targeting recovery: priorities of the spinal cord-injured population. Journal of Neurotrauma *21*, 1371–1383.

Anderson, A.J., Piltti, K.M., Hooshmand, M.J., Nishi, R.A., and Cummings, B.J. (2017). Preclinical Efficacy Failure of Human CNS-Derived Stem Cells for Use in the Pathway Study of Cervical Spinal Cord Injury. Stem Cell Rep *8*, 249–263.

Anderson, M.A., Burda, J.E., Ren, Y., Ao, Y., O'Shea, T.M., Kawaguchi, R., Coppola, G., Khakh, B.S., Deming, T.J., and Sofroniew, M.V. (2016). Astrocyte scar formation aids central nervous system axon regeneration. Nature *532*, 195.

Anderson, M.A., O'Shea, T.M., Burda, J.E., Ao, Y., Barlatey, S.L., Bernstein, A.M., Kim, J.H., James, N.D., Rogers, A., Kato, B., Wollenberg, AL., Kawaguchi, R., Coppola, G., Wang, C., Deming, T.J., He, Z., Courtine, C., and Sofrienew, M.V. (2018). Required growth facilitators propel axon regeneration across complete spinal cord injury. Nature *561*, 396–400.

Angeli, C.A., Boakye, M., Morton, R.A., Vogt, J., Benton, K., Chen, Y., Ferreira, C.K., and Harkema, S.J. (2018). Recovery of Over-Ground Walking after Chronic Motor Complete Spinal Cord Injury. New England Journal of Medicine *379*, 1244–1250.

Ashley, C., and Ridgway, E.B. (1968). Simultaneous Recording of Membrane Potential, Calcium Transient and Tension in Single Muscle Fibres. Nature *219*, 2191168a0.

Assinck, P., Duncan, G.J., Hilton, B.J., Plemel, J.R., and Tetzlaff, W. (2017). Cell transplantation therapy for spinal cord injury. Nature Neuroscience *20*, 637.

Ballermann, M., and Fouad, K. (2006). Spontaneous locomotor recovery in spinal cord injured rats is accompanied by anatomical plasticity of reticulospinal fibers. The European Journal of Neuroscience *23*, 1988–1996.

Barbeau, H., and Rossignol, S. (1987). Recovery of locomotion after chronic

spinalization in the adult cat. Brain Res *412*, 84–95.

Bareyre, F., Kerschensteiner, M., and Raineteau, O. (2004). The injured spinal cord spontaneously forms a new intraspinal circuit in adult rats.

Bareyre, F.M., Garzorz, N., Lang, C., Misgeld, T., Büning, H., and Kerschensteiner, M. (2011). In vivo imaging reveals a phase-specific role of STAT3 during central and peripheral nervous system axon regeneration. Proc National Acad Sci *108*, 6282–6287.

Barnabé-Heider, F., Göritz, C., Sabelström, H., Takebayashi, H., Pfrieger, F.W., Meletis, K., and Frisén, J. (2010). Origin of new glial cells in intact and injured adult spinal cord. Cell Stem Cell *7*, 470–482.

Bartanusz, V., Jezova, D., Alajajian, B., and Digicaylioglu, M. (2011). The blood-spinal cord barrier: morphology and clinical implications. Annals of Neurology *70*, 194–206.

Bartus, K., James, N.D., Didangelos, A., Bosch, K.D., Verhaagen, J., Yáñez-Muñoz, R.J., Rogers, J.H., Schneider, B.L., Muir, E.M., and Bradbury, E.J. (2014). Large-Scale Chondroitin Sulfate Proteoglycan Digestion with Chondroitinase Gene Therapy Leads to Reduced Pathology and Modulates Macrophage Phenotype following Spinal Cord Contusion Injury. J Neurosci *34*, 4822–4836.

Batchelor, P.E., Kerr, N.F., Gatt, A.M., Aleksoska, E., Cox, S.F., Ghasem-Zadeh, A., Wills, T.E., and Howells, D.W. (2010). Hypothermia Prior to Decompression: Buying Time for Treatment of Acute Spinal Cord Injury. J Neurotraum *27*, 1357–1368.

Becker, C., Lieberoth, B., Morellini F., Feldner, J., Becker, T., and Schachner M. (2004). L1. 1 is involved in spinal cord regeneration in adult zebrafish.

Belin, S., Nawabi, H., Wang, C., Tang, S., Latremoliere, A., Warren, P., Schorle, H., Uncu, C., Woolf, C.J., He, Z., and Steen, J.A. (2015). Injury-Induced Decline of Intrinsic Regenerative Ability Revealed by Quantitative Proteomics. Neuron *86*, 1000–1014.

Benevento, B.T., and Sipski, M.L. (2002). Neurogenic bladder, neurogenic bowel, and sexual dysfunction in people with spinal cord injury. Physical Therapy *82*, 601–612.

Benton, R.L., and Hagg, T. (2011). Vascular Pathology as a Potential Therapeutic Target in SCI. Translational Stroke Research *2*, 556–574.

Berry, M., Maxwell, W., Logan, A., Mathewson, A., McConnell, P., Ashhurst, D., and Thomas, G. (1983). Deposition of scar tissue in the central nervous system. Acta Neurochirurgica. Supplementum *32*, 31–53.

Bikson, M., Fox, J.E., and Jefferys, J.G. (2003). Neuronal Aggregate Formation Underlies Spatiotemporal Dynamics of Nonsynaptic Seizure Initiation. J Neurophysiol *89*, 2330–2333.

Bjorklund, A., and Stenevi, U. (1984). Intracerebral Neural Implants: Neuronal Replacement and Reconstruction of Damaged Circuitries. Annu Rev Neurosci *7*, 279–308.

Björklund, A., Schmidt, R.H., and Stenevi, U. (1980). Functional reinnervation of the neostriatum in the adult rat by use of intraparenchymal grafting of dissociated cell suspensions from the substantia nigra. Cell Tissue Res *212*, 39–45.

Black, I.B., and Woodbury, D. (2001). Adult Rat and Human Bone Marrow Stromal Stem Cells Differentiate into Neurons. Blood Cells Mol Dis *27*, 632–636.

Blesch, A., Lu, P., and Tuszynski, M.H. (2002). Neurotrophic factors, gene therapy, and neural stem cells for spinal cord repair. Brain Res Bull *57*, 833–838.

Bonizzato, M., Pidpruzhnykova, G., DiGiovanna, J., Shkorbatova, P., Pavlova, N., Micera, S., and Courtine, G. (2018). Brain-controlled modulation of spinal circuits improves recovery from spinal cord injury. Nature Communications *9*, 3015.

Bonner, J.F., Connors, T.M., Silverman, W.F., Kowalski, D.P., Lemay, M.A., and Fischer, I. (2011). Grafted neural progenitors integrate and restore synaptic connectivity across the injured spinal cord. The Journal of Neuroscience : The Official Journal of the Society for Neuroscience *31*, 4675–4686.

Boyden, E.S., Zhang, F., Bamberg, E., Nagel, G., and Deisseroth, K. (2005). Millisecond-timescale, genetically targeted optical control of neural activity. Nat Neurosci *8*, nn1525.

Bracken, M. (1997). Administration of methylprednisolone for 24 or 48 hours or tirilazad mesylate for 48 hours in the treatment of acute spinal cord injury. Results of the Third National Acute Spinal Cord Injury Randomized Controlled Trial. National Acute Spinal Cord Injury Study. Jama J Am Medical Assoc *277*, 1597–1604.

Bracken, M.B., Shepard, M., Collins, W.F., Holford, T.R., Young, W., Baskin, D.S., Eisenberg, H.M., Flamm, E., Leo-Summers, L., Maroon, J., Marshall, L.F., Perot, Jr., P.L, Piepmeier, J., Sonntag, V.K.H., Wagner, F.C., Wilberger, J.E., and Winn, HR. (1990). A Randomized, Controlled Trial of Methylprednisolone or Naloxone in the Treatment of Acute Spinal-Cord Injury. New Engl J Medicine *322*, 1405–1411.

Bradbury, E.J., Moon, L.D., Popat, R.J., King, V.R., Bennett, G.S., Patel, P.N., Fawcett, J.W., and McMahon, S.B. (2002). Chondroitinase ABC promotes functional recovery after spinal cord injury. Nature *416*, 636–640.

Braughler, M.J., and Hall, E.D. (1984). Effects of multi-dose methylprednisolone sodium succinate administration on injured cat spinal cord neurofilament degradation and energy metabolism. J Neurosurg *61*, 290–295.

Brock, J.H., Graham, L., Staufenberg, E., Im, S., and Tuszynski, M.H. (2017). Rodent Neural Progenitor Cells Support Functional Recovery After Cervical Spinal Cord Contusion. Journal of Neurotrauma.

Brösamle, C., Huber, A.B., Fiedler, M., Skerra, A., and Schwab, M.E. (2000). Regeneration of Lesioned Corticospinal Tract Fibers in the Adult Rat Induced by a Recombinant, Humanized IN-1 Antibody Fragment. J Neurosci *20*, 8061–8068.

Bundesen, L.Q., Scheel, T., Bregman, B.S., and Kromer, L.F. (2003). Ephrin-B2 and EphB2 Regulation of Astrocyte-Meningeal Fibroblast Interactions in Response to Spinal Cord Lesions in Adult Rats. J Neurosci *23*, 7789–7800.

Bunge, R., Puckett, W., Becerra, J., Marcillo, A., and Quencer, R. (1993). Observations on the pathology of human spinal cord injury. A review and classification of 22 new cases with details from a case of chronic cord compression with extensive focal demyelination. Adv Neurol *59*, 75–89.

Burda, J.E., and Sofroniew, M.V. (2014). Reactive gliosis and the multicellular response to CNS damage and disease. Neuron *81*, 229–248.

Byrne, A.B., Walradt, T., Gardner, K.E., Hubbert, A., Reinke, V., and Hammarlund, M. (2014). Insulin/IGF1 Signaling Inhibits Age-Dependent Axon Regeneration. Neuron *81*, 561–573.

Cafferty, W.B., Yang, S.-H.H., Duffy, P.J., Li, S., and rittmatter, S. (2007). Functional axonal regeneration through astrocytic scar genetically modified to digest chondroitin sulfate proteoglycans. The Journal of Neuroscience : The Official Journal of the Society for Neuroscience *27*, 2176–2185.

Cajal, S. (1928). Degeneration and Regeneration of the Nervous System. Oxford University Press.

Campenot, R.B. (1977). Local control of neurite development by nerve growth factor. Proc National Acad Sci *74*, 4516–4519.

Canty, A., Huang, L., Jackson, J., Little, G., Knott, G., Maco, B., and Paola, D.V. (2013). In-vivo single neuron axotomy triggers axon regeneration to restore synaptic density in specific cortical circuits. Nat Commun *4*, 2038.

Cao, G., Platisa, J., Pieribone, V.A., Raccuglia, D., Kunst, M., and Nitabach, M.N. (2013). Genetically Targeted Optical Electrophysiology in Intact Neural Circuits. Cell *154*.

Cao, Y., Krause, J.S., Saunders, L.L., and Clark, J.M. (2015). Impact of Marital Status on 20-Year Subjective Well-being Trajectories. Top Spinal Cord Inj Rehabilitation *21*,

208–217.

Capogrosso, M., Milekovic, T., Borton, D., Wagner, F., Moraud, E., Mignardot, J.-B., Buse, N., Gandar, J., Barraud, Q., Xing, D., Rey, E., Duis, S., Jianzhong, Y., Ko, W.K.D., Li, Q., Detemple, P., Denison, T., Micera, S., Bezard, E., Bloch, J., and Courtine, G. (2016). A brain–spine interface alleviating gait deficits after spinal cord injury in primates. Nature *539*, 284.

Cardenas, D.D., and Felix, E.R. (2009). Pain after Spinal Cord Injury: A Review of Classification, Treatment Approaches, and Treatment Assessment. Pm&R *1*, 1077–1090.

Carelli, S., Giallongo, T., Rey, F., Colli, M., Tosi, D., Bulfamante, G., Giulio, A., and Gorio, A. (2019). Neuroprotection, Recovery of Function and Endogenous Neurogenesis in Traumatic Spinal Cord Injury Following Transplantation of Activated Adipose Tissue. Cells *8*, 329.

Casha, S., Zygun, D., McGowan, D.M., Bains, I., Yong, W.V., and Hurlbert, J.R. (2012). Results of a phase II placebo-controlled randomized trial of minocycline in acute spinal cord injury. Brain *135*, 1224–1236.

Chang, D.-J., Oh, S.-H., Lee, N., Choi, C., Jeon, I., Kim, H., Shin, D., Lee, S., Kim, D., and Song, J. (2013). Contralaterally transplanted human embryonic stem cell-derived neural precursor cells (ENStem-A) migrate and improve brain functions in stroke-damaged rats. Exp Mol Medicine *45*, emm201393.

Chang, K.-J., Susuki, K., Dours-Zimmermann, M.T., Zimmermann, D.R., and Rasband, M.N. (2010). Oligodendrocyte Myelin Glycoprotein Does Not Influence Node of Ranvier Structure or Assembly. J Neurosci *30*, 14476–14481.

Chen, M., Geoffroy, C.G., Wong, H.N., Tress, O., Nguyen, M.T., Holzman, L.B., Jin, Y., and Zheng, B. (2016a). Leucine Zipper-bearing Kinase promotes axon growth in mammalian central nervous system neurons. Sci Rep-Uk *6*, srep31482.

Chen, T.-W., Wardill, T.J., Sun, Y., Pulver, S.R., Renninger, S.L., Baohan, A., Schreiter, E.R., Kerr, R.A., Orger, M.B., Jayaraman, V., Looger, L.L., Svoboda, K., and Kim, D.S. (2013). Ultrasensitive fluorescent proteins for imaging neuronal activity. Nature *499*, 295.

Chen, Y., He, Y., and DeVivo, M.J. (2016b). Changing Demographics and Injury Profile of New Traumatic Spinal Cord Injuries in the United States, 1972-2014. Archives of Physical Medicine and Rehabilitation *97*, 1610–1619.

Chivatakarn, O., Kaneko, S., He, Z., Tessier-Lavigne, M., and Giger, R.J. (2007). The Nogo-66 Receptor NgR1 Is Required Only for the Acute Growth Cone-Collapsing But Not the Chronic Growth-Inhibitory Actions of Myelin Inhibitors. J Neurosci *27*, 7117–

7124.

Cipriani, S., Ferrer, I., Aronica, E., Kovacs, G.G., Verney, C., Nardelli, J., Khung, S., Delezoide, A.-L., Milenkovic, I., Rasika, S., Manivet, P., Benifla, J., Deriot, N., Gressens, P., and Adle-Biassette H. (2018). Hippocampal Radial Glial Subtypes and Their Neurogenic Potential in Human Fetuses and Healthy and Alzheimer's Disease Adults. Cereb Cortex *28*, 2458–2478.

Cole, G.J., and McCabe, C.F. (1991). Identification of a developmentally regulated keratan sulfate proteoglycan that inhibits cell adhesion and neurite outgrowth. Neuron *7*, 1007–1018.

Courtine, G., Song, B., Roy, R.R., Zhong, H., Herrmann, J.E., Ao, Y., Qi, J., Edgerton, R.V., and Sofroniew, M.V. (2008). Recovery of supraspinal control of stepping via indirect propriospinal relay connections after spinal cord injury. Nat Med *14*, 69–74.

Courtine, G., Gerasimenko, Y., van den Brand, R., Yew, A., Musienko, P., Zhong, H., Song, B., Ao, Y., Ichiyama, R.M., Lavrov, I., Roy, R.R., Sofroniew, M.V., and Edgerton, V.R. (2009). Transformation of nonfunctional spinal circuits into functional states after the loss of brain input. Nature Neuroscience *12*, 1333–1342.

Cummings, B.J., Uchida, N., Tamaki, S.J., Salazar, D.L., Hooshmand, M., Summers, R., Gage, F.H., and Anderson, A.J. (2005). Human neural stem cells differentiate and promote locomotor recovery in spinal cord-injured mice. Proceedings of the National Academy of Sciences of the United States of America *102*, 14069–14074.

Cummings, B.J., Uchida, N., Tamaki, S.J., and Anderson, A.J. (2013). Human neural stem cell differentiation following transplantation into spinal cord injured mice: association with recovery of locomotor function. Neurol Res *28*, 474–481.

Curt, A., Hedel, H.J., Klaus, D., Dietz, V., and Group, S.E. (2008). Recovery from a Spinal Cord Injury: Significance of Compensation, Neural Plasticity, and Repair. J Neurotraum *25*, 677–685.

Curtis, E., Martin, J.R., Gabel, B., Sidhu, N., Rzesiewicz, T.K., Mandeville, R., Gorp, S., Leerink, M., Tadokoro, T., Marsala, S., Jamieson, C., Marsala, M., and Ciacci, J.D. (2018). A First-in-Human, Phase I Study of Neural Stem Cell Transplantation for Chronic Spinal Cord Injury. Cell Stem Cell *22*, 941-950.e6.

David, S., and Aguayo, A.J. (1981). Axonal elongation into peripheral nervous system "bridges" after central nervous system injury in adult rats. Science *214*, 931–933.

Davies, S.J., Fitch, M.T., Memberg, S.P., Hall, A.K., Raisman, G., and Silver, J. (1997). Regeneration of adult axons in white matter tracts of the central nervous system. Nature *390*, 37776.

Davies, S.J., Goucher, D.R., Doller, C., and Silver, J. (1999). Robust Regeneration of Adult Sensory Axons in Degenerating White Matter of the Adult Rat Spinal Cord. J Neurosci *19*, 5810–5822.

Decq, P. (2003). [Pathophysiology of spasticity]. Neuro-Chir *49*, 163–184.

Dietz, V., Wirz, M., Curt, A., and Colombo, G. (1998). Locomotor pattern in paraplegic patients: training effects and recovery of spinal cord function. Spinal Cord *36*, 3100590.

Ditunno, J., Little, J., Tessler, A., and Burns, A. (2004). Spinal shock revisited: a four-phase model. Spinal Cord *42*, 383–395.

Dizdaroglu, M., Jaruga, P., Birincioglu, M., and Rodriguez, H. (2002). Free radical-induced damage to DNA: mechanisms and measurement1,2 1This article is part of a series of reviews on “Oxidative DNA Damage and Repair.” The full list of papers may be found on the homepage of the journal. 2Guest Editor: Miral Dizdaroglu. Free Radical Bio Med *32*, 1102–1115.

Dou, C., and Levine, J. (1994). Inhibition of neurite growth by the NG2 chondroitin sulfate proteoglycan. J Neurosci *14*, 7616–7628.

Dulin, J.N., Adler, A.F., Kumamaru, H., Poplawski, G.H., Lee-Kubli, C., Strobl, H., Gibbs, D., Kadoya, K., Fawcett, J.W., Lu, P., and Tuszynski, M.H. (2018). Injured adult motor and sensory axons regenerate into appropriate organotypic domains of neural progenitor grafts. Nature Communications *9*, 84.

Duncan, G.J., Manesh, S.B., Hilton, B.J., Assinck, P., Liu, J., Moulson, A., Plemel, J.R., and Tetzlaff, W. (2018). Locomotor recovery following contusive spinal cord injury does not require oligodendrocyte remyelination. Nat Commun *9*, 3066.

Emiliani, V., Cohen, A.E., Deisseroth, K., and Häusser, M. (2015). All-Optical Interrogation of Neural Circuits. The Journal of Neuroscience *35*, 13917–13926.

Enomoto, M., Bunge, M., and Tsoulfas, P. (2013). A multifunctional neurotrophin with reduced affinity to p75NTR enhances transplanted Schwann cell survival and axon growth after spinal cord injury. Exp Neurol *248*, 170–182.

Eriksson, P.S., Perfilieva, E., Björk-Eriksson, T., Alborn, A.-M., Nordborg, C., Peterson, D.A., and Gage, F.H. (1998). Neurogenesis in the adult human hippocampus. Nat Med *4*, nm1198_1313.

Ertürk, A., Hellal, F., Enes, J., and Bradke, F. (2007). Disorganized Microtubules Underlie the Formation of Retraction Bulbs and the Failure of Axonal Regeneration. J Neurosci *27*, 9169–9180.

Farrar, M.J., Bernstein, I.M., Schlafer, D.H., Cleland, T.A., Fetcho, J.R., and Schaffer,

C.B. (2012). Chronic in vivo imaging in the mouse spinal cord using an implanted chamber. Nature Methods *9*, 297–302.

Fehlings, M., and Tator, C. (1995). The relationships among the severity of spinal cord injury, residual neurological function, axon counts, and counts of retrogradely labeled neurons after experimental spinal cord injury. Experimental Neurology *132*, 220–228.

Fehlings, M.G., Theodore, N., Harrop, J., Maurais, G., Kuntz, C., Shaffrey, C.I., Kwon, B.K., Chapman, J., Yee, A., Tighe, A., and McKerracher, L. (2011). A Phase I/IIa Clinical Trial of a Recombinant Rho Protein Antagonist in Acute Spinal Cord Injury. J Neurotraum *28*, 787–796.

Fehlings, M.G., Wilson, J.R., and Cho, N. (2014). Methylprednisolone for the Treatment of Acute Spinal Cord Injury: Counterpoint. Neurosurgery *61*, 36–42.

Felts, P.A., Baker, T.A., and Smith, K.J. (1997). Conduction in Segmentally Demyelinated Mammalian Central Axons. J Neurosci *17*, 7267–7277.

Fenno, L., Yizhar, O., and Deisseroth, K. (2011). The Development and Application of Optogenetics. Neuroscience *34*, 389–412.

Filous, A.R., Tran, A., Howell, J.C., Busch, S.A., Evans, T.A., Stallcup, W.B., Kang, S.H., Bergles, D.E., Lee, S., Levine, J.M., and Silver, J. (2014). Entrapment via Synaptic-Like Connections between NG2 Proteoglycan+ Cells and Dystrophic Axons in the Lesion Plays a Role in Regeneration Failure after Spinal Cord Injury. J Neurosci *34*, 16369–16384.

Fisher, R.E., Geiger, L.A., Stroik, L.K., Hutchins, E.D., George, R.M., Denardo, D.F., Kusumi, K., Rawls, A.J., and Wilson-Rawls, J. (2012). A Histological Comparison of the Original and Regenerated Tail in the Green Anole, Anolis carolinensis. Anatomical Rec *295*, 1609–1619.

Flynn, J.R., Brichta, A.M., Galea, M.P., Callister, R.J., and Graham, B.A. (2011). A horizontal slice preparation for examining the functional connectivity of dorsal column fibres in mouse spinal cord. Journal of Neuroscience Methods *200*, 113–120.

Freund, P., Schmidlin, E., Wannier, T., Bloch, J., Mir, A., Schwab, M.E., and Rouiller, E.M. (2006). Nogo-A–specific antibody treatment enhances sprouting and functional recovery after cervical lesion in adult primates. Nat Med *12*, nm1436.

Freund, P., Schmidlin, E., Wannier, T., Bloch, J., Mir, A., Schwab, M.E., and Rouiller, E.M. (2009). Anti-Nogo-A antibody treatment promotes recovery of manual dexterity after unilateral cervical lesion in adult primates – re-examination and extension of behavioral data. Eur J Neurosci *29*, 983–996.

Fujimoto, Y., Abematsu, M., Falk, A., Tsujimura, K., Sanosaka, T., Juliandi, B., Semi, K.,

Namihira, M., Komiya, S., Smith, A., and Nakashima, K. (2012). Treatment of a Mouse Model of Spinal Cord Injury by Transplantation of Human Induced Pluripotent Stem Cell-Derived Long-Term Self-Renewing Neuroepithelial-Like Stem Cells. Stem Cells *30*, 1163–1173.

Gad, P., Lee, S., Terrafranca, N., Zhong, H., Turner, A., Gerasimenko, Y., and Edgerton, V. (2018). Noninvasive activation of cervical spinal networks after severe paralysis. Journal of Neurotrauma.

Gaillard, A., Prestoz, L., Dumartin, B., Cantereau, A., Morel, F., Roger, M., and Jaber, M. (2007). Reestablishment of damaged adult motor pathways by grafted embryonic cortical neurons. Nat Neurosci *10*, 1294–1299.

García-Alías, G., and Fawcett, J.W. (2012). Training and anti-CSPG combination therapy for spinal cord injury. Exp Neurol *235*, 26–32.

Gardner, E.P., and Johnson, K.O. (2013). The Somatosensory System: Receptors and Central Pathways. In Principles of Neural Science, (McGraw-Hill), pp. 475–495.

Geoffroy, C.G., and Zheng, B. (2014). Myelin-associated inhibitors in axonal growth after CNS injury. Curr Opin Neurobiol *27*, 31–38.

Geoffroy, C.G., Lorenzana, A.O., Kwan, J.P., Lin, K., Ghassemi, O., Ma, A., Xu, N., Creger, D., Liu, K., He, Z., and Zheng, B. (2015). Effects of PTEN and Nogo Codeletion on Corticospinal Axon Sprouting and Regeneration in Mice. The Journal of Neuroscience : The Official Journal of the Society for Neuroscience *35*, 6413–6428.

Geoffroy, C.G., Hilton, B.J., Tetzlaff, W., and Zheng, B. (2016). Evidence for an Age-Dependent Decline in Axon Regeneration in the Adult Mammalian Central Nervous System. Cell Reports *15*, 238–246.

Gerasimenko, Y.P., Lu, D.C., Modaber, M., Zdunowski, S., Gad, P., Sayenko, D.G., Morikawa, E., Haakana, P., Ferguson, A.R., Roy, R.R., and Edgerton, V.R. (2015). Noninvasive Reactivation of Motor Descending Control after Paralysis. J Neurotraum *32*, 1968–1980.

Giehl, K.M., and Tetzlaff, W. (1996). BDNF and NT-3, but not NGF, Prevent Axotomy-induced Death of Rat Corticospinal Neurons In Vivo. Eur J Neurosci *8*, 1167–1175.

Gill, M.L., Grahn, P.J., Calvert, J.S., Linde, M.B., Lavrov, I.A., Strommen, J.A., Beck, L.A., Sayenko, D.G., Straaten, M.G., Drubach, D.I., Veith, D.D., Thoreson, A.R., Lopez, C., Gerasimenko, Y.P., Edgerton, V.R., Lee, K.H., and Zhao, K.D. (2018). Neuromodulation of lumbosacral spinal networks enables independent stepping after complete paraplegia. Nature Medicine *24*, 1677–1682.

Golden, K.L., Pearse, D.D., Blits, B., Garg, M.S., Oudega, M., Wood, P.M., and Bunge,

M. (2007). Transduced Schwann cells promote axon growth and myelination after spinal cord injury. Exp Neurol *207*, 203–217.

Grienberger, C., and Konnerth, A. (2012). Imaging Calcium in Neurons. Neuron *73*.

Grossman, R.G., Fehlings, M.G., Frankowski, R.F., Burau, K.D., Chow, D., Tator, C., Teng, A., Toups, E.G., Harrop, J.S., Aarabi, B., Shaffrey, C.I., Johnson, M.M., Harkema, S.J., Boakye, M., Guest, J.D., and Wilson, J.R. (2014). A Prospective, Multicenter, Phase I Matched-Comparison Group Trial of Safety, Pharmacokinetics, and Preliminary Efficacy of Riluzole in Patients with Traumatic Spinal Cord Injury. J Neurotraum *31*, 239–255.

Grynkiewicz, G., Poenie, M., and Tsien, R. (1985). A new generation of Ca2+ indicators with greatly improved fluorescence properties. J Biological Chem *260*, 3440–3450.

Guo, Y., Liu, S., Zhang, X., Wang, L., Zhang, X., Hao, A., Han, A., and Yang, J. (2014). Sox11 promotes endogenous neurogenesis and locomotor recovery in mice spinal cord injury. Biochem Bioph Res Co *446*, 830–835.

Hagg, T., Gulati, A.K., Behzadian, M.A., Vahlsing, H.L., Varon, S., and Manthorpe, M. (1991). Nerve growth factor promotes CNS cholinergic axonal regeneration into acellular peripheral nerve grafts. Exp Neurol *112*, 79–88.

Hagino, S., Iseki, K., Mori, T., Zhang, Y., Hikake, T., Yokoya, S., Takeuchi, M., Hasimoto, H., Kikuchi, S., and Wanaka, A. (2003). Slit and glypican-1 mRNAs are coexpressed in the reactive astrocytes of the injured adult brain. Glia *42*, 130–138.

Hall, E.D., and Braughler, J.M. (1982a). Glucocorticoid mechanisms in acute spinal cord injury: A review and therapeutic rationale. Surg Neurol *18*, 320–327.

Hall, E.D., and Braughler, M.J. (1982b). Effects of intravenous methylprednisolone on spinal cord lipid peroxidation and (Na+ + K+)-ATPase activity. J Neurosurg *57*, 247–253.

Hata, K., Fujitani, M., Yasuda, Y., Doya, H., Saito, T., Yamagishi, S., Mueller, B.K., and Yamashita, T. (2006). RGMa inhibition promotes axonal growth and recovery after spinal cord injury. J Cell Biology *173*, 47–58.

Hawthorne, A.L., Hu, H., Kundu, B., Steinmetz, M.P., Wylie, C.J., Deneris, E.S., and Silver, J. (2011). The Unusual Response of Serotonergic Neurons after CNS Injury: Lack of Axonal Dieback and Enhanced Sprouting within the Inhibitory Environment of the Glial Scar. J Neurosci *31*, 5605–5616.

He, Z., and Jin, Y. (2016). Intrinsic Control of Axon Regeneration. Neuron *90*, 437–451.

Hellal, F., Hurtado, A., Ruschel, J., Flynn, K.C., Laskowski, C.J., Umlauf, M., Kapitein,

L.C., Strikis, D., Lemmon, V., Bixby, J., Hoogenraad, C.C., and Bradke, F. (2011). Microtubule Stabilization Reduces Scarring and Causes Axon Regeneration After Spinal Cord Injury. Science *331*, 928–931.

Hess, M.J., and Hough, S. (2012). Impact of spinal cord injury on sexuality: broad-based clinical practice intervention and practical application. The Journal of Spinal Cord Medicine *35*, 211–218.

Ho, C.H., Triolo, R.J., Elias, A.L., Kilgore, K.L., DiMarco, A.F., Bogie, K., Vette, A.H., Audu, M.L., Kobetic, R., Chang, S.R., Chan, K.M., Dukelow, S., Bourbeau, D.J., Brose, S.W., Gustafson, K.J., Kiss, Z.H.T., and Mushahwar, V.K. (2014). Functional Electrical Stimulation and Spinal Cord Injury. Phys Med Rehabil Cli *25*, 631–654.

Hodgson, J.A., Roy, R.R., de Leon, R., Dobkin, B., and Edgerton, R.V. (1994). Can the mammalian lumbar spinal cord learn a motor task?. Medicine Sci Sports Exerc *26*, 1491.

Hofstetter, C., Schwarz, E., Hess, D., Widenfalk, J., Manira, E.A., Prockop, D.J., and Olson, L. (2002). Marrow stromal cells form guiding strands in the injured spinal cord and promote recovery. Proc National Acad Sci *99*, 2199–2204.

Holinski, B., Mazurek, K., Everaert, D., Toossi, A., Lucas-Osma, A., Troyk, P., Etienne-Cummings, R., Stein, R., and Mushahwar, V. (2016). Intraspinal microstimulation produces over-ground walking in anesthetized cats. J Neural Eng *13*, 056016.

Holland, S.M., Collura, K.M., Ketschek, A., Noma, K., Ferguson, T.A., Jin, Y., Gallo, G., and Thomas, G.M. (2016). Palmitoylation controls DLK localization, interactions and activity to ensure effective axonal injury signaling. Proc National Acad Sci *113*, 763–768.

Hu, H.Z., Granger, N., Pai, B.S., Bellamkonda, R.V., and Jeffery, N.D. (2018). Therapeutic efficacy of microtube-embedded chondroitinase ABC in a canine clinical model of spinal cord injury. Brain J Neurology *141*, 1017–1027.

Huntwork-Rodriguez, S., Wang, B., Watkins, T., Ghosh, A., Pozniak, C.D., Bustos, D., Newton, K., Kirkpatrick, D.S., and Lewcock, J.W. (2013). JNK-mediated phosphorylation of DLK suppresses its ubiquitination to promote neuronal apoptosis. J Cell Biology *202*, 747–763.

Hurlbert, J.R. (2000). Methylprednisolone for acute spinal cord injury: an inappropriate standard of care. J Neurosurg Spine *93*, 1–7.

Hurlbert, J.R. (2014). Methylprednisolone for the Treatment of Acute Spinal Cord Injury: Point. Neurosurgery *61*, 32–35.

Husch, A., Cramer, N., and Harris-Warrick, R.M. (2011). Long-duration perforated patch

recordings from spinal interneurons of adult mice. Journal of Neurophysiology *106*, 2783–2789.

hwab, J., Zhang, Y., Kopp, M.A., Brommer, B., and Popovich, P.G. (2014). The paradox of chronic neuroinflammation, systemic immune suppression, autoimmunity after traumatic chronic spinal cord injury. Experimental Neurology *258*, 121–129.

Jakeman, L.B., and Reier, P.J. (1991). Axonal projections between fetal spinal cord transplants and the adult rat spinal cord: A neuroanatomical tracing study of local interactions. J Comp Neurol *307*, 311–334.

Jayaprakash, N., Nowak, D., Eastwood, E., Krueger, N., Wang, Z., and Blackmore, M.G. (2019). Restoration of Direct Corticospinal Communication Across Sites of Spinal Injury. BioRxiv 546374.

Jeffery, N., Boudreau, E.C., Konarik, M., Mays, T., and Fajt, V. (2018). Pharmacokinetics and safety of oral glyburide in dogs with acute spinal cord injury. Peerj *6*, e4387.

Ji, B., Case, L.C., Liu, K., Shao, Z., Lee, X., Yang, Z., Wang, J., Tian, T., Shulga-Morskaya, S., Scott, M., He, Z., Relton, J.K., and Mi, S. (2008). Assessment of functional recovery and axonal sprouting in oligodendrocyte-myelin glycoprotein (OMgp) null mice after spinal cord injury. Mol Cell Neurosci *39*, 258–267.

Jin, D., Liu, Y., Sun, F., Wang, X., Liu, X., and He, Z. (2015). Restoration of skilled locomotion by sprouting corticospinal axons induced by co-deletion of PTEN and SOCS3. Nature Communications *6*, 8074.

Jones, L.L., Margolis, R.U., and Tuszynski, M.H. (2003). The chondroitin sulfate proteoglycans neurocan, brevican, phosphacan, and versican are differentially regulated following spinal cord injury. Exp Neurol *182*, 399–411.

Kadoya, K., Tsukada, S., Lu, P., Coppola, G., Geschwind, D., Filbin, M.T., Blesch, A., and Tuszynski, M.H. (2009). Combined Intrinsic and Extrinsic Neuronal Mechanisms Facilitate Bridging Axonal Regeneration One Year after Spinal Cord Injury. Neuron *64*.

Kadoya, K., Lu, P., Nguyen, K., Lee-Kubli, C., Kumamaru, H., Yao, L., Knackert, J., Poplawski, G., Dulin, J.N., Strobl, H., Takashima, Y., Biane, J., Conner, J., Zhang, S., and Tuszynski, M.H. (2016). Spinal cord reconstitution with homologous neural grafts enables robust corticospinal regeneration. Nature Medicine *22*, nm.4066.

Kaneko, S., Iwanami, A., Nakamura, M., Kishino, A., Kikuchi, K., Shibata, S., Okano, H.J., Ikegami, T., Moriya, A., Konishi, O., Nakayama, C., Kumagai, K., Kimura, T., Sato, Y., Goshima, Y., Taniguchi, M., Ito, M., He, Z., Toyama, Y., and Okano, H. (2006). A selective Sema3A inhibitor enhances regenerative responses and functional recovery of the injured spinal cord. Nat Med *12*, nm1505.

Kang, Z., Wang, C., Zepp, J., Wu, L., Sun, K., Zhao, J., Chandrasekharan, U., DiCorleto, P.E., Trapp, B.D., Ransohoff, R.M., Li, X. (2013). Act1 mediates IL-17-induced EAE pathogenesis selectively in NG2+ glial cells. Nat Neurosci *16*, 1401–1408.

Kanno, H., Pressman, Y., Moody, A., Berg, R., Muir, E.M., Rogers, J.H., Ozawa, H., Itoi, E., Pearse, D.D., and Bunge, M. (2014). Combination of engineered Schwann cell grafts to secrete neurotrophin and chondroitinase promotes axonal regeneration and locomotion after spinal cord injury. The Journal of Neuroscience : The Official Journal of the Society for Neuroscience *34*, 18381855.

Kasten, M., Sunshine, Secrist, E., Horner, P., and Moritz, C. (2013). Therapeutic intraspinal microstimulation improves forelimb function after cervical contusion injury. J Neural Eng *10*, 044001.

Katoh-Semba, R., Matsuda, M., Kato, K., and Oohira, A. (1995). Chondroitin Sulphate Proteoglycans in the Rat Brain: Candidates for Axon Barriers of Sensory Neurons and the Possible Modification by Laminin of their Actions. Eur J Neurosci *7*, 613–621.

Kawabata, S., Takano, M., Numasawa-Kuroiwa, Y., Itakura, G., Kobayashi, Y., Nishiyama, Y., Sugai, K., Nishimura, S., Iwai, H., Isoda, M., Shibata, S., Kohyama, J., Iwanami, A., Toyama, Y., Matsumoto, M., Nakamura, M., and Okano, H (2016). Grafted Human iPS Cell-Derived Oligodendrocyte Precursor Cells Contribute to Robust Remyelination of Demyelinated Axons after Spinal Cord Injury. Stem Cell Rep *6*, 1–8.

Keirstead, H.S., Nistor, G., Bernal, G., Totoiu, M., Cloutier, F., Sharp, K., and Steward, O. (2005). Human Embryonic Stem Cell-Derived Oligodendrocyte Progenitor Cell Transplants Remyelinate and Restore Locomotion after Spinal Cord Injury. J Neurosci *25*, 4694–4705.

Kerschensteiner, M., Schwab, M.E., Lichtman, J.W., and Misgeld, T. (2005). In vivo imaging of axonal degeneration and regeneration in the injured spinal cord. Nat Med *11*, 572–577.

Kirshblum, S.C., Waring, W., Biering-Sorensen, F., Burns, S.P., Johansen, M., Schmidt-Read, M., Donovan, W., Graves, D., Jha, A., Jones, L., Mulcahey, M.J., and Krassioukov, A. (2011). Reference for the 2011 revision of the International Standards for Neurological Classification of Spinal Cord Injury. The Journal of Spinal Cord Medicine *34*, 547–554.

Klapoetke, N.C., Murata, Y., Kim, S., Pulver, S.R., Birdsey-Benson, A., Cho, Y., Morimoto, T.K., Chuong, A.S., Carpenter, E.J., Tian, Z., Wang, J., Xie, Y., Yan, Z., Zhang, Y., Chow, B.Y., Surek, B., Melkonian, M., Jayaraman, V., Constantine-Paton, M., Wong, G., and Boyden, E.S. (2014). Independent optical excitation of distinct neural populations. Nature Methods *11*, 338–346.

Koffler, J., Samara, R.F., and Rosenzweig, E.S. (2014). Axon Growth and Regeneration, Methods and Protocols. Methods Mol Biology Clifton N J *1162*, 157–165.

Koffler, J., Zhu, W., Qu, X., Platoshyn, O., Dulin, J.N., Brock, J., Graham, L., Lu, P., Sakamoto, J., Marsala, M., Chen, S., and Tuszynski, M.H. (2019). Biomimetic 3D-printed scaffolds for spinal cord injury repair. Nature Medicine 1.

Kotter, M.R., Li, W.-W., Zhao, C., and Franklin, R.J. (2006). Myelin Impairs CNS Remyelination by Inhibiting Oligodendrocyte Precursor Cell Differentiation. J Neurosci *26*, 328–332.

Kucher, K., Johns, D., Maier, D., Abel, R., Badke, A., Baron, H., Thietje, R., Casha, S., Meindl, R., Gomez-Mancilla, B., Pfister, C., Rupp, R., Weidner, N., Mir, A., Schwab, M.E., and Curt, A. (2018). First-in-Man Intrathecal Application of Neurite Growth-Promoting Anti-Nogo-A Antibodies in Acute Spinal Cord Injury. Neurorehab Neural Re *32*, 578–589.

van Kuijk, A., Geurts, A., and van Kuppevelt, H. (2002). Neurogenic heterotopic ossification in spinal cord injury. Spinal Cord *40*, 3101309.

Kumamaru, H., Kadoya, K., Adler, A.F., Takashima, Y., Graham, L., Coppola, G., and Tuszynski, M.H. (2018). Generation and post-injury integration of human spinal cord neural stem cells. Nature Methods *15*, 723–731.

Kumamaru, H., Lu, P., Rosenzweig, E.S., Kadoya, K., and Tuszynski, M.H. (2019). Regenerating Corticospinal Axons Innervate Phenotypically Appropriate Neurons within Neural Stem Cell Grafts. Cell Reports *26*, 2329-2339.e4.

Kumar, K., Toth, C., Nath, R., and Laing, P. (1998). Epidural spinal cord stimulation for treatment of chronic pain—some predictors of success. A 15-year experience. Surg Neurol *50*, 110–121.

Kwon, B.K., Tetzlaff, W., Grauer, J.N., Beiner, J., and Vaccaro, A.R. (2004). Pathophysiology and pharmacologic treatment of acute spinal cord injury. Spine J *4*, 451–464.

Kwon, B.K., Stammers, A., Belanger, L.M., Bernardo, A., Chan, D., Bishop, C.M., Slobogean, G.P., Zhang, H., Umedaly, H., Giffin, M., Street, J., Boyd, M.C., Paquette, S.J., Fisher, C.G., and Dvorak, M.F. (2010). Cerebrospinal Fluid Inflammatory Cytokines and Biomarkers of Injury Severity in Acute Human Spinal Cord Injury. J Neurotraum *27*, 669–682.

Lammertse, D., Dungan, D., Dreisbach, J., Falci, S., Flanders, A., Marino, R., Schwartz, E., and on and Rehabilitation, N. (2007). Neuroimaging in Traumatic Spinal Cord Injury: An Evidence-based Review for Clinical Practice and Research. J Spinal Cord Medicine *30*, 205–214.

Lang, B.T., Cregg, J.M., DePaul, M.A., Tran, A.P., Xu, K., ck, S., Madalena, K.M., Brown, B.P., Weng, Y.-L.L., Li, S., Karimi-Abdolrezaee, S., Busch, S.A., Shen, Y., and Silver, J. (2014). Modulation of the proteoglycan receptor PTPσ promotes recovery after spinal cord injury. Nature.

LaPlaca, M.C., Simon, C.M., Prado, G.R., and Cullen, D.K. (2007). CNS injury biomechanics and experimental models. Progress in Brain Research *161*, 13–26.

Lee, J.K., Geoffroy, C.G., Chan, A.F., Tolentino, K.E., Crawford, M.J., Leal, M.A., Kang, B., and Zheng, B. (2010). Assessing Spinal Axon Regeneration and Sprouting in Nogo-, MAG-, and OMgp-Deficient Mice. Neuron *66*, 663–670.

Lee, S.M., Yune, T.Y., Kim, S.J., Park, D.W., Lee, Y.K., Kim, Y.C., Oh, Y.J., Markelonis, G.J., and Oh, T.H. (2003). Minocycline Reduces Cell Death and Improves Functional Recovery after Traumatic Spinal Cord Injury in the Rat. J Neurotraum *20*, 1017–1027.

Lemay, M.A., and Grill, W.M. (2004). Modularity of Motor Output Evoked By Intraspinal Microstimulation in Cats. J Neurophysiol *91*, 502–514.

de Leon, R., Hodgson, J., Roy, R., and Edgerton, V. (1998). Locomotor Capacity Attributable to Step Training Versus Spontaneous Recovery After Spinalization in Adult Cats. J Neurophysiol *79*, 1329–1340.

Lepore, A.C., and Fischer, I. (2005). Lineage-restricted neural precursors survive, migrate, and differentiate following transplantation into the injured adult spinal cord. Exp Neurol *194*, 230–242.

Levi, A.D., Casella, G., Green, B.A., Dietrich, D.W., Vanni, S., Jagid, J., and Wang, M.Y. (2010). Clinical Outcomes Using Modest Intravascular Hypothermia After Acute Cervical Spinal Cord Injury. Neurosurgery *66*, 670–677.

Levi, A.D., Okonkwo, D.O., Park, P., Jenkins, A.L., Kurpad, S.N., Parr, A.M., Ganju, A., Aarabi, B., Kim, D., Casha, S., Fehlings, M.G., Harrop, J.S., Anderson, K.D., Gage, A., Hsieh, J., Huhn, S., Curt, A., and Guzman, R. (2018). Emerging Safety of Intramedullary Transplantation of Human Neural Stem Cells in Chronic Cervical and Thoracic Spinal Cord Injury. Neurosurgery *82*, 562–575.

Lin, J.Y., Knutsen, P.M., Muller, A., Kleinfeld, D., and Tsien, R.Y. (2013). ReaChR: a red-shifted variant of channelrhodopsin enables deep transcranial optogenetic excitation. Nature Neuroscience *16*, 1499–1508.

Liu, K., Lu, Y., Lee, J.K., Samara, R., Willenberg, R., Sears-Kraxberger, I., Tedeschi, A., Park, K.K., Jin, D., Cai, B., Xu, B., Connolly, L., Steward, O., Zheng, B., and He, Z. (2010). PTEN deletion enhances the regenerative ability of adult corticospinal neurons. Nature Neuroscience *13*, 1075–1081.

Liu, K., Tedeschi, A., Park, K., and He, Z. (2011). Neuronal Intrinsic Mechanisms of Axon Regeneration. Annu Rev Neurosci *34*, 131–152.

Lorenzana, A.O., Lee, J.K., Mui, M., Chang, A., and Zheng, B. (2015). A Surviving Intact Branch Stabilizes Remaining Axon Architecture after Injury as Revealed by In Vivo Imaging in the Mouse Spinal Cord. Neuron.

Lu, D.C., Edgerton, V., Modaber, M., AuYong, N., Morikawa, E., Zdunowski, S., Sarino, M.E., Sarrafzadeh, M., Nuwer, M.R., Roy, R.R., Gerasimenko, Y. (2016). Engaging Cervical Spinal Cord Networks to Reenable Volitional Control of Hand Function in Tetraplegic Patients. Neurorehabilitation and Neural Repair *30*, 951–962.

Lu, J., Féron, F., Mackay-Sim, A., and Waite, P.M. (2002). Olfactory ensheathing cells promote locomotor recovery after delayed transplantation into transected spinal cord. Brain *125*, 14–21.

Lu, P., Wang, Y., Graham, L., McHale, K., Gao, M., Wu, D., Brock, J., Blesch, A., Rosenzweig, E.S., Havton, L.A., Zheng, B., Conner, J.M., Marsala, M., and Tuszynski, M.H. (2012). Long-Distance Growth and Connectivity of Neural Stem Cells after Severe Spinal Cord Injury. Cell *150*, 1264–1273.

Lu, P., Woodruff, G., Wang, Y., Graham, L., Hunt, M., Wu, D., Boehle, E., Ahmad, R., Poplawski, G., Brock, J., Goldstein, L., and Tuszynski, M.H. (2014). Long-Distance Axonal Growth from Human Induced Pluripotent Stem Cells after Spinal Cord Injury. Neuron *83*, 789–796.

Lu, P., Ceto, S., Wang, Y., Graham, L., Wu, D., Kumamaru, H., Staufenberg, E., and Tuszynski, M.H. (2017). Prolonged human neural stem cell maturation supports recovery in injured rodent CNS. Journal of Clinical Investigation.

Mahmood, A., Lu, D., and Chopp, M. (2004). Marrow Stromal Cell Transplantation after Traumatic Brain Injury Promotes Cellular Proliferation within the Brain. Neurosurgery *55*, 1185–1193.

Mao, Y., Nguyen, T., Sutherland, T., and Gorrie, C. (2016). Endogenous neural progenitor cells in the repair of the injured spinal cord. Neural Regen Res *11*, 1075–1076.

McKeon, R., Schreiber, R., Rudge, J., and Silver, J. (1991). Reduction of neurite outgrowth in a model of glial scarring following CNS injury is correlated with the expression of inhibitory molecules on reactive astrocytes. J Neurosci *11*, 3398–3411.

Mckeon, R.J., Höke, A., and Silver, J. (1995). Injury-Induced Proteoglycans Inhibit the Potential for Laminin-Mediated Axon Growth on Astrocytic Scars. Exp Neurol *136*, 32–43.

McKeon, R.J., Jurynec, M.J., and Buck, C.R. (1999). The Chondroitin Sulfate Proteoglycans Neurocan and Phosphacan Are Expressed by Reactive Astrocytes in the Chronic CNS Glial Scar. J Neurosci *19*, 10778–10788.

McQuarrie, I.G., and Grafstein, B. (1973). Axon Outgrowth Enhanced by a Previous Nerve Injury. Arch Neurol-Chicago *29*, 53–55.

Mecollari, V., Nieuwenhuis, B., and Verhaagen, J. (2014). A perspective on the role of class III semaphorin signaling in central nervous system trauma. Front Cell Neurosci *8*, 328.

Meletis, K., Barnabé-Heider, F., Carlén, M., Evergren, E., Tomilin, N., Shupliakov, O., and Frisén, J. (2008). Spinal cord injury reveals multilineage differentiation of ependymal cells. PLoS Biology *6*, e182.

Merkler, D., Metz, G.A., Raineteau, O., Dietz, V., Schwab, M.E., and Fouad, K. (2001). Locomotor Recovery in Spinal Cord-Injured Rats Treated with an Antibody Neutralizing the Myelin-Associated Neurite Growth Inhibitor Nogo-A. J Neurosci *21*, 3665–3673.

van Middendorp, J.J., Hosman, A.J.F., and Suhail, D.A.R. (2013). The effects of the timing of spinal surgery after traumatic spinal cord injury: a systematic review and meta-analysis. Journal of Neurotrauma *30*, 1781–1794.

Mishra, A.M., Pal, A., Gupta, D., and Carmel, J.B. (2017). Paired motor cortex and cervical epidural electrical stimulation timed to converge in the spinal cord promotes lasting increases in motor responses. The Journal of Physiology *595*, 6953–6968.

Mitra, P., and Brownstone, R.M. (2012). An in vitro spinal cord slice preparation for recording from lumbar motoneurons of the adult mouse. Journal of Neurophysiology *107*, 728–741.

Miyawaki, A., Llopis, J., Heim, R., McCaffery, M.J., Adams, J.A., Ikura, M., and Tsien, R.Y. (1997). Fluorescent indicators for Ca2+based on green fluorescent proteins and calmodulin. Nature *388*, 42264.

Mondello, S.E., Sunshine, M.D., Fischedick, A.E., Dreyer, S.J., Horwitz, G.D., Anikeeva, P., Horner, P.J., and Moritz, C.T. (2018). Optogenetic surface stimulation of the rat cervical spinal cord. Journal of Neurophysiology.

Moreno-Jiménez, E.P., Flor-García, M., Terreros-Roncal, J., Rábano, A., Cafini, F., Pallas-Bazarra, N., Ávila, J., and Llorens-Martín, M. (2019). Adult hippocampal neurogenesis is abundant in neurologically healthy subjects and drops sharply in patients with Alzheimer's disease. Nat Med *25*, 554–560.

Moxon, K., and Knudsen, E. (2017). Restoration of Hindlimb Movements after Complete

Spinal Cord Injury Using Brain-Controlled Functional Electrical Stimulation. Frontiers in Neuroscience *11*, 715.

Muir, E., Winter, D.F., Verhaagen, J., and Fawcett, J. (2019). Recent advances in the therapeutic uses of chondroitinase ABC. Exp Neurol *321*, 113032.

Mukhopadhyay, G., Doherty, P., Walsh, F.S., Crocker, P.R., and Filbin, M.T. (1994). A novel role for myelin-associated glycoprotein as an inhibitor of axonal regeneration. Neuron *13*, 757–767.

Müller, A., Hauk, T.G., and Fischer, D. (2007). Astrocyte-derived CNTF switches mature RGCs to a regenerative state following inflammatory stimulation. Brain *130*, 3308–3320.

Musk, E., and Neuralink (2019). An integrated brain-machine interface platform with thousands of channels. Biorxiv 703801.

Nagel, G., Szellas, T., Huhn, W., Kateriya, S., Adeishvili, N., Berthold, P., Ollig, D., Hegemann, P., and Bamberg, E. (2003). Channelrhodopsin-2, a directly light-gated cation-selective membrane channel. Proceedings of the National Academy of Sciences of the United States of America *100*, 13940–13945.

New, P., and Marshall, R. (2014). International Spinal Cord Injury Data Sets for non-traumatic spinal cord injury. Spinal Cord *52*, 123–132.

New, P., Farry, A., Baxter, D., and Noonan, V. (2013). Prevalence of non-traumatic spinal cord injury in Victoria, Australia. Spinal Cord *51*, 99.

Ng, M.T., Stammers, A.T., and Kwon, B.K. (2011). Vascular disruption and the role of angiogenic proteins after spinal cord injury. Translational Stroke Research *2*, 474–491.

Noonan, V.K., Fingas, M., Farry, A., Baxter, D., Singh, A., Fehlings, M.G., and Dvorak, M.F. (2012). Incidence and Prevalence of Spinal Cord Injury in Canada: A National Perspective. Neuroepidemiology *38*, 219–226.

Norenberg, M.D., Smith, J., and Marcillo, A. (2004). The pathology of human spinal cord injury: defining the problems. Journal of Neurotrauma *21*, 429–440.

Nori, S., Okada, Y., Nishimura, S., Sasaki, T., Itakura, G., Kobayashi, Y., Renault-Mihara, F., Shimizu, A., Koya, I., Yoshida, R., Kudoh, J., Koike, M., Uchiyama, Y., Ikeda, E., Toyama, Y., Nakamura, M., and Okano, H. (2015). Long-Term Safety Issues of iPSC-Based Cell Therapy in a Spinal Cord Injury Model: Oncogenic Transformation with Epithelial-Mesenchymal Transition. Stem Cell Reports *4*, 360–373.

Nori, S., Khazaei, M., Ahuja, C.S., Yokota, K., Ahlfors, J.-E., Liu, Y., Wang, J., Shibata, S., Chio, J., Hettiaratchi, M.H., Führmann, T., Shoichet, M.S., Fehlings, M.G. (2018). Human Oligodendrogenic Neural Progenitor Cells Delivered with Chondroitinase ABC

Facilitate Functional Repair of Chronic Spinal Cord Injury. Stem Cell Reports.

Nowak, A.P., Breedveld, V., Pakstis, L., Ozbas, B., Pine, D.J., Pochan, D., and Deming, T.J. (2002). Rapidly recovering hydrogel scaffolds from self-assembling diblock copolypeptide amphiphiles. Nature *417*, 424.

NSCISC (2019). National Spinal Cord Injury Statistical Center, Facts and Figures at a Glance.

O'Shea, T.M., Burda, J.E., and Sofroniew, M.V. (2017). Cell biology of spinal cord injury and repair. The Journal of Clinical Investigation *127*, 3259–3270.

Packer, A.M., Russell, L.E., Dalgleish, H.W., and Häusser, M. (2014). Simultaneous all-optical manipulation and recording of neural circuit activity with cellular resolution in vivo. Nature Methods *12*, 140–146.

Park, K.K., Liu, K., Hu, Y., Smith, P.D., Wang, C., Cai, B., Xu, B., Connolly, L., Kramvis, I., Sahin, M., and He, Z. (2008). Promoting axon regeneration in the adult CNS by modulation of the PTEN/mTOR pathway. Science (New York, N.Y.) *322*, 963–966.

Parr, A., Tator, C., and Keating, A. (2007). Bone marrow-derived mesenchymal stromal cells for the repair of central nervous system injury. Bone Marrow Transpl *40*, 1705757.

Pawar, K., Cummings, B.J., Thomas, A., Shea, L.D., Levine, A., Pfaff, S., and Anderson, A.J. (2015). Biomaterial bridges enable regeneration and re-entry of corticospinal tract axons into the caudal spinal cord after SCI: Association with recovery of forelimb function. Biomaterials *65*, 1–12.

Petreanu, L., Huber, D., Sobczyk, A., and Svoboda, K. (2007). Channelrhodopsin-2–assisted circuit mapping of long-range callosal projections. Nat Neurosci *10*, 663–668.

Pindzola, R.R., Doller, C., and Silver, J. (1993). Putative Inhibitory Extracellular Matrix Molecules at the Dorsal Root Entry Zone of the Spinal Cord during Development and after Root and Sciatic Nerve Lesions. Dev Biol *156*, 34–48.

Pineau, I., and Lacroix, S. (2007). Proinflammatory cytokine synthesis in the injured mouse spinal cord: Multiphasic expression pattern and identification of the cell types involved. J Comp Neurol *500*, 267–285.

Pinto, D.J., Patrick, S.L., Huang, W.C., and Connors, B.W. (2005). Initiation, Propagation, and Termination of Epileptiform Activity in Rodent Neocortex In Vitro Involve Distinct Mechanisms. J Neurosci *25*, 8131–8140.

Powers, B.E., Lasiene, J., Plemel, J.R., Shupe, L., Perlmutter, S.I., Tetzlaff, W., and Horner, P.J. (2012). Axonal Thinning and Extensive Remyelination without Chronic Demyelination in Spinal Injured Rats. J Neurosci *32*, 5120–5125.

Prevedel, R., Verhoef, A.J., Pernía-Andrade, A.J., Weisenburger, S., Huang, B.S., Nöbauer, T., Fernández, A., Delcour, J.E., Golshani, P., Baltuska, A., and Vaziri, A. (2016). Fast volumetric calcium imaging across multiple cortical layers using sculpted light. Nature Methods.

Purves, D. (1986). The trophic theory of neural connections. Trends Neurosci *9*, 486–489.

Raiker, S.J., Lee, H., Baldwin, K.T., Duan, Y., Shrager, P., and Giger, R.J. (2010). Oligodendrocyte-Myelin Glycoprotein and Nogo Negatively Regulate Activity-Dependent Synaptic Plasticity. J Neurosci *30*, 12432–12445.

Reier, P.J. (1985). Neural Tissue Grafts and Repair of the Injured Spinal Cord. Neuropath Appl Neuro *11*, 81–104.

Reimer, M., Sörensen, I., and of …, K.V. (2008). Motor neuron regeneration in adult zebrafish.

Reimer, M.M., Norris, A., Ohnmacht, J., Patani, R., Zhong, Z., Dias, T.B., Kuscha, V., Scott, A.L., Chen, Y.-C.C., Rozov, S., Frazer, S.L., Wyatt, C., Higashijima, S., Patton, E.E., Panula, P., Chandran, S., Becker, T., and Becker, C.G. (2013). Dopamine from the brain promotes spinal motor neuron generation during development and adult regeneration. Developmental Cell *25*, 478–491.

Richardson, P., and Verge, V. (1986). The induction of a regenerative propensity in sensory neurons following peripheral axonal injury. J Neurocytol *15*, 585–594.

Richardson, P., McGuinness, U., and Aguayo, A. (1980). Axons from CNS neurons regenerate into PNS grafts. Nature *284*, 264–265.

Roberts, W.J., and Smith, D.O. (1973). Analysis of Threshold Currents during Myostimulation of Fibres in the Spinal Cord. Acta Physiol Scand *89*, 384–394.

Rosenzweig, E.S., Courtine, G., Jindrich, D.L., Brock, J.H., Ferguson, A.R., Strand, S.C., Nout, Y.S., Roy, R.R., Miller, D.M., Beattie, M.S., Havton, L.A., Bresnahan, J.C., Edgerton, V.R., and Tuszynski, M.H. (2010). Extensive spontaneous plasticity of corticospinal projections after primate spinal cord injury. Nature Neuroscience *13*, 1505–1510.

Rotshenker, S. (2011). Wallerian degeneration: the innate-immune response to traumatic nerve injury. J Neuroinflamm *8*, 109.

Ruder, L., Takeoka, A., and Arber, S. Long-Distance Descending Spinal Neurons Ensure Quadrupedal Locomotor Stability. Neuron.

Rudge, J., and Silver, J. (1990). Inhibition of neurite outgrowth on astroglial scars in vitro. J Neurosci *10*, 3594–3603.

Ruschel, J., Hellal, F., Flynn, K.C., Dupraz, S., Elliott, D.A., Tedeschi, A., Bates, M., Sliwinski, C., Brook, G., Dobrindt, K., Peitz, M., Brüstle, O., Norenberg, M.D., Blesch, A., Weidner, N., Bunge, M.B., Bixby, J.L., and Bradke, F. (2015). Axonal regeneration. Systemic administration of epothilone B promotes axon regeneration after spinal cord injury. Science (New York, N.Y.) *348*, 347–352.

Sahay, K., Mehrotra, R., Sachdeva, U., and Banerji, A. (1992). Elastomechanical characterization of brain tissues. Journal of Biomechanics *25*, 319–326.

Sakka, L., Gabrillargues, J., and Coll, G. (2016). Anatomy of the Spinal Meninges. Oper Neurosurg *12*, 168–188.

Schanne, F., Kane, A., Young, E., and Farber, J. (1979). Calcium dependence of toxic cell death: a final common pathway. Science *206*, 700–702.

Schwab, M., and Caroni, P. (1988). Oligodendrocytes and CNS myelin are nonpermissive substrates for neurite growth and fibroblast spreading in vitro. J Neurosci *8*, 2381–2393.

Schwab, M.E., and Strittmatter, S.M. (2014). Nogo limits neural plasticity and recovery from injury. Curr Opin Neurobiol *27*, 53–60.

Seif, G.I., Nomura, H., and Tator, C.H. (2007). Retrograde Axonal Degeneration (Dieback) in the Corticospinal Tract after Transection Injury of the Rat Spinal Cord A Confocal Microscopy Study. J Neurotraum *24*, 1513–1528.

Sekiguchi, K.J., Shekhtmeyster, P., Merten, K., Arena, A., Cook, D., Hoffman, E., Ngo, A., and Nimmerjahn, A. (2016). Imaging large-scale cellular activity in spinal cord of freely behaving mice. Nature Communications *7*, 11450.

Sharp, K.G., Yee, K., and Steward, O. (2014). A re-assessment of long distance growth and connectivity of neural stem cells after severe spinal cord injury. Exp Neurol *257*, 186–204.

Shimoji, K., Higashi, H., Kano, T., Asai, S., and Morioka, T. (1971). [Electrical management of intractable pain]. Masui Jpn J Anesthesiol *20*, 444–447.

Shimomura, O., Johnson, F.H., and Saiga, Y. (1962). Extraction, Purification and Properties of Aequorin, a Bioluminescent Protein from the Luminous Hydromedusan, Aequorea. J Cell Physiol *59*, 223–239.

Silver, J., and Miller, J.H. (2004). Regeneration beyond the glial scar. Nature Reviews. Neuroscience *5*, 146–156.

Simpson, L.A., Eng, J.J., Hsieh, J.T., Wolfe, D.L., and Team, S. (2012). The health and life priorities of individuals with spinal cord injury: a systematic review. Journal of Neurotrauma *29*, 1548–1555.

Smith, G., and Stevenson, J. (1988). Peripheral nerve grafts lacking viable Schwann cells fail to support central nervous system axonal regeneration. Exp Brain Res *69*, 299–306.

Smith, P.D., Sun, F., Park, K., Cai, B., Wang, C., Kuwako, K., Martinez-Carrasco, I., Connolly, L., and He, Z. (2009). SOCS3 Deletion Promotes Optic Nerve Regeneration In Vivo. Neuron *64*, 617–623.

Snow, D.M., Steindler, D.A., and Silver, J. (1990). Molecular and cellular characterization of the glial roof plate of the spinal cord and optic tectum: A possible role for a proteoglycan in the development of an axon barrier. Dev Biol *138*, 359–376.

Sofroniew, M.V. (2018). Dissecting spinal cord regeneration. Nature *557*, 343–350.

Soleman, S., Yip, P.K., Duricki, D.A., and Moon, L. (2012). Delayed treatment with chondroitinase ABC promotes sensorimotor recovery and plasticity after stroke in aged rats. Brain *135*, 1210–1223.

Sorrells, S.F., Paredes, M.F., Cebrian-Silla, A., Sandoval, K., Qi, D., Kelley, K.W., James, D., Mayer, S., Chang, J., Auguste, K.I., Chang, E.F., Gutierrez, A.J., Kriegstein, A.R., Mathern, G.W., Oldham, M.C., Huang, E.J., Garcia-Verdugo, J.M., Yang, Z., Alvarez-Buylla, A. (2018). Human hippocampal neurogenesis drops sharply in children to undetectable levels in adults. Nature *555*, 377.

Spalding, K.L., Bergmann, O., Alkass, K., Bernard, S., Salehpour, M., Huttner, H.B., Boström, E., Westerlund, I., Vial, C., Buchholz, B.A., Possnert, G., Mash, D., Druid, H., and Frisén J. (2013). Dynamics of Hippocampal Neurogenesis in Adult Humans. Cell *153*, 1219–1227.

Steward, O., Sharp, K., Selvan, G., Hadden, A., Hofstadter, M., Au, E., and Roskams, J. (2006). A re-assessment of the consequences of delayed transplantation of olfactory lamina propria following complete spinal cord transection in rats. Exp Neurol *198*, 483–499.

Stokols, S., and Tuszynski, M.H. (2006). Freeze-dried agarose scaffolds with uniaxial channels stimulate and guide linear axonal growth following spinal cord injury. Biomaterials *27*, 443–451.

Stokols, S., Sakamoto, J., Breckon, C., Holt, T., Weiss, J., and Tuszynski, M.H. (2006). Templated Agarose Scaffolds Support Linear Axonal Regeneration. Tissue Eng *12*, 2777–2787.

Sun, F., Park, K.K., Belin, S., Wang, D., Lu, T., Chen, G., Zhang, K., Yeung, C., Feng, G., Yankner, B.A., He., Z. (2011). Sustained axon regeneration induced by co-deletion of PTEN and SOCS3. Nature *480*, 372–375.

Sunshine, M.D., Ganji, C.N., Reier, P.J., Fuller, D.D., and Moritz, C.T. (2018). Intraspinal microstimulation for respiratory muscle activation. Exp Neurol *302*, 93–103.

Suzuki, H., Ahuja, C.S., Salewski, R.P., Li, L., Satkunendrarajah, K., Nagoshi, N., Shibata, S., and Fehlings, M.G. (2017). Neural stem cell mediated recovery is enhanced by Chondroitinase ABC pretreatment in chronic cervical spinal cord injury. PloS One *12*, e0182339.

Syed, Y.A., Zhao, C., Mahad, D., Möbius, W., Altmann, F., Foss, F., Sentürk, A., Acker-Palmer, A., Lubec, G., Lilley, K., Franklin, R.J.M., Nave, K., Kotter, M.R.N. (2016). Antibody-mediated neutralization of myelin-associated EphrinB3 accelerates CNS remyelination. Acta Neuropathol *131*, 281–298.

Tabakow, P., Raisman, G., Fortuna, W., Czyz, M., Huber, J., Li, D., Szewczyk, P., Okurowski, S., Miedzybrodzki, R., Czapiga, B., Salomon, B., Halon, A., Li, Y., Lipiec, J., Kulczyk, A., and Jarmundowicz W. (2014). Functional Regeneration of Supraspinal Connections in a Patient With Transected Spinal Cord Following Transplantation of Bulbar Olfactory Ensheathing Cells With Peripheral Nerve Bridging. Cell Transplant *23*, 1631-1655(25).

Takeoka, A., and Arber, S. (2019). Functional Local Proprioceptive Feedback Circuits Initiate and Maintain Locomotor Recovery after Spinal Cord Injury. Cell Reports *27*, 71-85.e3.

Takeoka, A., Vollenweider, I., Courtine, G., and Arber, S. (2014). Muscle Spindle Feedback Directs Locomotor Recovery and Circuit Reorganization after Spinal Cord Injury. Cell *159*, 1626–1639.

Tang, X., Davies, J.E., and Davies, S. (2003). Changes in distribution, cell associations, and protein expression levels of NG2, neurocan, phosphacan, brevican, versican V2, and tenascin-C during acute to chronic maturation of spinal cord scar tissue. J Neurosci Res *71*, 427–444.

Tator, C. (1972). Acute spinal cord injury: a review of recent studies of treatment and pathophysiology. Canadian Medical Association Journal *107*, 143-5 passim.

Tator, C. (1995). Update on the pathophysiology and pathology of acute spinal cord injury. Brain Pathology (Zurich, Switzerland) *5*, 407–413.

Tetzlaff, W., Okon, E.B., Karimi-Abdolrezaee, S., Hill, C.E., Sparling, J.S., Plemel, J.R., Plunet, W.T., Tsai, E.C., Baptiste, D., Smithson, L.J., Kawaja, M.D., Fehlings, M.G., and

Kwon, B.K. (2011). A Systematic Review of Cellular Transplantation Therapies for Spinal Cord Injury. J Neurotraum *28*, 1611–1682.

Theodore, N., Hlubek, R., Danielson, J., Neff, K., Vaickus, L., Ulich, T.R., and Ropper, A.E. (2016). First Human Implantation of a Bioresorbable Polymer Scaffold for Acute Traumatic Spinal Cord InjuryA Clinical Pilot Study for Safety and Feasibility. Neurosurgery *79*, E305–E312.

Tian, L., Hires, A.S., and Looger, L.L. (2012). Imaging Neuronal Activity with Genetically Encoded Calcium Indicators. Cold Spring Harbor Protocols *2012*, pdb.top069609.

Tom, V.J., Steinmetz, M.P., Miller, J.H., Doller, C.M., and Silver, J. (2004). Studies on the Development and Behavior of the Dystrophic Growth Cone, the Hallmark of Regeneration Failure, in an In Vitro Model of the Glial Scar and after Spinal Cord Injury. J Neurosci *24*, 6531–6539.

Toossi, A., Everaert, D.G., Azar, A., Dennison, C.R., and Mushahwar, V.K. (2017). Mechanically Stable Intraspinal Microstimulation Implants for Human Translation. Ann Biomed Eng *45*, 681–694.

Tsien, R.Y. (1980). New calcium indicators and buffers with high selectivity against magnesium and protons: design, synthesis, and properties of prototype structures. Biochemistry-Us *19*, 2396–2404.

Tsuji, O., Sugai, K., Yamaguchi, R., Tashiro, S., Nagoshi, N., Kohyama, J., Iida, T., Ohkubo, T., Itakura, G., Isoda, M., Shinozaki, M., Fujiyoshi, K., Kanemura, Y., Yamanaka, S., Nakamura, M., Okano, H. (2018). Laying the groundwork for a first-in-human study of an iPSC-based intervention for spinal cord injury. STEM CELLS.

Tuszynski, M.H., and Steward, O. (2012). Concepts and Methods for the Study of Axonal Regeneration in the CNS. Neuron *74*, 777–791.

Wagner, F.B., Mignardot, J.-B., Goff-Mignardot, C.G., Demesmaeker, R., Komi, S., Capogrosso, M., Rowald, A., Seáñez, I., Caban, M., Pirondini, E., Vat, M., McCracken, L.A., Heimgartner, R., Fodor, I., Watrin, A., Seguin, P., Paoles, E., Keybus, K., Eberle, G., Schurch, B., Pralong, E., Becce, F., Prior, J., Buse, N., Buschman, R., Neufeld, E., Kuster, N., Carda, S., von Zitzewitz, J., Delattre, V., Denison, T., Lambert, H., Minassian, K., Block, J., and Courtine, G. (2018). Targeted neurotechnology restores walking in humans with spinal cord injury. Nature *563*, 65–71.

Waller, A. (1851). Experiments on the Section of the Glosso-Pharyngeal and Hypoglossal Nerves of the Frog, and Observations of the Alterations Produced Thereby in the Structure of Their Primitive Fibres. Edinb Medical Surg J *76*, 369–376.

Wang, D., and Fawcett, J. (2012). The perineuronal net and the control of CNS plasticity. Cell Tissue Res *349*, 147–160.

Wang, X., Yigitkanli, K., Kim, C.-Y., Sekine-Konno, T., Wirak, D., Frieden, E., Bhargava, A., Maynard, G., Cafferty, W., and Strittmatter, S.M. (2014). Human NgR-Fc Decoy Protein via Lumbar Intrathecal Bolus Administration Enhances Recovery from Rat Spinal Cord Contusion. J Neurotraum *31*, 1955–1966.

Wanner, I.B., Anderson, M.A., Song, B., Levine, J., Fernandez, A., Gray-Thompson, Z., Ao, Y., and Sofroniew, M.V. (2013). Glial scar borders are formed by newly proliferated, elongated astrocytes that interact to corral inflammatory and fibrotic cells via STAT3-dependent mechanisms after spinal cord injury. The Journal of Neuroscience : The Official Journal of the Society for Neuroscience *33*, 12870–12886.

Watkins, T.A., Wang, B., Huntwork-Rodriguez, S., Yang, J., Jiang, Z., Eastham-Anderson, J., Modrusan, Z., Kaminker, J.S., Tessier-Lavigne, M., and Lewcock, J.W. (2013). DLK initiates a transcriptional program that couples apoptotic and regenerative responses to axonal injury. Proc National Acad Sci *110*, 4039–4044.

Watson, C., and Kayalioglu, G. (2009). The Spinal Cord. 1–7.

Weidner, N., Ner, A., Salimi, N., and Tuszynski, M. (2001). Spontaneous corticospinal axonal plasticity and functional recovery after adult central nervous system injury. Proceedings of the National Academy of Sciences of the United States of America *98*, 3513–3518.

Weinmann, O., Schnell, L., Ghosh, A., Montani, L., Wiessner, C., Wannier, T., Rouiller, E., Mir, A., and Schwab, M.E. (2006). Intrathecally infused antibodies against Nogo-A penetrate the CNS and downregulate the endogenous neurite growth inhibitor Nogo-A. Mol Cell Neurosci *32*, 161–173.

Wells, J.E., Hurlbert, J.R., Fehlings, M.G., and Yong, W.V. (2003). Neuroprotection by minocycline facilitates significant recovery from spinal cord injury in mice. Brain *126*, 1628–1637.

Wen, Y., Yu, S., Wu, Y., Ju, R., Wang, H., Liu, Y., Wang, Y., and Xu, Q. (2015). Spinal cord injury repair by implantation of structured hyaluronic acid scaffold with PLGA microspheres in the rat. Cell and Tissue Research.

Wenger, N., Moraud, E.M., Gandar, J., Musienko, P., Capogrosso, M., Baud, L., Goff, C.G., Barraud, Q., Pavlova, N., Dominici, N., Minev, I.R., Asboth, L., Hirsch, A., Duis, S., Kreider, J., Mortera, A., Haverbeck, O., Kraus, S., Schmitz, F., DiGiovanna, J., van den Brand, R., ., Bloch, J., Detemple, P., Lacour, S.P.P., Bézard, E., Micera, S., and Courtine, G. (2016). Spatiotemporal neuromodulation therapies engaging muscle synergies improve motor control after spinal cord injury. Nature Medicine.

Wenzel, M., Hamm, J.P., Peterka, D.S., and Yuste, R. (2017). Reliable and Elastic Propagation of Cortical Seizures In Vivo. Cell Reports *19*, 2681–2693.

World Health Organization (WHO) (2013). Spinal Cord Injury. https://www.who.int/news-room/fact-sheets/detail/spinal-cord-injury.

Wictorin, K., Brundin, P., Gustavii, B., Lindvall, O., and Björklund, A. (1990). Reformation of long axon pathways in adult rat central nervous system by human forebrain neuroblasts. Nature *347*, 347556a0.

Wilson, J.R., and Fehlings, M.G. (2014). Riluzole for Acute Traumatic Spinal Cord Injury: A Promising Neuroprotective Treatment Strategy. World Neurosurg *81*, 825–829.

Witte, H., Neukirchen, D., and Bradke, F. (2008). Microtubule stabilization specifies initial neuronal polarization. J Cell Biology *180*, 619–632.

Woodbury, D., Schwarz, E.J., Prockop, D.J., and Black, I.B. (2000). Adult rat and human bone marrow stromal cells differentiate into neurons. J Neurosci Res *61*, 364–370.

Wu, D., Klaw, M.C., Connors, T., Kholodilov, N., Burke, R.E., Côté, M.-P., and Tom, V.J. (2017). Combining constitutively-active Rheb expression and chondroitinase promotes functional axonal regeneration after cervical spinal cord injury. Molecular Therapy.

Wu, S., Suzuki, Y., Ejiri, Y., Noda, T., Bai, H., Kitada, M., Kataoka, K., Ohta, M., Chou, H., and Ide, C. (2003). Bone marrow stromal cells enhance differentiation of cocultured neurosphere cells and promote regeneration of injured spinal cord. J Neurosci Res *72*, 343–351.

Wujek, J., and Lasek, R. (1983). Correlation of axonal regeneration and slow component B in two branches of a single axon. J Neurosci *3*, 243–251.

Xiao, Z., Tang, F., Tang, J., Yang, H., Zhao, Y., Chen, B., Han, S., Wang, N., Li, X., Cheng, S., Han, G., Zhao, C., Yang, X., Chen, Y., Shi, Q., Hou, S., Zhang, S., and Dai, J. (2016). One-year clinical study of NeuroRegen scaffold implantation following scar resection in complete chronic spinal cord injury patients. Science China. Life Sciences *59*, 647–655.

Xu, X., Guénard, V., Kleitman, N., Aebischer, P., and Bunge, M. (1995). A Combination of BDNF and NT-3 Promotes Supraspinal Axonal Regeneration into Schwann Cell Grafts in Adult Rat Thoracic Spinal Cord. Exp Neurol *134*, 261–272.

Yamawaki, N., Suter, B.A., Wickersham, I.R., and epherd, G. (2016). Combining Optogenetics and Electrophysiology to Analyze Projection Neuron Circuits. Cold Spring Harbor Protocols *2016*, pdb.prot090084.

Yan, D., and Jin, Y. (2012). Regulation of DLK-1 Kinase Activity by Calcium-Mediated

Dissociation from an Inhibitory Isoform. Neuron *76*, 534–548.

Yang, J.-L., Lin, Y.-T., Chuang, P.-C., Bohr, V.A., and Mattson, M.P. (2014). BDNF and Exercise Enhance Neuronal DNA Repair by Stimulating CREB-Mediated Production of Apurinic/Apyrimidinic Endonuclease 1. Neuromol Med *16*, 161–174.

Yao, R., Murtaza, M., Velasquez, T.J., Todorovic, M., Rayfield, A., Ekberg, J., Barton, M., and John, S.J. (2018). Olfactory Ensheathing Cells for Spinal Cord Injury. Cell Transplant *27*, 879–889.

Yizhar, O., Fenno, L.E., Prigge, M., Schneider, F., Davidson, T.J., O'Shea, D.J., Sohal, V.S., Goshen, I., Finkelstein, J., Paz, J.T., Stehfest, K., Fudim, R., Ramakrishnan, C., Huguenard, J.R., Hegemann, P., and Deisseroth, K. (2011). Neocortical excitation/inhibition balance in information processing and social dysfunction. Nature *477*, 171–178.

Yuste, R., and Katz, L.C. (1991). Control of postsynaptic Ca2+ influx in developing neocortex by excitatory and inhibitory neurotransmitters. Neuron *6*, 333–344.

Zhang, H., Fang, X., Huang, D., Luo, Q., Zheng, M., Wang, K., Cao, L., and Yin, Z. (2018). Erythropoietin signaling increases neurogenesis and oligodendrogenesis of endogenous neural stem cells following spinal cord injury both in vivo and in vitro. Mol Med Rep *17*, 264–272.

Zhang, N., Fang, M., Chen, H., Gou, F., and Ding, M. (2014). Evaluation of spinal cord injury animal models. Neural Regen Res *9*, 2008–2012.

Zhao, R., Andrews, M.R., Wang, D., Warren, P., Gullo, M., Schnell, L., Schwab, M.E., and Fawcett, J.W. (2013). Combination treatment with anti-Nogo-A and chondroitinase ABC is more effective than single treatments at enhancing functional recovery after spinal cord injury. Eur J Neurosci *38*, 2946–2961.

Zörner, B., and Schwab, M.E. (2010). Anti-Nogo on the go: from animal models to a clinical trial. Ann Ny Acad Sci *1198*, E22–E34.

Zörner, B., Bachmann, L.C., Filli, L., Kapitza, S., Gullo, M., Bolliger, M., Starkey, M.L., Röthlisberger, M., Gonzenbach, R.R., and Schwab, M.E. (2014). Chasing central nervous system plasticity: the brainstem's contribution to locomotor recovery in rats with spinal cord injury. Brain : A Journal of Neurology *137*, 1716–1732.

Zukor, K., Belin, S., Wang, C., Keelan, N., Wang, X., and He, Z. (2013). Short hairpin RNA against PTEN enhances regenerative growth of corticospinal tract axons after spinal cord injury. The Journal of Neuroscience : The Official Journal of the Society for Neuroscience *33*, 15350–15361.

CHAPTER 2

Graft-Host Synaptic Connectivity in Spinal Cord Injury Revealed by Calcium Imaging

Ceto S[1,2,3,*], Sekiguchi KJ[4], Takashima Y[1,3], Nimmerjahn A[4], Tuszynski MH[1,3,*]

[1]Department of Neurosciences and [2]Biomedical Sciences Graduate Program, University of California, San Diego, La Jolla, CA 92093 USA;

[3]Veterans Administration Medical Center, San Diego, La Jolla, CA 92161 USA;

[4]Waitt Advanced Biophotonics Center, Salk Institute for Biological Studies, La Jolla, CA 92037 USA

*Correspondence: sceto@ucsd.edu (S.C.) or mtuszynski@ucsd.edu (M.H.T)

Summary

Neural stem/progenitor cell grafts integrate into sites of spinal cord injury (SCI) and form anatomical and electrophysiological neuronal relays across lesions. To determine how grafts become synaptically organized and connect with host systems, we performed calcium imaging of neural progenitor cell grafts within sites of SCI, using both *in vivo* imaging and spinal cord slices. Stem cell grafts organize into localized synaptic networks that fire spontaneously with a predominance of excitatory activity. Following optogenetic stimulation of host corticospinal tract axons regenerating into grafts, distinct and segregated neuronal networks respond throughout the graft. Moreover, optogenetic stimulation of graft axons extending out from the lesion into the denervated spinal cord also trigger responses in local *host* neural networks. In vivo imaging reveals that behavioral stimulation of host elicits focal synaptic responses within grafts. Thus, remarkably, neural progenitor cell grafts form functional synaptic subnetworks in patterns paralleling the normal spinal cord.

INTRODUCTION

Eliciting regeneration of the injured adult central nervous system (CNS) is, despite recent progress, extraordinarily difficult. While experimental approaches targeting multiple mechanisms can succeed in promoting injured host axonal regeneration into and even beyond sites of spinal cord injury (SCI) (Alto et al., 2009; Assinck et al., 2017; Bráz et al., 2012; Jayaprakash et al., 2019b; Liu et al., 2010; Lu et al., 2012), the number and distance of host axonal regeneration is limited: typically, only hundreds of host axons regenerate for distances that rarely exceed 1-2 mm. In contrast,

recent reports indicate that neural progenitor cells (NPCs) or neural stem cells (NPCs) implanted into sites of SCI support quite extensive host axon regeneration into grafts occupying the lesion site, while axons emerging from the grafted neurons extend into the distal host spinal cord in very large numbers (tens to *hundreds of thousands* of axons) and for long distances (up to 50 mm) (Kadoya et al., 2016; Lu et al., 2012, 2014; Rosenzweig et al., 2018). Indeed, even after complete spinal cord transection, NPC and NSC grafts support significant functional improvement (Koffler et al., 2019; Lu et al., 2012), and this functional improvement is abolished if the spinal cord is re-transected immediately rostral to the lesion site, suggesting that novel synaptic relays have formed from host-to-graft-to-host across the lesion site.

Little is known, however, regarding the synaptic architecture generated in NPC and NSC grafts placed in host spinal cord lesion sites. It is clear that host axons regenerating into grafts form synaptic contacts onto graft neurons (Adler et al., 2017; Dulin et al., 2018; Kumamaru et al., 2019; Lu et al., 2012; Rosenzweig et al., 2018) and are capable of generating post-synaptic currents (Jayaprakash et al., 2016; Kadoya et al., 2016; Tornero et al., 2017) that can increased the firing rate of graft neurons (Jayaprakash et al., 2019). Similarly, graft neurons in sites of stroke in the cerebral cortex respond to optogenetic stimulation of thalamo-cortical axons as well as physiological tactile stimulation (Tornero et al., 2017). Graft neurons can also modulate activity in host neuron populations (Etlin et al., 2016; Steinbeck et al., 2015). However, how host axons regenerating into grafts influence graft activity has not been described, and several possibilities exist. First, regenerating host axons may form circumscribed synaptic connections that represent single axon-to-graft single neuronal relays,

representing highly circumscribed host-graft pairings. Second, regenerating host axons may recruit larger networks of graft neurons, activating multiple or dozens of graft neurons, functioning as a network that parallels previously described patterns of cortico-spinal projections in the intact spinal cord (Lemon, 2008; Ueno et al., 2018). A third possibility is that the graft functions as a transmitter of slow neural activation, as described in spreading depression or activation of the cortex (Bikson et al., 2003; Pinto et al., 2005; Wenzel et al., 2017); in this case, one would predict that activation of host motor axons regenerating into grafts would elicit a wave of excitation in the graft that could be slowly propagated across the graft in the lesion site. Given the benefit of NPC/NSC grafts in improving functional outcomes after SCI in both rodents (Brock et al., 2017; Kadoya et al., 2016; Koffler et al., 2019; Kumamaru et al., 2018; Lu et al., 2012, 2017) and primates (Rosenzweig et al., 2018) it is important to gain an improved understanding regarding which of these mechanisms may be operative.

Thus, to gain insight into the nature of synaptic connectivity and functionality between regenerating host axons and graft neurons in a spinal cord lesion, we optogenetically stimulated host corticospinal axons regenerating into NPC grafts placed into sites of mid-cervical SCI in rats. Graft neurons expressed a genetically encoded calcium indicator (Anderson et al., 2018; Kadoya et al., 2016; Liu et al., 2017; Lu et al., 2012), allowing whole-graft imaging of activity in up to hundreds of cells simultaneously in spinal cord slices. In addition, we performed live in vivo imaging of calcium activity during host stimulation. Finally, we probed the nature of graft-to-host synaptic connectivity by optogenetically stimulating graft-derived axons in host spinal cord neurons caudal to the lesion site that expressed calcium indicators, in slices. We now

find that regenerating host corticospinal axons elicit robust and widespread calcium responses in graft neurons, generating synchronous activity in assemblies of graft neurons that resemble physiological patterns of corticospinal inputs to intact spinal cords. In turn, stimulation of graft axons extending caudal to the lesion site also activates networks of host spinal neurons in slices. Moreover, in vivo calcium imaging reveals that graft neurons respond to sensory stimuli delivered to the host, including light touch, pinch, and cold air puff. These findings show that neural progenitor cells grafts form active synaptic networks within sites of SCI.

RESULTS

Experimental Design

We expressed the red-shifted channelrhodopsin Chrimson in corticospinal neurons using adeno-associated viral vectors (AAV) containing the pan-neuronal synapsin promoter (AAV-Syn-ChrimsonR-tdTomato) (Klapoetke et al., 2014). AAV-Syn-ChrimsonR-tdTomato was injected bilaterally into the motor cortices of postnatal day zero (P0) wild-type C57BL/6 mice, resulting in robust expression in corticospinal axons in the lumbar spinal cord (**Figure 1A-D**). Six to eight weeks later, mice underwent T12 dorsal column spinal cord lesions to transect the corticospinal motor projection. In the same session, embryonic day 12 (E12) spinal cord multipotent neural progenitor cells that expressed the calcium indicator GCaMP6f were grafted directly into the lesion site (Chen et al., 2013) (**Figure 1D,E**; **Figure S1**; see Methods). Six to ten weeks post-injury/grafting, animals were prepared for either live spinal cord slice observations (N =

Figure 2.1: Chrimson-expressing corticospinal axons regenerate robustly into GCaMP6f-expressing neural progenitor cell grafts

(A) Experimental timeline. Animals received cortical injections of AAV-ChrimsonR at postnatal day 0 (P0). T12 dorsal column lesions and acute NPC grafting were performed at 6 – 8 weeks of age. Calcium imaging was performed 6 – 8 weeks later. (B) Sagittal section of adult whole brain shows abundant expression of ChrimsonR-tdTomato in cortex following neonatal AAV injections. Neurons labeled with NeuN. Inset in (B) shown at higher magnification in (C). (D-E) Chrimson-labeled CST main tract axons (D) regenerate robustly into neural progenitor cell grafts expressing GCaMP6f in neurons (E) in a graft-specific, Cre-dependent manner. In all images, the dorsal aspect of the slice is at the top and the rostral aspect is at left. Scale bar, 2 mm (B); 200 μm (C-E). Brightness and contrast adjusted for clarity across entire images (B-E).

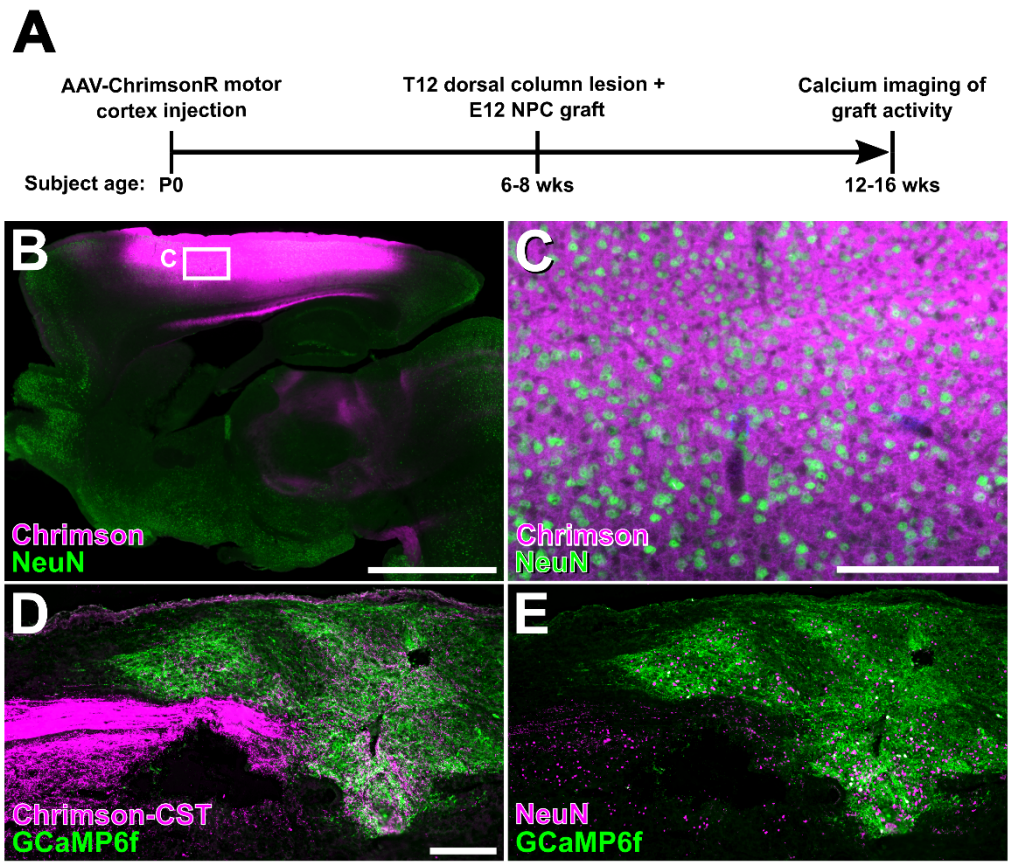
A
AAV-ChrimsonR motor cortex injection
T12 dorsal column lesion + E12 NPC graft
Calcium imaging of graft activity
Subject age: P0
6-8 wks
12-16 wks
B
C
Chrimson
NeuN
C
Chrimson
NeuN
D
Chrimson-CST
GCaMP6f
E
NeuN
GCaMP6f

27 animals) or *in vivo* calcium imaging (N = 15 animals), as described below. For animals undergoing slice preparation, most of the thoracic and lumbar cord was prepared in the sagittal plane.

Spinal Cord Slices

Using a custom filter set and a standard widefield electrophysiology microscope, corticospinal axons regenerating into neural progenitor cell grafts were stimulated with a 617 nm LED through the objective lens, and graft activity was imaged for neural activity (**Figure S2A**). Regions of interest (ROIs) with neuronal morphology and dynamic fluorescence were manually outlined (**Figure S2B-C**). The number of detectably active neurons in a field of view was in the range of 10-100 cells. In standard artificial cerebrospinal fluid (aCSF) recording solution, grafts displayed spontaneous activity and responses to stimulation of corticospinal axons regenerating into the lesion site filled with graft (**Figure S2D**). Addition of the potassium channel blocker 4-aminopyridine (4-AP, 100μM) (Blight et al., 1991; Liu et al., 2017; Strupp et al., 2017), a drug approved for human use, to the aCSF increased detectable spontaneous activity and responses to corticospinal stimulation (**Figure S2E-G**), and was used in most recordings. Episodes of activity in individual neurons were defined as periods of increasing fluorescence (positive first derivative of the change in fluorescence over time, ΔF/F, after noise subtraction) during fluorescence transients considered significantly above noise (based on a dynamic threshold incorporating the individual cell's calculated noise model and the decay kinetics of the calcium reporter) (Romano et al., 2017).

Spontaneous Activity: Grafts are Organized into Networks of Synchronously Active Neurons

Graft neurons exhibited spontaneous activity in single cells as well as in clusters of cells that were activated in broad, synchronous events at a rate of 2.33 ± 1.10 activations/min (n = 15 clusters in N = 4 animals) (**Figure 2A-C, Figure S3**). These groups consisted of 5.72 ± 0.46 cells that tended to neighbor one another topographically, although some clusters included more distantly spaced neurons (mean inter-ROI distance = 118 ± 27 μm; **Figure 2B**). The PCA-promax method of clustering synchronously active cells (Hendrickson and White, 1964; Peyrache et al., 2010; Romano et al., 2017) demonstrated that most individual neurons within grafts belonged to only a single cluster of cells, rather than contributing to multiple, distinct cell clusters (mean 4.7 ± 3.1% of cells belonging to more than one cell cluster). This largely independent arrangement of clusters suggests a degree of compartmentalization in the functional topography of grafts.

To confirm the validity of cell clusters that we identified based on patterns of concurrent spontaneous activity, we generated control “surrogate” clusters from the total pool of ROIs in each slice (Romano et al., 2017). At the beginning of the analysis pipeline, neurons are numbered by their location in the field of view from left to right. A cluster of synchronously active neurons is defined by a list of the numerical indices of the neurons belonging to that cluster. Surrogate clusters were generated by preserving these lists but shuffling the original neuron indexing. Thus, sets of surrogate clusters contained the same number of neurons in each cluster as the original set, and overlap between clusters was preserved. These surrogate control clusters were either

Figure 2.2: Clusters of graft neurons display episodes of synchronous activity and respond to CST stimulation

(A) Fluorescence traces of 93 graft cells exhibiting spontaneous activity. Red portions of traces indicate periods of significant activity as determined by first derivative rasterization. (B) Standard deviation projection of the run shown in (A) with all ROIs outlined in yellow and clusters of neurons with similar activity dynamics indicated by fill color. (C) First derivative raster plot (top) of traces from (A), with cells grouped into the clusters shown in (B). Cells above red line belonged to clusters. Significant activations of color-coded clusters are plotted below. (D) The mean activity of cells belonging to clusters was not significantly different from that in randomly (RSC) or topographically (TSC) generated surrogate clusters (N = 4 animals). (E) Cells in clusters showed significantly more pairwise correlation than those of surrogate clusters (N = 4 animals). (F) Same graft as in (B) with clusters extracted from a run with optogenetic CST stimulation. (G) As in (C), during a run with four trials of 500 ms, 20Hz CST stimulation. Scale bar, 200 μm (B,F). In all images, the dorsal aspect of the slice is at the top and the rostral aspect is at left. Brightness and contrast adjusted for clarity across entire images. Data are represented as mean ±SEM with significance determined by Welch's t-test (*$p<0.05$; NS, not significant).

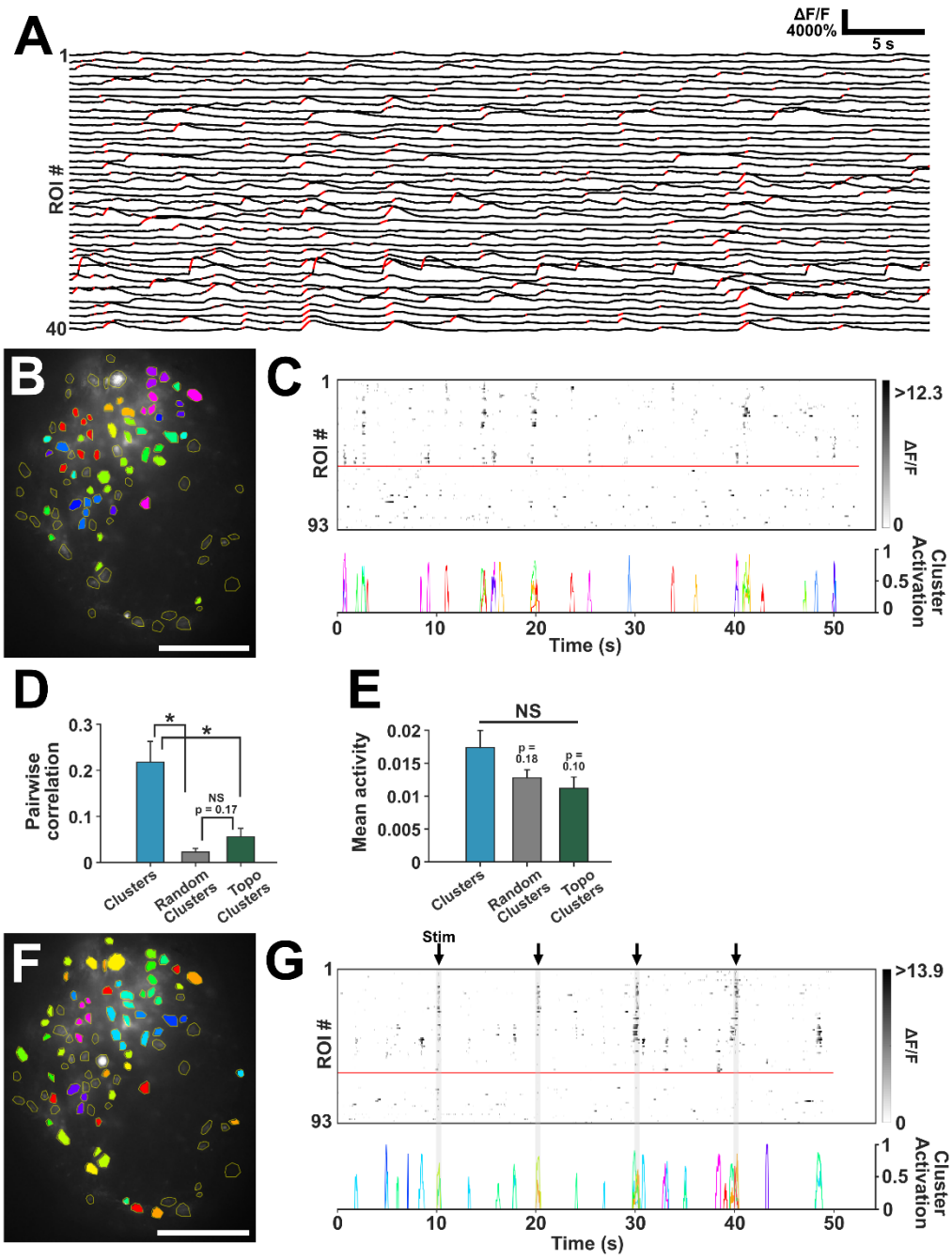
A
ΔF/F
4000%
5 s
1
ROI #
40
B
C
1
ROI #
93
>12.3
ΔF/F
0
1
0.5
0
Cluster Activation
0
10
20
30
40
50
Time (s)
D
Pairwise correlation
0.3
0.2
0.1
0
*
*
NS
p = 0.17
Clusters
Random Clusters
Topo Clusters
E
Mean activity
0.02
0.015
0.01
0.005
0
NS
p = 0.18
p = 0.10
Clusters
Random Clusters
Topo Clusters
F
G
Stim
1
ROI #
93
>13.9
ΔF/F
0
1
0.5
0
Cluster Activation
0
10
20
30
40
50
Time (s)

completely random groupings or topographically similar to the originally identified clusters in terms of the distances between cells within the clusters. One hundred random and 100 topographical surrogate controls were generated for each original cluster, and these control data sets were compared to *experimentally-identified* clusters. Experimentally identified clusters had similar levels of mean activity per cell compared to surrogates, but much higher pairwise activity correlation between cells, indicating that the clusters were not merely groups of cells with increased activity but assemblies of cells grouped either by direct connectivity or shared pre-synaptic inputs (Carrillo-Reid et al., 2016; Yuste, 2015) (**Figure 2D-E**).

Corticospinal Input-Evoked Network Activity: Graft Neuronal Clusters Fire Synchronously

Next, we sought to identify patterns of synaptic organization in grafts following stimulation of host corticospinal axons regenerating into grafts. Optogenetic stimulation of corticospinal axons within grafts activated *the same graft neuronal clusters* that were identified based on spontaneous activity. Indeed, 22.5 ± 13.2% of clusters that displayed spontaneous activations in a 50 s imaging run also responded to stimulation with cluster-wide activation of neurons in the same run (n = 18 clusters in N = 4 animals, **Figure 2F-G**), suggesting specificity in response patterns to corticospinal stimulation rather than all-or-nothing graft activation. Cluster responses began immediately following stimulus onset and decayed quickly; slow patterns of graft excitation and propagation through grafts were never observed. Grafts therefore efficiently encode inputs within preexisting neural networks. To compare these activity patterns to normal

spinal cord processing of CST inputs, we also performed these experiments in intact spinal cord slices (**Figure S4**). In parallel with graft responses, spinal cord neurons of the medial and dorsal gray matter displayed spontaneous activity in individual neurons and synchronously active clusters, both of which could be activated by optogenetic CST stimulation.

Graft neuron response properties

Graft neurons displayed robust calcium responses to corticospinal optogenetic stimulation within hundreds of milliseconds of stimulus onset (**Figure 3A-C**). At the low magnification used for population calcium imaging, subthreshold fluctuations in membrane potential are not generally detectable above noise, whereas single action potentials can be resolved with modern genetically encoded calcium indicators such as GCaMP6f (Emiliani et al., 2015; Lin and Schnitzer, 2016). We therefore interpret the fast-rising and slow-decaying fluorescence transients observed in response to corticospinal stimulation to be the result of one or more action potentials firing in graft neurons. The fluorescence traces in responding cells began to rise immediately following stimulus onset and reached their temporal midpoint to peak fluorescence less than halfway through the 500 ms stimulus (**Figure 3E**), indicating that the responses saturate in less than half a second. These responses were mediated through excitatory transmission, as indicated by their disappearance in the presence of the glutamatergic blocker 6,7-dinitroquinoxaline-2,3-dione (DNQX) (**Figure 3E,F**). The magnitude of response strength (average $\Delta F/F$ over 1 s following stimulus onset) and percent of responding cells ($\Delta F/F \geq 100\%$) increased with increasing power of the LED stimulation

Figure 2.3: Graft neurons are activated by optogenetic stimulation of regenerated CST axons

(A) One second average of ΔF/F video immediately prior to stimulation onset shows a small number of spontaneously active graft neurons. (B-C) As in (A), immediately following stimulation onset. GCaMP6f fluorescence in several graft cells increases in response to stimulation of regenerated CST axons (cyan numbered arrows in C). (D) Example traces from cells labeled in (C) during a 50 s period over which four CST stimuli (vertical cyan bars) were delivered. Stimuli consisted of 500 ms-long 20 Hz trains of 10 ms pulses of 617 nm light. Irradiance at the slice was 4.49 mW/mm^2. Significant fluorescence transients are highlighted in red. Cells display varying response strengths as well as spontaneous activity. (E) Mean response traces with ±SEM shade of n = 7 cells in one slice to 12 trials in standard recording conditions, + 100 μM 6,7-dinitroquinoxaline-2,3-dione (DNQX), and after DNQX washout. Responses were abolished by the AMPA and kainite receptor antagonist DNQX, indicating the presence of excitatory synaptic connections from CST axons onto graft neurons. (F) Mean response strengths from (E), quantified over one second following stimulus onset. (G) Mean response strength quantified as in (G) in response to increasing 617 nm LED irradiance. Responses in n = 16 cells in one slice increased in strength with increasing irradiance but began to plateau at higher irradiance. (H) The percentage of cells activated (activation threshold = 100% ΔF/F) by CST stimulation also increased with increasing 617 nm LED irradiance. In all images, the dorsal aspect of the slice is at the top and the rostral aspect is at left. Brightness and contrast adjusted for clarity across entire images. Scale bar, (A-C), 200 μm. Two-group comparisons were tested with Welch's t-test (**$p<0.01$; NS, not significant). Data are represented as mean ±SEM unless otherwise indicated.

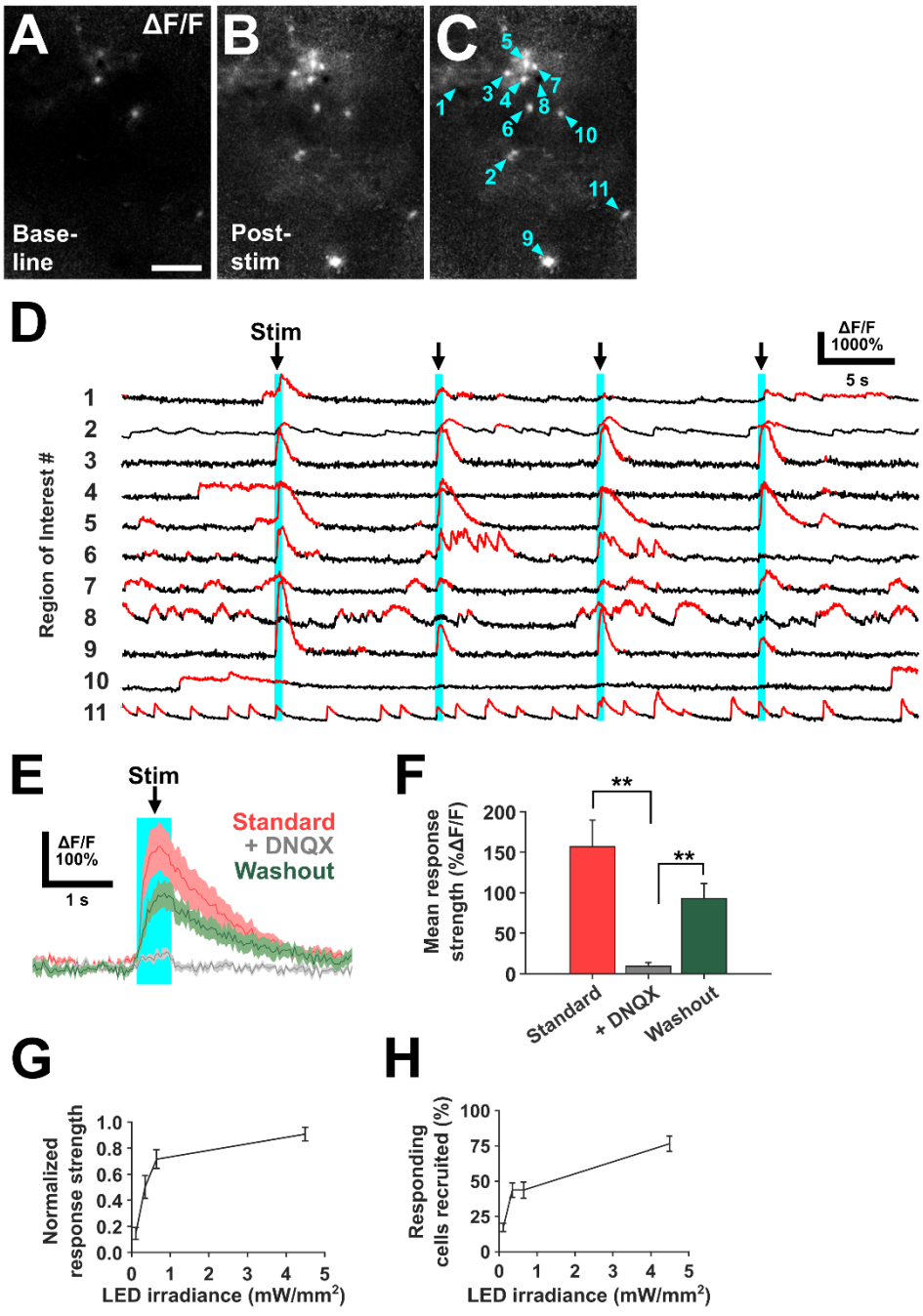
A
ΔF/F
Base-
line
B
Post-
stim
C
1
2
3
4
5
6
7
8
9
10
11
D
Stim
ΔF/F
1000%
5 s
Region of Interest #
1
2
3
4
5
6
7
8
9
10
11
E
Stim
ΔF/F
100%
1 s
Standard
+ DNQX
Washout
F
Mean response
strength (%ΔF/F)
200
150
100
50
0
**
**
Standard
+ DNQX
Washout
G
Normalized
response strength
1.0
0.8
0.6
0.4
0.2
0.0
0
1
2
3
4
5
LED irradiance (mW/mm²)
H
Responding
cells recruited (%)
100
75
50
25
0
0
1
2
3
4
5
LED irradiance (mW/mm²)

(**Figure 3G,H**), demonstrating that graft responses encode stimulus strength. When AAV-Chrimson was not injected into the cortex, graft cells did not respond to LED stimulation in the absence of opsins (N = 6 animals; **Figure S2H**), indicating that graft responses to are not artifacts of direct photoactivation by the light stimulus.

Cells throughout grafts responded to corticospinal stimulation, even at the most caudal aspect, furthest from the point at which the main tract of corticospinal axons enters the graft (**Figure 4A-C**). While the density of ChrimsonR-tdTomato-labeled axons varied throughout different regions of grafts, as previously observed (Dulin et al., 2018; Kumamaru et al., 2019), response strength to corticospinal stimulation in a given cell was uncorrelated with the brightness of tdTomato signal in the corresponding region of interest (n = 68 cells in N = 3 animals; response strength and tdTomato brightness normalized to their respective maximum in each imaging field; **Figure 4D-E**). Thus, graft cells are activated by corticospinal stimulation in all regions of grafts, including the distal aspect that contains the preponderance of caudally-projecting cells (Lu et al., 2019).

Graft axon stimulation of host neurons

Having observed this activation of *clusters* of cells throughout grafts following stimulation of regenerating corticospinal axons, we next sought to determine whether grafts could in turn activate host spinal neurons caudal to the injury site. We mixed AAV-Syn-FLEX-ChrimsonR-tdTomato vectors with Syn1-Cre neural progenitor cells just prior to grafting acutely into T12 dorsal column lesions. This yielded graft-specific expression of ChrimsonR-tdTomato, which was readily detectable in *axons* extending out from the graft borders and into the distal host spinal cord (**Figure 5A-B**). Three to

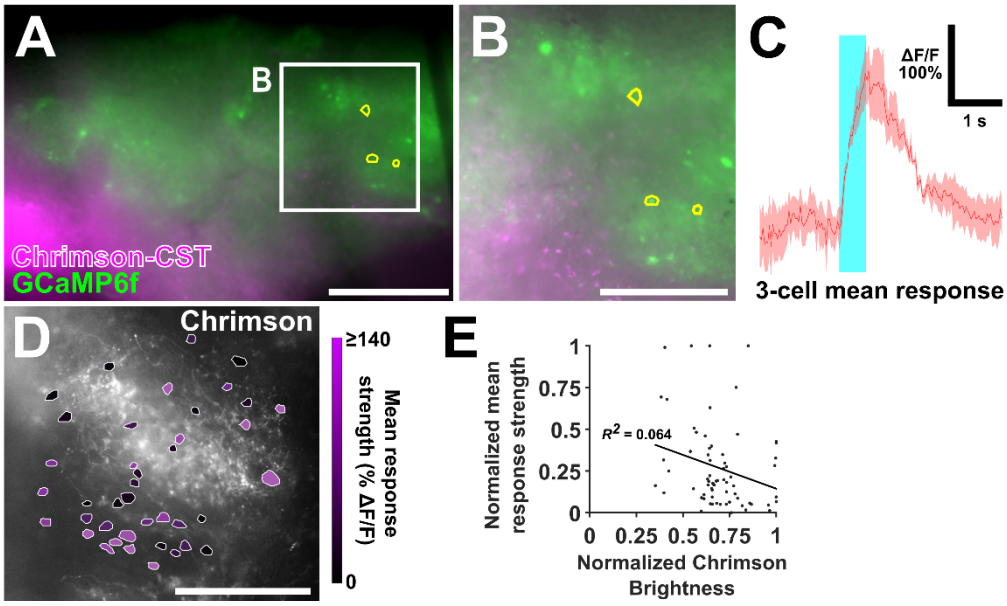

Figure 2.4: Graft neurons respond to CST stimulation even in areas of low Chrimson expression and in sensory neuron clusters.

(A) Overview of an exceptionally large graft with three cells in the most caudal area that responded to CST stimulation outlined in yellow. (B) Higher magnification of inset from (A) showing attenuation of Chrimson axon presence rostral to location of responding cells. (C) Mean ±SEM shade traces of the responses of the three cells in (A-B) to 12 trials of the same optogenetic stimulation (vertical cyan bar) as in Figure 2D. (D) Overlay of response strength in graft cells on native ChrimsonR-tdTomato fluorescence showing responsive cells in areas of both high and low Chrimson brightness. (E) No correlation was seen between the response strength and Chrimson brightness in n=68 cells from N=3 animals. Response strength and Chrimson brightness were normalized to the respective maximums in each field of view. A least-squares linear fit to the data is shown. In all images, the dorsal aspect of the slice is at the top and the rostral aspect is at left. Brightness and contrast adjusted for clarity across entire images. Scale bars, 300 μm (A); 150 μm (B, D).

four weeks after grafting, AAV9-Syn-GCaMP6f was injected 1.2 mm caudal to grafts into host central gray matter (**Figure 5A-B**). When imaged 6-8 weeks after grafting, a total of 15 host neurons were detected (in 2 out of 18 animals) that responded to whole-field stimulation of graft axons (**Figure 5C-F**). Responding cells were located in the medial and dorsal gray matter, but no responses could be detected in ventral motor pools. This may have been a result of poor GCaMP6f expression in more ventral regions, however, as numerous graft axons were visible in these areas, whereas minimal spontaneous cell activity or anti-GFP immunoreactivity was observed (**Figure 5B**). Responses were eliminated with DNQX administration, indicating that host responses to graft axon stimulation were mediated through excitatory synaptic transmission (**Figure 5G**). The latency of these responses was less than 200 ms, showing that, as in grafts, responses peaked before the end of the 500 ms light stimulus. Thus, neural progenitor cell grafts are capable of activating host neurons below spinal cord lesions.

In vivo imaging of graft activity

Preceding studies in slices demonstrated that host axons stereotypically activated *clusters* of graft neurons when stimulated optogenetically. To examine activation of graft neurons by behavioral stimulation of the host, we turned to in vivo imaging of graft activity (Farrar et al., 2012; Sekiguchi et al., 2016). Animals underwent T12 dorsal column spinal cord lesions followed by placement of E12 neural progenitor cell grafts expressing GCaMP6f into the lesion site. Six to ten weeks later, spinal stabilization hardware and imaging windows were implanted over the dorsal surface of

Figure 2.5: Host neurons are activated by optogenetic stimulation of axons extending from grafts

(A) Grafts expressing Chrimson extended axons into host gray and white matter rostral and caudal to the lesion site. (B) Inset from (A) showing graft axon innervation of regions of GCaMP6f-expressing host spinal cord neurons caudal to the lesion. Note the attenuation of GCaMP6f labeling in more ventral gray matter (bottom). (C) One second average $\Delta F/F$ image of host spinal cord neurons just prior to stimulus onset. (D) As in (C), one second following onset of 500 ms optogenetic stimulation of graft axons. (E) Mean response strength map of host neurons over one second following stimulus onset. (F) Individual cell fluorescence traces of the cells in (E) show abundant spontaneous activity as well as consistent responses in some cells to graft axon stimulation. (G) Mean ±SEM traces of n = 5 responding cells from one slice before and after wash-in of 100 μM DNQX, showing that grafts form excitatory synaptic connections with host neurons below the lesion. In all images, the dorsal aspect of the slice is at the top and the rostral aspect is at left. Brightness and contrast adjusted for clarity across entire images. Scale bars, 300 μm (A); 100 μm (B-E).

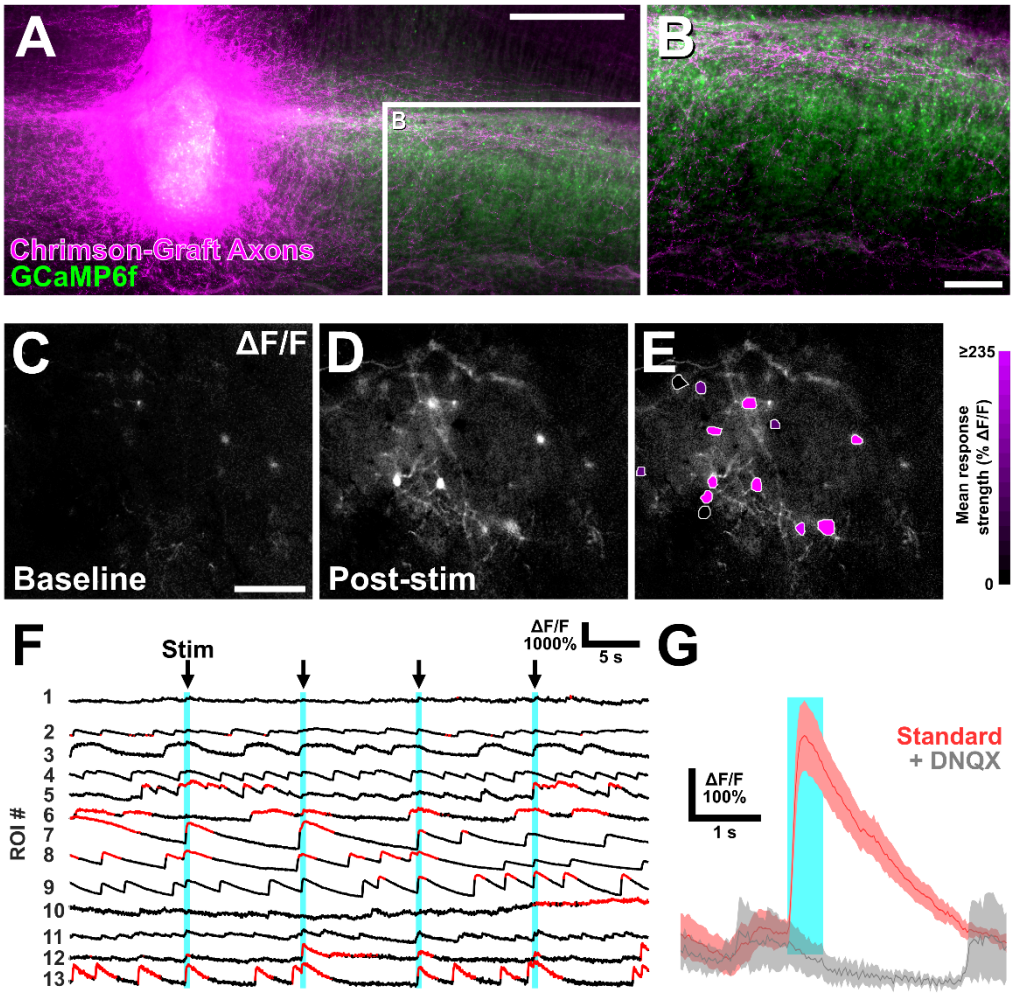
A
B
Chrimson-Graft Axons
GCaMP6f
B
C
ΔF/F
Baseline
D
Post-stim
E
≥235
Mean response strength (% ΔF/F)
0
F
Stim
ΔF/F 1000%
5 s
ROI #
1
2
3
4
5
6
7
8
9
10
11
12
13
G
ΔF/F 100%
1 s
Standard
+ DNQX

grafts, as previously described (Farrar et al., 2012; Sekiguchi et al., 2016). Grafts were imaged one hour after window implantation. With a detectable depth of imaging of approximately 100 μm into grafts, we observed spontaneous activity of graft neurons (**Figure 6A-C**). When the host was stimulated by hindpaw pinch (**Figure 6D-E**), light touch of the lower back (**Figure 6F-G**), or passive movement of the hindlimb (**Figure 6H**),individual graft neuronal responses were detected in four out of seven animals with detectable graft activity. These responses could be consistently reproduced without diminishing in strength over repeated stimuli. Cells typically responded to a single stimulus type, though two neighboring ROIs responded to both hindlimb movement and light touch of the lower back in one animal (**Figure 6F-H**). Thus, host sensory systems functionally connect to grafts and elicit synaptic responses.

DISCUSSION

Calcium imaging reveals that host axons regenerating into neural progenitor cell grafts placed into sites of SCI activate clusters of responsive graft neurons. Regenerating host axons do not appear to nonspecifically activate slow waves of activity through grafts; instead, host activation of graft neuronal clusters is a pattern that recapitulates responses of intact spinal systems (Johannssen and Helmchen, 2013; Sekiguchi et al., 2016). Considering the highly anomalous milieu that we are studying, i.e., “developing” neural tissue placed in an *adult* spinal cord lesion site, it is remarkable that the resulting patterns of synaptic connectivity resemble intact spinal cord responses. Moreover, we show that grafts not only respond to optogenetic stimulation of regenerating host axons, but to *behavioral* stimulation of the host. Graft neurons

Figure 2.6: Graft neurons respond to sensory stimuli in vivo

(A-C) Baseline average ΔF/F image of a graft neuron over a one second period just prior to (A) and one second following onset of a spontaneous calcium transient (B) in a single graft neuron with transgenic GCaMP6f expression in an anesthetized animal. (C) Fluorescence trace of the calcium transient shown in (C). (D) Maximum projection image of in vivo calcium activity during a period of three hindpaw pinch stimuli. ROIs (yellow outlines) include both neuronal soma and processes. (E) Fluorescence traces of the activity in the ROIs shown in (D) during hindpaw pinch stimuli (purple trace). Graft neurons showed variable response latency and consistency. (F) Standard deviation projection of viral GCaMP6f expression in vivo over a period of light touch stimuli. ROIs are highlighted in yellow. (G) Several ROIs responded consistently to light touch stimuli. (H) Two cropped ROIs from the same field of view as (E) responded consistently to movement of the hindlimb through its range of motion by the experimenter. These ROIs, which may be part of a single neuron or neuron cluster, were on the left side of the graft and responded to left hindlimb movement (green bars) but not right hindlimb movement (pink bars). Brightness and contrast adjusted for clarity across entire images. Scale bars, (A-B), 25 μm; (D), 30 μm; (F), 50 μm.

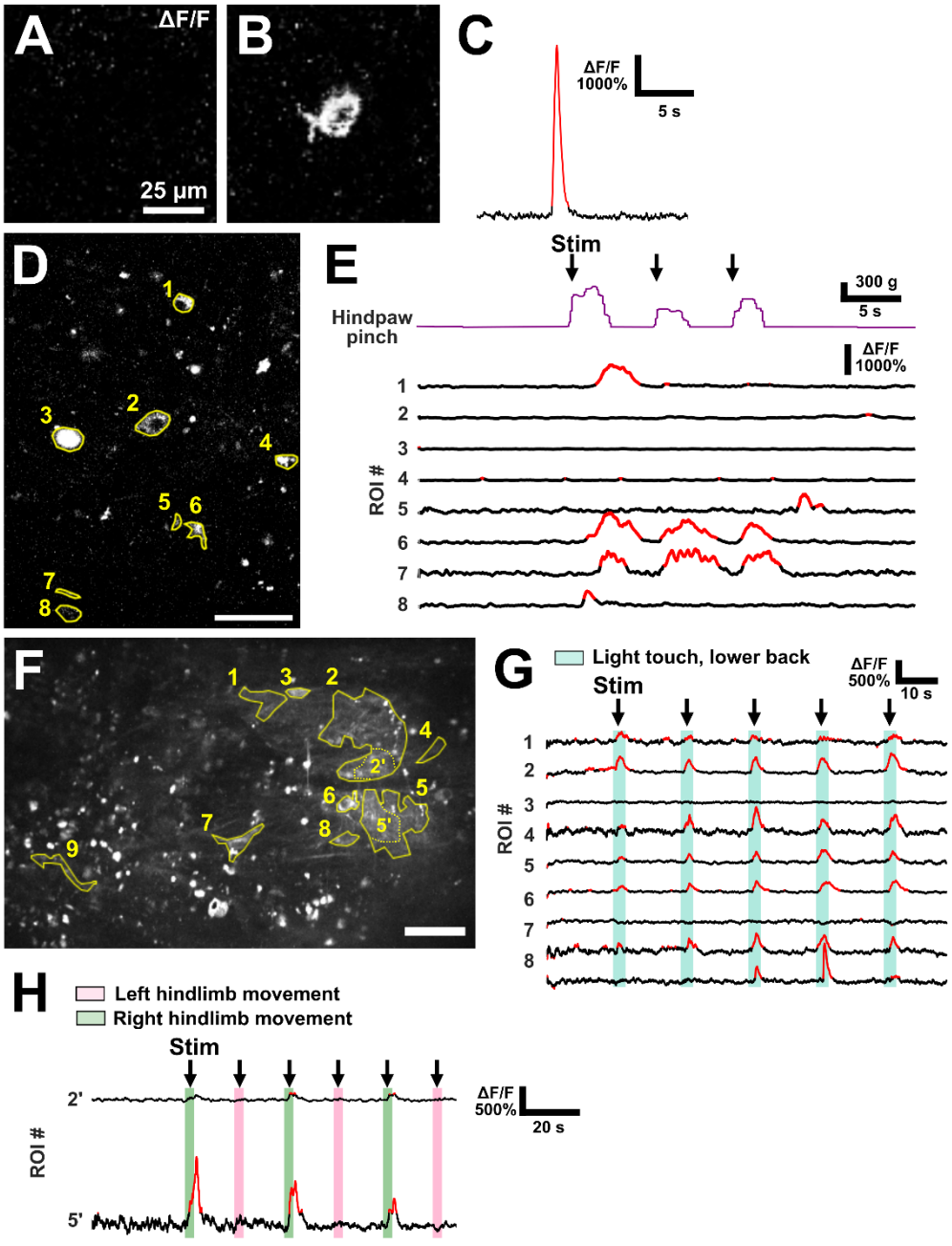
A
ΔF/F
25 μm
B
C
ΔF/F
1000%
5 s
D
1
2
3
4
5
6
7
8
E
Stim
Hindpaw
pinch
300 g
5 s
ΔF/F
1000%
ROI #
F
G
Light touch, lower back
Stim
ΔF/F
500%
10 s
H
Left hindlimb movement
Right hindlimb movement
Stim
2'
5'
ΔF/F
500%
20 s

respond to corticospinal input as quickly as is detectable with calcium imaging methods. The latency of the temporal midpoint to peak response amplitude was 100-300 msec, and cell fluorescence began to increase within one to two imaging frames (about 30 -60 ms) of stimulus onset cells throughout grafts. These findings indicate that, rather than gradually 'turning on' the graft through a slowly spreading wave of excitation, corticospinal input is capable of activating graft neurons on a timescale of tens to hundreds of milliseconds. Similar response latencies were obtained for host neurons below the lesion to graft axon stimulation. While the underlying electrical activity which gives rise to GCaMP6f fluorescence spikes occurs on a much shorter timescale (Chen et al., 2013), even an extremely conservative fluorescence-based estimation would place the time for a full relay across the lesion at no more than a few hundred milliseconds.

In the dorsal column lesion model employed in this study, regenerating corticospinal axons were present throughout the rostro-caudal length of the graft, and responses to corticospinal stimulation were also observed over this rostral-to-caudal range. Similarly, response strength did not depend on local density of Chrimson-expressing fibers. These widespread responses to light stimulation could be due to the dendritic processes of graft neurons extending into areas of denser Chrimson-expressing axon innervation or through polysynaptic connections with other graft cells receiving direct corticospinal input. Among all spontaneously active neuron clusters in grafts, approximately one-fourth responded to corticospinal stimulation. This limited responsiveness could reflect an incomplete extent of axonal regeneration, but it could also indicate that regenerating corticospinal axons may elicit responses from

subdomains of grafts containing appropriate corticospinal target neurons, as suggested in recent studies (Kumamaru et al., 2019; Dulin et al., 2018).

Findings of this study suggest that host axons regenerating into neural stem cell grafts recapitulate synaptic patterns of organization of the intact spinal cord. Future experiments will aim to address some of the limitations of this study. First, the depth of calcium visualization in our in vivo imaging experiments was ~100μm, which is too superficial to visualize most of the regenerating corticospinal axons, which tend to penetrate deeper regions of the grafts. New imaging methods, including the use of intraspinal prisms, may in the future allow assessment of graft responses to motor behaviors in aware, behaving animals after SCI (Andermann et al., 2013; Chia and Levene, 2010). Second, levels of calcium reporter expression likely varied among individual graft neurons, and more equivalent expression levels in grafts derived from transgenic rats expressing GCaMP using CRISPR may improve graft imaging. Third, development of more sensitive calcium indicators may also improve imaging methods. Finally, we note that the continued development of red-shifted optogenetic tools may present the exciting future possibility of stimulating graft neurons either transdermally or with implanted actuators, allowing assessment of whether synchronizing of graft activity with motor behaviors in awake animals may further improve the functional efficacy of grafts.

CONCLUSION

Calcium imaging combined with optogenetic stimulation is a novel and viable approach to interrogate synaptic connectivity between host and neural stem/progenitor

cell graft neurons. We now find that grafts receive synaptic inputs from regenerating host axons, forming clusters of synchronously active neurons, and graft axons also form synaptically active outputs onto host neurons below the lesion. In vivo calcium imaging shows the functional integration of host inputs to grafts. These findings lend further support to the potential feasibility of transplanting neural stem cells to treat spinal cord injury.

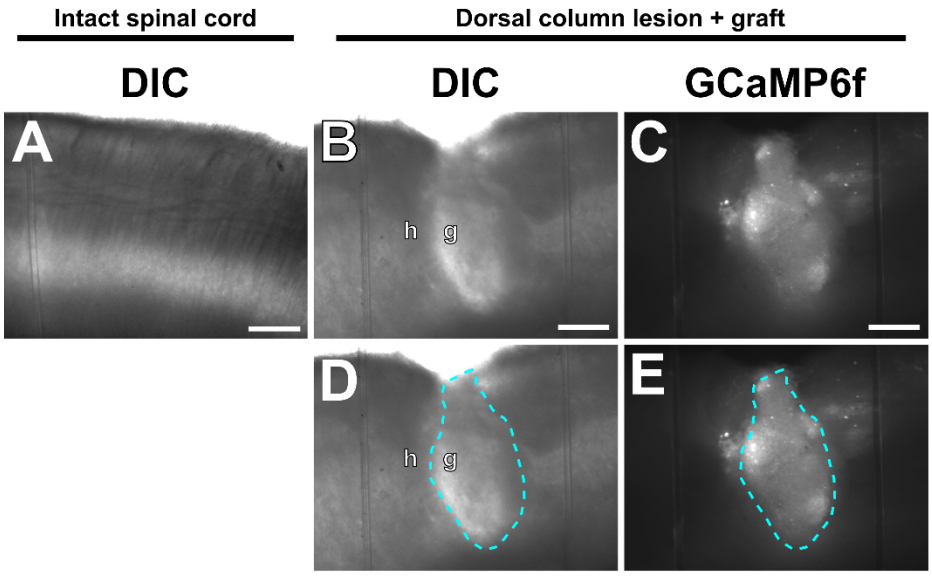

Figure 2.S1: Functional GCaMP6f expression is seen in more graft cells with non-Cre-dependent expression; graft boundaries can be conservatively delineated by morphology under differential interference contrast (DIC)

(A) DIC image of an intact spinal cord slice in the sagittal plane. (B) DIC image of a spinal cord slice with a dorsal column lesion and NPC graft (g). Note the clear disruption to the host (h) tissue continuity and differing texture of the graft and host. (C) Standard deviation projection of 50 s calcium imaging video from the same field of view as in (B) showing graft cells with dynamic GCaMP6f fluorescence. Graft cells transgenically expressed Cre recombinase under the synapsin promoter and were mixed with a Cre-dependent GCaMP6f AAV prior to grafting for graft-specific GCaMP6f expression. (D) Same image as in (B) with graft border drawn based on morphology under DIC. (E) Same image as in (C) with border drawn in (D) superimposed, showing that the border drawn based on gross morphology does not extend beyond the area of graft-specific GCaMP6f expression. In all images, the dorsal aspect of the slice is at the top and the rostral aspect is at left. Scale bars, 300 μm (A-C). Brightness and contrast adjusted for clarity across entire images (A-E).

Figure 2.S2: 4-AP increases graft spontaneous activity and response to CST stimulation

(A) Light path for widefield, all-optical stimulation and imaging in acute slice prep. A 470 nm LED excites GCaMP6f for imaging neuronal activity, while a 617 nm LED stimulates regenerated CST axons expressing Chrimson. LED1, 470 nm mounted LED; LED 2, 617 nm mounted LED; LPD, long-pass dichroic mirror; DM, deflecting mirror; BPD, band-pass dichroic mirror. Condensers and excitation and emission filters not shown for simplicity. (B,C) Standard deviation projection of GCaMP6f fluorescence in a NPP graft, with regions of interest (ROIs) outlined in yellow in (C). ROIs, referred to interchangeably as cells or neurons, were identified based on activity in calcium imaging videos and outlined on the standard deviation projection of the video to find the precise boundaries of dynamic GCaMP6f fluorescence. (D) Traces of the change in fluorescence over baseline of the 93 cells outlined in (C) in recording solution with no drug added. Over the 50 s shown, 4 trials of optogenetic CST stimulation (vertical cyan bars) were performed at 10 s intervals. Stimulation consisted of two 10 ms pulses from a 617 nm LED with a 50 ms start-to-start separation. Modest levels of spontaneous activity were observed and responses to stimulation were rare. (E) As in (C), after wash-in of 100 μM 4-AP. Extensive spontaneous activity was observed, as well as robust responses to CST stimulation. (F) Quantification of mean activity (imaging frames with significant upward fluorescence transients divided by total frames – see Methods for neuronal activity deconvolution procedure) before and after 4-AP wash-in in n=123 cells in N=3 animals during runs without stimulation. (G) Quantification of mean response strength to 8 trials of CST stimulation (same protocol as in C-D, but with longer 500 ms train at 20Hz) before and after 4-AP wash-in in n=53 cells in N= 3 animals. (H) Traces of change in fluorescence over baseline of 28 graft cells from an animal that did not receive AAV-Chrimson injections. While cells exhibited abundant spontaneous activity, no response to light stimulation was observed in N = 6 six animals with no AAV-Chrimson injections, indicating that the responses seen in graft neurons to optogenetic stimulation of regenerated CST axons are not the result of direct photostimulation of non-opsin-expressing graft cells. Scale bar, 200 μm (B). In both images, the dorsal aspect of the slice is at the top and the rostral aspect is at left. Brightness and contrast adjusted for clarity across entire images (A-B). Two-group comparisons were tested with Welch's t-test (**$p<0.01$). Data are represented as mean ±SEM.

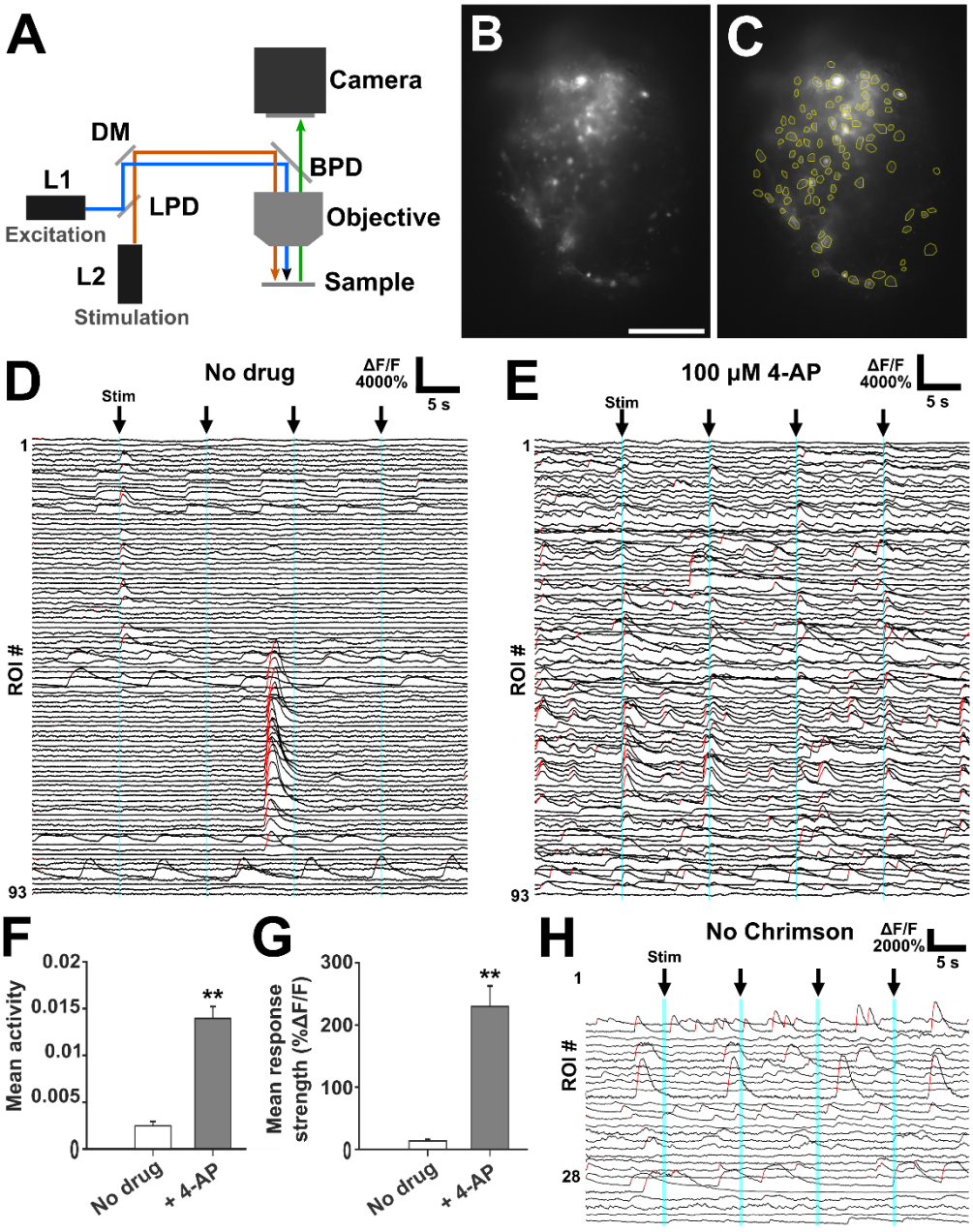
A
Camera
DM
BPD
L1
LPD
Objective
Excitation
L2
Sample
Stimulation
B
C
D
No drug
ΔF/F
4000%
5 s
Stim
1
ROI #
93
E
100 μM 4-AP
ΔF/F
4000%
5 s
Stim
1
ROI #
93
F
Mean activity
0.02
0.015
0.01
0.005
0
**
No drug
+ 4-AP
G
Mean response strength (%ΔF/F)
300
200
100
0
**
No drug
+ 4-AP
H
No Chrimson
ΔF/F
2000%
5 s
Stim
1
ROI #
28

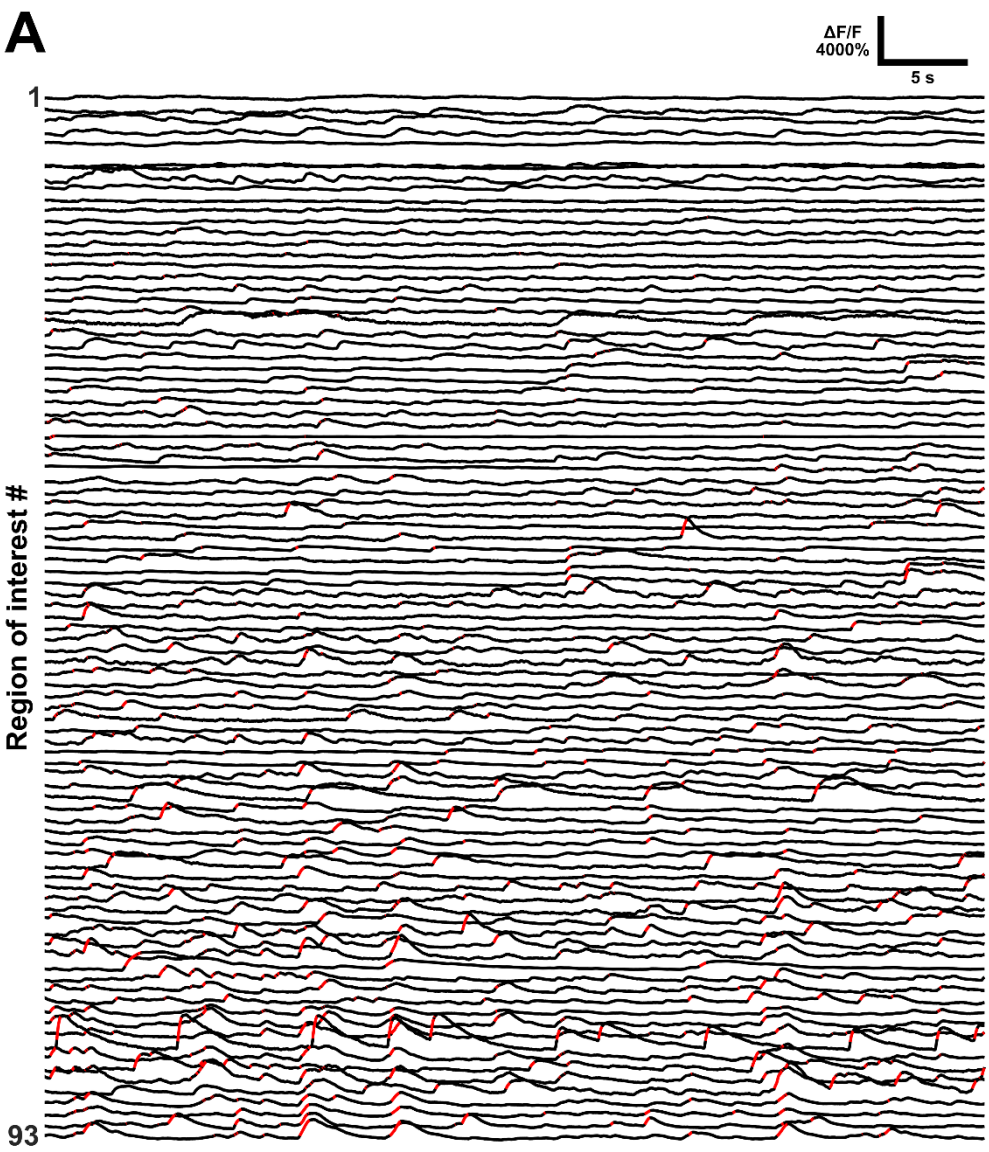

Figure 2.S3: Graft neurons exhibit spontaneous activity in individual neurons and groups of synchronously active neurons

(A) Fluorescence traces of all graft neurons analyzed in **Figure 2** displaying varying frequencies and patterns of activity. Traces are ordered from lowest mean activity (top) to highest mean activity (bottom).

Figure 2.S4: Optogenetic stimulation of corticospinal axons activates individual neurons and neuron clusters in intact host spinal cord

(A) Fluorescence traces of host neurons showing spontaneous activity and responses to 500 ms optogenetic stimulation of corticospinal axons. (B) Standard deviation projection of the run shown in (A) with all ROIs outlined in yellow and clusters of neurons with similar activity dynamics indicated by fill color. (C) First derivative raster plot (top) of traces from (A), with cells grouped into the clusters shown in (B). Cells above red line belonged to clusters. Significant activations of color-coded clusters are displayed below. Scale bar, 200 μm (B).

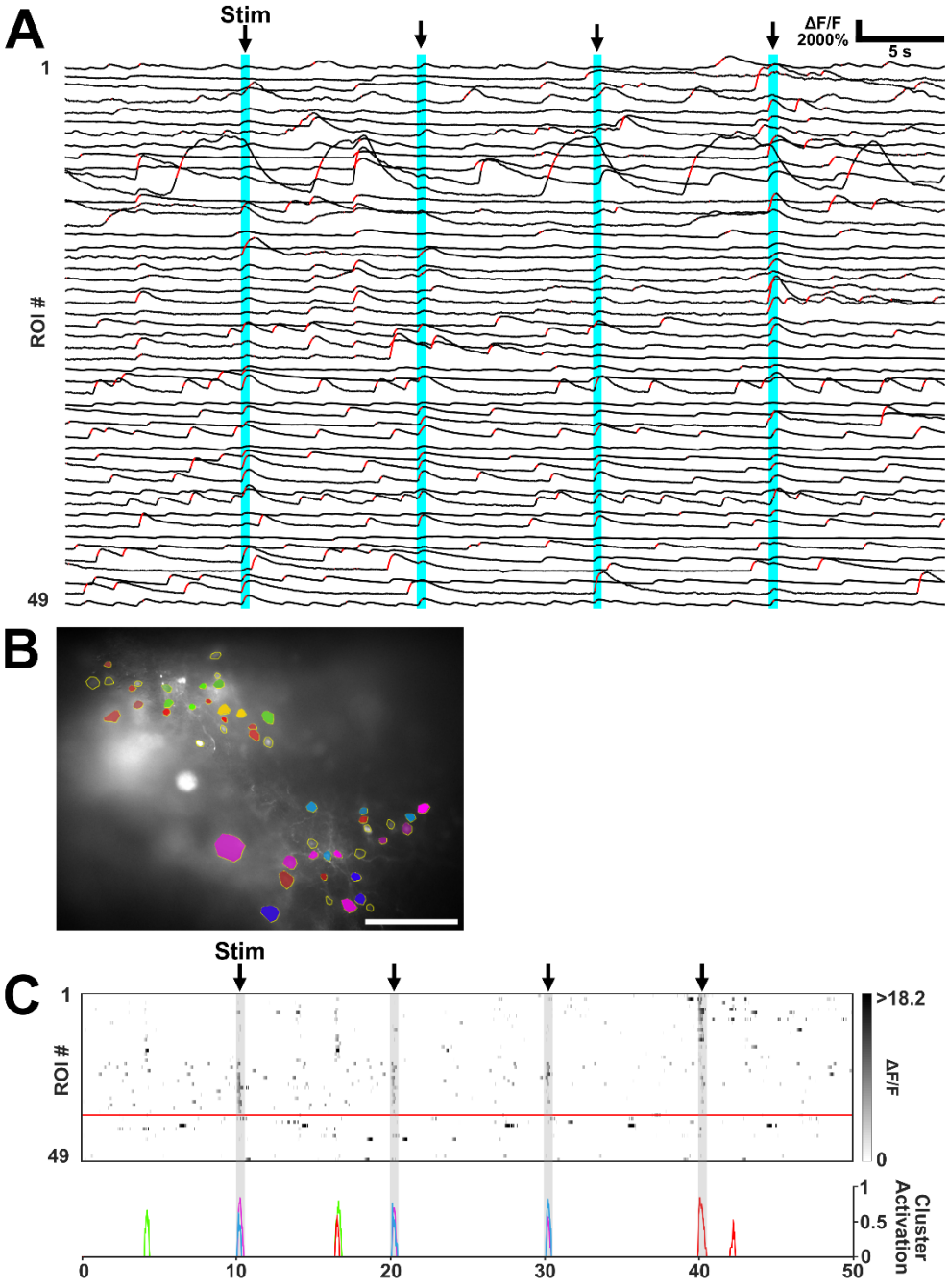
A
Stim
ΔF/F
2000%
5 s
1
ROI #
49
B
C
Stim
1
ROI #
49
>18.2
ΔF/F
0
1
0.5
0
Cluster Activation
0
10
20
30
40
50

References

Adler, A.F., Lee-Kubli, C., Kumamaru, H., Kadoya, K., and Tuszynski, M.H. (2017). Comprehensive Monosynaptic Rabies Virus Mapping of Host Connectivity with Neural Progenitor Grafts after Spinal Cord Injury. Stem Cell Reports *8*, 1525–1533.

Andermann, M.L., Gilfoy, N.B., Goldey, G.J., Sachdev, R., Wölfel, M., McCormick, D.A., Reid, C.R., and Levene, M.J. (2013). Chronic Cellular Imaging of Entire Cortical Columns in Awake Mice Using Microprisms. Neuron *80*, 900–913.

Anderson, M.A., O'Shea, T.M., Burda, J.E., Ao, Y., Barlatey, S.L., Bernstein, A.M., Kim, J.H., James, N.D., Rogers, A., Kato, B., Wollenber, A.L., Kawaguchi, R., Coppola, G., Wang, C., Deming, T.J., He, Z., Courtine, G., and Sofroniew, MV. (2018). Required growth facilitators propel axon regeneration across complete spinal cord injury. Nature *561*, 396–400.

Blight, A.R., Toos, J.P., Uer, M.S., and Widmer, W.R. (1991). The Effects of 4-Aminopyridine on Neurological Deficits in Chronic Cases of Traumatic Spinal Cord Injury in Dogs: A Phase I Clinical Trial. Journal of … *8*, 103–119.

Carrillo-Reid, L., Tecuapetla, F., and of …, T.D. (2008). Encoding network states by striatal cell assemblies.

Carrillo-Reid, L., Yang, W., Bando, Y., Peterka, D.S., and Yuste, R. (2016). Imprinting and recalling cortical ensembles. Science *353*, 691–694.

Chen, T.-W., Wardill, T.J., Sun, Y., Pulver, S.R., Renninger, S.L., Baohan, A., Schreiter, E.R., Kerr, R.A., Orger, M.B., Jayaraman, V., Looger, L.L., Svoboda, K., and Kim, D.S. (2013). Ultrasensitive fluorescent proteins for imaging neuronal activity. Nature *499*, 295.

Chia, T.H., and Levene, M.J. (2010). Multi-Layer In Vivo Imaging of Neocortex Using a Microprism. Cold Spring Harbor Protocols *2010*, pdb.prot5476.

Dulin, J.N., Adler, A.F., Kumamaru, H., Poplawski, G.H., Lee-Kubli, C., Strobl, H., Gibbs, D., Kadoya, K., Fawcett, J.W., Lu, P., and Tuszynski, M.H. (2018). Injured adult motor and sensory axons regenerate into appropriate organotypic domains of neural progenitor grafts. Nature Communications *9*, 84.

Edelstein, A.D., Tsuchida, M.A., Amodaj, N., Pinkard, H., Vale, R.D., and Stuurman, N. (2014). Advanced methods of microscope control using μManager software. Journal of Biological Methods *1*.

Emiliani, V., Cohen, A.E., Deisseroth, K., and Häusser, M. (2015). All-Optical Interrogation of Neural Circuits. The Journal of Neuroscience : The Official Journal of the Society for Neuroscience *35*, 13917–13926.

Etlin, A., Bráz, J.M., Kuhn, J.A., Wang, X., Hamel, K.A., Llewellyn-Smith, I.J., and Basbaum, A.I. (2016). Functional Synaptic Integration of Forebrain GABAergic Precursors into the Adult Spinal Cord. The Journal of Neuroscience : The Official Journal of the Society for Neuroscience *36*, 11634–11645.

Farrar, M.J., Bernstein, I.M., Schlafer, D.H., Cleland, T.A., Fetcho, J.R., and Schaffer, C.B. (2012). Chronic in vivo imaging in the mouse spinal cord using an implanted chamber. Nature Methods *9*, 297–302.

Hendrickson, A.E., and White, P. (1964). PROMAX: A QUICK METHOD FOR ROTATION TO OBLIQUE SIMPLE STRUCTURE. Brit J Statist Psych *17*, 65–70.

Husch, A., Cramer, N., and Harris-Warrick, R.M. (2011). Long-duration perforated patch recordings from spinal interneurons of adult mice. Journal of Neurophysiology *106*, 2783–2789.

Johannssen, H.C., and Helmchen, F. (2013). Two-photon imaging of spinal cord cellular networks. Experimental Neurology *242*, 18–26.

Kadoya, K., Lu, P., Nguyen, K., Lee-Kubli, C., Kumamaru, H., Yao, L., Knackert, J., Poplawski, G., Dulin, J.N., Strobl, H., Takashima, Y., Biane, J., Conner, J., Zhang, S., and Tuszynski, M.H. (2016). Spinal cord reconstitution with homologous neural grafts enables robust corticospinal regeneration. Nature Medicine *22*, nm.4066.

Kerkut, G.A., and Bagust, J. (1995). The isolated mammalian spinal cord. Prog Neurobiol *46*, 1–48.

Klapoetke, N.C., Murata, Y., Kim, S., Pulver, S.R., Birdsey-Benson, A., Cho, Y., Morimoto, T.K., Chuong, A.S., Carpenter, E.J., Tian, Z., Wang, J., Xie, Y., Yan, Z., Zhang, Y., Chow, B.Y., Surek, B., Melkonian, M., Jayaraman, V., Constantine-Paton, M., Wong, G., Boyden, E.S. (2014). Independent optical excitation of distinct neural populations. Nature Methods *11*, 338–346.

Kumamaru, H., Lu, P., Rosenzweig, E.S., Kadoya, K., and Tuszynski, M.H. (2019). Regenerating Corticospinal Axons Innervate Phenotypically Appropriate Neurons within Neural Stem Cell Grafts. Cell Reports *26*, 2329-2339.e4.

Lin, M.Z., and Schnitzer, M.J. (2016). Genetically encoded indicators of neuronal activity. Nature Neuroscience *19*, 1142–1153.

Liu, Y., Wang, X., Li, W., Zhang, Q., Li, Y., Zhang, Z., Zhu, J., Chen, B., Williams, P.R., Zhang, Y., Yu, B., Gu, X., He, Z. (2017). A Sensitized IGF1 Treatment Restores Corticospinal Axon-Dependent Functions. Neuron *95*, 817-833.e4.

Lu, P., Wang, Y., Graham, L., McHale, K., Gao, M., Wu, D., Brock, J., Blesch, A.,

Rosenzweig, E.S., Havton, L.A., Zheng, B., Conner, J.M., Marsala, M., and Tuszynski, M.H. (2012). Long-Distance Growth and Connectivity of Neural Stem Cells after Severe Spinal Cord Injury. Cell *150*, 1264–1273.

Lu, P., Gomes-Leal, W., Anil, S., Dobkins, G., Huie, R.J., Ferguson, A.R., Graham, L., and Tuszynski, M. (2019). Origins of Neural Progenitor Cell-Derived Axons Projecting Caudally after Spinal Cord Injury. Stem Cell Reports.

Madisen, L., Garner, A.R., Shimaoka, D., Chuong, A.S., Klapoetke, N.C., Li, L., van der Bourg, A., Niino, Y., Egolf, L., Monetti, C., Gu, H., Mills, M., Cheng, A., Tasic, B., Nguyen, T.N., Sunkin, S.M., Benucci, A., Nagy, A., Miyawaki, A., Helmchen, F., Empson, R.M., Knöpfel, T., Boyden, E.S., Reid, R.C., Carandini, M., and Zeng, H. (2015). Transgenic mice for intersectional targeting of neural sensors and effectors with high specificity and performance. Neuron *85*, 942–958.

Mitra, P., and Brownstone, R.M. (2012). An in vitro spinal cord slice preparation for recording from lumbar motoneurons of the adult mouse. Journal of Neurophysiology *107*, 728–741.

Peyrache, A., Benchenane, K., Khamassi, M., Wiener, S.I., and Battaglia, F.P. (2010). Principal component analysis of ensemble recordings reveals cell assemblies at high temporal resolution. J Comput Neurosci *29*, 309–325.

Romano, S.A., Pérez-Schuster, V., Jouary, A., Boulanger-Weill, J., Candeo, A., Pietri, T., and Sumbre, G. (2017). An integrated calcium imaging processing toolbox for the analysis of neuronal population dynamics. PLoS Computational Biology *13*, e1005526.

Schneider, C.A., Rasband, W.S., and Eliceiri, K.W. (2012). NIH Image to ImageJ: 25 years of image analysis. Nature Methods *9*, 671–675.

Sekiguchi, K.J., Shekhtmeyster, P., Merten, K., Arena, A., Cook, D., Hoffman, E., Ngo, A., and Nimmerjahn, A. (2016). Imaging large-scale cellular activity in spinal cord of freely behaving mice. Nature Communications *7*, 11450.

Steinbeck, J.A., Choi, S.J., Mrejeru, A., Ganat, Y., Deisseroth, K., Sulzer, D., Mosharov, E.V., and Studer, L. (2015). Optogenetics enables functional analysis of human embryonic stem cell-derived grafts in a Parkinson's disease model. Nature Biotechnology *33*, 204–209.

Strupp, M., Teufel, J., Zwergal, A., Schniepp, R., Khodakhah, K., and Feil, K. (2017). Aminopyridines for the treatment of neurologic disorders. Neurology: Clinical Practice *7*, 65–76.

Thévenaz, P., Ruttimann, U., and Unser, M. (1998). A pyramid approach to subpixel registration based on intensity. IEEE Transactions on Image Processing : A Publication of the IEEE Signal Processing Society *7*, 27–41.

Yuste, R. (2015). From the neuron doctrine to neural networks. Nature Reviews. Neuroscience *16*, 487–497.

Zhu, Y., Romero, M.I., Ghosh, P., Ye, Z., Charnay, P., Rushing, E.J., Marth, J.D., and Parada, L.F. (2001). Ablation of NF1 function in neurons induces abnormal development of cerebral cortex and reactive gliosis in the brain. Gene Dev *15*, 859–876.

Chapter 2, in full, is currently being prepared for submission for publication of the material. Ceto, Steven; Sekiguchi, Kohei J.; Takashima, Yoshio T.; Nimmerjahn, Axel; Tuszynski, Mark H. The dissertation author was the primary investigator and author of this material. He designed and performed the experiments, processed and analyzed the data, and wrote the manuscript.

Chapter 3

Prolonged human neural stem cell maturation supports recovery in injured rodent CNS

This chapter appears in its published form: Lu P, Ceto S, Wang Y, Graham L, Wu D, Kumamaru H, Staufenberg E, and Tuszynski MH (2017) J Clin Invest 127(9):3287-3299.

JCI The Journal of Clinical Investigation

Prolonged human neural stem cell maturation supports recovery in injured rodent CNS

Paul Lu, … , Eileen Staufenberg, Mark H. Tuszynski

J Clin Invest. 2017;127(9):3287-3299. https://doi.org/10.1172/JCI92955.

Research Article Neuroscience

Neural stem cells (NSCs) differentiate into both neurons and glia, and strategies using human NSCs have the potential to restore function following spinal cord injury (SCI). However, the time period of maturation for human NSCs in adult injured CNS is not well defined, posing fundamental questions about the design and implementation of NSC-based therapies. This work assessed human H9 NSCs that were implanted into sites of SCI in immunodeficient rats over a period of 1.5 years. Notably, grafts showed evidence of continued maturation over the entire assessment period. Markers of neuronal maturity were first expressed 3 months after grafting. However, neurogenesis, neuronal pruning, and neuronal enlargement continued over the next year, while total graft size remained stable over time. Axons emerged early from grafts in very high numbers, and half of these projections persisted by 1.5 years. Mature astrocyte markers first appeared after 6 months, while more mature oligodendrocyte markers were not present until 1 year after grafting. Astrocytes slowly migrated from grafts. Notably, functional recovery began more than 1 year after grafting. Thus, human NSCs retain an intrinsic human rate of maturation, despite implantation into the injured rodent spinal cord, yet they support delayed functional recovery, a finding of great importance in planning human clinical trials.

Prolonged human neural stem cell maturation supports recovery in injured rodent CNS

Paul Lu,[1,2] Steven Ceto,[2,3] Yaozhi Wang,[2] Lori Graham,[2] Di Wu,[2] Hiromi Kumamaru,[2] Eileen Staufenberg,[2] and Mark H. Tuszynski[1,2]

[1]VA San Diego Healthcare System, San Diego, California, USA. [2]Department of Neurosciences and [3]Biomedical Sciences Graduate Program, UCSD, La Jolla, California, USA.

Neural stem cells (NSCs) differentiate into both neurons and glia, and strategies using human NSCs have the potential to restore function following spinal cord injury (SCI). However, the time period of maturation for human NSCs in adult injured CNS is not well defined, posing fundamental questions about the design and implementation of NSC-based therapies. This work assessed human H9 NSCs that were implanted into sites of SCI in immunodeficient rats over a period of 1.5 years. Notably, grafts showed evidence of continued maturation over the entire assessment period. Markers of neuronal maturity were first expressed 3 months after grafting. However, neurogenesis, neuronal pruning, and neuronal enlargement continued over the next year, while total graft size remained stable over time. Axons emerged early from grafts in very high numbers, and half of these projections persisted by 1.5 years. Mature astrocyte markers first appeared after 6 months, while more mature oligodendrocyte markers were not present until 1 year after grafting. Astrocytes slowly migrated from grafts. Notably, functional recovery began more than 1 year after grafting. Thus, human NSCs retain an intrinsic human rate of maturation, despite implantation into the injured rodent spinal cord, yet they support delayed functional recovery, a finding of great importance in planning human clinical trials.

Introduction

Neural stem cells (NSCs) differentiate into neurons and glia and can potentially replace lost neural systems after central nervous system (CNS) injury (1–8). When implanted into sites of spinal cord injury (SCI), rat- and human-derived multipotent neural progenitor cells, human embryonic stem cell–derived (ESC-derived) NSCs, and human induced pluripotent stem cell–derived (iPSC-derived) NSCs all extend very large numbers of axons over long distances and form synapses with host neurons (4, 5) that in some cases support functional improvement (4, 8–10). These findings suggest the potential for human translation; indeed, NSC clinical trials for SCI have begun, and more are planned (ClinicalTrials.gov).

Yet a question of great relevance to the design, implementation, and performance of clinical trials remains: at what rate will human NSCs mature when grafted to sites of SCI? This is important for several reasons: if human NSCs mature rapidly, then it is reasonable to assess outcomes on a typical clinical trial time frame of months. In contrast, if NSC maturation parallels normal human development and cells mature over much longer time periods (see below), then clinical trials must be designed over very extended time periods. Prolonged maturation in turn raises fundamental biological questions: will injured host axons and neurons remain responsive to NSC grafts if the latter are mature and capable of sustaining function only months or even years after grafting? If chronically injured host axons retract from injury sites over the time period that human grafts are maturing, can neural circuitry be reconstituted? If NSC-derived axons are pruned over time (as during neural development), might functional benefits be lost?

The human gestational period is 280 days; rat gestation is 21 days (11). At birth, the human brain roughly corresponds to a postnatal day 7 rat brain based on body/brain weight ratios, and a 2- to 3-year-old human brain corresponds to a postnatal day-20 rat brain (11). Yet most NSC grafting studies have been performed over relatively short survival times of weeks to a few months in vivo (3, 5, 9, 12). Moreover, it is possible that the rodent environment, especially the adult traumatic environment, will alter the fate or rate of human NSC maturation; these questions have, until the present, remained unanswered. Previous studies have examined the differentiation and maturation of human fetus–derived NSCs (13), oligodendrocyte progenitors (14, 15), glial progenitor cells (6, 16), or human ESC-derived neurons (17, 18); however, none of these studies examined human neural cell maturation in an adult rodent CNS trauma model. In addition, human cells were transplanted either into embryonic or neonatal rodents, but not into adult animals; the developing CNS environment is distinct from the adult CNS, potentially influencing the differentiation and maturation of human NSCs. An assessment of the fate and maturation of human ESC–derived NSCs in adult lesion models is important not only for stem cell biology, but also for the practical and realistic design of translational human trials involving NSCs for SCI and other human disorders. Accordingly, we examined the nature and time course of human NSC maturation in adult rats that underwent SCI. Post-grafting time periods ranged from 1 month to 1.5 years.

▶ Related Commentary: p. 3284

Conflict of interest: The authors have declared that no conflict of interest exists.
Submitted: January 20, 2017; **Accepted:** June 27, 2017.
Reference information: *J Clin Invest.* 2017;127(9):3287–3299.
https://doi.org/10.1172/JCI92955.

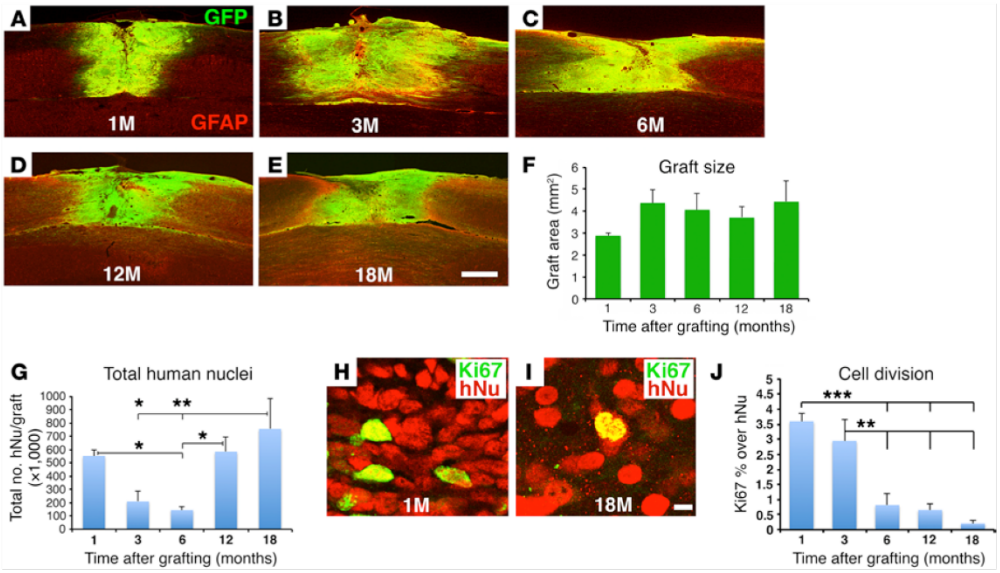

Figure 1. H9-NSC graft morphology and Ki67 immunolabeling. (**A**–**E**) Graft size was stable over time in the C5 hemisection lesion site, and grafts were well integrated with the host. GFP and GFAP double-labeling (horizontal sections). (**F**) Grafts nonsignificantly expanded from 1 to 3 months after grafting ($P = 0.6$, by ANOVA) and were stable in size thereafter. Data represent the mean ± SEM. (**G**) The total number of grafted human cells (detected by hNu, a human-specific cell marker) was significantly reduced at 3 and 6 months, but recovered by 12 and 18 months. $P < 0.05$, by ANOVA and $^{**}P < 0.001$ and $^{*}P < 0.05$, by Fisher's exact post-hoc test. Data represent the mean ± SEM. (**H**–**J**) Cell proliferation was significantly reduced after 3 months. hNu indicates the human-specific nucleus marker; Ki67 labels proliferating cells. $P < 0.0001$, by ANOVA and $^{***}P < 0.001$ and $^{**}P < 0.01$, by Fisher's exact post-hoc test comparing results at 1 and 3 months with results at 6, 12, and 18 months, respectively. Data represent the mean ± SEM. For **F**, **G**, and **J**: 1 month, $n = 3$; 3 months, $n = 3$; 6 months, $n = 5$; 12 months, $n = 3$; and 18 months, $n = 4$. Scale bars: 550 μm (**A**–**E**); 7 μm (**H** and **I**).

Results

We used the widely available H9 human NSC line, derived from human ESCs (Gibco Human Neural Stem Cells) (19, 20). This NSC line is well characterized: it expresses the NSC-specific markers nestin and SOX2 and differentiates into neurons, oligodendrocytes, and astrocytes (21). H9 NSCs were transduced to express GFP and were harvested and embedded in fibrin matrices containing a growth factor cocktail (see Methods and ref. 4) to promote NSC survival and retention in the lesion site. Cells were transplanted into C5 spinal cord lateral hemisection lesion sites in immunodeficient rats (total $n = 18$) 2 weeks after the SCI. Right hemisections are large lesions that entirely remove the right half of the spinal cord, thereby impairing function of the ipsilateral forelimb (22). Control rats ($n = 5$) underwent the same hemisection lesions and injections of the fibrin matrix containing the growth factor cocktail, without NSCs. NSC-grafted subjects were perfused at serial time points after grafting: 1 month ($n = 3$); 3 months ($n = 3$); 6 months ($n = 5$); 12 months ($n = 3$); and 18 months ($n = 4$). Control subjects were perfused 12 months after lesioning. Behavioral analysis of the affected forelimb was conducted monthly for those NSC-grafted subjects that survived for 12 ($n = 7$) or 18 ($n = 4$) months and control subjects ($n = 5$) that survived for 12 months.

H9 NSC graft size is stable over time. GFP-expressing human NSCs survived well and filled C5 hemisection sites at each survival time point (Figure 1, A–E). Graft size tended to increase from 1 to 3 months, but was stable thereafter (Figure 1F). The total number of grafted human cells, assessed by the human-specific nuclear marker hNu, was maximal 1 month after grafting, declined at 3 and 6 months after grafting, and then gradually recovered by 12 and 18 months (Figure 1G). Double-labeling of grafted cells for hNu and the cell proliferation marker Ki67 demonstrated that 3.6% ± 0.2% and 3.0% ± 0.7% of grafted human cells were proliferating 1 and 3 months after grafting, respectively, but this number was significantly and substantially reduced to 0.8% ± 0.4% and 0.7% ± 0.2% by 6 and 12 months after grafting, respectively (Figure 1, H–J). Cell division was further attenuated by 18 months after grafting to only 0.2% ± 0.1% ($P < 0.0001$, by ANOVA; $P < 0.01$, by Fisher's exact post-hoc test comparing 18 months with 1 and 3 months, respectively) (Figure 1, H–J). Indeed, we detected no Ki67 labeling in 2 of 4 subjects 18 months after grafting. Approximately 70% of dividing Ki67-labeled cells colocalized with human-specific nestin, indicating that many dividing cells in grafts were dividing NSCs (Supplemental Figure 1; supplemental material available online with this article; https://doi.org/10.1172/JCI92955DS1). Some of these dividing NSCs were clustered, as was seen with NSC niches (23). These data indicate that grafted H9 human NSCs became nearly entirely postmitotic, without tumor formation, in lesion sites at long post-grafting time periods, an important safety consideration for human clinical application.

Grafted human neurons mature gradually over 18 months. One month after grafting, human NSCs densely expressed the immature neuronal marker doublecortin (DCX) (Figure 2A), but not the

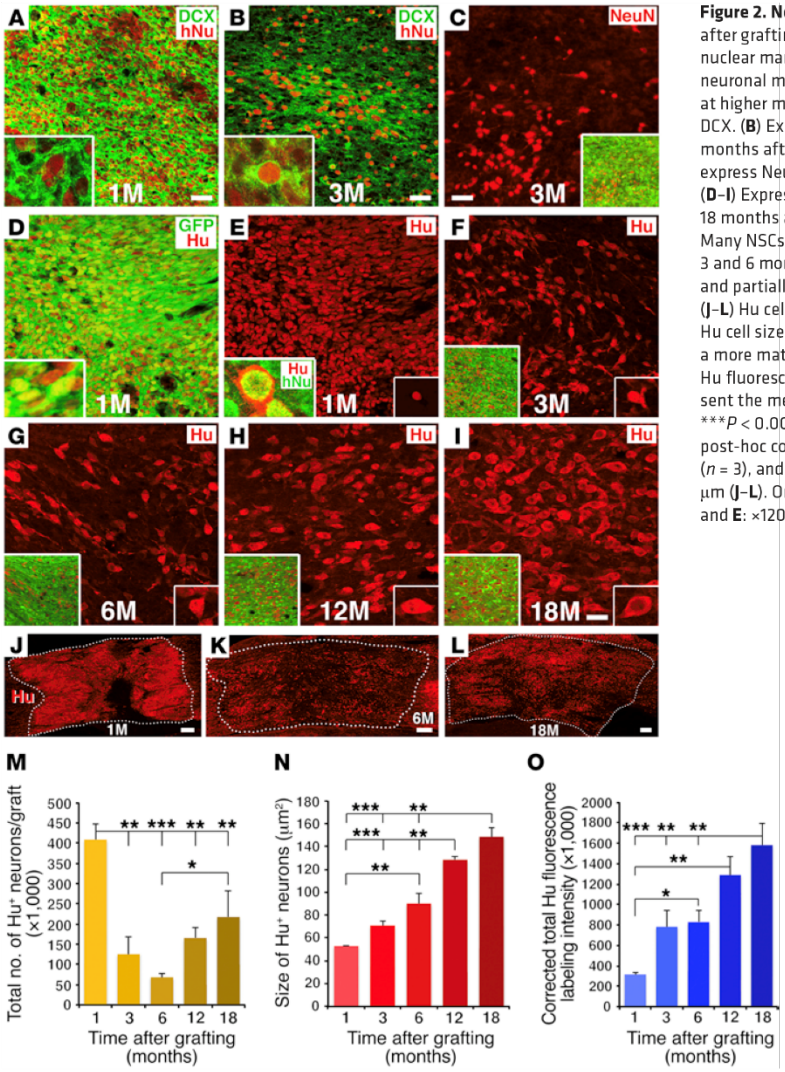

Figure 2. Neuronal maturation over time. (**A**) One month after grafting, human H9-NSCs expressed the human nuclear marker hNu; many cells also expressed the immature neuronal marker DCX in the cytoplasm. Inset shows image at higher magnification and colocalization of hNu and DCX. (**B**) Expression of DCX was substantially reduced by 3 months after grafting, and (**C**) at this time point, cells first express NeuN. Inset images show higher magnification. (**D**–**I**) Expression of the pan-neuronal marker Hu from 1 to 18 months after grafting. Insets show higher magnification. Many NSCs, labeled for GFP, also expressed Hu at 1 month. At 3 and 6 months, Hu$^+$ cell numbers were substantially reduced and partially recovered by 12 and 18 months (quantified in **M**). (**J**–**L**) Hu cell distribution in the graft at 1, 6, and 18 months. Hu cell size increased over time (quantified in **N**) and adopted a more mature neuronal morphology. (**O**) Quantification of Hu fluorescence labeling intensity over time. All data represent the mean ± SEM. $P < 0.001$, ANOVA (**M**–**O**) and $^{***}P < 0.001$, $^{**}P < 0.01$, and $^{*}P < 0.05$, by Fisher's exact post-hoc comparison test for 1 ($n = 3$), 3 ($n = 3$), 6 ($n = 5$), 12 ($n = 3$), and 18 months ($n = 4$). Scale bars: 32 μm (**A**–**I**); 250 μm (**J**–**L**). Original magnification of Images in insets: **A**, **B**, **D**, and **E**: ×1200; **C**, **F**–**I**: ×400.

mature neuronal marker NeuN. By 3 months, we observed that DCX expression in grafts was reduced, and at 6 months and thereafter was restricted to small subregions of grafts (Figure 2B and Supplemental Figure 2, A–C). NeuN expression was first evident 3 months after grafting and persisted thereafter (Figure 2C and Supplemental Figure 2, D–F). Notably, the number, size, and intensity of NeuN-expressing cells in grafts appeared to increase from 3 months to 1 year after grafting, an observation that was confirmed on quantification (Figure 2C and Supplemental Figure 2, D–F and J–L). Thus, neurons exhibited evidence of gradual maturation over a full year after grafting.

To assess changes in the total number of grafted neurons over time, we used the specific neuronal marker Hu, which is expressed by all neurons, including both immature and mature postmitotic neurons (24–26) and is distinct from the hNu antibody, which specifically labels human nuclei but is not restricted to neurons (Figure 2, A, B, E inset, and Supplemental Figure 2, G–I). We found that Hu labeled all immature neurons that expressed DCX both in vitro and in vivo (Supplemental Figure 3, A–C, and G–I) and all NeuN-expressing neurons both in vitro and in vivo (Supplemental Figure 3, D–F and J–L). Using Hu/hNu double labeling, we quantified the total number of grafted neurons, neuron size, and Hu-labeling intensity over time.

The proportion of all grafted cells that expressed the neuronal marker Hu (Hu/hNu) steadily decreased over time to 1 year and then stabilized: 76% ± 4% of all cells expressed Hu at 1 month; 60% ± 5% at 3 months; 49% ± 3% at 6 months; 29% ± 2% at 12 months; and 29% ± 3% at 18 months, a gradual reduction that was significant ($P < 0.0001$, by 1-way ANOVA). Interestingly, the total number of grafted human NSCs expressing the neuronal marker Hu was maximal 1 month after grafting, as assessed using semistereological methods (Figure 2, D, E, J, and M). At later time points, as neurons matured, the number of neurons expressing Hu had a 70%

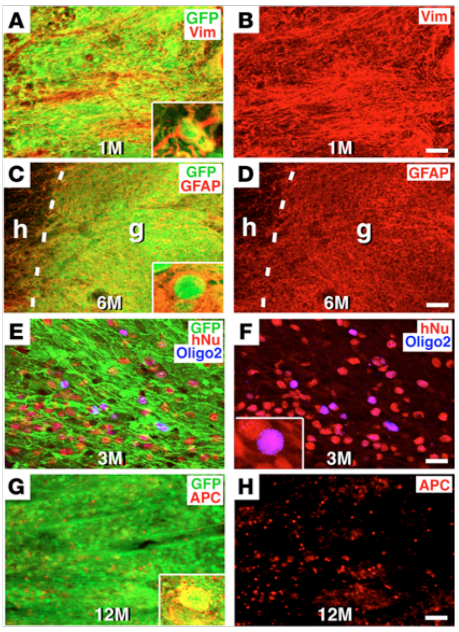

Figure 3. Glial maturation over time. (**A** and **B**) GFP and vimentin (Vim) immunolabeling revealed colocalization of grafted human cells expressing GFP with the glial progenitor marker vimentin 1 month after grafting. Inset in **A** is a higher-magnification image. (**C** and **D**) The mature astrocyte marker GFAP was not detectable in human NSC grafts until 6 months after implantation. Dashed lines indicate the host/graft (h/g) interface. Inset in **C** is a higher magnification image showing colocalization of GFP and GFAP. (**E** and **F**) The oligodendroglial marker Oligo2 was first detectable 3 months after grafting and colocalized with GFP and hNu markers. (**G** and **H**) However, the more mature oligodendrocyte marker APC was first detected only 12 months after NSC grafting and colocalized with GFP (inset in **G**). Scale bars: 60 μm (**A**–**D**, **G**, and **H**); 24 μm (**E** and **F**). Original magnification of images in insets (**A**, **C**, **F**, **G**): ×600.

reduction 3 months after grafting ($P < 0.001$, by 1-way ANOVA; $P < 0.001$ vs. 1 month after grafting, by Fisher's exact post-hoc test) and an 83% reduction 6 months after grafting ($P < 0.0001$ vs. 1 month after grafting, by Fisher's exact post-hoc test) (Figure 2, F, G, K, and M). Yet after 6 months, we found that the number of grafted human neurons expressing Hu progressively recovered: at 12 months, cell numbers increased by 2.4-fold compared with the numbers at 6 months and further increased by 3.2-fold at 18 months ($P < 0.05$ vs. 6 months after grafting, by Fisher's exact post-hoc test) (Figure 2, H, I, L, and M). The final total number of grafted cells expressing Hu after 18 months represented 53% of the original number of Hu cells at 1 month (Figure 2, I, L, and M). Similarly, quantification of the number of neurons expressing the mature neuronal marker NeuN was lowest at 3 and 6 months and increased at 12 and 18 months (Figure 2C and Supplemental Figure 2, D–F, and J). As expected, the total number of NeuN-labeled cells was lower than the number of Hu-labeled cells, because Hu detects both immature and mature neurons (25) (Figure 2, C–L, and Supplemental Figures 2 and 3), and because NeuN does not recognize all classes of mature neurons (27). These findings indicate that grafted NSCs undergo dynamic neurogenesis: neuron numbers are maximal 1 month after grafting and then exhibit a delayed phase of reduction 3–6 months after grafting, followed by gradual recovery. DAPI staining at 3 and 6 months confirmed the presence of nuclear fragmentation in some grafted human cells, consistent with apoptotic cell death (28) (Supplemental Figure 4). As noted above, nearly 1% of grafted cells continued to express the cell division marker Ki67 through 1 year after grafting (Figure 1J), and small amounts of cells expressed DCX through 18 months (Figure 2, A and B, and Supplemental Figure 2, A–C), constituting a newly dividing cell pool that may reconstitute neuron numbers; only 0.2% of cells expressed Ki67 by 18 months, a point at which neuron numbers had stabilized.

Neuronal hypertrophy is an indication of continuing cell maturation (29). While total neuron numbers dropped and then recovered over time, mean Hu-labeled neuron size gradually and significantly increased by 3-fold over successive post-grafting time points through 12 months ($P < 0.0001$, by ANOVA) (Figure 2N). Moreover, the mean intensity of Hu neuronal reaction product per neuron also increased over time ($P < 0.001$, by 1-way ANOVA) (Figure 2O). Cells also gradually adopted a more mature, pyramid-like morphology over time (Figure 2, D–I). We observed parallel changes in size and intensity of NeuN-labeled cells (Figure 2C and Supplemental Figure 2, D–F, K, and L).

Collectively, the preceding data indicate that, following a 1- to 3-month period of delayed cell loss, grafted neurons will mature steadily over the ensuing 12 months. This time period corresponds to a normal human time course of neuronal maturation, despite graft placement into an injured adult rodent environment.

The spatial distribution of neurons in the graft also evolved over time. One month after grafting, cells were relatively homogeneously distributed in the lesion site (Figure 2, A, D, E, and J). However, by 3 and 6 months, when we observed extensive loss of cells expressing neuronal markers, cell distribution in the graft was uneven, with some regions containing clusters of Hu-expressing cells and other regions showing attenuated cell density (Figure 2, B, C, F, G, and K). However, by 18 months, both Hu- and NeuN-labeled cells were more uniformly distributed through the graft/lesion site (Figure 2, I and L, and Supplemental Figure 2F). These findings, when taken together with the time course of neuron numbers in grafts, indicate that the period of subacute delayed cell loss may leave clusters of surviving NSCs or neuronal progenitor cells that gradually proliferate and distribute throughout the lesion site over a prolonged period of 1 year. Eventually, a mature neural environment forms in what would otherwise be an empty lesion site.

Grafted human glia mature gradually over 12 months. The expression of mature glial markers also occurred over a protracted, human-like time period (Figure 3). The glial progenitor marker vimentin was present at the earliest time point assessed, i.e., 1 month (Figure 3, A and B), and expression was continuously detected thereafter. The mature astrocytic cell marker GFAP was first detected within grafted cells 6 months after grafting, a late time point corresponding to human neural development (30) (Figure 3, C and D). At 18 months, we found that 48% ± 1% of grafted, GFP-labeled NSCs expressed GFAP immunoreactivity.

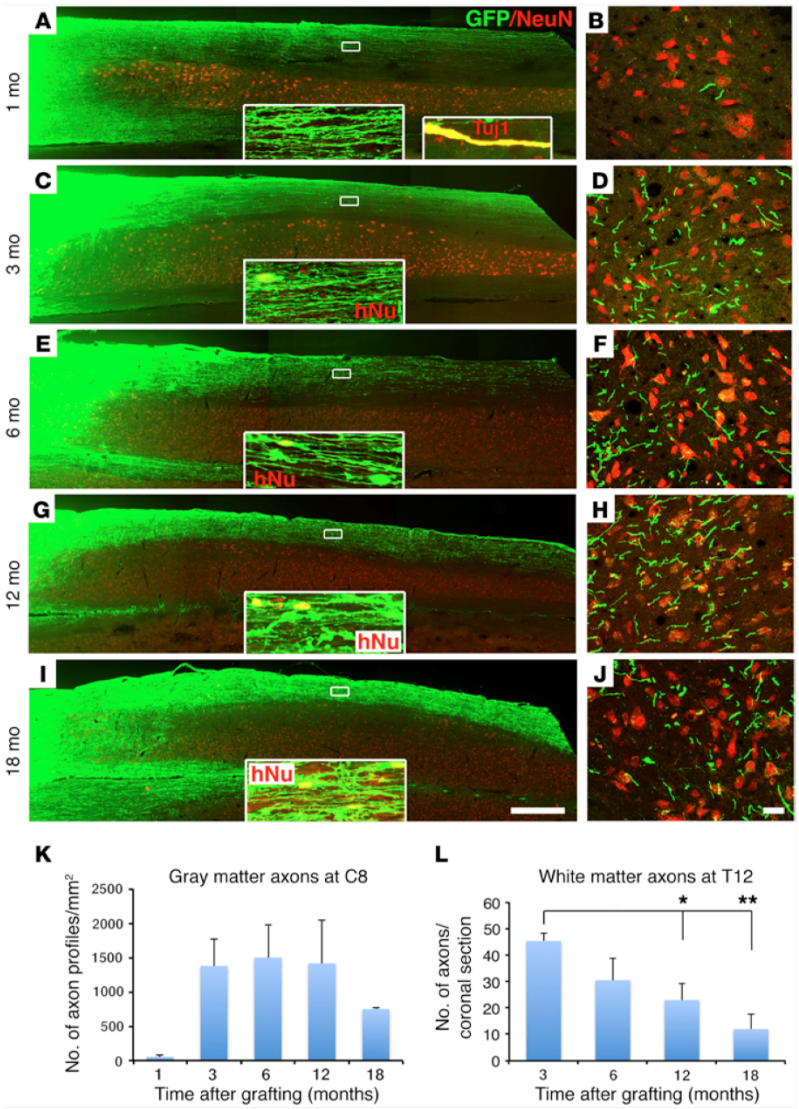

Figure 4. Axonal extension from H9-NSC grafts. (**A** and **B**) Very large numbers of GFP-labeled human axons extended from the lesion site (far left side of the image) caudally after 1 month. (**A**) Horizontal section and (**B**) C8 coronal section. NeuN labels gray matter. Inset images show higher magnification of axons extending caudally in white matter, 3 mm caudal to the graft. The second inset in **A** shows colocalization of GFP with the axonal marker Tuj1, indicating the identity of many GFP processes as axons at 1 month. (**C**) Axons persisted 3 months after grafting, although glial migration was also evident at this point, as identified by the human nucleus marker hNu (inset; see also Figure 5). Because NSCs did not migrate into host gray matter, axon numbers over time could be quantified in gray matter. (**D**) A larger number of NSC-derived axons were evident in C8 gray matter at 3 months compared with those seen at 1 month, as quantified in **K**. (**E** and **F**) Six months after grafting, axons remained detectable in white and gray matter caudal to the lesion site. (**G** and **H**) By 12 months, a reduction in axon numbers caudal to the lesion site was observed, as quantified in C8 gray matter in **K**. (**I** and **J**) Further attenuation of axon numbers was evident at 18 months. (**K**) Quantification of human NSC-derived axons in C8 gray matter. Data represent the mean ± SEM. $P = 0.14$, by ANOVA for 1 ($n = 3$), 3 ($n = 3$), 6 ($n = 5$), 12 ($n = 3$), and 18 months ($n = 4$). (**L**) Glial migration did not reach T12, thus GFP-labeled axon numbers could be reliably quantified over time at T12. A gradual reduction in axon numbers was evident. $P < 0.05$, by ANOVA; $^*P < 0.05$ and $^{**}P < 0.01$, by Fisher's exact post-hoc test for 1 ($n = 3$), 3 ($n = 3$), 6 ($n = 5$), 12 ($n = 3$), and 18 months ($n = 3$). Scale bars: 800 μm (**A**, **C**, **E**, **G**, and **I**); 25 μm (**B**, **D**, **F**, **H**, and **J**). Original magnification: ×1200 for GFP-TUJ1 and ×600 for other inset images.

Oligodendrocyte maturation was the most prolonged of all the primary CNS cell types. The early oligodendroglial marker Oligo2 (31) was detected as early as 3 months after grafting (Figure 3, E and F). We used an adenomatous polyposis coli (APC) antibody to detect mature oligodendrocytes, because it labels the cell body (allowing clear quantification), and we used clone CC-1 of the APC antibody, because it is reportedly more specific for oligodendrocytes than polyclonal APC antibodies (32, 33). Notably, cells first expressed APC only 12 months after grafting (Figure 3, G and H). The proportion of all grafted GFP-labeled cells that coexpressed APC was 12% ± 1% at 12 months and 11% ± 1% at 18 months.

Having identified that the maturation of NSCs follows a human temporal course of development, we next sought to determine whether there was evidence of axonal pruning, another important aspect of developmental neurobiology.

Human axons project in large numbers over long distances, but their numbers are gradually reduced. As we reported previously (4, 5), human GFP-labeled axons emerged from grafts placed in the lesion site and extended rapidly and in large numbers over very long distances in the lesioned adult rat CNS (Figure 4). At the earliest time point sampled, 1 month after grafting, GFP-labeled axons had already extended 10 spinal segments caudally from the C5 lesion site to the T6 spinal cord, a distance of 27 mm (Figure 4, A and B, Supplemental Figure 5, A and B, and Supplemental Table 1). Axons also extended rostrally for a distance of 15 mm to the brainstem (Supplemental Figure 5, C and D, and Supplemental Table 1). The identity of these GFP-labeled processes as axons was confirmed by colocalization with the axonal marker βIII-tubulin (Tuj1) (Figure 4A, inset). Notably, while axons were present in both white and gray matter, many more axons were located in

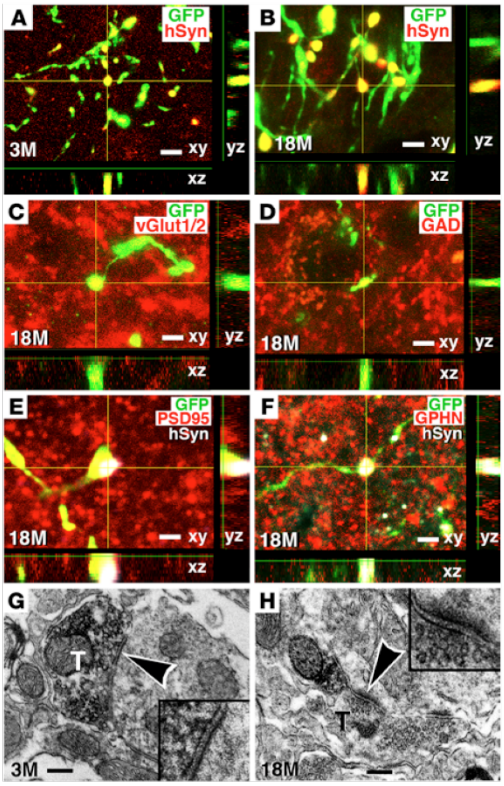

Figure 5. Connectivity of human axons with host neurons. (**A** and **B**) GFP-immunoreactive human axons in host gray matter at C8 expressed hSyn at both 3 and 18 months after grafting, suggesting the formation of presynaptic elements. (**C** and **D**) Some GFP-immunoreactive human axonal terminals expressed (**C**) vGlut1/2, suggesting the presence of excitatory synapses, or (**D**) GAD65/67, suggesting inhibitory synaptic terminals. (**E** and **F**) GFP and hSyn labeled presynaptic elements at human axonal terminals and were closely associated with individual excitatory and inhibitory postsynaptic proteins labeled with (**E**) PSD95 and (**F**) GPHN (all at C8 gray matter from subjects that survived 18 months). (**G** and **H**) Electron microscopy confirmed that DAB-labeled, GFP-expressing human axon terminals (T) formed synapses (arrowheads) with host dendrites (see insets) 3 months and 18 months after grafting. Synapses were asymmetric and contained rounded vesicles, suggesting excitatory synapses in these views. Scale bars: 3 μm (**A**, **B**, and **D**); 3.5 μm (**C**); 3 μm (**E**); 2.5 μm (**F**); 550 nm (**G** and **H**). Original magnification in **G** and **H** insets: ×15,000.

white matter than gray matter at the 1-month time point; branching into gray matter was relatively infrequent (Figure 4, A and B, and Supplemental Figure 5, A–D).

By 3 months after grafting, axons extended over even longer distances. Axons now reached the L4 spinal cord, a distance of 57 mm or 21 spinal segments (Figure 4, C and D, Supplemental Figure 5, E–H, and Supplemental Table 1). Axons also extended longer distances in the rostral direction over a distance of 48 mm, extending as far as the cortex and olfactory bulb, as previously reported (4, 5) (Supplemental Figure 5, I–N, and Supplemental Table 1). Moreover, the number of axons present in host gray matter (measured at the C8 spinal level, 3 spinal segments caudal to the lesion site) increased markedly (nearly 100-fold) from 1 to 3 months after grafting (Figure 4, B, D, and K). Notably, both the maximum distance over which axons extended and their density in host gray matter reached a maximum at 3 months (Figure 4, Supplemental Figure 5, E–N, and Supplemental Table 1). Neither maximum axon growth distance nor total axon numbers increased at the longer time points of 6, 12, and 18 months (Figure 4, E–J). Indeed, total axon numbers measured in white matter at the T12 spinal segment were maximal at 3 months and steadily declined by 75% at 18 months after grafting ($P < 0.05$, by ANOVA) (Figure 4L and Supplemental Figure 6, A–D). Interestingly, axon density in host gray matter (measured at the C8 level) was also reduced at the 18-month time point, but these reductions occurred later compared with white matter losses and were less extensive: axon numbers in host gray matter were approximately 50% of the numbers detected at 3 months (Figure 4K), although this late reduction was not significant ($P < 0.1$, by ANOVA; $P = 0.3$, by Fisher's exact post-hoc test comparing 12 months with 18 months after grafting). We measured axon numbers in host white matter at the T12 level, because we could clearly distinguish human axons from migrating human glia at this level (glia were never present at T12 except in 1 surviving 18 months that was excluded for axon number counting).

We further confirmed the identity of GFP-labeled processes as axons using the human-specific mature axonal marker neurofilament 70 (NF-70) (34). Expression of human NF-70 was clearly detected 12 and 18 months after grafting (Supplemental Figure 6, E and F), but not at 6 months or earlier time points, indicating that human axons, like human neurons, exhibit a protracted time course of maturation when grafted to sites of rodent SCI. We also observed colocalization of GFP-labeled axons with the early and late axonal marker Tuj1 (Figure 4A, inset).

Human axons in white matter frequently branched into host gray matter and formed axon terminal–like structures (Supplemental Figure 7A). Graft-derived human axons terminated in different zones of host gray matter, including dorsal, intermediate, and ventral host gray matter, with a preponderance of terminals in intermediate and ventral gray matter (Supplemental Figure 7, B–E).

Notably, human axons formed synapses with host rat neurons as early as 3 months after grafting (Figure 5A), despite the fact that neurons continued to mature for another 15 months. Synapses were also readily detected 18 months after grafting, indicating that synaptic projections onto host neurons could remain stable over time (Figure 5B). Some human axon terminals that projected onto host neurons were excitatory , as evidenced by the expression of vesicular glutamate transporter 1 and 2 (vGlut1/2) (Figure 5C). Other synapses expressed inhibitory transmitter markers (Figure 5D). In addition, human presynaptic elements were closely associated with the excitatory postsynaptic marker postsynaptic density 95 (PSD95) (Figure 5E) (35) and the inhibitory postsynaptic protein gephyrin (GPHN) (Figure 5F) (36). Immunoelectron microscopy confirmed synapse formation between GFP-labeled, graft-derived human axons and host rat neurons at both 3 and 18 months after grafting (Figure 5, G and H).

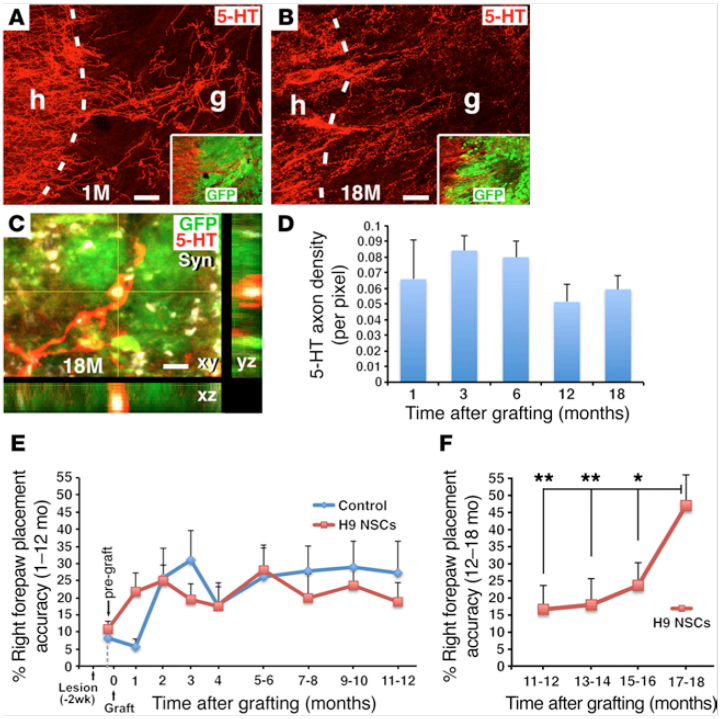

Figure 6. Host axonal regeneration and behavioral outcomes. (**A** and **B**) Host 5-HT–labeled serotonergic axons regenerated into GFP-expressing human NSC grafts in a C5 hemisection lesion site 1 and 18 months after grafting. Dashed lines indicate the host/graft (h/g) interface. (**C**) Higher-magnification image shows 5-HT–labeled host axons regenerating into a GFP-expressing human NSC graft. The 5-HT–labeled structures colocalized with Syn in a *Z*-stack image, 18 months after grafting. (**D**) 5-HT quantification reveals that host serotonergic penetration of grafts was stable over time ($P = 0.7$, by ANOVA), for 1 ($n = 3$), 3 ($n = 3$), 6 ($n = 5$), 12 ($n = 3$), and 18 months ($n = 4$). (**E**) Forepaw placement accuracy on a behavioral grid-walking task was measured monthly for the first 4 months and bimonthly thereafter. Following an initial period of modest recovery from 0 to 2 months after lesioning, functional performance thereafter was stable in both grafted ($n = 7$) and control lesion ($n = 5$) groups and did not improve from 1 to 12 months ($P = 0.62$, by 2-way repeated-measures ANOVA comparing graft and lesion-only groups from 1 to 12 months). The control group was perfused at a preplanned anatomical endpoint of 12 months. (**F**) Functional testing in NSC-grafted animals continuing beyond 12 months ($n = 4$) revealed a significant, 2.7-fold late recovery of function compared with their own stable functional baseline at 12 months. $^{**}P < 0.02$ and $^{*}P < 0.05$, by post-hoc Fisher's exact test comparing performance at 18 months at the indicated time points. Scale bars: 58 μm (**A** and **B**); 8 μm (**C**).

Host axons stably penetrate human NSC grafts. We examined host serotonergic axon penetration of human NSC grafts, as serotonergic systems play important modulatory roles in motor function (37, 38). We found that serotonergic axons penetrated grafts as early as 1 month after injury, and the distance of penetration and density of serotonergic axons in grafts remained stable up to 18 months after grafting (Figure 6, A, B, and D). Thus, in contrast to axons growing out of NSC grafts, adult axons regenerating into NSC grafts were stable and were not reduced in number over time. Serotonin (5-HT) somata were not present in human NSC grafts, indicating that serotonergic axons in grafts were host derived. In addition, regenerated serotonergic host axons expressed synaptophysin (Syn) (Figure 6C), suggesting potential synaptic connectivity with grafted neurons.

Function. Because human NSCs gradually mature over 18 months, prolonged time periods may be required to observe the functional effects of these cells compared with grafts of rodent NSCs, which mature far more rapidly and can support functional improvement within 3 months (4, 8, 39). Complete C5 right hemisection lesions cause lasting deficits in forelimb use, which can be assessed by measuring forepaw placement as animals walk on an irregular grid. Over a 1- to 12-month period, the functional performance of both grafted and lesioned control groups was identical ($P = 0.62$, by 2-way repeated-measures ANOVA) (Figure 6E). Moreover, while forepaw placement improved slightly from month 0 after lesioning to month 2 in all lesioned animals, as expected, function thereafter did not improve further, up to 1 year (ANOVA $P = 0.87$ for the grafted group from months 2 through 12 after lesioning). However, beginning at month 12, performance in the grafted group improved progressively from 17% accuracy in right forepaw placement to 47% accuracy by month 18, a 2.7-fold improvement that was statistically significant ($P < 0.01$, by ANOVA comparing all time points in the grafted group between 12 and 18 months; $P < 0.01$, by Fisher's exact post-hoc test comparing month 12 with month 18) (Figure 6F). The control group animals were sacrificed at month 12 as a preplanned study anatomical endpoint. However, performance of all lesioned animals plateaued 2 months after injury (Figure 6E) and would not have been expected to improve spontaneously after month 12 (40). Moreover, human clinical trials would be designed to detect late, within-subjects improvement from a chronic, stable baseline score, as in this study, because patients typically show little or no improvement in function at chronic post-injury time points (41–43).

Glial migration from human grafts into host white matter. We observed a slow and persistent migration of human astrocytes from the graft site into the host spinal cord over 18 months (Figure 7 and Supplemental Figure 8). Migrating GFP-immunoreactive cells were colabeled for the human cell–specific nuclear marker hNu and for the mature astrocyte marker GFAP (Figure 7), but did not colocalize with either neuronal (NeuN, Tuj1), oligodendroglial (APC, Oligo2, NG2) (Supplemental Figure 8, H and I), or NSC (nestin) markers (data not shown). Astrocytes migrated from the lesion site at a rate of 2 to 3 mm per month. One month after grafting, cell migration from the lesion site was not evident, but we observed migration into host white matter by 3 months after grafting for a distance of 5 to 6 mm (Figure 7, A and B, and Supplemental Table 1). This increased to

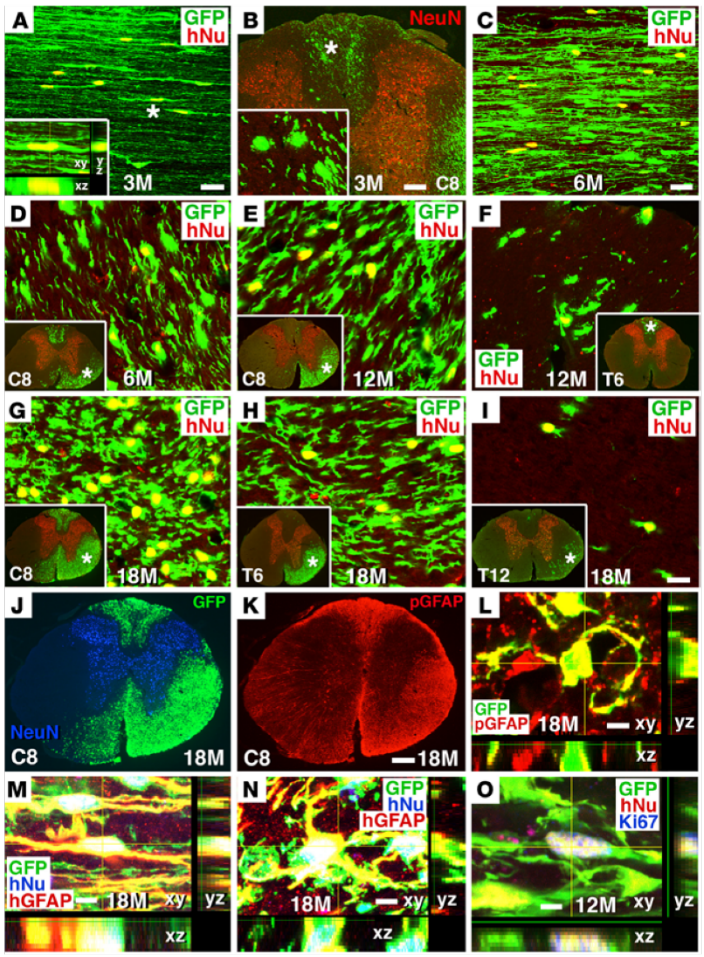

Figure 7. Human glial migration from graft site into host white matter. (**A** and **B**) Human NSCs migrated out of the graft into host white matter, beginning 3 months after grafting, as indicated by colocalization of GFP with the human-specific nuclear marker hNu. (**A**) Horizontal section 3 mm caudal to the graft (inset is a *Z*-stack image); (**B**) coronal section at C8 (inset is a higher-magnification image from the dorsal column region, indicated by an asterisk). (**C** and **D**) More extensive human NSC migration was evident 6 months after grafting at the same level as in **A**, 3 mm caudal to the graft. (**E** and **F**) Human cell migration at C8 and T6 after 12 months; insets show regions of sampling, colabeled for NeuN. (**G**–**I**) Human cell migration at C8, T6, and T12 at 18 months. (**J** and **K**) Migrated human cells (GFP$^+$) colocalized with pan-GFAP (pGFAP); C8 coronal section 18 months after grafting. (**L**) Confocal *Z*-stack image showing colocalization of GFP and pGFAP at C8. (**M** and **N**) *Z*-stack images showing colocalization of GFP$^+$ and hNu$^+$ human cells with the human-specific astroglial marker hGFAP, 18 months after grafting. (**M**) Horizontal section 3 mm caudal to the graft; (**N**) coronal section at C8. (**O**) *Z*-stack image showing GFP and hNu coexpressing the cell proliferation marker Ki67, 12 months after grafting in a C7 horizontal section. Scale bars: 28 μm (**A** and **C**); 100 μm (**B**); 18 μm (**D**–**I**); 260 μm (**J** and **K**); 3 μm (**L**); 7 μm (**M**); 5 μm (**N** and **O**). Original magnification of insets: ×1200 (**A**); ×400 (**B**); ×40 (**D**–**I**).

12 to 15 mm at 6 months (Figure 7, C and D, and Supplemental Figure 8, A and B); 24 to 36 mm at 12 months (Figure 7, E and F, Supplemental Figure 8, C and D, and Supplemental Table 1); and up to 45 mm at 18 months (Figure 7, G–I, Supplemental Figure 8, E–G, and Supplemental Table 1). Migration occurred in both rostral and caudal directions (Figure 7 and Supplemental Figure 8), but only in white matter; no human astrocytes were detected in host gray matter (Figure 7 and Supplemental Figure 8). Cells divided as they migrated, as evidenced by occasional labeling for Ki67 in these migrating cells (Figure 7O). In host white matter, we quantified the proportion of human cells that expressed Ki67 at spinal level C8, three segments below the lesion site, and this proportion gradually declined over time: 4.6% ± 0.7% at 6 months; 3.4% ± 2.8% at 12 months; and 0.34% ± 0.21% at 18 months. Most migrating human astrocytes had typical bipolar astrocyte morphology, with long processes that were oriented in a rostrocaudal direction (Figure 7 and Supplemental Figure 9A). Human astrocytic processes were closely associated with vascular endothelium, labeled by REC1, and surrounded blood vessels (Supplemental Figure 9B), suggesting the formation of a blood-brain barrier (44).

Ectopic cell collections were rare. It has been reported that grafts of NSCs can form ectopic cell deposits remote from the site of grafting (45, 46). In this experiment, remote cell deposits occurred in 2 of 18 animals (11%) (Supplemental Figure 9, C–F), and local extra-pial cell spreading was confined to 1 to 2 spinal segments from the graft site in 5 of 18 animals (28%). None of these extra-axial cell collections resulted in detectable compression or damage to underlying host neural tissue, even after 18 months, and labeling for astrocyte and microglial/macrophage markers failed to reveal evidence of a host response to the overlying human cells (Supplemental Figure 9, C and D). One remote ectopic cell deposit was present on the dorsal spinal cord surface at T12 cord in an animal surviving 12 months (Supplemental Figure 9C), and a second remote cell deposit was present in the dorsal medulla of an animal surviving 18 months (Supplemental Figure 9, E and F). In neither case was there secondary compression of the underlying host spinal cord or brainstem after this prolonged time period.

Discussion

We report here what to our knowledge is the longest survival period to date — 18 months — of NSCs implanted into sites of neurotrauma; to our surprise, we found evidence of continued stem cell maturation throughout this period. Neurons continued to hypertrophy and increase NeuN expression; mature astrocyte markers first appeared 6 months after grafting; and mature oligodendrocyte markers were not evident until 12 months after grafting. These findings clearly indicate that intrinsic human maturation "programs" are retained by NSCs placed in sites of neurotrauma and that neither the adult environment, the injured environment, nor the rodent environment alters this prolonged developmental time course. Moreover, recovery of forelimb function is supported by human NSC grafts, but only after mature cell markers of both neuronal and glial lineages are expressed.

In another parallel with normal human development, axons extended early and profusely from neural implants, and their numbers were pruned over 1 year to approximately half their original numbers in gray matter and to one-quarter their original numbers in white matter (Figure 4). These reductions are consistent with observations in neural development (47). This reduction in axon numbers observed in our study is not likely to be attributable to a downregulation in expression of the reporter gene GFP, since it is expressed under the ubiquitin promoter. Developmental cell death is another feature of normal nervous system development (48), and our grafted human NSCs exhibited a reduction of approximately 40% in total cell numbers from 3 months to 6 months after grafting. Interestingly, neuron numbers recovered at 12 and 18 months, points at which neurons also became more evenly distributed throughout the graft in the lesion site (Figure 2).

Human NSC–derived axons grew into both caudal and rostral host regions, including some ectopic regions such as the cerebral cortex and olfactory bulb. While ectopic axonal growth could result in adverse functional effects, the number of axons reaching these ectopic targets was very small, and gross functional deficits were not noted in these animals. In addition, axons may not reach these distant targets in the substantially longer human nervous system. Future long-term studies will be required to fully characterize the safety of this approach. Notably, neurons did not migrate from the lesion site, but astrocytes slowly migrated into host white matter at a rate of 2 to 3 mm per month. By 12 to 18 months, human glia represented a substantial proportion of astrocytes in host white matter both caudal and rostral to the lesion site (Figure 7 and Supplemental Figure 8), raising potential safety concerns. However, adverse effects of this glial outgrowth were not evident as either tumor formation or deterioration in forelimb function over time. Previously, Goldman and colleagues reported long-term safety and efficacy after administration of human glial progenitor cells in rodent demyelinating disease models (15), and Zhang and colleagues reported the functional integration of human-derived astrocytes into intact rodent spinal cord, including investment of astrocytic processes around host neurons and extension of end feet around blood vessels (44). Similarly, ectopic clusters of cells that have been previously reported (45, 46) with our grafting technique were only rarely observed at prolonged time points (2 of 12 animals surviving 6 months or longer) and did not compress the spinal cord. Nonetheless, for optimization of safety, grafting techniques can be used that minimize graft cell leakage into the cerebrospinal fluid after implantation in closed lesion sites; such measures eliminate ectopic cell collections (8).

Overall, our NSC grafts generated from the human ESC line H9 preliminarily showed acceptable safety outcomes over this prolonged experiment. Grafts did not expand over time, and cell division steadily declined over time, with a complete absence of dividing cell markers in 2 of the 4 animals examined at 18 months. This is useful long-term safety data for potential future human clinical trials.

The observation that NSC grafts continue to mature for at least 18 months and support late functional recovery has important implications for the design of human clinical trials. We propose that preplanned clinical outcome measures will need to be focused on equally long time points after grafting. Reliance on earlier time points for primary outcome measures could lead to a misleadingly negative interpretation of outcomes; instead, trial design will need to account for the prolonged developmental biology of NSCs.

Methods

Human ESC-derived NSCs. Generation of the human H9 ESC line and differentiation of NSCs from these ESCs have been described previously (19, 20). Briefly, human H9 ESCs were derived from the inner cell mass of a blastocyst-stage embryo with a normal female XX karyotype; these cells expressed primate ESC markers but not other early lineage markers (19). H9 ESCs were induced to differentiate into NSCs by embryonic body and neural tube–like structure formation in response to the presence of FGF-2. Differentiated NSCs were isolated by selective enzymatic digestion and further purified on the basis of differential adhesion (20). The H9 ESC–derived NSCs (H9-NSCs) expressed the NSC marker nestin and were able to differentiate into neurons, astrocytes, and oligodendrocytes in vitro following withdrawal of FGF-2. The H9-NSC line was obtained from Aruna Biomedical and Invitrogen (Thermo Fisher Scientific). We purchased H9-NSCs from Invitrogen (catalog N7800-100) and cultured H9-NSCs as a monolayer on a CELLstart coated flask (Thermo Fisher Scientific) in KnockOut DMEM/F-12 with supplement and FGF-2 and EGF. To track the transplanted human NSCs in vivo, we transduced proliferating H9-NSCs with lentiviral vectors expressing GFP (49). Approximately 95% of the H9-NSCs expressed GFP.

In vivo studies. A total of 26 adult female athymic, T cell–deficient nude rats (Harlan Laboratories) weighing 180–200 g were used in this study. The animals were deeply anesthetized using a combination (2 ml/kg) of ketamine (25 mg/ml), xylazine (1.3 mg/ml), and acepromazine (0.25 mg/ml) under aseptic conditions. All 26 rats received a right C5 hemisection as described previously (5, 50). Briefly, following C5 dorsal laminectomy, the dura was cut longitudinally and retracted. A 1.5-mm-long block of the right spinal cord was excised using a combination of iridectomy scissors and microaspiration, with visual verification to ensure complete transection ventrally, medially, and laterally. The lesion was closed, and the subjects were treated with the antibiotics ampicillin (3–5 mg/kg/day) via a s.c. daily injection for 1 to 2 weeks and amoxicillin and sulfamethoxazole in the drinking water (0.5 mg/ml) continuously until sacrificed.

Two subjects died one day after C5 hemisection, and one animal was perfused one week after C5 hemisection due to systemic illness (prior to grafting); none of the animals died after stem cell grafting.

The remaining 23 subjects were randomly divided into human NSC graft ($n = 18$) or control ($n = 5$) groups. Two weeks later, cultured human H9-NSCs were trypsinized, washed with PBS, and resuspended at a concentration of 250,000 cells/μl. Cells were mixed into a fibrin matrix containing a growth factor cocktail to promote survival and retention in the lesion site, as previously described (4, 5). The fibrin and growth cocktail alone (lacking NSCs, in controls) or human NSCs (5 μl) in the fibrin and growth factor cocktail were microinjected into the subacute lesion cavity using a pulled glass micropipette with an inner diameter of 40 μm, connected to a Picospritzer II (General Valve). Cells were injected into 6 sites encompassing the lesioned hemicord: 2 side-by-side injections were made at the center of the lesion cavity, spaced 0.5 mm apart (in the mediolateral plane); 2 side-by-side injections were made 0.5 mm rostral to the center of the lesion site, spaced 0.5 mm apart (in the mediolateral plane); and 2 side-by-side injections were made 0.5 mm caudal to the center of the lesion site, spaced 0.5 mm apart (in the mediolateral plane). Approximately 1 μl cell matrix per site was injected, for a total volume of approximately 5 to 6 μl. Injections were stopped if reflux occurred. After human NSC transplantation or vehicle injection, the animals were sacrificed at different time points as a time-course study of NSC survival, differentiation, and maturation: 1 month ($n = 3$); 3 months ($n = 3$); 6 months ($n = 5$); 12 months ($n = 3$ for the NSC group and $n = 5$ for the controls); and 18 months ($n = 4$).

Functional testing. Forepaw placement was examined on a gridwalk task. Footfalls were measured in 5-minute test sessions recorded on video as animals walked on a 38 cm^2 plastic-coated wire mesh field containing 3-cm^2 openings. Each forepaw was scored for the total number of steps and the total number of missteps. Step and misstep numbers were added to obtain the total number of placements. By convention, the right forepaw correct placement was calculated by dividing the number of steps by the total number of placements (steps plus missteps) (5, 51). Functional testing was performed for all animals surviving to 12 months (7 grafted animals and 5 controls) and continued for an additional 6 months for 4 grafted animals. The lesioned control animals did not continue functional testing beyond 12 months, because they had reached a preplanned anatomical endpoint for comparison with grafted animals. Initial testing was performed 1.5 weeks after C5 hemisection to obtain post-lesion scores, and then testing was performed monthly for 4 months and at least bimonthly thereafter (5, 51, 52).

Anatomical analysis. Rats were transcardially perfused with 4% paraformaldehyde in 0.1 M phosphate buffer (pH = 7.4) and post-fixed overnight. Spinal cords and brains were dissected out and transferred to 30% sucrose for 72 hours. A 12-mm length of spinal cord containing the NSC graft in the middle was entirely sectioned horizontally through its ventral-to-dorsal axis on a cryostat set at 30-μm thickness, and the horizontal sections were serially collected into 24-well plates for immunohistochemical analysis. In addition, the remaining spinal cord was blocked into 1- to 2-mm segments at C2, C8, T6, T12, and L4 spinal cord levels for coronal sections, and the whole right hemisphere of the brain was sectioned sagittally and collected into 24-well plates. Free-floating spinal cord and brain sections were processed for immunohistochemical analysis with the following primary antibodies: (a) GFP rabbit polyclonal antibody (A6455; Invitrogen, Thermo Fisher Scientific; 1:3,000) and GFP chicken polyclonal antibody (ab13970; Abcam; 1:3,000) for GFP labeling to assess grafted cell survival, differentiation, and processes outgrowth; (b) hNu mouse monoclonal antibody (MAB1281, clone 235-1; EMD Millipore; 1:200) for human nuclei labeling to assess grafted human cell bodies; (c) rabbit polyclonal antibody (ab16667, Abcam; 1:500) for Ki67 labeling to assess proliferating cells; d) mouse monoclonal antibody (10C2; Gene Tex; 1:500) for neural cell markers, including human-specific nestin; goat polyclonal DCX antibody (sc-8066; Santa Cruz Biotechnology Inc.; 1:1,000) for immature neurons; Hu human antibody for immature and mature neurons (1:1,000; a gift of Robert Darnel, Rockefeller University, New York, New York, USA) (25); Tuj1 mouse monoclonal antibody (MO15013; Neuromics; 1:200) for immature and mature neurons; NeuN mouse monoclonal antibody (ab104224, clone 1B7; Abcam; 1:1,000) for mature neuronal nuclei; goat polyclonal choline acetyltransferase (ChAT) antibody (AB144P; EMD Millipore; 1:200) for mature spinal motor neurons; human-specific NF-70 mouse monoclonal antibody (MAB5294, clone DP5 2.7.3; EMD Millipore; 1:1,500) to label human axons; 5-HT rabbit polyclonal antibody (20080; ImmunoStar; 1:10,000) for mature raphespinal neurons and axons; mouse monoclonal Syn antibody (MAB5258, clone SY38; EMD Millipore; 1:1,000) for presynaptic proteins expressed on both human and rodent synapses; hSyn mouse monoclonal antibody (NBP1-19222, clone EP10, Novus; 1:1,500) for human presynaptic proteins; vGlut1/2 mouse monoclonal antibody (MAB5502, clone 3C10.2, MAB5504, clone 8G9.2, Chemicon; 1:1,000) to label glutamatergic terminals; glutamic acid decarboxylase 65 or 67 (GAD65/67) to label GABAergic neurons/terminals (GAD65 goat polyclonal antibody, catalog AF2247, from R&D Systems, or GAD67 mouse monoclonal antibody, catalog MAB5406, clone 1G10.2, from EMD Millipore; 1:1,000); PSD-95 rabbit polyclonal antibody (ab18258, Abcam; 1:500) to label postsynapse density; GPHN rabbit polyclonal antibody (ab32206, Abcam; 1:1,000) to label postsynapse density; GFAP mouse monoclonal antibody (MAB360, clone GA5, EMDMillipore; 1:1,500) to label astrocytes; human-specific GFAP (hGFAP) rabbit polyclonal antibody (TA302094; OriGene; 1:1,000); APC mouse monoclonal antibody (OP80, clone CC-1; Oncogene; 1:800) to label oligodendrocytes; Oligo2 rabbit polyclonal antibody (18953; IBL; 1:200) to label immature and mature oligodendrocytes; vimentin mouse monoclonal antibody (MAB3400, clone V9; EMD Millipore; 1:80) to label immature oligodendrocytes; NG2 rabbit polyclonal antibody (AB5320; EMD Millipore; 1:400) to label immature oligodendrocytes; CNPase mouse monoclonal antibody (NE1020, clone SMI-91; EMD Millipore; 1:200) to label immature oligodendrocytes; PDGFR-α goat polyclonal antibody (sc-31178; Santa Cruz Biotechnology Inc.; 1:500) to label immature oligodendrocytes; GalC mouse monoclonal antibody (MAB342, clone mGalC; EMD Millipore; 1:100) to label immature oligodendrocytes; A2B5 mouse monoclonal antibody (ab-53521, clone 105; Abcam; 1:100) to label glial progenitors; myelin basic protein (MBP) rabbit polyclonal antibody (AB980; EMD Millipore; 1:250) to label myelin; and nestin mouse monoclonal antibody (556309, clone rat 401; BD Biosciences; 1:200) to label NSCs. Sections were incubated overnight at 4°C for primary antibodies individually or in combination and then incubated with Alexa 488–, 594–, or 647–conjugated goat or donkey secondary antibodies (Invitrogen, Thermo Fisher Scientific; 1:500) for 2.5 hours at room temperature. The sections were then washed, mounted on uncoated slides, and coverslipped with Fluoromount-G (SouthernBiotech).

The NSC graft area was measured using ImageJ software (NIH) on images of fixed box size at 1,600 × 1,200 pixels and ×20 magnification, using every sixth horizontal section that contained GFP-expressing graft. The pixel value was converted into mm^2 to obtain the average graft area in mm^2 per section. The ratio of Hu^+ neurons in

the NSC graft was determined by counting individual cells labeled for Hu within a fixed box size of 1,024 × 1,024 pixels in confocal images at ×600 magnification within the graft, divided by the total number of cells per sample box labeled with the human nuclear antigen hNu. Two randomly selected fields from the graft epicenter in two randomly selected horizontal sections were counted in each subject for each label. Exposure times were adjusted such that the brightest cell in each image was just below saturation. For each animal, 2 sections were quantified, with 1 grayscale image from both the rostral and caudal halves of the graft, for a total of 4 images per animal. For quantification of the size of Hu^+ and $NeuN^+$ neurons, images were converted to 8-bit and cropped to an 800 × 800 pixel region in the center of the original 1,024 × 1,024 pixel images. The dimensions of the cropped images were 155 × 155 μm. Each Hu^+ or $NeuN^+$ cell was outlined with the freehand tool and measured for area. Cells that extended to the borders of the image were not counted. The areas of Hu^+ or $NeuN^+$ cells in each animal were averaged and converted from pixels to square micrometers to produce the average Hu or NeuN size value.

The peak Hu and NeuN fluorescence intensity of grafted cells was quantified using ImageJ. A ×400 image was captured from horizontal sections in areas containing both the rostral and caudal halves of each graft and in which the brightest, most homogenous distribution of $NeuN^+$ cells could be found. An exposure time of 141 ms was used for all images. Bright, relatively large, and in-focus cell perimeters were outlined freehand, and an adjacent background area was selected for each cell. Corrected total cell fluorescence was calculated by subtracting the product of the area of a cell and the mean gray value of its respective background selection from the integrated density of the cell. A total of 20 cells from 2 sections were analyzed for each subject.

For estimation of the total number of Hu^+ and $NeuN^+$ neurons, 2 sections per subject were imaged at ×200 using a Keyence BZ-X710 automated fluorescence microscope. Each graft region was imaged in its entirety by stitching together full-focused, 960 × 720 pixel images captured automatically on the basis of 4 edge points representing the furthest extent of the graft (defined by dense GFP signal) in each x–y direction. At each edge point, the top and bottom planes of the *Z*-stack to be captured were set. A slice interval of 1.5 μm was used for all images. The exposure was set to a point at which the brightest Hu^+ or $NeuN^+$ cell in the graft was just below saturation. Images were captured in both 488-nm (GFP) and 594-nm (Hu or NeuN) channels during each run. Images were then analyzed using Fiji software (ImageJ). Graft regions were outlined with the Polygon Selection tool. The graft border was defined as the edge of continuous, dense, and homogenous GFP signal. Ectopic GFP^+ regions were not included as part of the graft. The area outside of the graft was then cleared from the image, and the red Hu or NeuN channel was isolated for analysis. A series of repeating 400 × 400 pixel regions of interest (ROIs) was then superimposed on the image, with 400 pixels between ROIs on the *x* axis, and 200 pixels on the *y* axis, resulting in one-third sampling of the graft area in each image. Within each ROI, Hu^+ or $NeuN^+$ cells with visible nucleoli contained entirely within the cropped graft were counted. Cells lying on the border of the ROI were only counted on the top and right edges. All ROIs containing any amount of graft area were quantified. The graft area was measured by setting the brightness threshold between 1 and 255, eliminating all pixels with a brightness value of 0 (the cropped out area of the original image), and using the Measure function. For each image, the number of Hu^+ or $NeuN^+$ cells was divided by the area of the graft in that image and averaged with the values for the other image from that subject to obtain the average Hu or NeuN density as number/square pixel. This density was then converted to the number of neurons/mm^2 and multiplied by the average total graft area and the total number of sections per subject to obtain the estimated total number of neurons/graft.

To estimate the total number of human cells in grafts (labeled for hNu), we calculated the ratio of Hu-labeled neurons to total hNu-labeled human nuclei in thin (1-μm) double-labeled (hNu/Hu) sections at ×600 magnification. Ratios were quantified from 2 anatomical regions per graft, and regions were pseudo-randomly selected by StereoInvestigator software. The total number of Hu-labeled cells per graft was divided by the ratio of Hu/hNu as follows: total number of human cells = (total number of Hu neurons)/(ratio of Hu/hNu). This procedure was used because individual hNu-labeled cells could not be individually resolved and quantified due to their high packing density, whereas Hu-labeled neurons could be individually resolved and quantified.

Glial cell differentiation was determined by counting individual cells labeled for GFAP and APC within a fixed box size of 1,024 × 1,024 pixels at ×400 magnification within the graft, divided by the total number of cells per sample box labeled with the human nuclear antigen hNu. Two randomly selected fields from the graft epicenter were counted in every 12th section in each animal for each label. The number of GFAP- and APC-labeled cells was counted in each grafted animal and divided by the mean number of hNu-labeled nuclei in the sampled field. Similar methods were used to quantify Ki67-labeled cells divided by the number of hNu^+ cells to obtain the percentage of Ki67 cells in the graft and at the C8 spinal cord level.

The ratio of migrating human cells expressing the glial marker hGFAP was determined by counting hGFAP and hNu double-labeled cells and dividing by the total number of hNu cells from ×400 *Z*-stack images taken from C8 coronal sections. The images were taken from 3 areas of the right-sided spinal cord white matter in which migrating, GFP-labeled cells were located: the dorsal columns, ventral white matter, and lateral white matter. The ratio of GFAP labeled glia in each area was averaged for each subject.

The number of GFP-labeled human axon profiles in gray matter of C8 coronal sections was counted from a ×400 *Z*-stack image in the medial central gray region including laminae 5–7, which human axons predominately innervated; there was no human glial cell migration in this region. Quantification of 2 coronal sections was done, and an average axonal profile number was obtained by adding total axon numbers in each of 2 sections and dividing by 2 (the number of sampled sections per animal). In addition, the number of axons in the whole right side of spinal cord white matter from two T12 coronal sections per subject was manually counted and averaged. One subject that survived 18 months was excluded because of the presence of glial processes at the T12 level.

The density of 5-HT–labeled serotonergic axons penetrating grafts in lesion sites was quantified as previously described (53). Briefly, a series of 1-in-12 sections was labeled for 5-HT to visualize serotonergic axons. The rostral lesion/graft border was identifiable as a region of GFP-labeled grafted cells that also expressed NeuN (graft-derived neurons did not migrate from the lesion site). The number of pixels occupied by graft at ×100 magnification was measured. The immunolabeled 5-HT axons within the graft were converted to black and white images, and the thresholding values of images were chosen,

such that only immunolabeled axons were measured and light, nonspecific background labeling was not detected. The total number of 5-HT–labeled pixels was divided by the graft area to obtain the mean axon density per pixel of graft.

To assess synapse formation between human axonal terminals and host neurons, a segment of spinal cord at the T3 level from two 3-month surviving and two 18-month surviving animals was refixed with 4% paraformaldehyde and 0.25% glutaraldehyde overnight. Horizontal sections were cut on a vibratome set at 50-μm intervals and processed for light-level observation of GFP immunolabeling using DAB and nickel chloride following the methods of Knott et al. (54). The host spinal cord gray matter containing GFP-labeled axons was then microscopically dissected and post-fixed with 1% osmium tetroxide, dehydrated, and embedded in Durcupan resin (Sigma-Aldrich). These samples were sectioned at a thickness of 60 nm using an ultramicrotome. Individual BDA-labeled axons or axonal terminals were located and assessed using an FEI 200KV Sphera microscope at the UCSD CryoElectron Microscopy Core Facility.

Statistics. For all quantification procedures, observers were blinded to the nature of the experimental manipulation. Comparisons among groups were tested by ANOVA (JMP software) at a designated significance level of $P < 0.05$ and followed by Fisher's exact post-hoc test between individual groups. Data are presented as the mean ± SEM. For behavioral analysis, repeated-measures ANOVA was used to assess group differences over time, with Fisher's exact post-hoc test.

Study approval. All the animal experiments were approved by the IACUC of the VA–San Diego Healthcare System, and NIH guidelines for laboratory animal care and safety were strictly followed.

Author contributions

PL, SC, and MT designed the experiments. YW, LG, and EB performed the behavioral tests. DW and PL prepared cell cultures. YW, DW, and HK performed histology. PL, SC, YW, DW, and HK acquired data. PL, SC, and MT analyzed data and wrote the manuscript.

Acknowledgments

This work was supported by the Veterans Administration Gordon Mansfield Collaborative Consortium for Spinal Cord Injury Research (1I50RX001706-01); Veterans Adminstration Merit Review grants (1 I01 BX001252-01A2 and 1 I21 RX00084-01A1); the NIH (NS09881 and EB014986); the Craig H. Neilsen Foundation; the California Institute for Regenerative Medicine; the Dr. Miriam and Sheldon G. Adelson Medical Research Foundation; and the Bernard and Anne Spitzer Charitable Trust.

Address correspondence to: Mark H. Tuszynski, Department of Neurosciences, 0626, University of California, San Diego, La Jolla, California 92093, USA. Phone: 858.534.8857; Email: mtuszynski@ucsd.edu.

1. Wictorin K, Brundin P, Gustavii B, Lindvall O, Björklund A. Reformation of long axon pathways in adult rat central nervous system by human forebrain neuroblasts. *Nature*. 1990;347(6293):556–558.
2. Lepore AC, Fischer I. Lineage-restricted neural precursors survive, migrate, and differentiate following transplantation into the injured adult spinal cord. *Exp Neurol*. 2005;194(1):230–242.
3. Tsuji O, et al. Therapeutic potential of appropriately evaluated safe-induced pluripotent stem cells for spinal cord injury. *Proc Natl Acad Sci U S A*. 2010;107(28):12704–12709.
4. Lu P, et al. Long-distance growth and connectivity of neural stem cells after severe spinal cord injury. *Cell*. 2012;150(6):1264–1273.
5. Lu P, et al. Long-distance axonal growth from human induced pluripotent stem cells after spinal cord injury. *Neuron*. 2014;83(4):789–796.
6. Han X, et al. Forebrain engraftment by human glial progenitor cells enhances synaptic plasticity and learning in adult mice. *Cell Stem Cell*. 2013;12(3):342–353.
7. Blaya MO, Tsoulfas P, Bramlett HM, Dietrich WD. Neural progenitor cell transplantation promotes neuroprotection, enhances hippocampal neurogenesis, and improves cognitive outcomes after traumatic brain injury. *Exp Neurol*. 2015;264:67–81.
8. Kadoya K, et al. Spinal cord reconstitution with homologous neural grafts enables robust corticospinal regeneration. *Nat Med*. 2016;22(5):479–487.
9. Nori S, et al. Grafted human-induced pluripotent stem-cell-derived neurospheres promote motor functional recovery after spinal cord injury in mice. *Proc Natl Acad Sci U S A*. 2011;108(40):16825–16830.
10. Iwai H, et al. Allogeneic neural stem/progenitor cells derived from embryonic stem cells promote functional recovery after transplantation into injured spinal cord of nonhuman primates. *Stem Cells Transl Med*. 2015;4(7):708–719.
11. Semple BD, Blomgren K, Gimlin K, Ferriero DM, Noble-Haeusslein LJ. Brain development in rodents and humans: Identifying benchmarks of maturation and vulnerability to injury across species. *Prog Neurobiol*. 2013;106–107:1–16.
12. Nutt SE, et al. Caudalized human iPSC-derived neural progenitor cells produce neurons and glia but fail to restore function in an early chronic spinal cord injury model. *Exp Neurol*. 2013;248:491–503.
13. Brüstle O, et al. Chimeric brains generated by intraventricular transplantation of fetal human brain cells into embryonic rats. *Nat Biotechnol*. 1998;16(11):1040–1044.
14. Windrem MS, et al. Fetal and adult human oligodendrocyte progenitor cell isolates myelinate the congenitally dysmyelinated brain. *Nat Med*. 2004;10(1):93–97.
15. Windrem MS, et al. Neonatal chimerization with human glial progenitor cells can both remyelinate and rescue the otherwise lethally hypomyelinated shiverer mouse. *Cell Stem Cell*. 2008;2(6):553–565.
16. Windrem MS, et al. A competitive advantage by neonatally engrafted human glial progenitors yields mice whose brains are chimeric for human glia. *J Neurosci*. 2014;34(48):16153–16161.
17. Wernig M, et al. Functional integration of embryonic stem cell-derived neurons in vivo. *J Neurosci*. 2004;24(22):5258–5268.
18. Nicholas CR, et al. Functional maturation of hPSC-derived forebrain interneurons requires an extended timeline and mimics human neural development. *Cell Stem Cell*. 2013;12(5):573–586.
19. Thomson JA, et al. Embryonic stem cell lines derived from human blastocysts. *Science*. 1998;282(5391):1145–1147.
20. Zhang SC, Wernig M, Duncan ID, Brüstle O, Thomson JA. In vitro differentiation of transplantable neural precursors from human embryonic stem cells. *Nat Biotechnol*. 2001;19(12):1129–1133.
21. Chang DJ, et al. Contralaterally transplanted human embryonic stem cell-derived neural precursor cells (ENStem-A) migrate and improve brain functions in stroke-damaged rats. *Exp Mol Med*. 2013;45:e53.
22. Khaing ZZ, et al. Assessing forelimb function after unilateral cervical spinal cord injury: novel forelimb tasks predict lesion severity and recovery. *J Neurotrauma*. 2012;29(3):488–498.
23. Lin R, Iacovitti L. Classic and novel stem cell niches in brain homeostasis and repair. *Brain Res*. 2015;1628(Pt B):327–342.
24. Barami K, Iversen K, Furneaux H, Goldman SA. Hu protein as an early marker of neuronal phenotypic differentiation by subependymal zone cells of the adult songbird forebrain. *J Neurobiol*. 1995;28(1):82–101.
25. Ince-Dunn G, et al. Neuronal Elav-like (Hu) proteins regulate RNA splicing and abundance to control glutamate levels and neuronal excitability. *Neuron*. 2012;75(6):1067–1080.
26. Greenlee JE, et al. Neuronal uptake of anti-Hu antibody, but not anti-Ri antibody, leads to cell death in brain slice cultures. *J Neuroinflammation*. 2014;11:160.

27. Sarnat HB, Nochlin D, Born DE. Neuronal nuclear antigen (NeuN): a marker of neuronal maturation in early human fetal nervous system. *Brain Dev*. 1998;20(2):88–94.
28. Tamagno E, et al. H2O2 and 4-hydroxynonenal mediate amyloid beta-induced neuronal apoptosis by activating JNKs and p38MAPK. *Exp Neurol*. 2003;180(2):144–155.
29. Yamaguchi K, Goto N. Development of the human magnocellular red nucleus: a morphological study. *Brain Dev*. 2006;28(7):431–435.
30. Lukás Z, Dráber P, Bucek J, Dráberová E, Viklický V, Stasková Z. Expression of vimentin and glial fibrillary acidic protein in human developing spinal cord. *Histochem J*. 1989;21(12):693–701.
31. Zhou Q, Wang S, Anderson DJ. Identification of a novel family of oligodendrocyte lineage-specific basic helix-loop-helix transcription factors. *Neuron*. 2000;25(2):331–343.
32. Lang J, et al. Adenomatous polyposis coli regulates oligodendroglial development. *J Neurosci*. 2013;33(7):3113–3130.
33. Bin JM, Harris SN, Kennedy TE. The oligodendrocyte-specific antibody 'CC1' binds Quaking 7. *J Neurochem*. 2016;139(2):181–186.
34. Reubinoff BE, et al. Neural progenitors from human embryonic stem cells. *Nat Biotechnol*. 2001;19(12):1134–1140.
35. Keith D, El-Husseini A. Excitation control: Balancing PSD-95 function at the synapse. *Front Mol Neurosci*. 2008;1:4.
36. Tyagarajan SK, Fritschy JM. Gephyrin: a master regulator of neuronal function? *Nat Rev Neurosci*. 2014;15(3):141–156.
37. Ribotta MG, Provencher J, Feraboli-Lohnherr D, Rossignol S, Privat A, Orsal D. Activation of locomotion in adult chronic spinal rats is achieved by transplantation of embryonic raphe cells reinnervating a precise lumbar level. *J Neurosci*. 2000;20(13):5144–5152.
38. Musienko P, et al. Controlling specific locomotor behaviors through multidimensional monoaminergic modulation of spinal circuitries. *J Neurosci*. 2011;31(25):9264–9278.
39. Lynskey JV, et al. Delayed intervention with transplants and neurotrophic factors supports recovery of forelimb function after cervical spinal cord injury in adult rats. *J Neurotrauma*. 2006;23(5):617–634.
40. Houle JD, Tessler A. Repair of chronic spinal cord injury. *Exp Neurol*. 2003;182(2):247–260.
41. Geisler FH, Dorsey FC, Coleman WP. Recovery of motor function after spinal-cord injury--a randomized, placebo-controlled trial with GM-1 ganglioside. *N Engl J Med*. 1991;324(26):1829–1838.
42. Fawcett JW, et al. Guidelines for the conduct of clinical trials for spinal cord injury as developed by the ICCP panel: spontaneous recovery after spinal cord injury and statistical power needed for therapeutic clinical trials. *Spinal Cord*. 2007;45(3):190–205.
43. Oh SK, Choi KH, Yoo JY, Kim DY, Kim SJ, Jeon SR. A phase III clinical trial showing limited efficacy of autologous mesenchymal stem cell therapy for spinal cord injury. *Neurosurgery*. 2016;78(3):436–447; discussion 447.
44. Chen H, et al. Human-derived neural progenitors functionally replace astrocytes in adult mice. *J Clin Invest*. 2015;125(3):1033–1042.
45. Tuszynski MH, et al. Neural stem cell dissemination after grafting to CNS injury sites. *Cell*. 2014;156(3):388–389.
46. Steward O, Sharp KG, Yee KM, Hatch MN, Bonner JF. Characterization of ectopic colonies that form in widespread areas of the nervous system with neural stem cell transplants into the site of a severe spinal cord injury. *J Neurosci*. 2014;34(42):14013–14021.
47. Low LK, Cheng HJ. Axon pruning: an essential step underlying the developmental plasticity of neuronal connections. *Philos Trans R Soc Lond B Biol Sci*. 2006;361(1473):1531–1544.
48. Pozniak CD, Radinovic S, Yang A, McKeon F, Kaplan DR, Miller FD. An anti-apoptotic role for the p53 family member, p73, during developmental neuron death. *Science*. 2000;289(5477):304–306.
49. Taylor L, Jones L, Tuszynski MH, Blesch A. Neurotrophin-3 gradients established by lentiviral gene delivery promote short-distance axonal bridging beyond cellular grafts in the injured spinal cord. *J Neurosci*. 2006;26(38):9713–9721.
50. Lu P, et al. Motor axonal regeneration after partial and complete spinal cord transection. *J Neurosci*. 2012;32(24):8208–8218.
51. Gensel JC, Tovar CA, Hamers FP, Deibert RJ, Beattie MS, Bresnahan JC. Behavioral and histological characterization of unilateral cervical spinal cord contusion injury in rats. *J Neurotrauma*. 2006;23(1):36–54.
52. Schallert T, Fleming SM, Leasure JL, Tillerson JL, Bland ST. CNS plasticity and assessment of forelimb sensorimotor outcome in unilateral rat models of stroke, cortical ablation, parkinsonism and spinal cord injury. *Neuropharmacology*. 2000;39(5):777–787.
53. Lu P, Jones LL, Tuszynski MH. BDNF-expressing marrow stromal cells support extensive axonal growth at sites of spinal cord injury. *Exp Neurol*. 2005;191(2):344–360.
54. Knott GW, Holtmaat A, Trachtenberg JT, Svoboda K, Welker E. A protocol for preparing GFP-labeled neurons previously imaged in vivo and in slice preparations for light and electron microscopic analysis. *Nat Protoc*. 2009;4(8):1145–1156.

Supplementary Figures

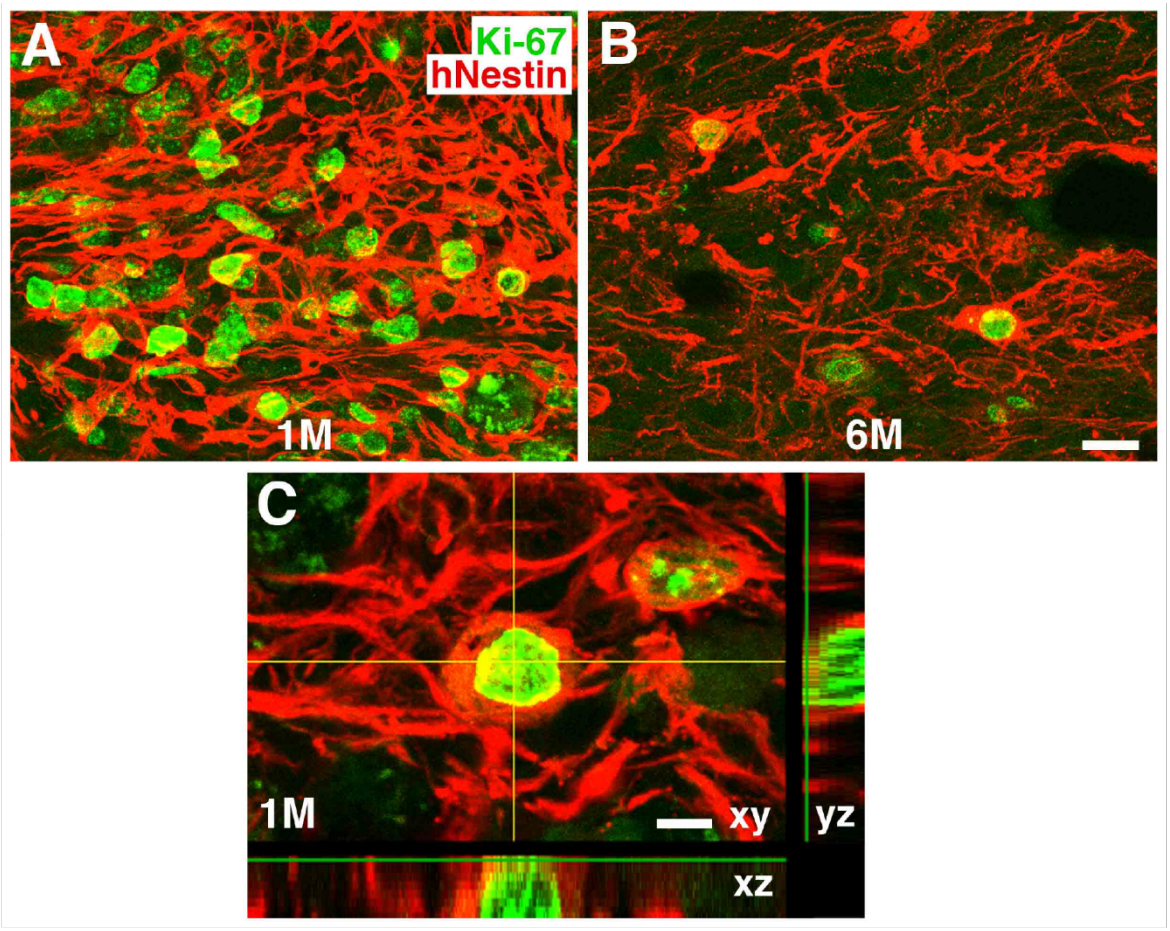

Suppl Fig. 1: Co-localization of Some Ki-67+ Cells with Human-specific Nestin in the Human Cell Graft

(A-B) Double labeling of **Ki67** and human-specific nestin **(hNestin)** reveals that some **Ki67**-labeled, dividing cells co-localize with **nestin,** 1 and 6 months post-grafting. **(C)** A high magnification confocal z-stack image shows a single **nestin**-labeled cells co-localized with **Ki67** at xy, xz, and yz views from 1-month grafted sample. Scale bar, 16 µm (A-B), 6 µm (C).

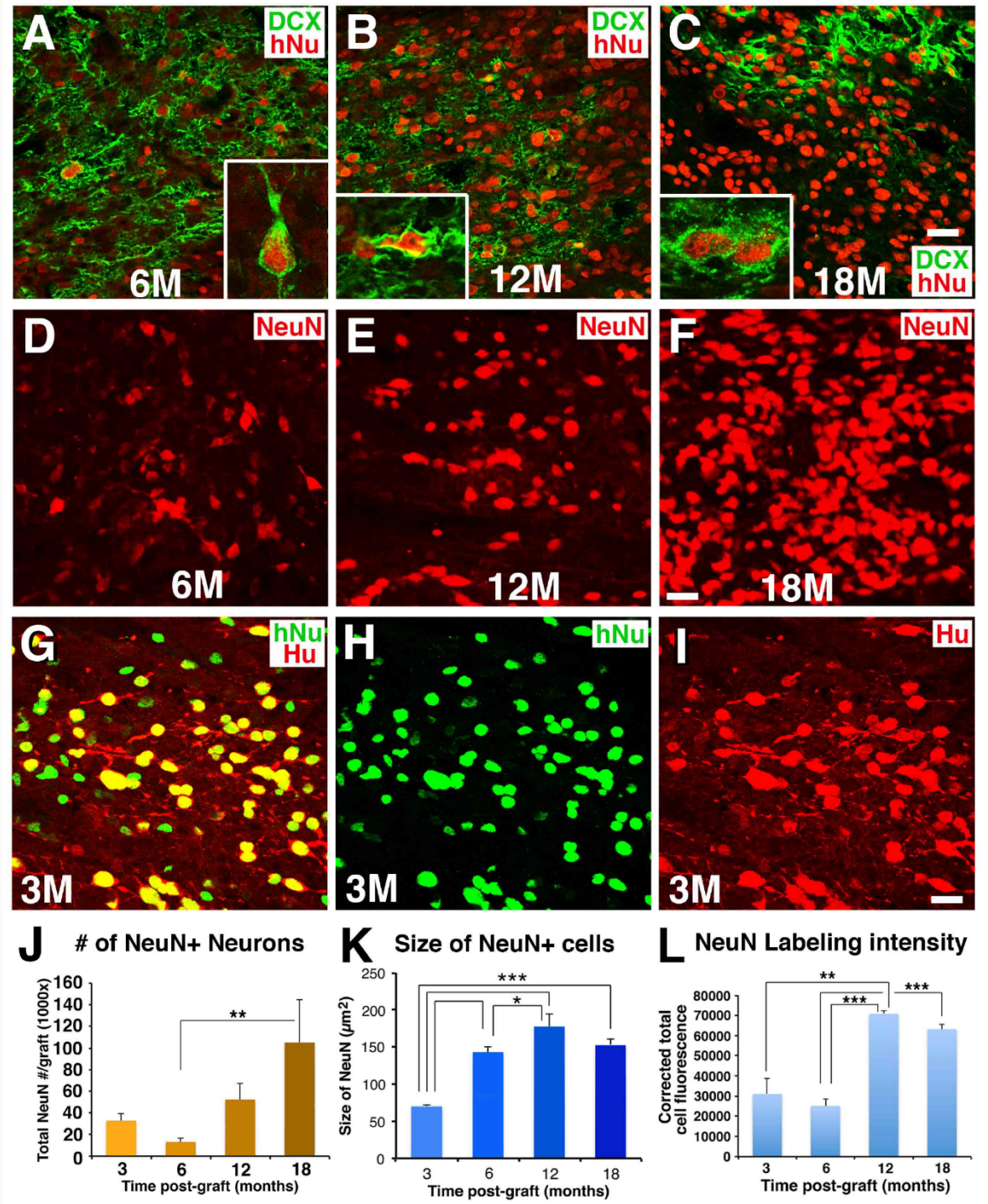

Suppl Fig. 2: Doublecortin (DCX), NeuN and Hu Labeling
(A-C) Doublecortin (**DCX**) and human nuclear (**hNu**) immunolabeling reveal persistent expression of **DCX** at 6, 12, 18 months post-graft (insets show examples of **DCX** and **hNu** double labeling); this labeling is patchy and progressively rarer in longer term

grafts. **(D-F)** **NeuN** labeling is persistent at 6, 12 and 18 months post-grafting. The density and size of **NeuN+** cells increased over time (quantified in J, K), consistent with Hu labeling at Fig. 2. **(G-I)** Double labeling for the human cell marker **hNu** and the neuronal marker **Hu** reveals that the majority of hNu-labeled cells co-localized with Hu 3-months post-grafting. **(J)** Quantification of total **NeuN$^+$** neurons 3, 6, 12 and 18 months post-grafting. **(K-L)** Quantification of **NeuN** size, and fluorescent label intensity. For J-L, $P<0.001$, ANOVA and ***$p<0.001$; **$p<0.01$; *$p<0.05$, post-hoc Fischer's comparison, 1 (n=3), 3 (n=3), 6 (n=5), 12 (n=3), and 18 months (n=4). Scale bar 32µm, A-F; 24µm, G-I.

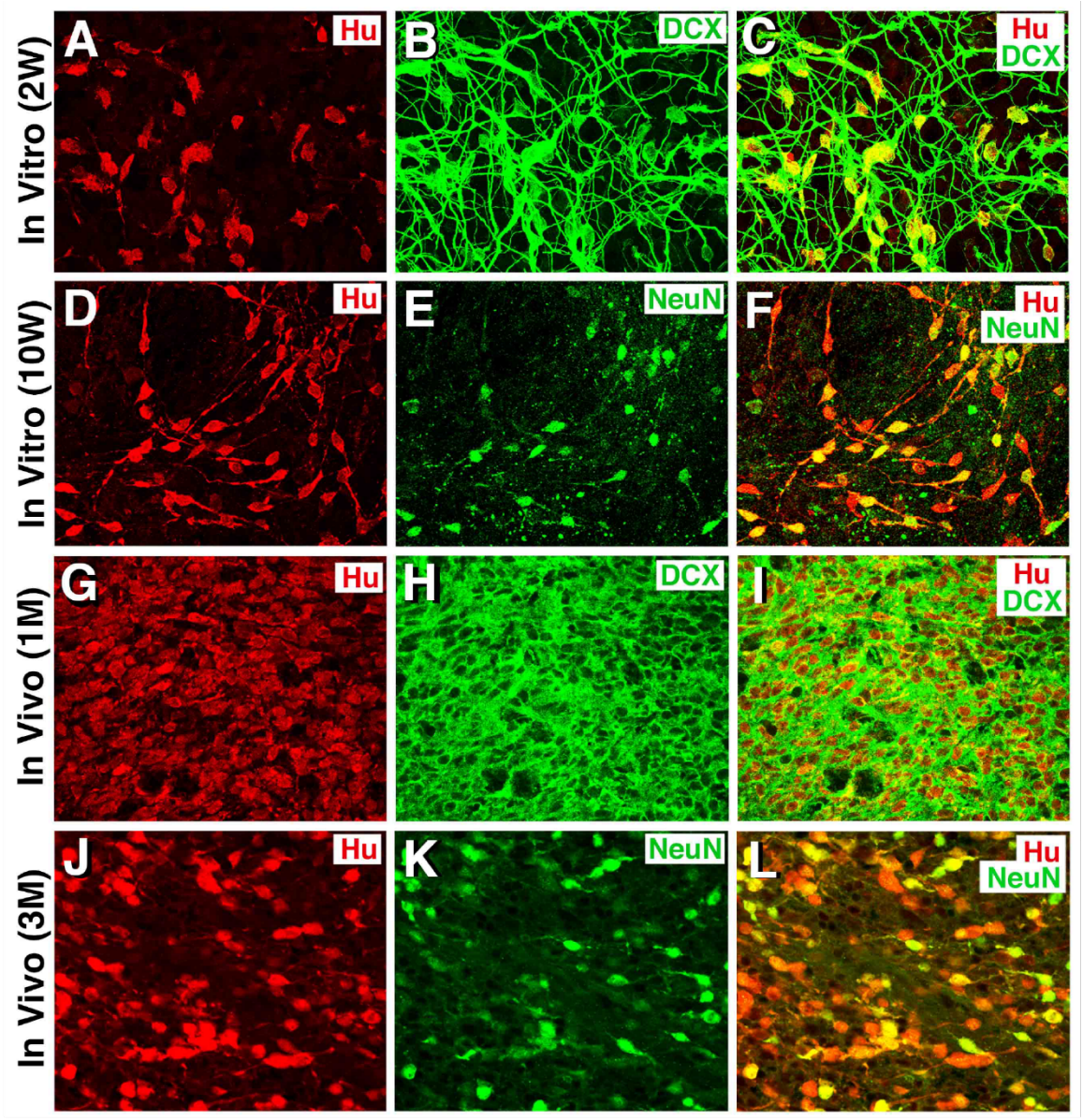

Suppl Fig. 3: Hu Labeling In Vitro and In Vivo

(A-C) The pan-neuronal label **Hu** and the early neuronal marker doublecortin **(DCX)** co-localize in H9-derived NSCs after 2 weeks in vitro, under a differentiation protocol. **(D-F)** After 10 weeks in vitro, NSCs mature and now predominantly co-localize with the mature neuronal marker **NeuN. (G-I)** After one month in vivo, grafted H9 NSCs co-localize for **Hu** and **DCX** in graft**. (J-L)** 3 months after in vivo grafting, NSCs predominantly co-localize for **Hu** and **NeuN**. Scale bar: 24 µm.

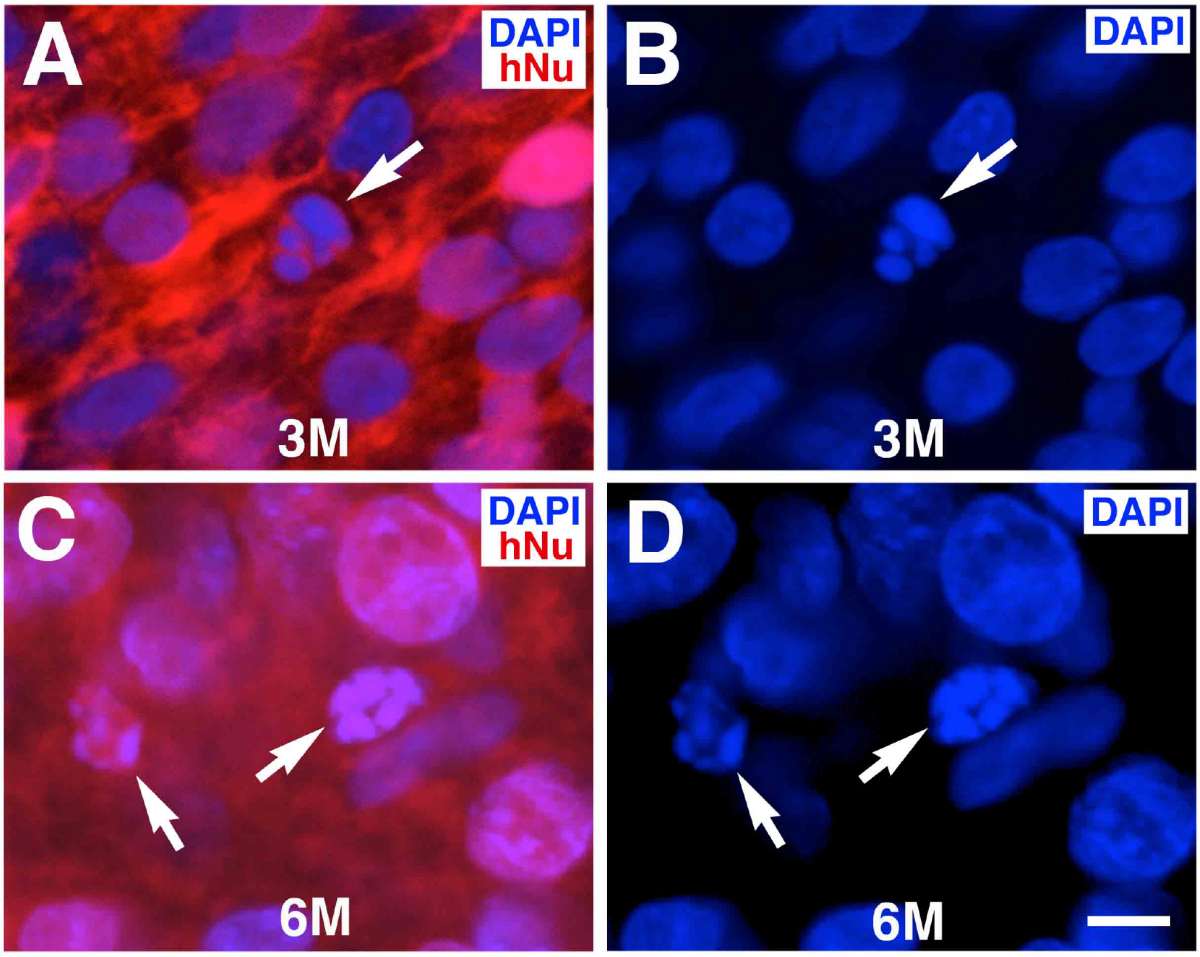

Suppl Fig. 4: DAPI Staining
DAPI immunolabeling reveals nuclear fragmentation (arrows) in human NSC graft identified by human cell specific marker **hNu** at (**A-B**) 3 and (**C-D**) 6 months post-grafting. Scale bar: 5 µm.

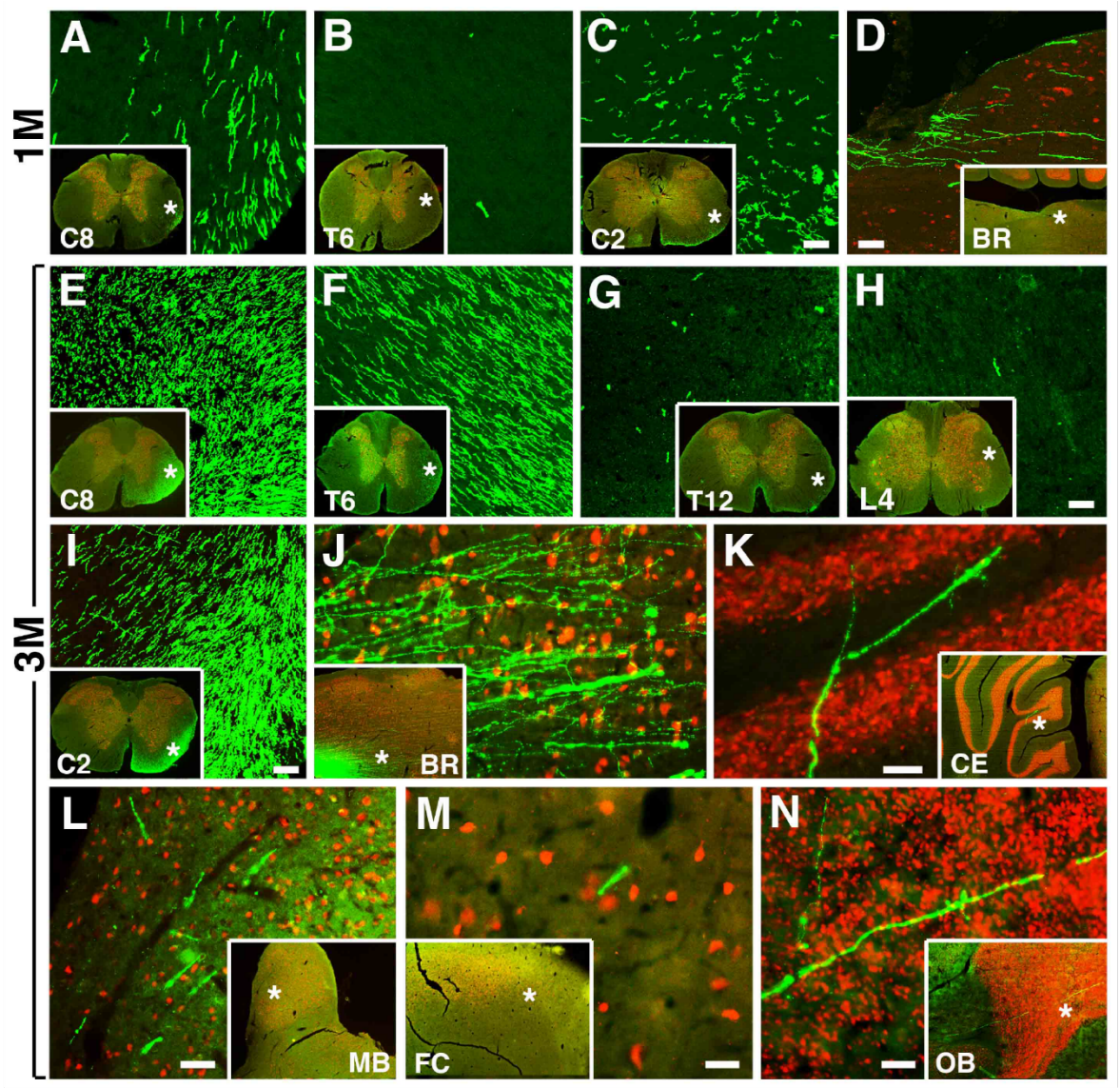

Suppl Fig. 5: Long-Distance Axonal Growth from H9-Derived NSCs at 1 and 3 Months Post-Grafting

(A-D) GFP and NeuN immunolabeling reveals GFP positive axons from human H9-NSCs graft at C5 hemisection site at 1 month extended caudally into **(A)** C8 and *as far* as into **(B)** T6 spinal cord (coronal view), and rostrally into **(C)** C2 and **(D)** brainstem (BS). * at inset indicates region of sampling. **(E-N)** GFP labeled human axons at 3 months post-graft extended caudally into **(E)** C8, **(F)** T6, **(G)** T12 and *as far* as into **(H)** L4, and rostrally into **(I)** C2 and **(J)** brainstem (BR), **(K)** cerebellum (CE), **(L)** midbrain (MB), **(M)** front cortex (FC) and **(N)** olfactory bulb (OB). Scale bar: A-C, 30μm; D, 50μm; E-I, 30μm; J, 55μm; K-M, 50μm; N, 45μm.

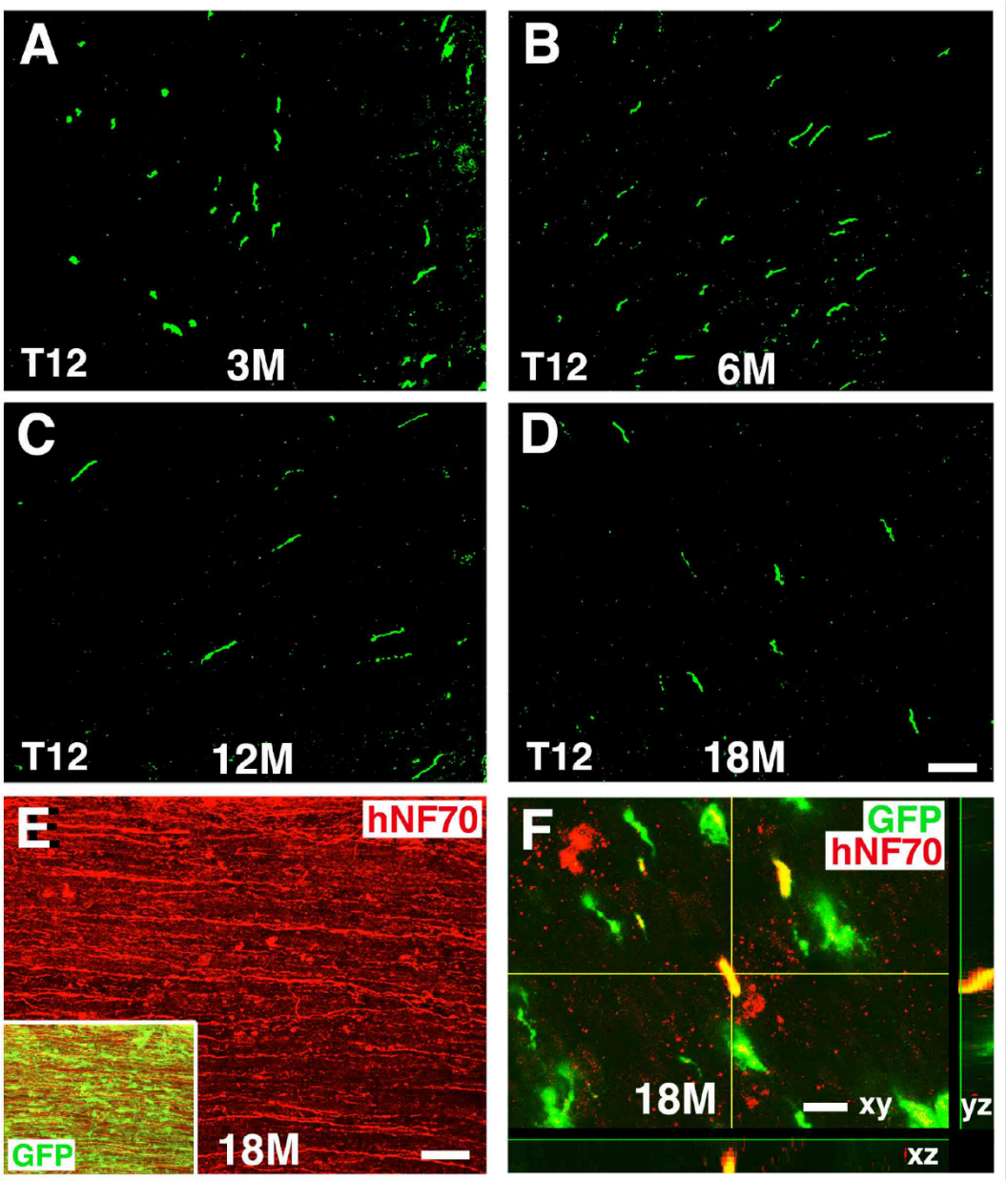

Suppl Suppl Fig. 6: Long-Term Persistence and Maturation of Graft-Derived Human Axons

(A-D) **GFP**-immunoreactive human axons in coronal sections of host white matter at T12 (16 spinal segments caudal to the lesion site) 3, 6, 12 and 18 months post-grafting. Axons were not found in this level at 1 month post-grafting. Migrating glia did not reach this level 18 months post-grafting, allowing quantification of GFP-labeled axon numbers as a function of time (except in one 18-month subject that was excluded from axon counts, due to glial migration). **(E)** Human-specific NF70 (**hNF70**) labeling reveals persistence of human axons in host white matter 18 months post-grafting, 2mm caudal to the lesion site. Inset shows double labeling of hNF70 and **GFP** that detects both large

migrating glia and fine axons. **(F)** A confocal z-stack image shows co-localization of fine **GFP+** human axons with **hNF70** in a C8 coronal section at 18 months post-graft. Migrating glial cells and processes are also present, labeled only for **GFP**. Scale bar = 30 μm (A-D); 48μm (E); 4μm (F).

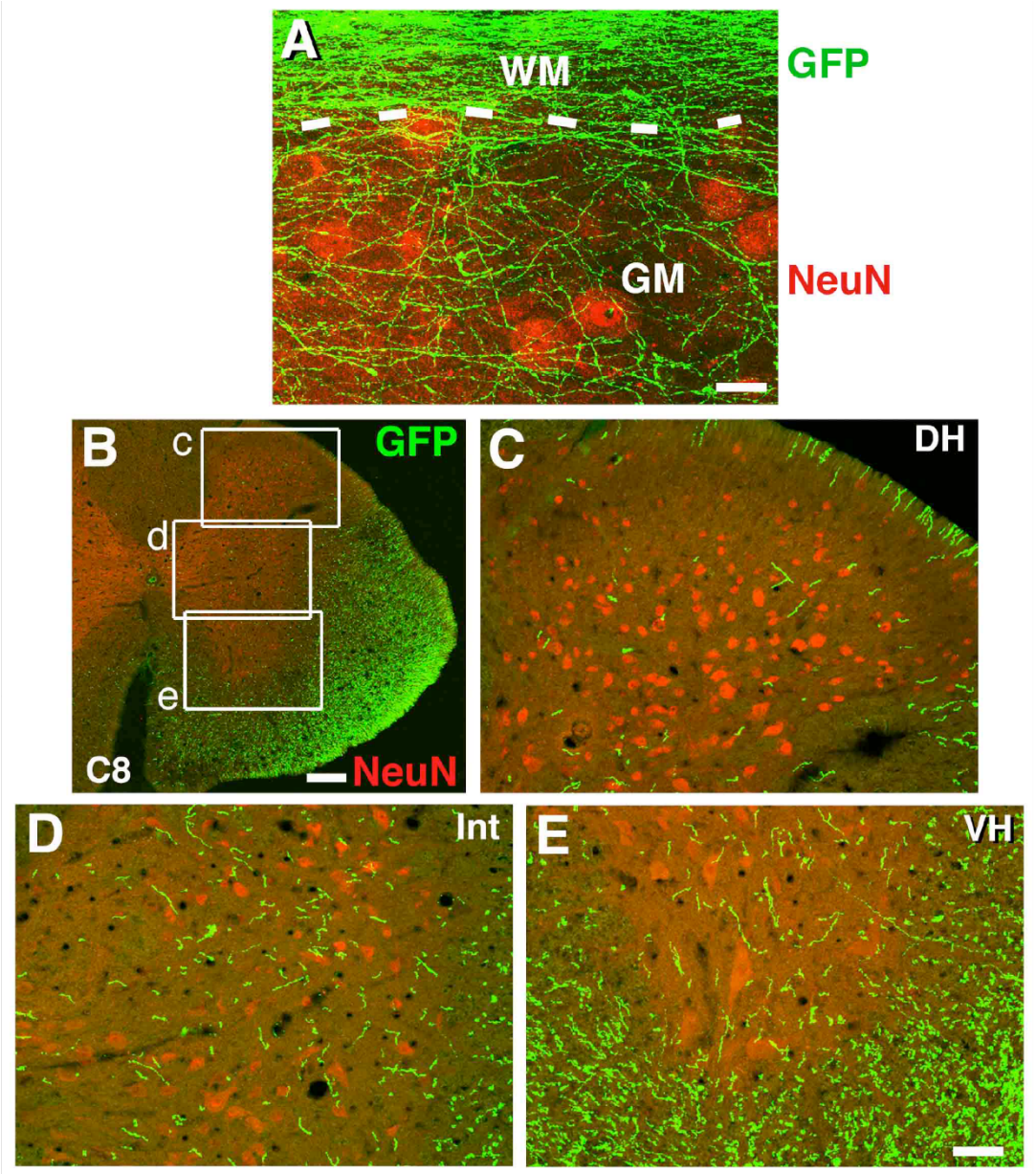

Suppl Fig. 7: Human Axons Terminate in Host Gray Matter Regions
(A) GFP-labeled human axons in host white matter (WM) branch and enter host gray matter (**GM**, indicated by regions of NeuN labeling), 3 months post-grafting. Axons branch and arborize extensively. Horizontal section, 2mm caudal to graft; dashed lines indicate interface of white and gray matter. **(B)** GFP+ human axons terminate in different zones of host gray matter, 3 months post-grafting in a coronal section view at C8, 3 segments caudal to the graft. **(C-E)** High magnification views from boxed area in panel B showing human axons in host **(C)** dorsal horn (DH) gray matter, **(D)** intermediate zone (Int) gray matter, and **(E)** ventral horn (VH) gray matter. Scale bar = 48 µm (A); 128 µm (B); 32µm (C-D).

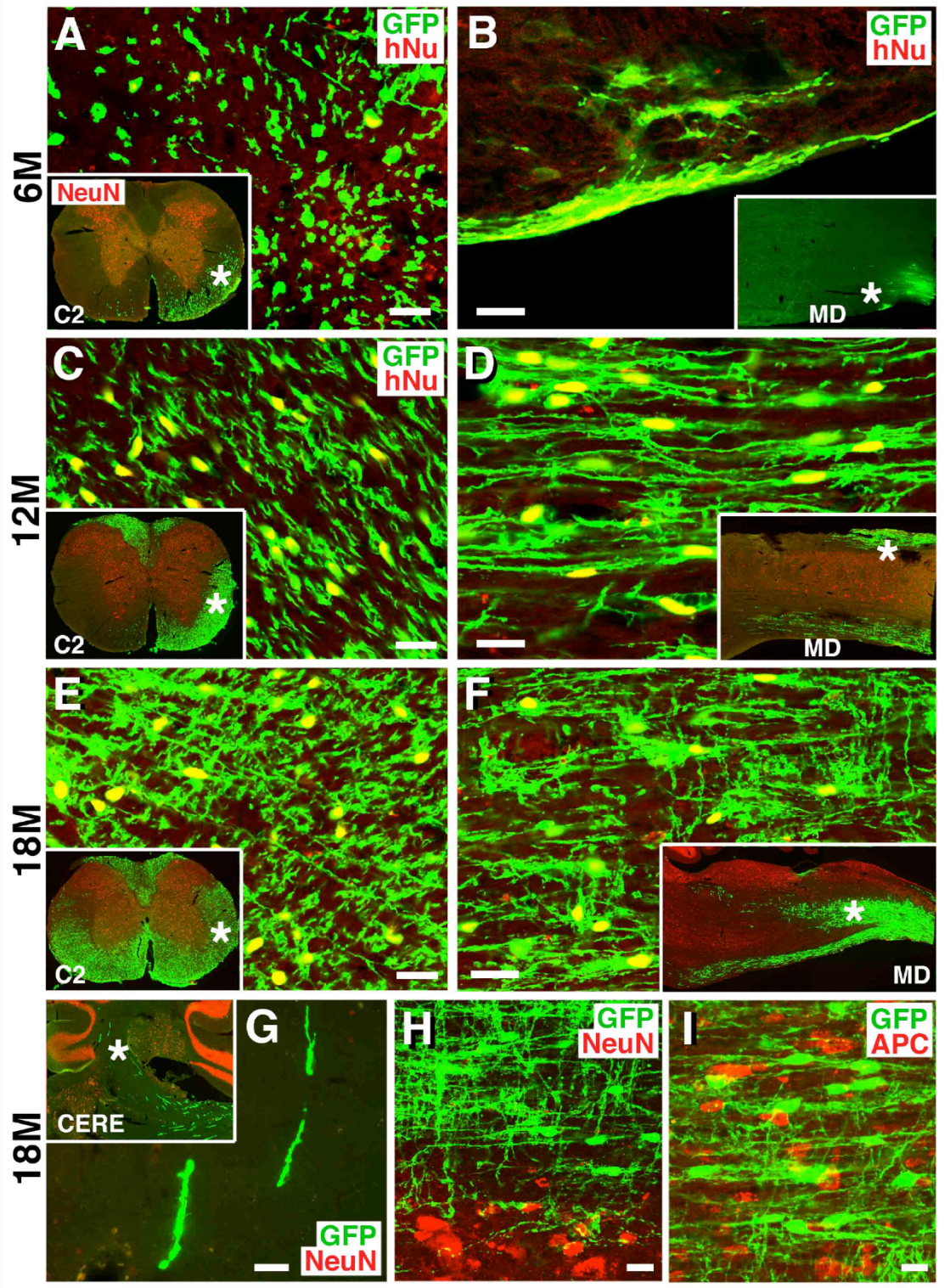

Suppl. Fig. 8: Rostral Migration of Human Cells

(A) **GFP+** and human nuclear+ (**hNu+**) cells were observed at C2, 6 mo post-grafting. Low magnification inset indicates section location; **NeuN** labels host gray matter

neurons. *indicates region of higher magnification view. **(B)** **GFP+** human cells labeled with **hNu+** in ventral medulla (MD), 6 mo post-grafting. **(C-D)** **GFP+** and **hNu+** human cells migrated rostrally toward **(C)** C2 and **(D)** dorsal medulla (MD), 12 months post-grafting. **(E-F)** **GFP+** and **hNu+** human cells migrated into **(E)** C2 and **(F)** medulla (MD) 18 mo post-grafting. **(G)** Thick **GFP+** human cell processes in cerebellum (CERE), 18 mo post-grafting. (**H-I)** **GFP+** human cells do not co-localize with **(H)** the neuronal marker **NeuN,** or **(I)** the oligodendrocyte marker **APC** (horizontal sections, 3mm from graft). Scale bar: A, C, E, 22μm; B, 25 μm; D, F, 32μm; G, 40μm; H, 25μm; I,18 μm.

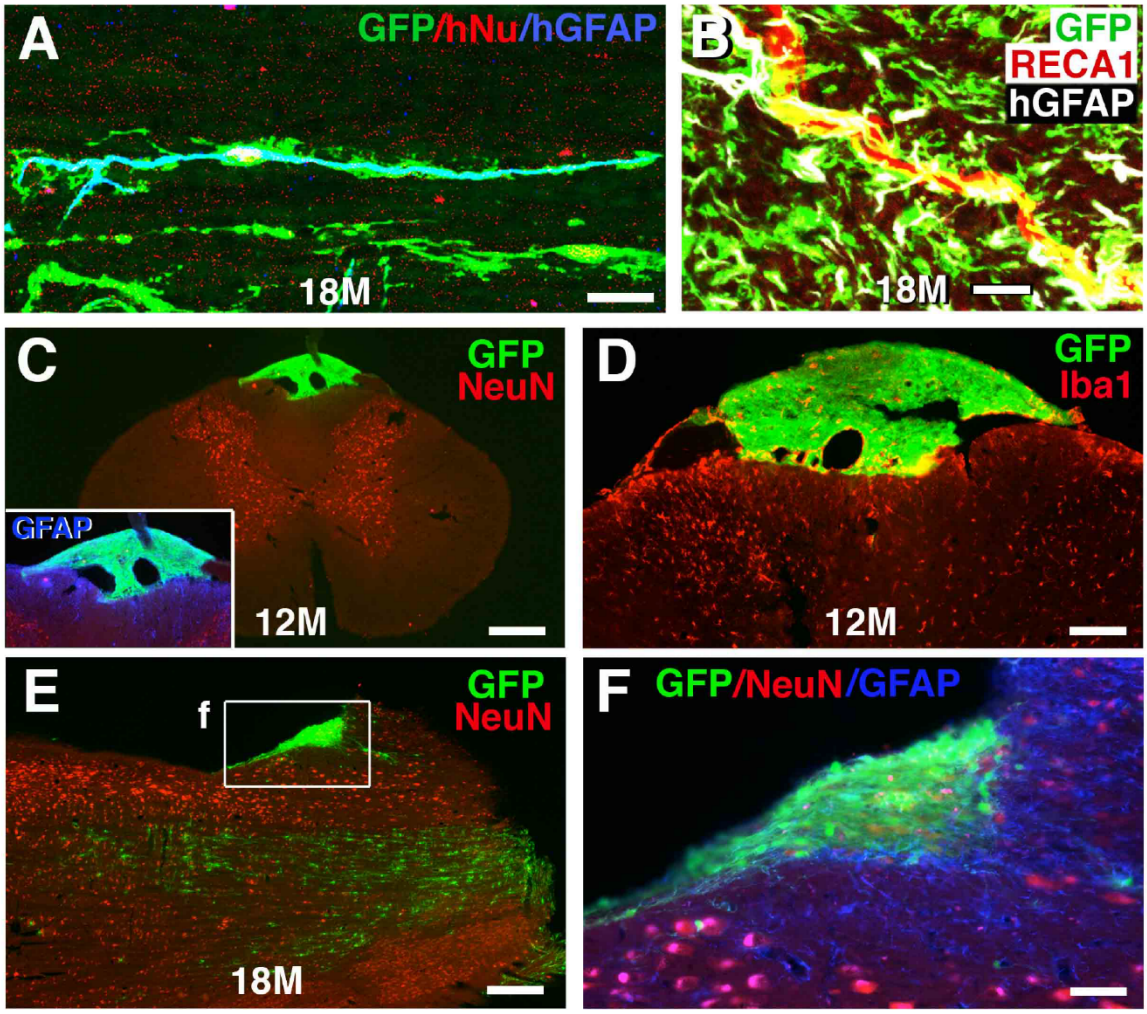

Suppl. Fig. 9: Morphology of Human Migrating Glia
(A) Morphology of a migrating **GFP+, hNu+** human cell that co-localizes with the human-specific astrocyte marker GFAP (**hGFAP**) in white matter, 2mm caudal to an 18-month graft site. **(B)** A migrated **GFP+** and **hGFAP+** (white) human glial cell associated with a host **RECA1+** endothelial cell in host white matter (coronal section at C8, 18 months post-graft). **(C)** **GFP+** human cells occasionally form a remote cell collection on the surface of host cord (coronal section at T12, 12 months post-graft). Inset shows differentiation of GFAP positive glia. **(D)** Graft does not express macrophage specific marker **Iba1**, and host cord under ectopic cell deposit does not show upregulation of **Iba1** immunoreactivity. **(E)** **GFP**-labeled sparse human cell deposit on dorsal surface of brainstem 18 months post-grafting. **NeuN** labels gray matter neurons. (**F**) A high magnification view from boxed area in E. **GFAP** labels astrocytes. Scale bars: 24μm (A); 13μm (B); 300 μm (C); 120 μm (D); 300 μm (E); 60 μm (F).

Table 1. Distance of Axonal Growth and Glial Migration

Time	Rat ID	Caudal								Rostral													
		C8		T6		T12		L4		C2		BR		CE		MB		HT /ST		FC		OB	
		Axons	Glia	Axons	Glia	Axons	Glia	Axons	Glia	Axons	Glia	Axons	Glia	Axons	Glia	Axons	Glia	Axons	Glia	Axons	Glia	Axons	Glia
1M	1	√		√						√		√											
	2	√								√													
	3	√		√						√													
3M	4	√		√		√		√		√		√		√		√		√		√		√	
	5	√	√	√		√		√		√		√		√		√		√		√			
	6	√		√		√				√		√		√		√		√					
6M	7	√	√	√		√		√		√	√	√	√	√		√		√		√			
	8	√	√	√		√		√		√	√	√		√		√		√					
	9	√	√	√		√		√		√		√		√		√		√		√			
	10	√	√	√		√				√	√	√		√		√		√		√			
	11	√		√		√				√	√	√		√		√		√		√			
12M	12	√	√	√	√	√				√	√	√	√	√		√		√		√			
	13	√	√	√		√				√	√	√	√	√		√		√		√			
	14	√	√	√	√	√				√	√	√		√		√							
18M	15	√	√	√		√		√		√	√	√	√	√	√	√		√		√		√	
	16	√	√	√	√	√	√	√		√	√	√	√	√		√		√					
	17	√	√	√	√	√		√		√	√	√	√	√	√	√		√		√		√	
	18	√	√	√		√		√		√	√	√	√			√		√					

BR, brainstem; CE, cerebellum; MB, midbrain; HT, hypothalamus; ST, stratum; FC, front cortex; OB, olfactory bulb.

Chapter 3, in full, is a reprint of the material as it appears in The Journal of Clinical Investigation 2017 Sep 1; 127(9): 3287–3299. Lu, Paul; Ceto, Steven; Wang, Yaozhi; Graham, Lori; Wu, Di; Kumamaru, Hiromi; Staufenberg, Eileen; and Tuszynski, Mark., American Society for Clinical Investigation, 2017. The dissertation author was the second author of this paper. He captured images, designed analysis methods, processed and analyzed data, wrote a portion of the manuscript, and edited the manuscript.

Chapter 4

General Discussion

Discussion

Many host axon populations regenerate into NPC/NSC grafts placed in sites of spinal cord injury, and graft cells mature into neurons which extend axons long distances into host tissue. To determine the nature of host activation of graft neurons and graft activation of host neurons, we employed optogenetic stimulation and recording techniques in acute spinal cord slices and performed in vivo imaging of spontaneous and sensory-evoked graft activity. This dissertation has demonstrated that stimulation of regenerating CST axons evokes excitatory synaptic responses in both individual graft neurons and clusters of spontaneously active graft neurons, while no evidence of slowly spreading excitation was observed. In turn, stimulation of graft axons elicits excitatory synaptic responses in host neurons caudal to the injury site. Individual graft neurons also respond to multiple sensory stimuli in vivo. Low sample sizes of responding neurons prevented analysis of the network-level effects of both graft axon stimulation on host neurons and sensory stimulation on graft neurons. Finally, human NSCs grafted into rodent SCI continue to mature over 18 months and support functional recovery at accordingly late time points. Below, the major findings of this dissertation will be discussed, and future directions to build on this work will be outlined.

Optical stimulation and recording is a novel and robust method for interrogating host-graft connectivity.

Previously used methods of testing synaptic connectivity between host and graft neurons are prone to artifacts and limited in scope. Gross extracellular stimulation and recording on either side of a graft, even when guided stereotactically, is ambiguous with regard to the exact cell populations being tested due to the unrestricted spread of current through tissue. It is also possible that stimulation of the spinal cord at one level may cause muscle twitches and associated body movement that could result in reflex responses in the spinal cord on the distal side of the lesion, potentially confounding results that indicate the presence of a neuronal relay. Implantable electrodes and electrode arrays offer more precise recording of single neurons, but it is not always clear exactly which cells are being recorded, especially in grafts of variable morphology. While whole-cell electrophysiology provides unrivaled precision in recording of neuronal activity, it is limited by the number of cells that can be patched simultaneously and the depth at which stable patches can be made. The optogenetic approach used in this dissertation circumvents all these shortcomings. Transfection of corticospinal neurons with ChrimsonR allowed specific stimulation of CST axons with orange light, while graft-specific expression of GCaMP6f enabled calcium imaging of dozens of graft neurons in the green spectrum. The same approach was then successfully adapted for stimulation of graft axons and recording of host neuron responses. Calcium imaging of graft activity was possible in both acute slice and in vivo preparations.

Although calcium imaging has become a widely used tool in the study of intact CNS tissues, it has seen relatively little use in assessing NPC/NSC graft function.

Perhaps the best example was the use of chronic 2-photon calcium imaging to track the functional integration of late embryonic cortical neurons transplanted into lesions of the visual cortex (Falkner et al., 2016). Graft neurons expressing the slow GCaMP6 variant, GCaMP6s, responded to visual stimuli in vivo, and the tuning of responses to stimuli of different directional orientation sharpened over 15 weeks following transplantation. However, the lack of stimulation of specific, identified host inputs into the graft leaves some uncertainty regarding the dynamics of host inputs into the graft, and mono- versus poly-synaptic nature of such inputs. In a traumatic brain injury model, NPC grafts transplanted into cortical lesions were loaded with the synthetic calcium indicator Oregon Green Bapta-1 (OGB-1) and imaged in vivo (Lin et al., 2018). Graft cells expressed the fluorescent protein DsRed, enabling identification of graft cells by co-labeling. Spontaneous calcium transients were observed in graft neurons, but neither graft responses to host stimuli nor graft activation of host neurons were assessed. Another group recently implanted brain organoids grown in culture into an aspirative lesion in the retrosplenial cortex of young adult mice and performed in vivo calcium imaging of graft cells. In these experiments, the red-shifted genetically encoded calcium indicator jRGECO1a was expressed in graft neurons through viral injection into GFP-expressing graft sites (Mansour et al., 2018). Graft neurons showed synchronous spontaneous activity, but connectivity with host systems was not assessed by calcium imaging. Finally, an insightful analysis of early NSC graft integration in host circuits used an organotypic striatal slice culture combined with calcium imaging to show that, prior to neuronal maturation and synapse formation, NSCs communicate with host neurons via gap junctions (Jäderstad et al., 2010). Synchronous calcium transients were observed

in host and graft cells, and it was proposed that NSC support of host cells through gap junctions may enhance host neuron survival after the explant procedure. To our knowledge, no other studies have utilized calcium imaging in spinal cord grafts, and no studies have combined calcium imaging with optogenetics to probe the synaptic connectivity between host and NPC/NSC grafts in any region of the nervous system. Thus, the approach taken in this dissertation is entirely novel, and it provides a platform to assess many more host-graft connections simultaneously than any other established methodology.

One of the key advantages of this technique is its simple and cost-effective implementation. A standard slice electrophysiology setup (a staple component of many neuroscience laboratories) can be readily and inexpensively adapted for all-optical experiments. The primary add-ons needed are two light-emitting diodes (LEDs) for stimulation and recording, two LED drivers, mounting hardware, and a custom filter cube. While advanced cameras for high speed imaging of dim signals can benefit data quality, a standard electrophysiology camera is sufficient for most widefield imaging experiments. Free, open-source software is available for image acquisition and analysis (https://micro-manager.org).

Despite the advantages of the all-optical approach, it comes with several limitations. First, successful stimulation and recording is highly dependent on expression levels of both the opsin and the calcium indicator. Insufficient or off-target ChrimsonR expression can prevent efficient stimulation of the desired axon populations, regardless of how many axons are physically present in the target location. Switching to neonatal AAV-ChrimsonR injections from adult injections dramatically increased the

efficiency of CST axon labeling. Using consistent skull positioning and landmarks was critical to obtaining robust CST labeling in the lumbar spinal cord, as only one injection site per hemisphere was used, leaving little room for error. Lastly, although we successfully stimulated CST axons with bright ChrimsonR-tdTomato expression induced just after birth, it has previously been reported that high expression levels of channelrhodopsins for prolonged time periods can result in altered axonal morphology and targeting (Miyashita et al., 2013). These effects were far stronger with in utero DNA electroporation than with viral transduction in adult animals, however, perhaps in part due to the early stage in development at which expression began.

Achieving the optimal level of GCaMP6f expression was also a difficult task. We initially generated GCaMP6f-expressing grafts by crossing Syn1-Cre males to Floxed-STOP-GCaMP6f females, and though we obtained some usable data in vivo, the expression was quite dim and, after a few generations of breeding, became unusable. This led us to use adeno-associated viral vectors, which must be appropriately titrated to yield functional expression; too little expression cannot be detected above noise, whereas too much expression can saturate cells so that no changes during activity can be seen. One must also be mindful of the fact that calcium indicators are also calcium buffers, and excessive expression can significantly alter calcium dynamics and cell physiology (Grienberger and Konnerth, 2012). We found that, although functional expression could be obtained by mixing Cre-dependent GCaMP6f vectors with Syn1-Cre NPCs just prior to grafting, a higher proportion of graft cells could be imaged by injecting non-Cre-dependent vectors intraparenchymally 3-4 weeks after grafting. This method sacrifices graft-specificity of GCaMP6f expression, but we found that, when

viewing acute slices with graft-specific GCaMP6f expression, graft regions could be faithfully delineated under differential interference contrast (DIC) by their notably distinct gross morphology compared to intact tissue. While this conservative approach likely leaves out some graft cells at the host-graft interface from the analysis, it provides a more complete picture of neuronal activity in the interior of the graft. Because the graft-host borders were not clear from the dorsal surface of the spinal cord, in vivo imaging was exclusively performed in animals with graft-specific GCaMP6f expression.

Grafts display spontaneous single-neuron activity as well as synchronous bursting activity in clusters of neurons.

In standard recording buffer with no drug added, grafts in acute slices displayed modest levels of spontaneous activity, both at the single neuron level and in clusters of synchronously active cells. The rate of such activity and the number of active neurons significantly increased following addition of 100 μM 4-AP. This concentration is roughly 100 times the plasma concentration after a typical 10 mg dose in human patients (Alviña and Khodakhah, 2010; Strupp et al., 2017); thus, we do not equate our slice recording conditions to a therapeutic use of the drug. Though addition of high concentration 4-AP clearly creates non-physiological conditions, it reveals a greater activity potential than would have otherwise been observable. Indeed, some acute slices appeared to be mostly silent prior to 4-AP wash-in. The seemingly random activation of individual neurons spread throughout the graft, interspersed with cluster activity, closely resembled that observed in intact spinal cord slices in the presence of 4-AP. This was particularly apparent in the most dorsal laminae, where large synchronous

bursts occurred across the entire field of view. Dorsal horn neuron activity rates were lower and more in line with in vivo calcium imaging studies prior to 4-AP wash-in (Johannssen and Helmchen, 2010; Sekiguchi et al., 2016), though synchronous activity was still observed.

Electrophysiological studies of superficial dorsal horn neurons in monkeys, cats, and rodents have demonstrated the presence of both irregular and regular spontaneous firing patterns (Hentall, 1977; Kumazawa and Perl, 1978; Sandkühler and Eblen-Zajjur, 1994). In an acute slice study using microelectrode arrays to record from up to four superficial dorsal horn neurons simultaneously, only 10% of cells showed correlated firing (Roza et al., 2016). Interestingly, every group of neurons displaying such activity contained at least one irregular fast-bursting (IFB) neuron, which sporadically discharged short (usually 2 – 5 spikes) bursts at ~100 Hz, suggesting that such neurons may play a role in coordinating synchronous activity. The same group later showed that while spontaneous activity was inhibited by cocktails including antagonists of both excitatory and inhibitory synaptic transmission in irregular fast-bursting neurons, clock-like neurons with regular firing patterns were mostly unaffected by this treatment (Lucas-Romero et al., 2018). Clock-like neurons were, however, often inhibited by specific ion channel blockers of persistent sodium and hyperpolarization-activated currents. These results may explain the presence of sporadic high amplitude calcium transients in some cells (putative irregular fast-bursting neurons) and rhythmic, low amplitude transients in other cells (putative clock-like neurons) in both graft and host tissue. Synchronously active clusters may then be driven by the activity of one or more irregular fast-bursting neurons contained within.

Spontaneous, synchronous activity has also been observed in more ventral neurons in neonatal and young (postnatal day 6-14) rodent spinal cord preparations (Kwan et al., 2010; Wilson et al., 2007, 2010; Zhong et al., 2010). In whole cord or thick slice neonatal and young preparations, spontaneous activation of central pattern generator (CPG) neurons can be observed in synchrony with activity in attached nerve root fibers with bath application of excitatory agonists such as N-methyl-D-aspartate (NMDA) or 5-hydroxytyptamine (5-HT), a phenomenon termed “fictive locomotion” (Cazalets et al., 1992). Central pattern generator circuits consist of both excitatory neurons involved in motor neuron activation (Kwan et al., 2010; Wilson et al., 2007) and inhibitory neurons involved in suppressing activity of motor neurons innervating opposing muscles (Wilson et al., 2010). As NPC grafts in this dissertation were generated from whole embryonic spinal cords, it is possible that the spontaneous activity patterns observed in these grafts contain contributions from both dorsal sensory- and medial/ventral motor-like networks that self-assemble in the presence of both sensory and motor axon innervation from the host.

Regenerating corticospinal axons form functional synapses with graft neurons that can elicit single neuron and neuronal cluster activity.

Optogenetic stimulation of ChrimsonR-expressing corticospinal axons regenerating into grafts resulted in calcium transient responses in graft neurons that began immediately after stimulation onset. Although we generally stimulated with trains of light pulses for 500 ms, responses began decaying prior to the end of the stimuli, indicating responses had already saturated by this point. Whether this saturation was

initiated in the presynaptic CST axons or the postsynaptic graft neurons was unclear. While continuous light pulses fail to drive action potentials in ChrimsonR-expressing cells after only a few spikes, trains of short pulses, such as those used in our experiments, can continuously drive action potentials with each pulse over several seconds (Klapoetke et al., 2014). Thus, it is likely that graft neurons either stopped firing or the total population of GCaMP6f molecules in graft neurons became saturated with calcium prior to the end of the stimulus. We did not observe consistent calcium responses with substantially longer latencies than the immediate responses reported. Although calcium transients that began several hundred milliseconds or longer after a single stimulus were sometimes observed, such transients never occurred with a consistent latency, indicating that they were likely coincidental spontaneous transients. Likewise, we did not see any slowly spreading waves of activity or depression, such as those observed in the cortex (Bikson et al., 2003; Pinto et al., 2005; Wenzel et al., 2017).

Graft neurons activated by CST stimulation showed diverse patterns of spontaneous activity. Some of these neurons were rarely if ever active without stimulation, whereas others exhibited spontaneous calcium transients either in an independent fashion or as part of synchronous bursts of activity in clusters of cells. In addition to pointing to different levels of connectivity among graft neurons, this may also indicate a diversity in the cell types responding to CST stimulation. Roughly a quarter of spontaneously active neuron clusters were activated by CST stimulation, suggesting that the majority of these clusters do not receive extensive corticospinal input. Supporting this hypothesis, clusters of dorsal horn-like sensory neuron clusters that self-

assembled in NPC grafts were previously reported to be avoided by regenerating CST axons (Dulin et al., 2018), which mostly innervated areas of more dispersed motor interneurons (Kumamaru et al., 2019). Importantly, CST stimulation activated neurons throughout the graft volume, even in caudal regions where fewer CST axons were observed. Due to the slow dynamics of calcium imaging relative to electrophysiological recordings, it was impossible to determine if these caudal responses (or, indeed, any graft responses) were the result of monosynaptic connections with corticospinal fibers or a polysynaptic relay with either graft cells or CST-activated host neurons that also innervated grafts; the sparsity of observable CST axons in these regions, however, supports the latter possibility. Blockade of excitatory synaptic transmission with 6,7-dinitroquinoxaline-2,3-dione (DNQX) ablated responses, confirming that they were in fact synaptic in nature. While bath application of tetrodotoxin (TTX) in addition to 4-AP can be used to confirm that responses are monosynaptic (continued 4-AP-enhanced response after TTX addition indicates a monosynaptic connection, because TTX blocks action potential propagation) (Cho et al., 2013), this technique relies on the detection of subthreshold responses by electrophysiological recordings, which precludes its use with calcium imaging.

Our findings of fast synaptic responses in graft cells to host stimulation parallel those of previous studies in the spinal cord (Etlin et al., 2016; Jayaprakash et al., 2019; Kadoya et al., 2016) and brain (Tornero et al., 2017; Wuttke et al., 2018) using optogenetic stimulation and electrophysiological recordings. For example, acute slice whole-cell patch recordings made from NPC graft neurons in a similar dorsal column lesion model in rats showed short latency excitatory post-synaptic currents (EPSCs) in

response to light stimulation of CST axons expressing Channelrhodopsin-2 (ChR2) (Kadoya et al., 2016). However, the present study was limited by the fact that only the most superficial neurons in the slice could be patched due to the high density of cell bodies in the graft compared to intact tissue. Responding cells were rare and EPSC amplitudes low, possibly due to the severing of a large fraction of the dendritic architecture of these superficial cells during the slicing procedure. In a preprint released this year using the same injury and graft model, in vivo recordings were made from a 32-channel shank electrode inserted into injury site (Jayaprakash et al., 2019). Eleven percent of spontaneously active units showed an increase in firing rate during optogenetic CST stimulation, compared to 65% of spontaneously active units located 0.5 mm rostral to the lesion center. While it is likely that at least some of the lesion site recordings were from NPC graft-derived neurons, the precise locations of the electrodes displaying responses in the injury/graft site were not determined by post-hoc tissue analysis, leaving open the possibility that these recordings were from spared host neurons. Therefore, assuming the widely validated premise that fast-rising, high-amplitude calcium transients in neurons are the result of cell firing (Chen et al., 2013; Emiliani et al., 2015; Grienberger and Konnerth, 2012), the findings of the present dissertation are the first unambiguous demonstration that regenerating CST axons can drive action potentials in graft targets.

Outgrowing graft axons form functional synapses onto host neurons below lesions.

An essential component of the neuronal relay hypothesis is that graft neurons not only receive synaptic input from the host, but in turn extend axons and form synapses onto distal host targets. Indeed, we found that stimulation of ChrimsonR-expressing graft axons resulted in post-synaptic responses in host neurons caudal to the injury. As in CST-to-graft connections, responses began immediately following stimulus onset and peaked prior to the end of the 500 ms stimulus, indicating response saturation. While we could not determine if these particular responses were monosynaptic or polysynaptic, logic dictates that if any host response is observed to graft-specific stimulation, at least some connections (observed or not) must be monosynaptic. Additionally, the neuropil damage created in the acute slice preparation makes detection of polysynaptic responses less likely with each additional synapse. Due to the low number of responding cells, we were not able to assess the cell cluster activation patterns of graft stimulation in the host. Additionally, poor GCaMP6f expression in ventral host spinal cord regions precluded observation of graft connectivity to these areas. Although we did observe graft axon innervation of ventral spinal cord, the dorsal column lesion does not provide the maximum opportunity for ventral graft axon outgrowth, as most of the white matter disrupted by this lesion is in the dorsal half of the spinal cord, and graft axons preferentially grow along both intact and degenerating white matter tracts (Poplawski et al., 2018).

Several factors may have contributed to the low number of responding host neurons. First, because NPC grafts into dorsal column lesions are relatively small compared to other lesion models (Brock et al., 2017; Kadoya et al., 2016; Lu et al., 2012), fewer neurons were present from which axons could extend. Furthermore, these

axons grew both rostrally and caudally into white and gray matter, distributing the total output. In contrast, the dorsal column lesion severs ~98% of corticospinal axons (Weidner et al., 2001), which are then in direct apposition to subsequently placed NPC grafts. This provided a much greater opportunity for dense innervation of ChrimsonR-expressing axons in the imaging site during CST-to-graft connectivity experiments. While such dense innervation may not be necessary to elicit post-synaptic responses in vivo, with all connections intact, the requirement for suprathreshold responses for detection by calcium imaging in acute slice preparations could set an artificially high bar for the strength of observable connectivity. Another important difference in assessing connectivity from host to graft and graft to host is that graft cells are substantially younger than host cells, as they are grafted at an embryonic development stage into adult hosts. We and others have noted that slice tissue health and electrical recording access/stability declines with increasing age of the animal (Husch et al., 2011; Mitra and Brownstone, 2012), so it is possible that fewer host neurons receiving graft input were healthy enough to display robust calcium responses than graft neurons receiving CST input. In agreement with findings that larger ventral spinal cord neurons are more vulnerable to ischemia in slice preparations than dorsal horn neurons (Mitra and Brownstone, 2012; Nohda et al., 2007), we observed notably more active neurons in the dorsal aspect of slices, particularly in the superficial dorsal laminae with the smallest neuronal cell bodies. Finally, the strength of graft synapses onto host neurons simply may not be as strong as those from corticospinal axons onto graft neurons. Little is currently known about these synapses, and it may be that persistent cortical output through regenerating CST axons strengthens host-to-graft connections, as observed in

connections made by sprouting CST axons (Jiang et al., 2019; Mishra et al., 2017; Zareen et al., 2017), but such stimulation is not present to the same degree in caudally projecting graft axons.

Earlier investigations of graft modulation of host circuitry were performed with electrophysiological recordings from host neurons and optogenetic stimulation of graft neurons (Etlin et al., 2016; Mansour et al., 2018; Wuttke et al., 2018). Embryonic cortical neurons transplanted into intact cortex evoked low-amplitude, subthreshold responses with millisecond-scale latency in host neurons in both ipsilateral and contralateral cortical hemispheres (Wuttke et al., 2018). In another study, stimulation of brain organoids grafted into retrosplenial cortex resulted in short-latency local field potential responses in host tissue rostral to the graft (Mansour et al., 2018). However, channelrhodopsin-2 viral vector expression was not genetically limited to graft cells, raising questions about possible direct stimulation of host neurons. Lastly, ChR2-expressing GABAergic progenitor cells from the medial ganglionic eminence (MGE) transplanted into intact spinal cord produced low-latency post-synaptic hyperpolarizations in adjacent host neurons when light-stimulated (Etlin et al., 2016). Because these grafted neurons were inhibitory, they could not by definition drive action potentials in host neurons. Thus, our findings of fast activation of host neurons by optogenetic stimulation of NPC graft axons are in line with previous analyses of graft synaptic output, and they represent the first direct evidence of such functional connections made by grafts placed into sites of spinal cord injury.

Sensory stimulation activates graft neurons in vivo

Two-photon calcium imaging through a glass coverslip mounted on the dorsal surface of the spinal cord enabled detection of graft neuron activity in vivo. Transgenic expression of GCaMP6f ensured graft-specific calcium imaging. While spontaneous activity in graft neurons was occasionally observed, much of the activity seen was evoked by sensory stimuli. Graft cells responded to hindpaw pinch, hindlimb movement, and light touch of the lower back. Such responses could be consistently driven by repeated stimulation trials, and the majority of responding cells only responded to a single type of stimulus, suggesting the presence of circumscribed connections from sensory afferents onto individual graft neurons. While we did not quantify response latency due to the imprecise timing of manual stimuli, our qualitative impression was that the latency of in vivo responses was longer and more variable than in acute slices, perhaps due to differing stimulus strength thresholds required to elicit responses. Pilot experiments of CST stimulation in vivo did not yield detectable graft responses (data not shown), and large motion artifacts in the z-plane during awake imaging prevented analysis of calcium activity during locomotion or other voluntary behaviors. These motion artifacts may have been due to the different surgical procedures required for imaging previously injured and grafted regions of the spinal cord compared to imaging of intact cord (Sekiguchi et al., 2016). In intact animals, laminectomies over the imaging area were performed by drilling down and cutting laminae after spinal column stabilization with imaging chamber hardware, whereas laminectomies were performed with rongeurs prior to spinal stabilization in injured animals. Additionally, laminectomies were centered at the T12 vertebra in injured animals, a point at which there is far more

curvature of the spine than the L4-L5 laminectomies performed in intact animals, which made aligning multiple vertebral segments in a single plane for hardware mounting virtually impossible.

A major limitation of in vivo imaging was the superficial depth at which neuronal activity could be detected. At this depth of no more than 100 μm below the surface of the spinal cord, many fewer graft neurons were present than in more ventral regions, as seen by NeuN immunofluorescent labeling. We could not, therefore, analyze population activity among graft neurons to verify whether or not the synchronously active clusters observed in acute slices were also present in vivo. Additionally, fewer CST axons innervate these superficial regions, which could potentially explain why responses were not seen to CST stimulation in vivo.

As previously discussed, no studies of which we are aware have assessed host input to grafts in sites of SCI by calcium imaging. However, the responses to sensory stimulation which we observed in graft neurons were similar to those reported in dorsal horn neurons of the intact spinal cord (Johannssen and Helmchen, 2010; Sekiguchi et al., 2016). In both of these studies and in ours, neurons responded to hindpaw pinch with comparable calcium transient waveforms. Sekiguchi and colleagues reported that dorsal horn neurons exhibited a much higher mean activity rate in awake animals than those under isoflurane anesthesia, which could explain why we saw modest levels of activity in our experiments, which were all performed in anesthetized animals. Interestingly, in one animal with transgenic GCaMP6f expression in all graft cell types (including glia) due to germline recombination in a Synapsin-Cre male breeder (Rempe et al., 2006), large-scale, spontaneous calcium transients were observed that appeared

similar to coordinated transients seen in dorsal horn astrocytes (Sekiguchi et al., 2016) (data not shown). The high density of small, active processes was unique to this non-neuronally-restricted expression of GCaMP6f, indicating that it was likely astrocyte activity. Thus, in vivo calcium imaging in NPC grafts recapitulated spontaneous activity and sensory responses seen in intact spinal cord, suggesting that these grafts integrate with host circuits and reconstitute damaged spinal cord.

Human neural stem cell grafts mature at an intrinsic rate and support functional recovery at accordingly later timepoints when grafted into rodent SCI

In a second study, we analyzed the maturation of human neural stem cells over an 18-month time period following grafting into cervical hemisection SCI in rats. We found that, despite a dramatic decline in the number of dividing graft cells over time, graft size did not significantly change between time points, an important demonstration of the long-term safety of this line of human NSCs. Despite this static gross morphology, interesting changes took place among the cells within the grafts. Both the total number of human nuclei and the number of neurons in the graft dropped from 1 – 6 months after grafting, but then rose significantly between 6, 12, and 18 months. Mature neurons labeling for NeuN did not appear until three months, and the size and neuronal marker labeling intensity of neurons continued to increase up to 18 months. Following a similarly prolonged course of maturation, mature astrocytes did not appear until 6 months, and mature oligodendrocytes did not appear until 12 months. The number of graft-derived axons in the host white matter steadily declined over the entire experiment, but axon numbers in gray matter were more stable, suggesting that axons

which form synapses in host gray matter are protected from pruning, as occurs in normal development (Low and Cheng, 2006). Importantly, improvement in forepaw placement in gridwalk testing was not seen until 18 months post-grafting, indicating that human NSC grafts may require much longer periods of time to fully mature and functionally integrate with host circuitry than rodent grafts. In addition, human NSC-derived glia migrated long distances from lesion sites into host white matter. While an interesting finding that matched previous studies of human grafts into rodents (Chen et al., 2015; Windrem et al., 2008), we did not observe this phenomenon in a subsequent study of human NSCs implanted into primate SCI (Rosenzweig et al., 2018), suggesting human glial migration in rats may be a result of the larger phylogenetic difference between these species.

The human gestational period of 280 days is over 13 times longer than the 21 days of rats (Semple et al., 2013). The present results indicate that placement into a novel environment did not prevent human NSCs from undergoing a normal human rate of maturation. Neither the traumatic, adult, nor rodent nature of the surrounding environment altered the intrinsic developmental programs within these cells. This prolonged maturation and the associated late functional improvements have important implications for future studies of NSC grafts in both animal models and human clinical trials. Prior studies of NSC grafts have only evaluated outcomes over weeks to a few months (Lu et al., 2012; Nori et al., 2011; Nutt et al., 2013; Tsuji et al., 2010), but our results indicate that time points of well over one year post-grafting must be included for a proper assessment to be made of the full potential of grafts to improve functional outcomes.

Future Directions

The present work has shown that NPC grafts are activated by host synaptic input and can in turn drive activity in distal host neurons. While understanding these steps individually is an important achievement, it must now be determined to what extent such grafts truly relay electrophysiological signals across sites of SCI, and in what manner. Perhaps the most clear-cut method of evaluating the contribution of graft-mediated relay circuits is to stimulate inputs on one side of the graft and record from host neurons below, before and after silencing graft activity. Genetic tools for silencing specific cells are already available. For example, inhibitory designer receptors exclusively activated by designer drugs (DREADDs), such as hM4Di (Armbruster et al., 2007), can hyperpolarize neurons when bound to an administrable ligand. This hyperpolarization effectively silences neuronal activity, and circuit interrogation can then reveal the contribution of the silenced population. Such a strategy has been employed to demonstrate the function of detour circuits and compensatory sprouting in SCI (Chen et al., 2018; Siegel et al., 2015). If silencing of grafts reduced or eliminated signals transmitted across lesions and also abrogated functional improvements, this would provide definitive evidence of a functional relay.

Such experiments would benefit from a more severe lesion model than the dorsal column lesion to properly evaluate function deficits and graft-mediated improvements, as compensation by other descending pathways can restore substantial function spontaneously in rodents (Krajacic et al., 2010; Whishaw et al., 1998). One such lesion, the lateral hemisection (Lu et al., 2017; Robinson and Lu, 2017), would both allow

assessment of unilateral limb function with less spontaneous recovery and create a wider rostro-caudal lesion that would enable calcium imaging studies of how activity spreads across larger distances more similar to human injury (Norenberg et al., 2004). Because few CST axons regenerate further than 1 mm into NPC grafts (Kadoya et al., 2016), a large hemisection in which a 1.5-2 mm rostro-caudal block of tissue is aspirated would likely require polysynaptic relays through grafts for signals from CST axons to reach caudal host targets. Additionally, complete removal and replacement of endogenous tissue with grafted cells might increase the number of graft cells accessible with in vivo imaging, as host tissue can often close around the dorsal aspect of grafts into narrow wire knife lesions. Graft activity should also be assessed in more clinically relevant lesions such as contusions (Brock et al., 2017), which can result in some white matter sparing but also exhibit large rostro-caudal spread. Finally, calcium imaging of graft cells implanted in biomimetic scaffolds would be of great value in deciphering how signals are propagated through linear channels (Koffler et al., 2019) compared to unrestricted volumes.

To achieve optical access to deeper regions of grafts in vivo, new approaches are necessary. For instance, implantable microprisms have been used in the cerebral cortex to image multiple dorso-ventral layers simultaneously (Andermann et al., 2013; Chia and Levene, 2010; Wenzel et al., 2017). Microprisms are essentially glass cubes cut in half diagonally, with a reflective coating on the inside surface of the hypotenuse that reflects excitation and fluorescence emission light to produce a vertical imaging plane. If placed such that the vertical surface of the prism faces to the right or left in the spinal cord, the resulting imaging plane would be similar to the sagittal sections

prepared in our acute slice experiments. In fact, we tried this approach in the dorsal column lesion model, but we found that the injury site was too tough for smooth insertion of the prism. One way to avoid this issue would be to perform a unilateral lesion such as a hemisection, so that the prism could be inserted in the intact half of the spinal cord and then used to image the injured/grafted side.

New activity indicators could also improve the number of neurons with detectable activity, the imaging depth, and the temporal resolution of activity dynamics. The recently published jGCaMP7 series of genetically encoded calcium indicators (GECIs) improves upon the in vivo performance of the GCaMP6 family by increasing the signal to noise ratio and fraction of cells with detectable activity (Dana et al., 2019). New red-shifted GECIs have also been developed with the improved dynamics, one of which (jRCaMP1a) does not display photoswitching with blue light illumination, allowing its combined used with blue light stimulation of channelrhodopsins (Dana et al., 2016). Red calcium indicators allow greater imaging depths due to the decreased scattering of longer wavelength light. This could prove especially beneficial for in vivo imaging, though slice imaging could also benefit because deeper regions of the slice could contain cells with better-preserved connections after cutting. Finally, genetically encoded voltage indicators (GEVIs), whose fluorescence changes with the transmembrane potential of expressing cells, are continuing to improve (Abdelfattah et al., 2019; Lin and Schnitzer, 2016; St-Pierre et al., 2015). Voltage-based imaging allows detection of both action potentials and subthreshold changes in membrane potential, which could be of particular interest in slice preparations for visualization of subthreshold responses not visible with calcium imaging. Additionally, the millisecond

timescale of voltage indicator dynamics could allow much more precise visualization of the spread of activity through grafts, potentially revealing the presence of both mono- and polysynaptic connections. However, a major disadvantage of these fast dynamics is that they require accordingly fast imaging (>300 Hz for imaging of 2 ms action potentials), which necessitates the use of high excitation intensity that could cause thermal or photochemical tissue damage and cross-talk in all-optical stimulation and recording (Emiliani et al., 2015; Lin and Schnitzer, 2016). Recording at such high framerates also requires an expensive high-speed camera and a large amount of computational power for data processing and analysis.

New optogenetic actuators are also improving the sensitivity and temporal resolution of light stimulation. A novel red-shifted channelrhodopsin developed by structure-based genome mining, ChRmine drives substantially higher amplitude photocurrents than Chrimson (Marshel et al., 2019). Remarkably, it was used to individually stimulate, in 3-dimensional volumes, populations of neurons whose activity was associated with specific visual stimuli. Stimulation of these representative neurons drove the same behavioral response in mice as when they saw the visual stimulus. Another group developed a variant of Chrimson, vf-Chrimson, with such fast kinetics that it could be used to drive action potentials in fast interneurons to their frequency limit of ~250 Hz (Mager et al., 2018a, 2018b). A second variant, f-Chrimson, which had slower channel-closing kinetics but increased sensitivity to lower light intensity, was used in the implementation of an optogenetic cochlear implant to restore some hearing function in deaf mice (Mager et al., 2018a). These studies inspire the use of red-shifted opsins not just for circuit interrogation, but also for functional stimulation to strengthen

new circuitry during rehabilitation. For example, optogenetic stimulation of graft neurons could be combined with epidural stimulation of the spinal cord and/or motor cortex to facilitate Hebbian plasticity between graft and host (Capogrosso et al., 2016; Hebb, 1949; Mishra et al., 2017).

Graft-host circuitry could be further dissected with cell type-specific expression methods. While we restricted expression of both ChrimsonR and GCaMP6f to neurons via expression from the pan-neuronal Synapsin promoter, many transgenic mouse lines are available that express Cre recombinase in specific neuronal subtypes (Daigle et al., 2018; Harris et al.). These mice can be crossed to mice with Cre-dependent transgenic expression of calcium indicators or injected with Cre-dependent viruses. Unfortunately, the expression patterns of many available Cre lines have not been characterized in the spinal cord, but some important spinal cord neuron types have been specifically labeled by Cre drivers, such as V2a interneurons in Chx10-Cre mice (Hayashi et al., 2018). The advent of CRISPR/Cas9 gene editing tools has made generation of transgenic lines much quicker and cheaper (Adli, 2018), thus making it simpler to acquire custom strains based on desired spinal cord expression patterns, which can be viewed for many genes in the atlas created by the Allen Institute (http://mousespinal.brain-map.org/). Uncovering which cell types contribute (or don't contribute) to distinct activity patterns within grafts would aid in the optimization of cell culture conditions to direct differentiation of stem cells toward the most beneficial classes of neural stem cells, as was achieved in the development of spinalized NSCs (Kumamaru et al., 2018).

Finally, future experiments, especially those with human cells, should incorporate longer timepoints to allow grafts to fully mature and functionally integrate with host

circuitry. Methods such as calcium imaging and extracellular recordings with microelectrode arrays that can measure graft activity could be used to assess how spontaneous activity patterns and responses to host stimulation change as graft neurons mature, and to see whether such changes correlate with improvements in behavioral function. Studies in the brain suggest that this is likely the case (Avaliani et al., 2014; Falkner et al., 2016; Niclis et al., 2017). With the great sacrifice of animal lives, experimenter time, and research funds that go into each study of NPC/NSC grafts in spinal cord injury and other disorders of the central nervous system, it is a shame to potentially misinterpret the results of an experiment due to insufficient study length. As much as we would like a quick fix, the nervous system matures slowly, and therapeutic strategies that rely on the transplantation of developing neural tissue should not be expected *a priori* to elicit functional improvements on an accelerated timescale.

Conclusion

Understanding the neurophysiological effects of synaptic connectivity between neural stem cell grafts and host circuitry is essential to evaluating and improving the efficacy of neuronal relays as a mechanism of spinal cord injury repair. The present works demonstrates the utility of all-optical circuit interrogation in this endeavor, showing that graft neurons spontaneously self-assemble into synchronously active subnetworks, respond to motor and sensory stimuli, and can activate distal host neurons. Given sufficient time to completely mature and strengthen connections with host circuitry, neural stem cells indeed form the functional building blocks of a neuronal relay.

References

Abdelfattah, A.S., Kawashima, T., Singh, A., Novak, O., Liu, H., Shuai, Y., Huang, Y.-C., Campagnola, L., Seeman, S.C., Yu, J., Zheng, J., Grmm, J.B., Patel, R., Friedrich, J., Mensh, B.D., Paninski, L., Macklin, J.J., Murphy, G.J., Podgorski, K., Lin, B., Chen, T., Turner, G.C., Liu, Z., Koyama, M., Svoboda, K., Ahrens, M.B., Lavis, L.D., and Schreiter, E.R. (2019). Bright and photostable chemigenetic indicators for extended in vivo voltage imaging. Science *365*, 699–704.

Adli, M. (2018). The CRISPR tool kit for genome editing and beyond. Nat Commun *9*, 1911.

Alviña, K., and Khodakhah, K. (2010). The therapeutic mode of action of 4-aminopyridine in cerebellar ataxia. The Journal of Neuroscience : The Official Journal of the Society for Neuroscience *30*, 7258–7268.

Andermann, M.L., Gilfoy, N.B., Goldey, G.J., Sachdev, R., Wölfel, M., McCormick, D.A., Reid, C.R., and Levene, M.J. (2013). Chronic Cellular Imaging of Entire Cortical Columns in Awake Mice Using Microprisms. Neuron *80*, 900–913.

Armbruster, B.N., Li, X., Pausch, M.H., Herlitze, S., and Roth, B.L. (2007). Evolving the lock to fit the key to create a family of G protein-coupled receptors potently activated by an inert ligand. Proc National Acad Sci *104*, 5163–5168.

Avaliani, N., Sørensen, A., Ledri, M., Bengzon, J., Koch, P., Brüstle, O., Deisseroth, K., Andersson, M., and Kokaia, M. (2014). Optogenetics Reveal Delayed Afferent Synaptogenesis on Grafted Human-Induced Pluripotent Stem Cell-Derived Neural Progenitors. STEM CELLS *32*, 3088–3098.

Bikson, M., Fox, J.E., and Jefferys, J.G. (2003). Neuronal Aggregate Formation Underlies Spatiotemporal Dynamics of Nonsynaptic Seizure Initiation. J Neurophysiol *89*, 2330–2333.

Brock, J.H., Graham, L., Staufenberg, E., Im, S., and Tuszynski, M.H. (2017). Rodent Neural Progenitor Cells Support Functional Recovery After Cervical Spinal Cord Contusion. Journal of Neurotrauma.

Capogrosso, M., Milekovic, T., Borton, D., Wagner, F., Moraud, E., Mignardot, J.-B., Buse, N., Gandar, J., Barraud, Q., Xing, D., Rey, E., Duis, S., Jianzhong, Y., Ko, W.D., Li, Q., Detemple, P., Denison, T., Micera, S., Bezard, E., Bloch, J., and Courtine, G. (2016). A brain–spine interface alleviating gait deficits after spinal cord injury in primates. Nature *539*, 284.

Cazalets, J., Sqalli-Houssaini, Y., and Clarac, F. (1992). Activation of the central pattern generators for locomotion by serotonin and excitatory amino acids in neonatal rat. J Physiology *455*, 187–204.

Chen, B., Li, Y., Yu, B., Zhang, Z., Brommer, B., Williams, P., Liu, Y., Hegarty, S., Zhou, S., Zhu, J., Guo, H., Lu, Y., Zhang, Y., Gu, X., and He, Z. (2018). Reactivation of Dormant Relay Pathways in Injured Spinal Cord by KCC2 Manipulations. Cell.

Chen, H., Qian, K., Chen, W., Hu, B., Blackbourn, L.W., Du, Z., Ma, L., Liu, H., Knobel, K.M., Ayala, M., and Zhang, S. (2015). Human-derived neural progenitors functionally replace astrocytes in adult mice. J Clin Invest *125*, 1033–1042.

Chen, T.-W., Wardill, T.J., Sun, Y., Pulver, S.R., Renninger, S.L., Baohan, A., Schreiter, E.R., Kerr, R.A., Orger, M.B., Jayaraman, V., Looger, L.L., Svoboda, K., and Kim, D.S. (2013). Ultrasensitive fluorescent proteins for imaging neuronal activity. Nature *499*, 295.

Chia, T.H., and Levene, M.J. (2010). Multi-Layer In Vivo Imaging of Neocortex Using a Microprism. Cold Spring Harbor Protocols *2010*, pdb.prot5476.

Cho, J., Deisseroth, K., and Neuron, B.V. (2013). Synaptic encoding of fear extinction in mPFC-amygdala circuits.

Daigle, T.L., Madisen, L., Hage, T.A., Valley, M.T., Knoblich, U., Larsen, R.S., Takeno, M.M., Huang, L., Gu, H., Larsen, R., Mills, M., Bosma-Moody, A., Siverts, L.A., Walker, M., Graybuck, L.T., Yao, Z., Fong, O., Nguyen, T.N., Garren, E., Lenz, G.H., Chavarha, M., Pendergraft, J., Harrington, J., Hirokawa, K.E., Harris, J.A., Nicovich, P.R., McGraw, M.J., Ollerenshaw, D.R., Smith, K.A., Baker, C.A., Ting, J.T., Sunkin, S.M., Lecoq, J., Lin, M.Z., Boyden, E.S., Murphy, G.J., da Costa, N.M., Waters, L.L., Tasic, B., and Zeng, H. (2018). A Suite of Transgenic Driver and Reporter Mouse Lines with Enhanced Brain-Cell-Type Targeting and Functionality. Cell *174*, 465-480.e22.

Dana, H., Mohar, B., Sun, Y., Narayan, S., Gordus, A., Hasseman, J.P., Tsegaye, G., Holt, G.T., Hu, A., Walpita, D., Patel, R., Macklin, J.J., Bargmann, C.I., Ahrens, M.B., Schreiter, E.R., Jayaraman, V., Looger, L.L., Svoboda, K., and Kim, D.S. (2016). Sensitive red protein calcium indicators for imaging neural activity. Elife *5*, e12727.

Dana, H., Sun, Y., Mohar, B., Hulse, B.K., Kerlin, A.M., Hasseman, J.P., Tsegaye, G., Tsang, A., Wong, A., Patel, R., Macklin, J.J., Chen, Y., Konnerth, A., Jayaraman, V., Looger, L.L., Schreter, E.R., Svoboda, K., and Kim, D.S. (2019). High-performance calcium sensors for imaging activity in neuronal populations and microcompartments. Nat Methods *16*, 649–657.

Dulin, J.N., Adler, A.F., Kumamaru, H., Poplawski, G.H., Lee-Kubli, C., Strobl, H., Gibbs, D., Kadoya, K., Fawcett, J.W., Lu, P., and Tuszynski, M.H. (2018). Injured adult motor and sensory axons regenerate into appropriate organotypic domains of neural progenitor grafts. Nature Communications *9*, 84.

Emiliani, V., Cohen, A.E., Deisseroth, K., and Häusser, M. (2015). All-Optical Interrogation of Neural Circuits. The Journal of Neuroscience *35*, 13917–13926.

Etlin, A., Bráz, J.M., Kuhn, J.A., Wang, X., Hamel, K.A., Llewellyn-Smith, I.J., and Basbaum, A.I. (2016). Functional Synaptic Integration of Forebrain GABAergic Precursors into the Adult Spinal Cord. The Journal of Neuroscience : The Official Journal of the Society for Neuroscience *36*, 11634–11645.

Falkner, S., Grade, S., Dimou, L., Conzelmann, K.-K., Bonhoeffer, T., Götz, M., and Hübener, M. (2016). Transplanted embryonic neurons integrate into adult neocortical circuits. Nature *539*, nature20113.

Grienberger, C., and Konnerth, A. (2012). Imaging Calcium in Neurons. Neuron *73*.

Harris, J.A., Hirokawa, K.E., Sorensen, S.A., Gu, H., Mills, M., Ng, L.L., Bohn, P., Mortrud, M., Ouellette, B., Kidney, J., Smith, K.A., Dang, C., Sunkin, S., Bernard, A., Oh, S., Madisen, L., and Zeng, H. (2014). Anatomical characterization of Cre driver mice for neural circuit mapping and manipulation. Frontiers in Neural Circuits *8*.

Hayashi, M., Hinckley, C.A., Driscoll, S.P., Moore, N.J., Levine, A.J., Hilde, K.L., Sharma, K., and Pfaff, S.L. (2018). Graded Arrays of Spinal and Supraspinal V2a Interneuron Subtypes Underlie Forelimb and Hindlimb Motor Control. Neuron *97*, 869-884.e5.

Hebb, D.O. (1949). The organization of behavior; a neuropsychological theory.

Hentall, I. (1977). A novel class of unit in the substantia gelatinosa of the spinal cat. Exp Neurol *57*, 792–806.

Husch, A., Cramer, N., and Harris-Warrick, R.M. (2011). Long-duration perforated patch recordings from spinal interneurons of adult mice. Journal of Neurophysiology *106*, 2783–2789.

Jäderstad, J., Jäderstad, L.M., Li, J., Chintawar, S., Salto, C., Pandolfo, M., Ourednik, V., Teng, Y.D., Sidman, R.L., Arenas, E., Snyder, E.Y., and Herlenius, E. (2010). Communication via gap junctions underlies early functional and beneficial interactions between grafted neural stem cells and the host. Proceedings of the National Academy of Sciences of the United States of America *107*, 5184–5189.

Jayaprakash, N., Nowak, D., Eastwood, E., Krueger, N., Wang, Z., and Blackmore, M.G. (2019). Restoration of Direct Corticospinal Communication Across Sites of Spinal Injury. BioRxiv 546374.

Jiang, Y.-Q.Q., Armada, K., and Martin, J.H. (2019). Neuronal activity and microglial activation support corticospinal tract and proprioceptive afferent sprouting in spinal circuits after a corticospinal system lesion. Experimental Neurology 113015.

Johannssen, H.C., and Helmchen, F. (2010). In vivo Ca2+ imaging of dorsal horn

neuronal populations in mouse spinal cord. J Physiology *588*, 3397–3402.

Kadoya, K., Lu, P., Nguyen, K., Lee-Kubli, C., Kumamaru, H., Yao, L., Knackert, J., Poplawski, G., Dulin, J.N., Strobl, H., Takashima Y., Biane, J., Conner, J., Zhang, S., and Tuszynski, M.H. (2016). Spinal cord reconstitution with homologous neural grafts enables robust corticospinal regeneration. Nature Medicine *22*, nm.4066.

Klapoetke, N.C., Murata, Y., Kim, S., Pulver, S.R., Birdsey-Benson, A., Cho, Y., Morimoto, T.K., Chuong, A.S., Carpenter, E.J., Tian, Z., Wang, J., Xie, Y., Yan, Z., Zhang, Y., Chow, B.Y., Surek, B., Melkonian, M., Jayaraman, V., Constantine-Paton, M., Wong, G., and Boyden, E.S. (2014). Independent optical excitation of distinct neural populations. Nature Methods *11*, 338–346.

Koffler, J., Zhu, W., Qu, X., Platoshyn, O., Dulin, J.N., Brock, J., Graham, L., Lu, P., Sakamoto, J., Marsala, M., Chen, S., and Tuszynski, M.H. (2019). Biomimetic 3D-printed scaffolds for spinal cord injury repair. Nature Medicine 1.

Krajacic, A., Weishaupt, N., Girgis, J., Tetzlaff, W., and Fouad, K. (2010). Training-induced plasticity in rats with cervical spinal cord injury: Effects and side effects. Behav Brain Res *214*, 323–331.

Kumamaru, H., Kadoya, K., Adler, A.F., Takashima, Y., Graham, L., Coppola, G., and Tuszynski, M.H. (2018). Generation and post-injury integration of human spinal cord neural stem cells. Nature Methods *15*, 723–731.

Kumamaru, H., Lu, P., Rosenzweig, E.S., Kadoya, K., and Tuszynski, M.H. (2019). Regenerating Corticospinal Axons Innervate Phenotypically Appropriate Neurons within Neural Stem Cell Grafts. Cell Reports *26*, 2329-2339.e4.

Kumazawa, T., and Perl, E. (1978). Excitation of marginal and substantia gelatinosa neurons in the primate spinal cord: Indications of their place in dorsal horn functional organization. J Comp Neurol *177*, 417–434.

Kwan, A.C., Dietz, S.B., Zhong, G., Harris-Warrick, R.M., and Webb, W.W. (2010). Spatiotemporal dynamics of rhythmic spinal interneurons measured with two-photon calcium imaging and coherence analysis. J Neurophysiol *104*, 3323–3333.

Lin, M.Z., and Schnitzer, M.J. (2016). Genetically encoded indicators of neuronal activity. Nature Neuroscience *19*, 1142–1153.

Lin, G., He, X., Liang, F., Guo, Y., Sunnassee, G., Chen, J., Cao, X., Chen, Y., Pan, G., Pei, Z., and Tan, S. (2018). Transplanted human neural precursor cells integrate into the host neural circuit and ameliorate neurological deficits in a mouse model of traumatic brain injury. Neurosci Lett *674*, 11–17.

Low, L.K., and Cheng, H.-J. (2006). Axon pruning: an essential step underlying the

developmental plasticity of neuronal connections. Philosophical Transactions of the Royal Society of London. Series B, Biological Sciences *361*, 1531–1544.

Lu, P., Wang, Y., Graham, L., McHale, K., Gao, M., Wu, D., Brock, J., Blesch, A., Rosenzweig, E.S., Havton, L.A., Zheng, B., Conner, J.M., Marsala, M., and Tuszynski, M.H. (2012). Long-Distance Growth and Connectivity of Neural Stem Cells after Severe Spinal Cord Injury. Cell *150*, 1264–1273.

Lu, P., Ceto, S., Wang, Y., Graham, L., Wu, D., Kumamaru, H., Staufenberg, E., and Tuszynski, M.H. (2017). Prolonged human neural stem cell maturation supports recovery in injured rodent CNS. Journal of Clinical Investigation.

Lucas-Romero, J., Rivera-Arconada, I., Roza, C., and Lopez-Garcia, J.A. (2018). Origin and classification of spontaneous discharges in mouse superficial dorsal horn neurons. Sci Rep-Uk *8*, 9735.

Mager, T., de la Morena, D., Senn, V., Schlotte, J., D´Errico, A., Feldbauer, K., Wrobel, C., Jung, S., Bodensiek, K., Rankovic, V., Browne, L., Huet, A., Jüttner, J., Wood, P.G., Letzkus, J.J., Moser, T., and Bamberg, E. (2018a). High frequency neural spiking and auditory signaling by ultrafast red-shifted optogenetics. Nat Commun *9*, 1750.

Mager, T., de la Morena, D.L., Shevchenko, V., Senn, V., Wood, P.G., Letzkus, J.J., Gordeliy, V., Moser, T., and Bamberg, E. (2018b). Improved Microbial Rhodopsins for Ultrafast Red-Shifted Optogenetics. Biophys J *114*, 669a.

Mansour, A., Gonçalves, T.J., Bloyd, C.W., Li, H., Fernandes, S., Quang, D., Johnston, S., Parylak, S.L., Jin, X., and Gage, F.H. (2018). An in vivo model of functional and vascularized human brain organoids. Nature Biotechnology *36*, 432.

Marshel, J.H., Kim, Y., Machado, T.A., Quirin, S., Benson, B., Kadmon, J., Raja, C., Chibukhchyan, A., Ramakrishnan, C., Inoue, M., Shane, J.C., McKnight, D.J., Yoshizawa, S., Kato, H.E., Ganguli, S., and Deisseroth, K. (2019). Cortical layer–specific critical dynamics triggering perception. Science *365*, eaaw5202.

Mishra, A.M., Pal, A., Gupta, D., and Carmel, J.B. (2017). Paired motor cortex and cervical epidural electrical stimulation timed to converge in the spinal cord promotes lasting increases in motor responses. The Journal of Physiology *595*, 6953–6968.

Mitra, P., and Brownstone, R.M. (2012). An in vitro spinal cord slice preparation for recording from lumbar motoneurons of the adult mouse. Journal of Neurophysiology *107*, 728–741.

Miyashita, T., Shao, Y.R., Chung, J., Pourzia, O., and Feldman, D.E. (2013). Long-term channelrhodopsin-2 (ChR2) expression can induce abnormal axonal morphology and targeting in cerebral cortex. Frontiers in Neural Circuits *7*.

Niclis, J.C., Turner, C., Durnall, J., ugal, S., Kauhausen, J.A., Leaw, B., Dottori, M., Parish, C.L., and Thompson, L.H. (2017). Long-Distance Axonal Growth and Protracted Functional Maturation of Neurons Derived From Human Induced Pluripotent Stem Cells After Intracerebral Transplantation. Stem Cells Translational Medicine.

Nohda, K., Nakatsuka, T., Takeda, D., Miyazaki, N., Nishi, H., Sonobe, H., and Yoshida, M. (2007). Selective Vulnerability to Ischemia in the Rat Spinal Cord. Spine *32*, 1060–1066.

Norenberg, M.D., Smith, J., and Marcillo, A. (2004). The pathology of human spinal cord injury: defining the problems. Journal of Neurotrauma *21*, 429–440.

Nori, S., Okada, Y., Yasuda, A., Tsuji, O., Takahashi, Y., Kobayashi, Y., Fujiyoshi, K., Koike, M., Uchiyama, Y., Ikeda, E., Toyama, Y., Yamanaka, S., Nakamura, M., and Okano, H. (2011). Grafted human-induced pluripotent stem-cell–derived neurospheres promote motor functional recovery after spinal cord injury in mice. Proc National Acad Sci *108*, 16825–16830.

Nutt, S.E., Chang, E.-A., Suhr, S.T., Schlosser, L.O., Mondello, S.E., Moritz, C.T., Cibelli, J.B., and Horner, P.J. (2013). Caudalized human iPSC-derived neural progenitor cells produce neurons and glia but fail to restore function in an early chronic spinal cord injury model. Exp Neurol *248*, 491–503.

Pinto, D.J., Patrick, S.L., Huang, W.C., and Connors, B.W. (2005). Initiation, Propagation, and Termination of Epileptiform Activity in Rodent Neocortex In Vitro Involve Distinct Mechanisms. J Neurosci *25*, 8131–8140.

Poplawski, G.H., Lie, R., Hunt, M., Kumamaru, H., Kawaguchi, R., Lu, P., Schäfer, M.K., Woodruff, G., Robinson, J., Canete, P., Dulin, J.N., Geoffroy, C.G., Menzel, L., Zheng, B., Coppola, G., and Tuszynski, M.H. (2018). Adult rat myelin enhances axonal outgrowth from neural stem cells. Science Translational Medicine *10*.

Rempe, D., Vangeison, G., Hamilton, J., Li, Y., Jepson, M., and Federoff, H.J. (2006). Synapsin I Cre transgene expression in male mice produces germline recombination in progeny. Genesis *44*, 44–49.

Robinson, J., and Lu, P. (2017). Optimization of trophic support for neural stem cell grafts in sites of spinal cord injury. Experimental Neurology.

Rosenzweig, E.S., Brock, J.H., Lu, P., Kumamaru, H., Salegio, E.A., Kadoya, K., Weber, J.L., Liang, J.J., Moseanko, R., Hawbecker, S., Huie, R.J., Havton, L.A., Nout-Lomas, Y.S., Ferguson, A.R., Beattie, M.S., Bresnahan, J.C., and Tuszynski, M.H. (2018). Restorative effects of human neural stem cell grafts on the primate spinal cord. Nature Medicine *24*, 484.

Roza, C., Mazo, I., Rivera-Arconada, I., Cisneros, E., Alayón, I., and López-García, J.A.

(2016). Analysis of spontaneous activity of superficial dorsal horn neurons in vitro: neuropathy-induced changes. Pflügers Archiv - European J Physiology *468*, 2017–2030.

Sandkühler, J., and Eblen-Zajjur, A.A. (1994). Identification and characterization of rhythmic nociceptive and non-nociceptive spinal dorsal horn neurons in the rat. Neuroscience *61*, 991–1006.

Sekiguchi, K.J., Shekhtmeyster, P., Merten, K., Arena, A., Cook, D., Hoffman, E., Ngo, A., and Nimmerjahn, A. (2016). Imaging large-scale cellular activity in spinal cord of freely behaving mice. Nature Communications *7*, 11450.

Semple, B.D., Blomgren, K., Gimlin, K., Ferriero, D.M., and Noble-Haeusslein, L.J. (2013). Brain development in rodents and humans: Identifying benchmarks of maturation and vulnerability to injury across species. Prog Neurobiol *106*, 1–16.

Siegel, C.S., Fink, K.L., rittmatter, S., and Cafferty, W.B. (2015). Plasticity of intact rubral projections mediates spontaneous recovery of function after corticospinal tract injury. The Journal of Neuroscience : The Official Journal of the Society for Neuroscience *35*, 1443–1457.

St-Pierre, F., Chavarha, M., and Lin, M.Z. (2015). Designs and sensing mechanisms of genetically encoded fluorescent voltage indicators. Curr Opin Chem Biol *27*, 31–38.

Strupp, M., Teufel, J., Zwergal, A., Schniepp, R., Khodakhah, K., and Feil, K. (2017). Aminopyridines for the treatment of neurologic disorders. Neurology: Clinical Practice *7*, 65–76.

Tornero, D., Tsupykov, O., Granmo, M., Rodriguez, C., Grønning-Hansen, M., Thelin, J., Smozhanik, E., Laterza, C., Wattananit, S., Ge, R., Tatarishvili, J., Grealish, S., Brüstle, O., Skibo, G., Parmar, M., Schouenborg, J., Lindvall, O., and Kokaia, Z. (2017). Synaptic inputs from stroke-injured brain to grafted human stem cell-derived neurons activated by sensory stimuli. Brain *140*, 692–706.

Tsuji, O., Miura, K., Okada, Y., Fujiyoshi, K., Mukaino, M., Nagoshi, N., Kitamura, K., Kumagai, G., Nishino, M., Tomisato, S., Higashi, H., Nagai, T., Katoh, H., Kohda, K., Matsuzaki, Y., Yuzaki, M., Ikeda, E., Toyama, Y., Nakamura, M., Yamanaka, S., and Okano, H. (2010). Therapeutic potential of appropriately evaluated safe-induced pluripotent stem cells for spinal cord injury. Proc National Acad Sci *107*, 12704–12709.

Weidner, N., Ner, A., Salimi, N., and Tuszynski, M. (2001). Spontaneous corticospinal axonal plasticity and functional recovery after adult central nervous system injury. Proceedings of the National Academy of Sciences of the United States of America *98*, 3513–3518.

Wenzel, M., Hamm, J.P., Peterka, D.S., and Yuste, R. (2017). Reliable and Elastic

Propagation of Cortical Seizures In Vivo. Cell Reports *19*, 2681–2693.

Whishaw, I.Q., Gorny, B., and Sarna, J. (1998). Paw and limb use in skilled and spontaneous reaching after pyramidal tract, red nucleus and combined lesions in the rat: behavioral and anatomical dissociations. Behav Brain Res *93*, 167–183.

Wilson, J.M., Dombeck, D.A., Díaz-Ríos, M., Harris-Warrick, R.M., and Brownstone, R.M. (2007). Two-Photon Calcium Imaging of Network Activity in XFP-Expressing Neurons in the Mouse. J Neurophysiol *97*, 3118–3125.

Wilson, J.M., Blagovechtchenski, E., and Brownstone, R.M. (2010). Genetically Defined Inhibitory Neurons in the Mouse Spinal Cord Dorsal Horn: A Possible Source of Rhythmic Inhibition of Motoneurons during Fictive Locomotion. J Neurosci *30*, 1137–1148.

Windrem, M.S., Schanz, S.J., Guo, M., Tian, G.-F., Washco, V., Stanwood, N., Rasband, M., Roy, N.S., Nedergaard, M., Havton, L.A., Wang, S., and Goldman, S.A. (2008). Neonatal Chimerization with Human Glial Progenitor Cells Can Both Remyelinate and Rescue the Otherwise Lethally Hypomyelinated Shiverer Mouse. Cell Stem Cell *2*, 553–565.

Wuttke, T.V., Markopoulos, F., Padmanabhan, H., Wheeler, A.P., Murthy, V.N., and Macklis, J.D. (2018). Developmentally primed cortical neurons maintain fidelity of differentiation and establish appropriate functional connectivity after transplantation. Nature Neuroscience *21*, 517–529.

Zareen, N., inozaki, Ryan, D., Alexander, H., Amer, A., Truong, D.Q., Khadka, N., Sarkar, A., Naeem, S., Bikson, M., and Martin, J.H. (2017). Motor cortex and spinal cord neuromodulation promote corticospinal tract axonal outgrowth and motor recovery after cervical contusion spinal cord injury. Experimental Neurology *297*, 179–189.

Zhong, G., Droho, S., Crone, S.A., Dietz, S., Kwan, A.C., Webb, W.W., Sharma, K., and Harris-Warrick, R.M. (2010). Electrophysiological Characterization of V2a Interneurons and Their Locomotor-Related Activity in the Neonatal Mouse Spinal Cord. J Neurosci *30*, 170–182.